U.S. DEPARTMENT OF ENERGY | National Energy Technology Laboratory

OFFICE OF FOSSIL ENERGY

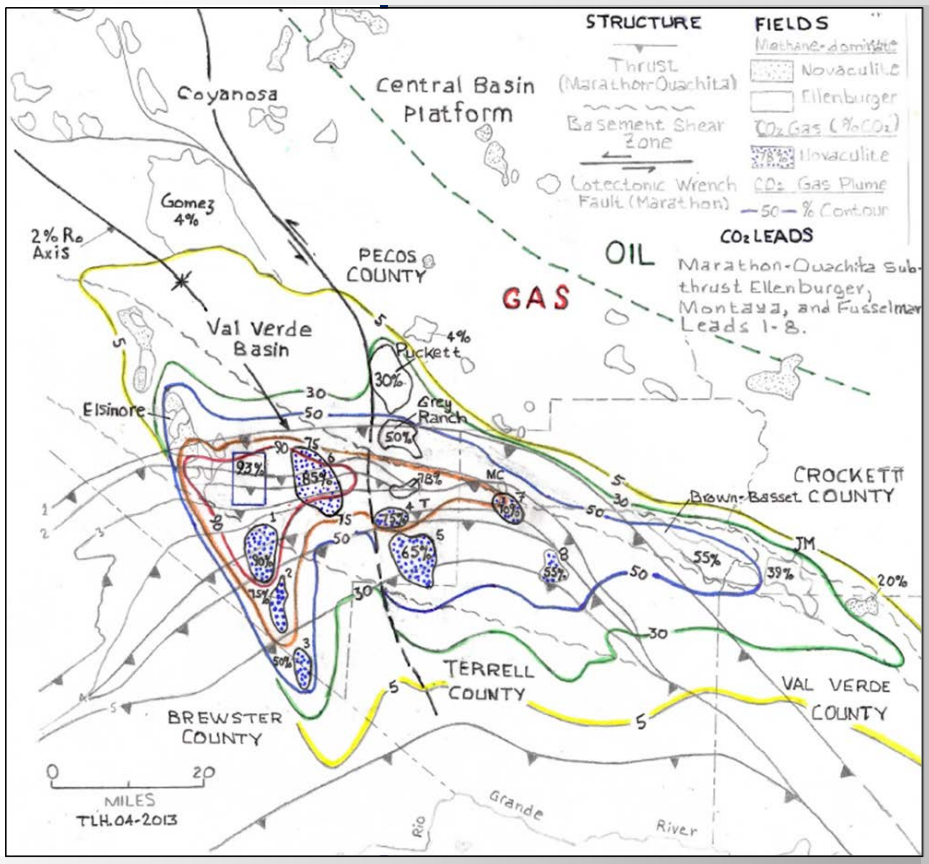

Subsurface Sources of CO_2 in the United States
Volume II: Exploration of CO_2 Systems

March 26, 2014

DOE/NETL-2014/1641

Working Paper

Disclaimer

This report was prepared as an account of work sponsored by an agency of the United States Government. Neither the United States Government nor any agency thereof, nor any of their employees, makes any warranty, express or implied, or assumes any legal liability or responsibility for the accuracy, completeness, or usefulness of any information, apparatus, product, or process disclosed, or represents that its use would not infringe privately owned rights. Reference therein to any specific commercial product, process, or service by trade name, trademark, manufacturer, or otherwise does not necessarily constitute or imply its endorsement, recommendation, or favoring by the United States Government or any agency thereof. The views and opinions of authors expressed therein do not necessarily state or reflect those of the United States Government or any agency thereof.

All exhibits have been created by Enegis, LLC, unless otherwise noted.

Author List:

Jeffrey Eppink, RG, RGph, MBA, Tom L. Heidrick,
Ramon Alvarado, Michael Marquis
Enegis, LLC

National Energy Technology Laboratory (NETL)

Phil DiPietro
Strategic Energy Analysis and Planning Division

Energy Sector Planning and Analysis (ESPA)

Robert Wallace
Booz Allen Hamilton, Inc.

This report was prepared by Energy Sector Planning and Analysis (ESPA) for the United States Department of Energy (DOE), National Energy Technology Laboratory (NETL). This work was completed under DOE NETL Contract Number DE-FE0004001. This work was performed under ESPA Task 150.07.05.

The authors wish to acknowledge the excellent guidance, contributions, and cooperation of the NETL staff, particularly:

Ms. Traci Rodosta

Ms. Evelyn Dale

DOE Contract Number DE-FE0004001

This page intentionally left blank.

Table of Contents

Executive Summary 1
1 Introduction 7
2 Overview and Methodology 8
2.1 Subsurface CO_2 Systems 8
2.1.1 CO_2 Sourcing 8
2.1.2 CO_2 Migration 8
2.1.3 CO_2 Trap 8
2.1.4 CO_2 Reservoir and Seal 8
2.1.5 CO_2 Origins 9
2.1.6 Tectonostratigraphic Characterization of Undiscovered CO_2 Traps 11
2.1.7 Timing of CO_2 Charge 15
2.2 Undiscovered CO_2 Resource Assessment 15
2.2.1 CO_2 Accumulations 15
2.2.2 Characteristics of CO_2 Fields 17
3 Play Fairways and Leads—Undiscovered 19
3.1 Identified Late-Cretaceous Laramide Fairways and Undiscovered CO_2 Leads 20
3.1.1 Mid-Continent Fairway 20
3.1.2 North American Kimberlite-Carbonatite-Lamproite Occurrences 31
3.1.3 Marathon Tectonic Compartmentalization and Foreland Stress Field 58
3.2 Identified Mid-Tertiary Fairways and Undiscovered CO_2 Leads 86
3.3 Identified Mid- to Late-Tertiary Fairways and Undiscovered CO_2 Lead 124
4 Estimates for GIIP and TRR 140
5 Closing Ideas, Concepts, and Observations 143
6 References 145
Appendix 1 Disaggregated Field Results from CREAM 155

Exhibits

Exhibit ES-1 Subsurface Sources of CO_2 in the Lower 48 United States: Discovered Reservoirs and Leads for Undiscovered Reservoirs 2
Exhibit ES-2 Estimates of gas-initially-in-place and technically recoverable resources for undiscovered leads for CO_2 in the United States, and key input variables for the volumetric calculations 4
Exhibit ES-3 Structural contour map top Permian in the Lincoln County porphyry belt. Shows Mid-Tertiary intrusions, faults, folds and principal mining districts (modified from Kelley and Thompson, 1964; used with permission) 6
Exhibit 2-1 Schematic cross-section showing hydrocarbon trapping mechanism and play types, Wind River Basin, Wyoming (Willis and Groshong, 1993; used with permission)..... 14
Exhibit 2-2 Stratigraphic trap types (after Biddle and Wielchowsky, undated) 15
Exhibit 2-3 Characteristics of discovered CO_2 field occurrences..... 16
Exhibit 3-1 Undiscovered CO_2 fairways and leads..... 19
Exhibit 3-2 Undiscovered CO_2 leads 20
Exhibit 3-3 Late Cretaceous igneous intrusive fairways 21
Exhibit 3-4 Sketch map summarizing principal structural and stratigraphic elements of the Mississippi Interior Salt Basin (modified after Pilger, 1981) 22
Exhibit 3-5 Map of principal intrusions comprising the AAP and general limit of lamprophyre dikes (adapted from Eby, 1987)..... 24
Exhibit 3-6 Magnet Cove intrusive complex (adapted from Howard and Chandler, 2007)..... 25
Exhibit 3-7 Radiometric summary of Mississippi, Arkansas, and Kansas lamproite and mafic-alkalic Laramide intrusions (data summarized from Brookins [1967, 1970], Brookins and Nasaer [1971], and Cullers et al. [1982])..... 27
Exhibit 3-8 Location map of the Riley and Marshall Counties kimberlite occurrences (modified after Berendsen and Weis, 2001; with fault interpretation by Enegis, LLC; used with permission)..... 29
Exhibit 3-9 Geologic map of Precambrian basement with major lithologies, Riley and Marshall Counties, Kansas (adapted from Berendsen and Weis, 2001; used with permission)..... 30
Exhibit 3-10 North American kimberlite-carbonatite-lamproite occurrences (125-1 Ma)..... 33
Exhibit 3-11 Map of the North American continent showing the location of several kimberlite, carbonatite, and lamproite intrusive complexes for the 175-1 Ma timeframe (150, 100, 75, 50, 25, and 5 Ma isochron lines by Enegis, LLC; modified after McCandless, 1999; used with permission)..... 34
Exhibit 3-12 Stylized model of a kimberlite magmatic system..... 35
Exhibit 3-13 Location map showing the leading edge of the Marathon-Ouachita fold-thrust belt and Permian foreland basins of west Texas (adapted from Hickman et al., 2009; used with permission)..... 36
Exhibit 3-14 Map generalizing the location of several subbasins and structural compartments of the Permian basin (modified from Hanson, 1991; used with permission)..... 37
Exhibit 3-15 Early Carboniferous (3A, Tournaisian, 356 Ma) and Late Carboniferous (3B, Moscovian, 306 Ma) (Scotese, 2003; used with permission) 38
Exhibit 3-16 Composite stratigraphic columns for the Marathon subthrust (left) and allochthon (right), Delaware-Val Verde foreland subbasins and Marathon facies (from Barden and Franklin, 2003)..... 40

Exhibit 3-17 Schematic diagram showing successive stages of tectonostratigraphic evolution of the Marathon overthrust belt (adapted from Hickman et al., 2009; used with permission).. 42
Exhibit 3-18 N-S schematic cross-section across the Marathon fold and thrust belt (from Barden and Franklin, 2003) 43
Exhibit 3-19 Diagrammatic SW-NE cross-section across the Marathon fold and thrust belt (from Barden and Franklin, 2003) 44
Exhibit 3-20 Isopach map of the Ellenburger formation, Permian Basin, west Texas (modified after Hanson et al., 1991; and Hoak, et al., 1998b; used with permission)..... 45
Exhibit 3-21 Structural contour map on top basement; contour interval is 1,000 ft, Permian basin region, West Texas (modified after Hoak et al., 1998a; used with permission; strain ellipsoid by Enegis, LLC) 47
Exhibit 3-22 Transverse (ENE-NE-bearing) cross-sections showing complex fold and thrust relationships developed along the Central Basin Platform Margin, southern Permian Basin, Texas (adapted from Shumaker, 1992; and Hoak, et al., 1998a)..... 50
Exhibit 3-23 Structural cross-section illustrating complex Pennsylvanian-Early Permian basement-involved fold and thrust relationships along the Central Basin Platform Margin, southern Permian Basin (adapted from Shumaker, 1992; Hoak, et al., 1998a)..... 51
Exhibit 3-24 Map of Marathon frontal thrusts, Marathon uplift, location of the Pinon field area, Longfellow-West Ranches, Thistle and Mckay Creek fields (from Barden and Franklin, 2003) 53
Exhibit 3-25 Structural contour map on top Caballos Novacullite, Longfellow-West Ranch leads (from Barden and Franklin, 2003) 54
Exhibit 3-26 Sequential forward model of a flat-ramp-flat fault-bend fold (modified from Suppe, 1983) 56
Exhibit 3-27 A, FMI image and core photo of Ellenburger fracture breccia development of a laminated mudstone. B, FMI image and core photo of a carbonate-matrix supported chaotic breccia, Ellenburger Dolomite, eastern Shelf, west Texas (images and core photos adapted from Cain and Hammes, 1997; used with permission)..... 57
Exhibit 3-28 Map locating the Central Basin Platform (gas/oil boundary is dashed green line), regional distribution of Ellenburger (blue) and Silurian-Devonian (orange) fields, and Marathon fold-thrust belt (adapted from Shumaker, 1992) 59
Exhibit 3-29 Simple left-lateral shear model showing sequentially deforming of a fixed circular area with successively increasing angles of internal shear (Øi, 22-67°) (adapted from Davis and Reynolds, 1996; used with permission) 61
Exhibit 3-30 Map compiles calculated depths to the 2.0% vitrinite reflectance (Ro) values for drilled strata from the Permian Basin, west Texas and southeastern New Mexico (adapted from Pawlewicz et al., 2005) 63
Exhibit 3-31 Vitrinite thermal maturity range with corresponding depth interval and geochemical event (after Pawlewicz et al., 2005)..... 64
Exhibit 3-32 Map of the Val Verde subbasin specifies the direction of increase in $CO_2/^3He$ ratios toward the Marathon fold-thrust belt (black arrows). CO_2 gas emplacement precedes CH_4 generation (Ballentine et al., 2001) (Contours (4, 30, 50, and 75 percent) added by Enegis, LLC)..... 65
Exhibit 3-33 Structural framework map of the Val Verde subbasin and Marathon-Ouachita fold-thrust belt, west Texas (structural details created with info from Shumaker, 1992; Barden and Franklin, 2003; and Enegis, LLC). The envisioned CO_2 plume is localized within the

Marathon allochthon; contoured CO_2 isograds given in percent contained gas and is the source of CO_2 charge for Leads 1-5 (blue stippled areas). Reservoirs are multiply brecciated Caballos Novaculaite (Units 1-3), which are tightly folded along with associated strata 66
Exhibit 3-34 Structural framework map of the Val Verde subbasin and Marathon-Ouachita fold-thrust belt, west Texas (structural details created with info from Shumaker, 1992; Barden and Franklin, 2003; and Enegis, LLC). The envisioned CO_2 plume is localized along the Permian basin detachment with traps localized within the Marathon subthrust facies (principally Ellenburger Dolomite). Contoured CO_2 isograds given in percent contained gas and represents the CO_2 source plume which charged Leads 1-8 (blue stippled area)..... 67
Exhibit 3-35 Map summarizes the Mesozoic and Cenozoic distribution of kimberlite, carbonatite and lamproite intrusive complexes recognized on the North American plate (adapted from McCandless, 1999; used with permission) 70
Exhibit 3-36 Radiometric age data, Great Plains Alkalic Province, Montana*..... 71
Exhibit 3-37 Paleo-tectonic and -geographic map of the western U.S. circa 50 Ma. Base map personal communication (Heidrick, 2013) 72
Exhibit 3-38 Schematic block diagram looks WNW across the American Northwest at the envisioned subduction regime at circa 50 Ma (adapted from Breitsprecher et al., 2003) 74
Exhibit 3-39 Succession of stylized, E-W-oriented, cross-sections across the American Northwest (adapted from Humphreys, 2009; used with permission) 75
Exhibit 3-40 Geologic sketch map of the Sweetgrass arch and Kevin-Sunburst anticline, North-Central Montana. Top Madison Limestone is contoured with a 1,000 ft interval (map modified after Shepard and Bartlow, 1986; limits of the Great Falls lineament after Mueller and Frost, 2006; used with permission) 77
Exhibit 3-41 Geologic map of the Kevin-Sunburst anticline, north-central Montana (adapted for the Montana Geological Society, 1985; used with permission)..... 78
Exhibit 3-42 A, Typical well log curves for principal stratigraphic units, Kevin-Sunburst field; and B, oblique, NW-SE-oriented, generalized cross-section across the Kevin-Sunburst anticline (data adapted from the Montana Geological Society, 1985; used with permission) 79
Exhibit 3-43 Structural contour map at top Mississippian Madison Limestone (100 ft contour interval) (adapted from the Montana Geological Society, 1985; used with permission) 80
Exhibit 3-44 Well log correlation and quantification of reservoir properties, Kevin-Sunburst anticline, Montana (adapted from Spangler, 2011; used with permission) 82
Exhibit 3-45 Regional tectonic sketch map of north-central Montana showing the location of three conventional leads (1, 2, and 4) and one unconventional stratigraphic trap (lead 3). Top Madison Limestone is contoured with 1,000 ft interval (adapted from Shepard and Bartow, 1986; used with permission) 83
Exhibit 3-46 Structural contour map top Duperow Formation shows location of wells penetrating Duperow reservoirs (300 ft contour interval) (adapted from Bowen, 2009; used with permission)..... 84
Exhibit 3-47 Structural contour map top Duperow Formation shows location of highest porous/permeable Units 1 and 2, Duperow Formation) (adapted from Bowen, 2009; used with permission)..... 85
Exhibit 3-48 Mid-Tertiary CO_2 fairway 86

Exhibit 3-49 Map depicting basins and uplifts in New Mexico, locations of fields with known CO_2 production, and the N-S-trending Carboniferous Pedernal uplift (adapted from Broadhead, et al., 2009; used with permission) 88
Exhibit 3-50 Regional tectonic framework map of SE New Mexico highlights the extent of the Pedernal uplift (dark grey) and principal Mid-Tertiary intrusions comprising the Lincoln County intrusive belt (modified from Kelley, 1971; and Yuras, 1991; used with permission) 89
Exhibit 3-51 A, presents a diagrammatic E-W cross-section through the Sierra Blanca intrusive complex and basin. Mescalero thrust added by Enegis, LLC (this study). B, typical gamma ray and resistivity logs, Bravo Dome field. (Exhibit A modified from Kelley and Thompson, 1964; Exhibit B adapted from Broadhead et al., 2009; used with permission) . 91
Exhibit 3-52 Sketch map of the Mid-Tertiary Trans-Pecos magmatic province, west Texas. The boundary between the alkalic (A) and calc-alkalic (CA) was extended to connect with the Lincoln County intrusive belt and (adapted from Barker, 1987; and Price et al., 1987; used with permission)..... 93
Exhibit 3-53 A, Subdivision of volcano-plutonic complexes at the Lincoln County porphyry belt (LCPB). Map outlines major mining districts (numbered, grey areas) and principal Mid-Tertiary intrusions comprising the LCPB; and B, histogram summarizes ages of igneous rocks from the LCPB area (adapted from McLemore and Zimmerer, 2009; used with permission)..... 95
Exhibit 3-54 Summary of intrusive-volcanic events and corresponding radiometric ages, Lincoln County magmatic belt, New Mexico (sources: McLemore, 2010; Allen and Foord, 1991; and references therein) 96
Exhibit 3-55 Map of New Mexico summarizes the regional distribution of radiometric ages of Mid-Tertiary (Oligocene, 33.7-23.8 Ma) rocks (adapted from Chapin et al., 2004; used with permission)..... 98
Exhibit 3-56 Map summarizes the distribution of the sixty-mile wide Great Plains margin belt of gold-silver deposits and consanguineous Tertiary intrusions of New Mexico (adapted from McLemore and North, 1987) 100
Exhibit 3-57 A, Stylized geologic cross-section depicts the blind syenite-carbonatite parental pluton and surficial intrusions and REE-Th-U alteration-mineralization (adapted from Staatz, 1992); B, envisioned petrogenetic relationship of parental alkalic intrusion, peripheral fenitized contact zone and late stage differentiated carbonatite (adapted from Schreiner, 1993; and Williams-Jones et al., 2000; with info from Richards, 1995)..... 102
Exhibit 3-58 Map summarizes the CO_2 content of gases from Upper Permian reservoirs, SE New Mexico. Content of contained subsurface CO_2 is contoured at 1, 5, and 10% (map and contoured CO_2 generalized from Broadhead et al., 2009; used with permission)..... 103
Exhibit 3-59 Structural contour map top Permian showing Mid-Tertiary intrusions, faults, folds and principal mining districts, LCPB. Contour interval is thousands of ft above sea level (modified from Kelley and Thompson, 1964; used with permission)..... 105
Exhibit 3-60 Structural contour map top Permian of the central portion of the LCPB showing undiscovered CO_2 conventional anticlinal Leads 1-4 and unconventional stratigraphic Lead 5 (modified from Kelley and Thompson, 1964; used with permission)..... 106
Exhibit 3-61 Structural contour map top Permian of the central portion of the LCPB showing location of unconventional Lead 6 associated with the Sierra Blanca intrusive center and basin flank (adapted from Kelley and Thompson, 1964; used with permission) 108

Exhibit 3-62 Tertiary structural framework map of North Park Basin, Colorado and adjoining Wyoming (modified from the compilations by Blackstone, 1977; Tweto, 1979). McCallum subsurface CO_2 gas fields are stippled 111
Exhibit 3-63 Tectonomagmatic evolution of North and Middle Park Basins, Colorado..... 112
Exhibit 3-64 Composite stratigraphic section and lithologic descriptions of Mesozoic and Cenozoic sedimentary rocks measured in the Northgate District, North Park Basin (based on Steven, l960) 113
Exhibit 3-65 Composite stratigraphic columns summarize formation and member nomenclature for the South, Middle, and North Park Basins, NW Colorado and SE Wyoming (from Wandrey and Barker, 1991) 114
Exhibit 3-66 Generalized Tertiary structural framework map of the Colorado Headwaters Basin (CHB), Middle and North Park Basins, north-central Colorado (compiled from Wellborn, 1977; Tweto, 1979; recent additions from Cole et al., 2010) 115
Exhibit 3-67 Modified structural framework map of Middle and North Park Basins, Colorado highlights Mid-Tertiary intrusive rocks (red boxes, which contain radiometric ages in Ma), Rabbit Ears intrusive plugs (black triangles), and principal structural compartments (modified after Cole et al., 2010; used with permission)..... 116
Exhibit 3-68 Structure contour map top Dakota Sandstone, Middle and North Park Basins, Colorado, and the McCallum anticline (500 ft contour interval). A-A' is the location of the cross-section across the North Park Basin (adapted from Wellborn, 1977) 118
Exhibit 3-69 Schematic ENE-WSW oriented cross-section (A-A' in Exhibit 3-67) constructed from Sheep Mountain, across North Park Basin and through the McCallum anticline..... 119
Exhibit 3-70 Detailed geologic map of the Braddock Peak intrusive and volcanic complex, Northern Never Summer Mountains, North Park, Colorado (modified after Cole and Braddock, 2009)..... 121
Exhibit 3-71 Structural framework map of North and Middle Park Basins, Colorado (adapted after Wellborn, 1977). Fourteen km of total shortening assumed and conserved along the Williams Range-Never Summer thrust belt (Erslev and Holdaway, 1999, and Erslev et al., 1999). 122
Exhibit 3-72 Map of the Colorado Plateau locates the San Juan Basin and highlights several, large Late Tertiary volcanic fields peripheral to this huge regional structural block (adapted from Gilfillan et al., 2008 and 2009) 125
Exhibit 3-73 Regional structural framework map of New Mexico shows mapped subsurface (black) and surface faults (blue); major Tertiary intrusive centers and dikes (red); and major reverse faults (orange) (adapted from Broadhead et al., 2009; used with permission) 126
Exhibit 3-74 Regional structural framework map of the Four Corners portraying dominate lineament orientations 128
Exhibit 3-75 Regional sketch map outlining principal positive structural blocks surrounding the San Juan Basin (yellow, stippled area). Syndepositional elements that were active and positive during the deposition of Leadville Limestone include the Zuni-Chaco slope, Paradox-Uncompahgre and Archuleta Arch-Nacimiento-uplift. The Four Corners platform block was inverted and uplifted during the Laramide orogeny (modified after Huffman and Condon, 1993)..... 130
Exhibit 3-76 E-W oriented cross-section across the San Juan Basin depicts the lower Paleozoic strata pinching out eastward against the syntectonic Archuleta, Nacimiento and Zuni-Chaco uplifts and highlands (adapted from Peterson, 1965) 131

Exhibit 3-77 Carboniferous-Permian correlation columns for the San Juan Basin, New Mexico (adapted from Huffman and Condon, 1993) 132
Exhibit 3-78 Isopach map of the Mississippian Leadville limestone, San Juan embayment, New Mexico shows the distribution of strata contoured at a 50 ft interval (adapted from Armstrong and Mamet, 1977; used with permission) 134
Exhibit 3-79 Location map of the Navajo Volcanic Field, Colorado Plateau, shows over 80 Tertiary age (28-19 Ma) volcanoes, dikes, sills and breccia pipes. Numerous petrochemically favorable intrusions are localized along the MHM-thrust belt placing them within the limits of the San Juan basin (adapted after Smith and Levy, 1976; and McGetchin et al., 1977; used with permission) 135
Exhibit 3-80 Map of CO_2 content in gases from Mississippian reservoirs in the San Juan Basin, New Mexico shows the progressive basinward increase in contained CO_2 and He gases (0.1 to 95.3% CO_2) (adapted from Broadhead et al., 2009; used with permission) 137
Exhibit 3-81 San Juan Basin-centered lead map locates the primary Leadville Limestone CO_2 objective (shown in blue) 138
Exhibit 4-1 Estimates of gas-initially-in-place and technically recoverable resources for undiscovered leads for CO_2 in the United States, and key input variables for the volumetric calculations 142
Exhibit A1-1 Risked GIIP estimates from CREAM 155
Exhibit A1-2 Risked accessible TRR estimates from CREAM 155

Acronyms and Abbreviations

AAP	Arkansas Alkalic Province
AAPG	American Association of Petroleum Geologists
Ag	Silver
AGS	Arkansas Geological Survey
Al	Aluminum
Ar	Argon
Au	Gold
Ba	Barium
BA	Billion years ago
Bcf	Billion cubic feet
C	Carbon
CA	Calc-alkalic
Ca	Calcium
CH_4	Methane
CHB	Colorado Headwaters Basin
Cl	Chlorine
CO_2	Carbon dioxide
Cu	Copper
DB-CP	Delaney Buttes-Cameron Pass
DOE	Department of Energy
E&P	Exploration and production
ENE	East-northeast
EOR	Enhanced oil recovery
ERR	Economically recoverable resources
ESE	East-southeast
ESPA	Energy Sector Planning and Analysis
F	Farallon
F	Flourine
Fe	Iron
FMI	Formation MicroImager
ft	Feet
FT	Fission track
Ga	Billion years ago
GIIP	Gas-initially-in-place
Gpa	Gigapascal
H_2O	Water
H_2S	Hydrogen sulfide
He	Helium
^3He	Helium 3 isotope
Hf	Hafnium
HFSE	High field strength elements
in	Inch
JE-M	Early-Middle Jurassic
K	Potassium or Cretaceous
K_2O	Potassium oxide
KAMA	Kansas, Arkansas, and Mississippi alkalic kimberlite-carbonatite
Kr	Krypton
LCPB	Lincoln County porphyry belt
LILE	Large-ion lithophile elements
LREE	Light rare-earth elements
M, m	Meter
Ma	Million years ago
MAP	Montana alkalic province
Mcfd	Thousand cubic feet per day
mD	Millidarcy
Mg	Magnesium
mi	Mile (s)
MMmt	Million metric tons
Mo	Molybedenum
MSL	Mean sea level
N_2	Nitrogen
N	North
NA	North American
Na	Sodium
Na_2O	Sodium oxide
Nb	Niobium
Nd	Neodymium
Ne	Neon
NE	Northeast
NETL	National Energy Technology Laboratory
NMBMMR	New Mexico Bureau of Mines and Mineral Resources
NNE	North-northeast
NNW	North-northwest
NW	Northwest
O_2	Oxygen
Os	Osmium
P	Phosphorus or Permian
ℙ	Pennsylvanian
Pd	Palladium
Pb	Lead
P/P	Porosity and permeability
Psi	Pounds per square inch
Pt	Platinum
Ra	Antitheic shears
Rb	Rubidium
Rcf	Reservoir cubic foot
Re	Rhenium
REE	Rare earth elements
RMAP	Rocky Mountain alkalic province
Ro	Vitrinite reflectance
Rs	Synthetic shears
Rscf	Reservoir standard cubic feet
S	South
scf	Standard cubic feet
Se	Selenium
SE	Southeast
SiO_2	Silica, (quartz)
SS	Sandstone
SSE	South-southeast
SSW	South-southwest
Sr	Strontium
Sri	Sr isotopic (initial)
SW	Southwest
T	Temperature

Ta	Tantalum
Tcf	Trillion cubic feet
TD	Total depth
Te	Tellurium
Th	Thorium
Ti	Titanium
TiO_2	Titanium oxide
TRR	Technically recoverable resources
TSR	Thermochemical sulfate reduction
U	Uranium
U.S.	United States
USGS	U.S. Geological Survey
W	Tungsten
WNW	West-northwest
WSW	West-southwest
Xe	Xenon
Y	Ytrium
yr	Year
Zr	Zirconium
°C	Celsius
°F	Fahrenheit

This page intentionally left blank.

Executive Summary

This document is a study of the genesis and tectonic setting of subsurface CO_2 systems in the United States. Its purpose is to better understand the potential for new discoveries of geologic accumulations and their implications for supply of CO_2 for enhanced oil recovery in the longer term. A companion NETL document, Volume 1, contains compiled information on discovered CO_2 reservoirs in the United States and presents volumetric calculations to estimate gas-initially-in-place (GIIP), technically recoverable resources (TRR), and economically recoverable resources (ERR).

A central observation is that most of the CO_2 accumulations are magmatic in origin, that is, the CO_2 was initially dissolved in intruding upwellings of magma as opposed to thermochemical degradation of hydrocarbon accumulations or other origination scenarios. This observation is based on the relatively high ratio of helium-3 isotope (^3He) to helium-4 isotope (^4He) found in reservoir gases, the ratio of other noble gas isotopes, and other geologic indications. Magmatic CO_2 systems begin with a point source or chimney where molten mantle rock rises through the Earth's crust and conveys dissolved CO_2 with it. Pressure and the force of buoyancy cause the CO_2 to migrate from its source along pathways and, where viable sealed traps with porous reservoir rock exist, deposits of CO_2 can occur.

Exhibit ES-1 shows that CO_2 deposits in the United States are found along discrete linear belts or fairways. Geologic evidence indicates that the associated magmatic intrusions and CO_2 emplacements occurred within narrow geologic episodes. Generally CO_2 sources tend to become younger as one goes from east to west. Jackson Dome, Valverde, and Kevin Dome can be associated with the Laramide orogeny (80-34 million years ago (Ma)). Sheep Mountain and Bravo Dome were emplaced during the Mid-Tertiary (38-22 Ma). McElmo, Jackson Dome, St. Johns and Doe Canyon are the youngest grouping of accumulations, emplaced during the Late Tertiary/Quaternary (12 Ma - current). There is some evidence that Bravo Dome is still filling.

Exhibit ES-1 Subsurface Sources of CO_2 in the Lower 48 United States: Discovered Reservoirs and Leads for Undiscovered Reservoirs

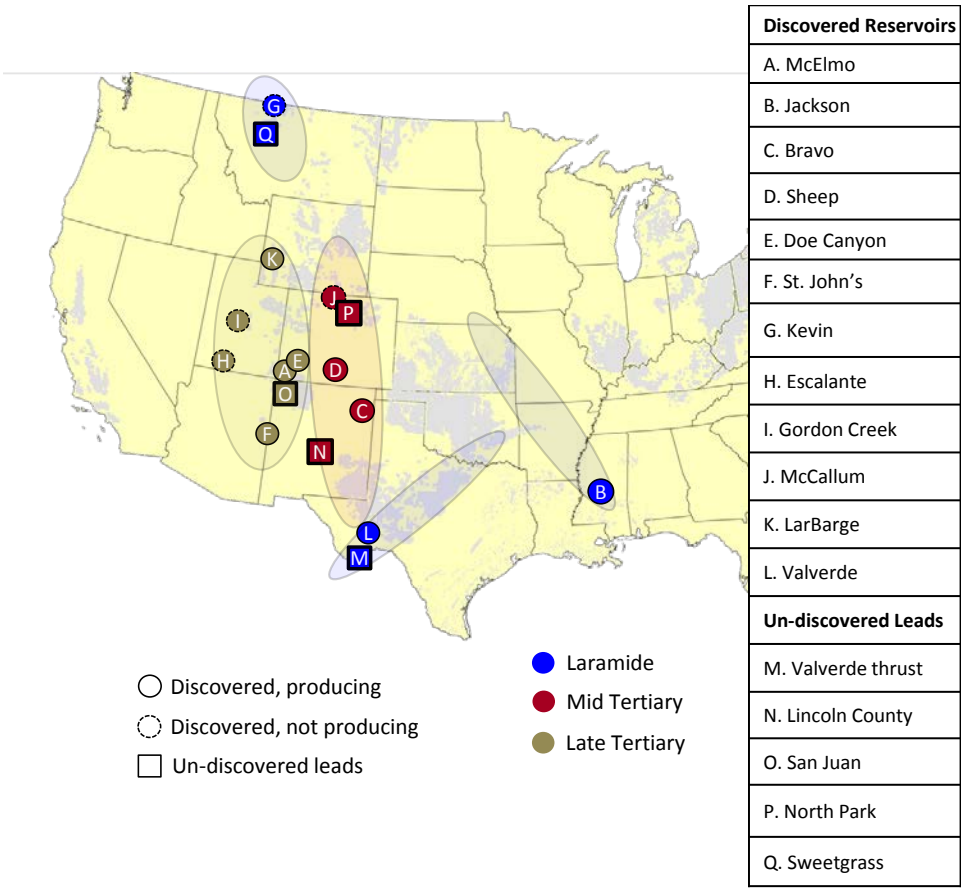

Discovered Reservoirs
A. McElmo
B. Jackson
C. Bravo
D. Sheep
E. Doe Canyon
F. St. John's
G. Kevin
H. Escalante
I. Gordon Creek
J. McCallum
K. LarBarge
L. Valverde
Un-discovered Leads
M. Valverde thrust
N. Lincoln County
O. San Juan
P. North Park
Q. Sweetgrass

The work was framed around an exploration for leads where undiscovered CO_2 reservoirs may occur. Known CO_2 reservoirs were used as a starting point for exploration. The five areas that screened as prospective to CO_2 are proximate to known CO_2 deposits and are expected to have resulted from the related magmatic events that formed the known sources.

- The San Juan lead in New Mexico is the largest in area, and unlike other leads, is an unconventional resource. The strata of interest in the San Juan basin are 13,500 feet below the surface, 4,000-6,000 feet deeper than current hydrocarbon production wells. Data from a small number of penetrations at this depth reveal produced gas containing 90 percent CO_2.
- Mapping of composition data from several natural gas production wells in the Val Verde region in the Permian Basin shows CO_2 concentrations trending higher for wells that are further south toward the Marathon Thrust zone. These data point to a magmatic chimney to the south. Two plays are identified, in the hanging wall and footwall (12,000 and 15,000 feet) of the Marathon thrust.

- The Sweetgrass Arch leads in Montana are in the same CO_2 system as Kevin Dome. The leads are areas where there are indications of traps along the apparent migration pathways.
- Lincoln County, New Mexico, is the most speculative of the leads. Well data with the elevated CO_2 concentrations and the presence of magmatic dikes provide evidence for emplacement of CO_2.
- The North Park area of Colorado contains two leads, indicated by the producing McCallum field, which is a trap in the hanging wall of the Never Summer thrust. One lead is an associated foot-wall trap. A second lead, located to the south, is co-tectonically associated with the McCallum backthrust.

Enough information was available to support estimates of GIIP and TRR for the undiscovered leads. Exhibit ES-2 presents key inputs for the volumetric calculation of risked GIIP and also the degradations for access and recoverability used to estimate TRR. Twenty-six leads in five geographic areas are estimated to contain 63 Tcf of risked CO_2 initially in place and 42 Tcf of risked technically recoverable CO_2 resource (TRR). Thirty-four Tcf of the risked TRR is contained in two areas: the San Juan basin in northwest New Mexico and the Val Verde basin in southwest Texas, both of which are near pipeline infrastructure that feeds the Permian Basin, a center of CO_2 use for enhanced oil recovery (EOR). From the Volume 1 Report on discovered CO_2 reservoirs, the aggregate TRR of fields feeding the Permian Basin is 43 TCF. Cummualtive production is 13 TCF leaving 30 TCF of remaining TRR. Therefor the undiscovered fields at San Juan and Val Verde have the potential to double the subsurface CO_2 TRR available in the Permian Basin region.

The aggregate estimates of GIIP and TRR should not be considered comprehensive within the lower 48 states. The number of areas examined was limited by the project budget and particular areas for study were selected where there was available data to support an analysis. At the same time, the results indicate that there are likely undiscovered CO_2 reservoirs in the United States of a magnitude that could contribute materially to CO_2 supply for EOR.

Exhibit ES-2 Estimates of gas-initially-in-place and technically recoverable resources for undiscovered leads for CO_2 in the United States, and key input variables for the volumetric calculations

Area	State	# leads	Area (all leads), M ac.	Pay, ft	Porosity %	Depth, Mft	Formation Volume Factor rcf/000cf	CO_2 %	Risk Factor	GIIP, Tcf	Access %	Recovery %	TRR, Tcf
San Juan (Leadville)	NM	1	1000	75	12	14	2.8	90	33	33.7	95	70	22.4
Val Verde (Marathon Sub thrust)	TX	8	96	650	5	15	2.5	74	31	10.2	95	70	6.8
Val Verde (Marathon thrust)	TX	5	49	225	16	12	2.3	77	33	6.9	95	70	4.6
Sweet Grass	MT	4	410	117	9	3.5	5.2	90	31	8.0	95	75	5.7
Lincoln County	NM	6	252	120	15	1.7	12.6	97	23	2.5	82	65	1.3
North Park	CO	2	36	95	18	5.5	2.9	95	27	1.9	51	70	0.7
Total		**26**	**1,844**							**63.2**			**41.5**

Conversion Factor: 52.9 $MMmtCO_2$/Tcf

Values for pay, porosity, depth, formation volume factor, CO_2 concentration, risk factor, access, and recovery are the weighted average (based on area) of the values for the leads within an area

A large amount of disparate data was assembled and analyzed to create the tectonic narratives that support the identification of the undiscovered leads. One of the challenges in CO_2 exploration and production (E&P) is that, unlike crude oil and coal, carbon dioxide molecules cannot be analyzed to develop a temperature and pressure history for an accumulation. Other evidences, which are less definitive, must be brought to bear. For example, Exhibit ES-3 illustrates one of the methods used to identify prospective areas. Areas of crustal weakness are likely places for magmatic intrusions and our study indicates that CO_2 reservoirs can occur in places where tectonic activity has created migratory fault pathways and anticlinal structural traps. Anticlines (sometimes called "arches") are linear features where strata of rock fold upward like a carpet pushed inward from two opposite sides. A fault can break the arch, offsetting it. The left pane of Exhibit ES-3 shows the Lincoln county structure as it is today, with the anticline shift at the tip of the green arrow. The right pane shows an imagination of the shift axis and how the area was before the shift. The shift is evidence of crustal weakness and an area that is prospective for magmatic CO_2 sourcing.

The study also shows that imbricate thrusts act as very effective, laterally contiguous, horizontal migration pathways for migrant supercritical CO_2 charge. This seems to be the case in the Val Verde basin/Marathon thrust belt; Lincoln County-Sierra Blanco basin/Mescalero thrust (Exhibit 3-51A); San Juan/Hogback thrust; Kevin dome/underlying Sweetgrass thrust; and McCallum/Never Summer thrust and backthrust.

Exhibit ES-3 Structural contour map top Permian in the Lincoln County porphyry belt. Shows Mid-Tertiary intrusions, faults, folds and principal mining districts (modified from Kelley and Thompson, 1964; used with permission)

Today

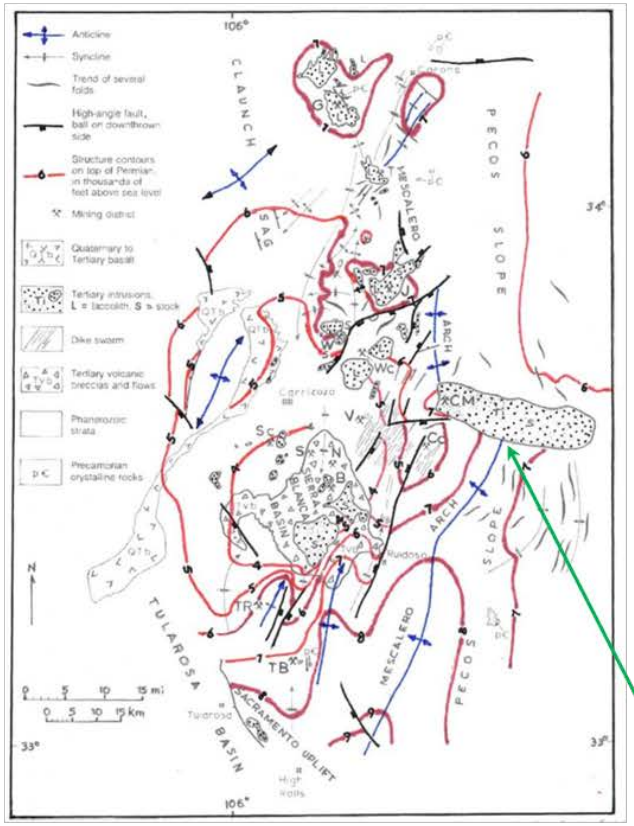

Before the Anticline Shift

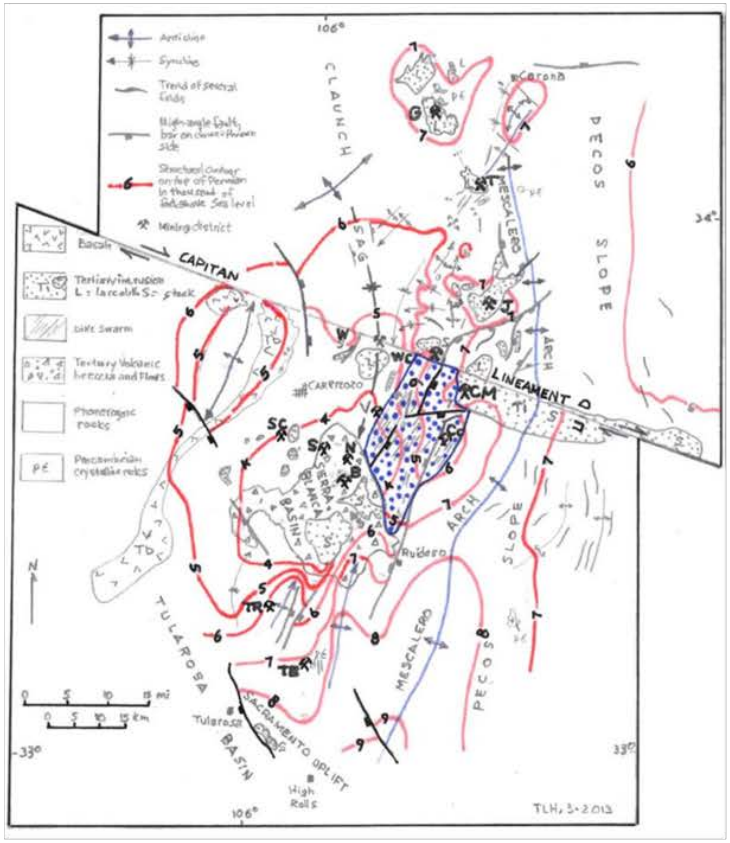

Area where a fault has evidently broken the arch (anticline) and shifted the northern part to the west, indicating crustal weakness and the potential for magmatic upswelling, CO_2 deposits.

1 Introduction

As discussed in *Volume I: Discovered Subsurface Sources of CO_2 in the Contiguous United States*, uncertainty surrounding the need for carbon dioxide (CO_2) for enhanced oil recovery (EOR) from advanced fossil-fuel platforms exists due to the lack of a comprehensive United States (U.S.)-based resource estimate of CO_2 available from subsurface sources. At the same time, the exploration for subsurface CO_2 deposits is not well developed, as discovered CO_2 deposits have generally been the by-product of oil and gas exploration. The expansion of existing CO_2 reserves and estimates and the identification of new major geologic plays of naturally occurring CO_2 could significantly impact the need for CO_2 from advanced fossil-fuel platforms beyond the 2030 timeframe. Given this set of circumstances, Energy Sector Planning and Analysis (ESPA) for the National Energy Technology Laboratory (NETL) requested assistance by Enegis, LLC, to conduct a screening study to characterize the subsurface sources of CO_2 as an initial step in assessing the impacts to the national energy strategy.

This report serves to provide a quantitative estimate of selected undiscovered geologic resources of CO_2 in the lower 48 U.S., where it provides an indicative (as opposed to comprehensive) examination of the country. Section 2 of the report presents an overview and methodology utilized for the undiscovered resource assessment. Section 3 presents play fairways and discusses individual leads, where a lead is defined as a set of conditions indicative for CO_2 deposit. Section 4 presents estimates of GIIP and TRR for the five undiscovered lead areas. Section 5 summarizes observations and insights gained from the analysis.

2 Overview and Methodology

CO_2 fairways are categorized according to the following orogenies:

- Early Cretaceous (125-85 Ma in the Mid-continent) and Laramide orogeny associations (80-34 million years ago [Ma])
- Mid-Tertiary and Early Miocene Uplift, Decompression, Extension, and Exhumation (34-20 Ma)
- Mid-Late Tertiary Uplift, Decompression, Extension, and Exhumation (20-5 Ma)

2.1 Subsurface CO_2 Systems

Although there are similarities to petroleum exploration, exploration for CO_2 is different in many ways. Geologic accumulations of CO_2, as with accumulations of other natural crustal gases, exist in discrete areas with conditions that are conducive to focusing, trapping, and storing migrant gas. These conditions are collectively referred to as a carbon system, which comprises a CO_2 source, a migration pathway, trap, and seal.

2.1.1 CO_2 Sourcing

Areas of ultramafic, mafic alkalic or felsic alkalic magmatic activity provide the most fertile sources for CO_2. Many such areas of favorable magmatism exist in the western United States, which provide a prime setting for CO_2 sourcing.

2.1.2 CO_2 Migration

As CO_2 is released from magma it is optimally focused along deep-penetrating crustal structures. CO_2 often migrates up shear zones and then laterally outward; or laterally along sub-horizontal frontal thrusts and secondarily upwards along sub-vertical fracture zones. Areas conducive to the focus and transmission of migrant CO_2 occur at fault bend geometries which promote extension, dilation and breccia development (e.g., pull-aparts). Large, through-going fractures, which cross to form broad “Xs” within the crust—whether horizontal or vertical—constitute particularly favorable pathways. Local, secondary migration is typically limited to distances of tens of miles outward from the primary depth-penetrating structures.

2.1.3 CO_2 Trap

Optimal traps are large, double-plunging foreland anticlines or domes located within 50 to 75 miles of frontal fold-thrust belts. Other traps include four-way closed, double-plunging anticlines of Carboniferous—Pennsylvanian-Permian (ℙ-P) or Laramide age which are typically smaller, structurally complex or involve composite traps.

2.1.4 CO_2 Reservoir and Seal

Reservoirs have characteristics identical to optimal methane reservoirs, with one principal exception—CO_2 becomes supercritical with modest pressure. Therefore, reservoirs deeper than about 2300 ft can hold significantly more resource than shallower reservoirs. The pressure at which CO_2 becomes supercritical is affected by geothermal gradient and mixture with other gases.

A topseal is needed to stop the upward migration of CO_2. An ideal seal is ductile and thick, such as shale, salt, anhydrite, and argillaceous limestone. Igneous sills or other fine-grained and/or cemented sediments can also provide sufficient seal.

2.1.5 CO_2 Origins

Exploration for CO_2 requires an understanding of the origin of the CO_2. There are several fundamentally different CO_2 gas formation processes. The two most important can be classified as (a) magmatic (or mantle) origin, and (b) thermal alteration of carbonates with magmatic sources dominant.

Magmatic Source

CO_2 and water (H_2O) are two of the dominant gases in magmas, but all magmas do not provide the same proportions or conditions to allow formation of large CO_2 deposits. Calc-alkalic magmas, related to island arcs and subduction zones, have high concentrations of H_2O and proportionally lower concentrations of CO_2; however, because the volumes of magma can be large, the total volume of CO_2 can be large. Nevertheless, trapping of CO_2 is a problem in arc settings because of the explosive eruption styles. Very different from calc-alkalic settings are intraplate settings where ultramafic or mafic-alkalic and felsic-alkalic magmas form. These magmas have high CO_2 content (percent) and are localized in relatively small subvertical plutons, plugs, diatremes, or breccias pipes spatially associated with co-tectonic domes and laccolithic complexes. The resultant geometries are optimal for the entrapment of focused CO_2 deposits.

Ultramafic, Mafic Alkalic, and Felsic Alkalic Sources

Ultramafic, mafic alkalic and felsic alkalic magmas carry the most CO_2 and are responsible for the majority of giant CO_2 accumulations. These are primitive magmas formed by small degrees of partial melting deep in the mantle. The magma that bears most CO_2 is alkalic and ultramafic or mafic, ranging from basanite to alkali basalt. The highest CO_2 is expected with the most basic (lowest SiO_2) and highest alkali (Na_2O+K_2O) magmas. High pressures (>3 Gigapascals (GPa), ~50-70 miles) are needed to form these magmas. CO_2 can be carried within these magmas and out-gassed at various stages of magma migration, or stream as a CO_2-rich fluid directly from the mantle.

These magmas are typically formed in “intraplate” settings, i.e., well inboard from subduction zones, within the non-subducting plate. These settings can be intraplate rifts with deep mantle sources, or related to changes in subduction patterns, such as slab rollback, where, typically because of slowing convergence, a subducting plate progressively steepens and attempts to rollback towards the subducting zone. This, in turn, causes up-welling of hot asthenosphere on the inboard side of the plate. Such an occurrence during the late Laramide is the mechanism of formation of the primitive, ultramafic, mafic alkalic, and felsic alkalic rocks occurring along the entire length of the Farallon subduction trend – from Colorado (U.S) to the East Mexican alkalic province.

Subduction Zone—Calc-Alkalic Arc Source

Magmatic gases, including H_2O and CO_2 are released with dissolution and outgassing on magma ascent and crystallization. In viscous magmas, such as calc-alkalic magmas, release of volatiles is a major cause for explosive eruptions, such as seen in volcanoes like Vesuvius. Although a

large volume of CO_2 can vent from calc-alkalic explosive volcanism, this mode of emplacement and differentiation does not promote concentrations of CO_2 or trapping of gases.

Venting not only occurs during eruptions, but can also occur more passively. Passive venting is seen above the subduction zone in Italy, where it is so strong in places it kills trees because their root zone becomes anoxic. Small animals and wild boars (with noses near the ground) die crossing these barren zones (Rogie et al., 2000; Kerrick, 2012). Whether the CO_2 is purely magmatic or generated by other mechanisms is not clear. A large fraction of the CO_2 generated from a subducting slab may be generated in the fore-arc. CO_2 generation in the arc region could result from the high heatflow and temperatures there (e.g., CO_2 generation by hydrothermal reactions at temperatures [T] >~300° Celsius [°C] as in basins such as the Salton Sea). The generation can be associated with the margins of specific intrusions, or generally distributed and related to high heat flow.

Thermal Alteration of Carbonates

CO_2 can be generated from silicate-carbonate mineral reactions in clastic sediments at temperatures above ~300°C. This origin is observed in hydrothermal systems and in deep rooted sedimentary basins (Cathles and Schoell, 2007). This is the prevalent origin of CO_2 in Southeast Asia (Malay Basin, Natuna Basin, and Gulf of Thailand). It is important to note that the carbonate-silicate reactions in clastic sediments are fundamentally different from thermal alteration of solid carbonates through contact metamorphism.

Sedimentary Basin Metamorphism

In the broadest terms, CO_2 is produced from carbonates in aqueous hydrothermal reactions at temperatures of ~300°C and in higher temperature (400-800°C depending on water availability [Kerrick and Connolly, 2001]). This can happen in sedimentary basins where burial is sufficient, or in situations where hydrothermal waters provide the heating as well as transport components for the reactions.

Sedimentary basins generate CO_2 when strata containing carbonate are deeply buried and heated to >~320°C. At these temperatures the partial pressure of CO_2 and steam are sufficient to form a separate vapor phase, which migrates upward, filling reservoirs with up to 100 percent CO_2 gas (Cathles and Schoell, 2007). In a basin setting, reaching such temperatures requires either deep burial (>~4 miles) or high heat flow. Cathles and Schoell (2007) showed how CO_2 could be generated from sediments in deep hot basins such as those in the South China Sea.

The first requirement for CO_2 generation is that a portion of the sediments needs to be heated to temperatures greater than 320°C. When this occurs, the partial pressures of CO_2 and H_2O (steam) exceed the pressures in the pore water, and a CO_2-steam gas phase separates from the pore waters. This gas phase can then migrate laterally and vertically.

The second requirement for filling a CO_2 reservoir is that silicate minerals containing carbonate-forming cations, such as calcium (Ca), iron (Fe), and magnesium (Mg), be titrated from the rock. The CO_2 in the gas dissolves in pore water as the gas migrates vertically and the dissolved CO_2 forms an acid which reacts quickly with the host sediments. If the host sediments contain aluminosilicates of Ca, Fe, or Mg these silicates will be dissolved and carbonates of these cations (calcite, siderite, magnesite, and dolomite) will form. Until these aluminosilicates are fully removed (titrated), the CO_2 pipe will not progress. This titration slows the advance of the CO_2 plume. But what is important to note is that, to supply the pipe with enough CO_2 to allow it to

reach a reservoir and fill it, a substantial volume of basin sediments must reach threshold temperatures (greater than 320°C).

CO_2 can be generated in a hydrothermal system such as the Salton Sea. A good example of such a system is the 1 x 3 miles Imperial CO_2 field, from which over one-half billion cubic feet (Bcf) of CO_2 was produced between 1934 and 1954 to make dry ice. It lies adjacent to the Salton Sea geothermal system. CO_2 and water vapor separated from hydrothermal waters when they circulated to depths shallow enough to allow phase separation (boiling). The water condensed and the CO_2 was trapped in sandstone reservoirs at 500 to 700 ft depth (Muffler and White, 1968).

Contact Metamorphism

Lastly, contact metamorphism by magmatic heating of carbonates is a potential source of CO_2 (Shieh and Taylor, 1969). Isotope analyses of CO_2 in fluid inclusions in a contact metamorphic assemblage with marine carbonates revealed typical marine $\delta^{13}C$ values between -4 and +2‰ (Yang et al., 2008). However, no literature on large accumulations of CO_2 that could be directly linked to contact metamorphism was found. We do not consider this process as being significant for CO_2 exploration.

Other Chemical Processes

Two other process related to chemical breakdown are important to understand the origin of CO_2, but do not in themselves generate large CO_2 deposits. These processes are thermochemical sulfate reduction (TSR) and biodegradation of hydrocarbons.

Thermal Sulfate Reduction

Thermochemical sulfate reduction is a process in which oils react with evaporites at temperatures above 160˚C to produce hydrogen sulfide (H_2S) and CO_2.

Biodegradation of Hydrocarbons

A minor source of CO_2 is the biodegradation of oils in shallow reservoirs at low temperatures. This CO_2 is isotopically enriched in ^{13}C; however, the volumetric potential of this process is small.

Overall, areas of ultramafic, mafic alkalic, and felsic alkalic magmatic activity provide the most fertile sources for CO_2. CO_2 can also be formed through thermal alteration of carbonates and other chemical processes.

2.1.6 Tectonostratigraphic Characterization of Undiscovered CO_2 Traps

Conventional Trap Types and Classification of Play Types

The characterization of subsurface CO_2 discoveries is found in Volume I. Discovered resources are located primarily in western North America (mainly the Colorado Plateau and southern Colorado Rocky Mountains). The western fields define a bimodal distribution of field sizes. The Big Piney-La Barge (Wyoming), Bravo and St. Johns/Springerville (New Mexico), and McElmo (Colorado) fields have reservoirs, which cover an area between 300 and 1,400 mi^2. In contrast, most remaining fields have reservoirs covering about 30 mi^2 or less. The Bravo and McElmo structures are, in part, fault-controlled traps, involving solitary, thin net pay reservoirs (50-100 ft), and therefore, cover much larger areas. This group of small to intermediate size

traps characterizes the most likely untested exploration targets in the region. The likelihood of discovering another Big Piney-La Barge structure containing >100 Tcf of potential in-place CO_2 in this well-explored region is very unlikely.

Suitable reservoirs with accompanying topseals do not appear to be a problem for much of the region. Dolomitized limestone strata are vertically stacked through the Paleozoic and Mesozoic stratigraphic column along with suitable sandstone and sandy conglomerate intervals. Depending on the local tectonostratigraphic setting, topseals are common and include anhydrite, salt, sabkha breccia, shale-mudstone-siltstone and Tertiary igneous sills throughout the Paleozoic and Mesozoic stratigraphic succession. Identified CO_2 gas in the western U.S. is trapped within: (a) Late Sevier-Laramide age (80-34 Ma) anticlines of modest structural relief averaging less than 1000 ft of structural closure; however, there is 3000 ft of relief at Big Piney-La Barge. Most traps are demonstrably underlain by low-angle, west-southwest (WSW)- or east-northeast (ENE)-dipping imbricate thrusts; and (b) low-relief, combination structure-stratigraphic traps associated with the formation of the "Ancestral Colorado Rocky Mountains" are found at Bravo Dome, New Mexico. Laramide anticlinal traps are predominately of the fault-bend and propagation fold classes with hanging-wall geometry largely dictated by the geometry of the underlying thrust and amount of shortening. Thrusts are both forward- and back-breaking with upright to asymmetric cylindrical folds with steep axial surfaces (Sheep Mountain and Sweetgrass); whereas, ENE-dipping thrusts are back-breaking, out of sequence, displacement thrusts with much broader, larger and laterally more contiguous folds (Moxa arch, La Barge).

Maps that combine the known distribution of mapped thrust and known/inferred distribution of CO_2-bearing ultramafic, mafic alkalic and felsic alkalic igneous centers help the explorationist focus in on the more prospective, CO_2 prone areas. It is the realization that: (a) only specific varieties of igneous rocks are CO_2 prone and contain large quantities of dissolved/immiscible CO_2; (b) widespread K- and/or Na-metasomatism associated with mafic-alkalic intrusive centers is indicative of consanguineous carbonatite emplacement at depth; (c) the suite of ultramafic, mafic alkalic and felsic alkalic intrusions fall within two diagnostic radiometric ages (36-22 Ma and 8 Ma-Recent); (d) ancillary but modest quantities of associated ultramafic kimberlite, lamprophyre and lamproite are petrochemically linked in time and space with small but significant amounts of carbonatite intrusions (immiscible supercritical CO_2 liquid); and (e) this unique assemblage of Mid-Tertiary (36-22 Ma) and Late Miocene-Recent ultramafic, mafic alkalic, and felsic alkalic intrusions only occur in areas of pronounced, focused crustal extension and co-tectonic rifting (Rio Grande graben), differential uplift (Colorado plateau) and along the hinge margin separating the Great Plains and the Rocky Mountain foreland provinces. The appreciation of these poorly understood and documented relationships by industry, academia and government provides this team with a distinct competitive edge. This advantage not only reduces exploration risk, but allows streamlining of the work processes required to define viable, untested CO_2 fairways, trends and leads in the western U.S. in the relatively short span of time provided for this study.

Optimal traps thus are large, Laramide, double-plunging foreland anticlines or domes located within 100-80 miles of frontal fold-thrust belts. Other traps include four-way closed, double-plunging anticlines of Pennsylvanian-Permian (Ancestral Rocky Mountains) or Laramide age which are typically smaller, structurally complex or involve composite traps.

Unconventional Traps

Basin-centered gas accumulations are typically characterized by regionally pervasive accumulations that are gas saturated, abnormally pressured, commonly lack a downdip water contact, and have low-permeability reservoirs. Our cursory review of travertine occurrences in the American Southwest shows that these unusual rocks are not distributed randomly. There is a pronounced alignment of travertine domes, craters, bicarbonate-rich springs, seeps and associated travertine build-ups along the Coyote Wash back-thrust which trends northwest (NW)-southeast (SE) and dips northeast (NE) beneath the trapping anticline running between St. Johns and Springerville, Arizona. Where the Coyote Wash thrust and the Supai-San Andreas reservoir-seal succession are breached by down-cutting along the Little Colorado River and a smaller distributary stream, there is a 6-mile-long by 2-mile-wide travertine field developed along the fault's trace. A second NW-SE alignment of smaller individual travertine build-ups, domes and bubbling CO_2 vents lie along the crest of the St. Johns/Springerville anticline. The bubbling domes and vents likewise suggest the San Andreas anhydrite topseal is being compromised and CO_2 reserves are leaking out of the trap along the axis of the field. The average CO_2 flux measured in rocks along or adjoining the thrust are likewise anomalously high (Allis, et al., 2005). Their work also demonstrates that numerous CO_2-prone seepages, geysers and bubbling vents with appreciable travertine build-ups are similarly localized along the west-northwest (WNW)-striking Little Grand Wash fault and within the NW-trending Ten Mile graben.

These observations are particular important in that both of these structures belong to a regionally pervasive set of N55°W-striking folds and faults constituting the Paradox fold and fault belt of SE Utah and SW Colorado. A projection of the Grand Wash fault zone and Ten Mile graben east-southeast (ESE) extends along a pronounced fold-fault zone extending from Monticello, Utah, to Cortez, Colorado. It is not a coincidence that the ~30 Tcf in place CO_2 resource at the McElmo anticline lies along the continuation of this zone toward Cortez. The petroleum industry has detailed the protracted structural and stratigraphic evolution of the Paradox basin commencing with its development during the formation of the "Ancestral Rocky Mountains" during the Pennsylvanian-Permian (325-260 Ma). Depth-penetrating bounding faults and co-tectonic pull-aparts allowed the basin to subside and fill with more than three miles of synorogenic debris shed from the flanking Uncomphagre uplift to the NE. The resultant intra-cratonic basin extends 165 mile in a NW-SE direction and is 120 miles in width. The depth-penetrating, crustal-scale bounding faults were ideally oriented for NE-SW-directed crustal reactivation and shortening during the Laramide orogeny and subsequent Oligocene uplift of the Colorado Plateau. The CO_2 gas surveys conducted by Allis et al. (2005), clearly show that the most recent Pliocene-Pleistocene uplift of the Colorado Plateau and Southern Colorado Rocky Mountains reactivated the ancestral Pennsylvanian-Permian framework elements; which in turn, controlled the emplacement of contemporaneous primitive CO_2-prone, alkali basalt along the axis of the Paradox and subsidiary Ten Mile grabens. It is suspected that this youthful, primitive magmatism provided the charge for the McElmo anticline. Similarly, the 6.6-3.6 Ma bimodal Silver Creek basalt-alaskite intrusive complex identified 24 miles ENE of McElmo at Rico, Colorado, is likewise part of this youthful intra-plate extension and coeval mafic-alkalic intrusive event (Larson, et al., 1994).

Tectonostratigraphic Classification of CO_2 Play Types

Tectonostratigraphic play types provide a framework for classification, and are best shown by example. Exhibit 2-1 identifies several tectonostratigraphic play types from the Wind River Basin in Wyoming. Note the stacked reservoir potential in the Madden, Pavillion and Horse Butte fields. Reservoir rocks range in age from the Mississippian Madison Limestone through Eocene strata.

Exhibit 2-1 Schematic cross-section showing hydrocarbon trapping mechanism and play types, Wind River Basin, Wyoming (Willis and Groshong, 1993; used with permission)

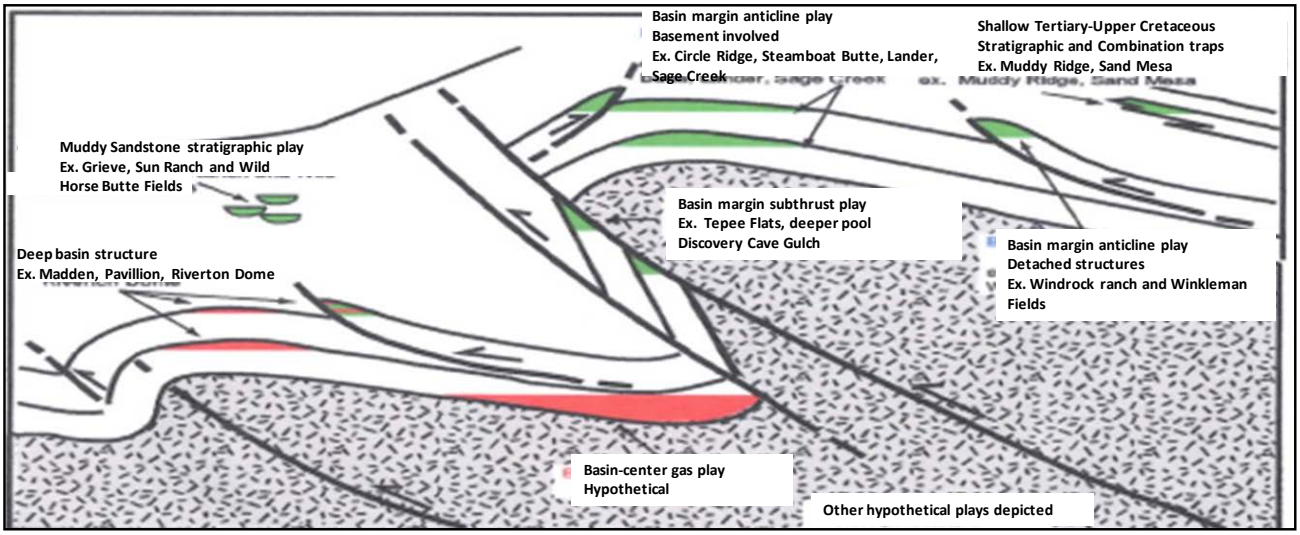

Types of structural plays include:

- Hanging-wall anticlinal traps
  - Crestal anticlines
  - Back-limb-out-of-the-syncline traps (rabbit ears)
  - Forelimb crowd structure with steep axial surfaces (rabbit ears)
- Intra-overthrust traps
  - Overturned, recumbent to intrafolial antiform
  - Multiple, imbricate repeated thrusted reservoirs
  - Intrafolial (solitary or imbricate) with subhorizontal axial surface
- Sub-thrust traps
  - Syncline-centered fracture and stratigraphy
  - Crestal anticlines
  - Back-limb-out-of-the-syncline traps (rabbit ears)
  - Forelimb crowd structure with steep axial surfaces (rabbit ears)
- Foreland basin floor (either foreland basin or subthrust)
  - Upthrusted box fold

Exhibit 2-2 shows stratigraphic traps from the San Juan Basin, where unconformities play a role in trapping natural gases.

Exhibit 2-2 Stratigraphic trap types (after Biddle and Wielchowsky, undated)

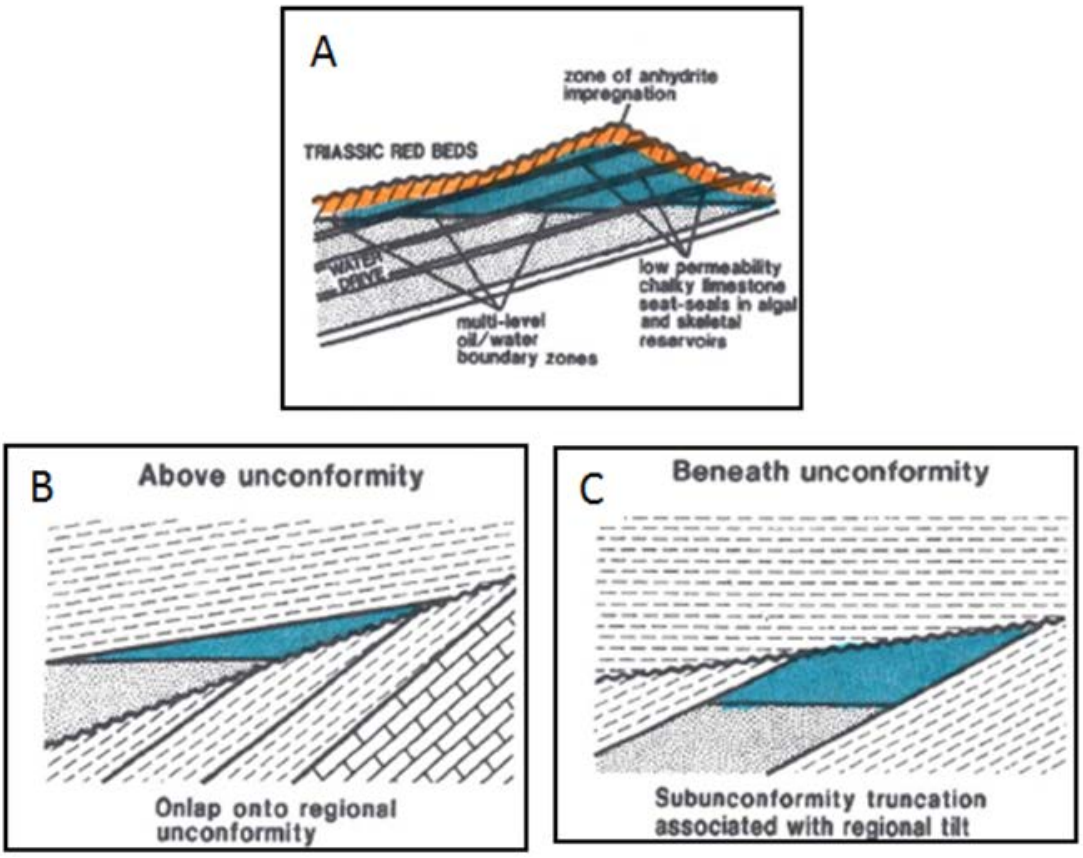

AAPG©1994, Reprinted by permission of the American Association of Petroleum Geologists (AAPG) whose permission is required for further use

2.1.7 Timing of CO_2 Charge

As CO_2 is released from magma it is optimally focused along deep-penetrating crustal structures. CO_2 often migrates along shear zones and then laterally outward. CO_2 can also migrate laterally along sub-horizontal frontal thrusts and secondarily upwards along orthogonal systems of sub-vertical fracture zones. Areas conducive to the focus and transmission of migrant CO_2 occur at fault bend geometries which promote extension, dilation, and breccia development (e.g., pull-aparts). Large, through-going fractures which cross to form broad "Xs" – whether horizontal or vertical – constitute particularly favorable pathways. Local, secondary migration is limited to distances of tens of miles outward from the primary depth-penetrating structures.

2.2 Undiscovered CO_2 Resource Assessment

2.2.1 CO_2 Accumulations

Most large deposits of CO_2 in the U.S. are of magmatic origin. Volume I describes the discovered CO_2 resource base. The characteristics of discovered fields provide a useful point-of-departure for examining undiscovered plays, which are compiled in Exhibit 2-3, where magmatic sources almost exclusively dominate.

Exhibit 2-3 Characteristics of discovered CO_2 field occurrences

Deposit	Reservoir, Trap, Seal	Comments CO_2 Origin
LaBarge – Big Piney (WY)	***Res***: SS, dolomite, fractured basement ***Trap***: Thrust, plunging asym anticline, 115 km long ***Seal***: Madison sabkha, karst breccia	Gases are stratified, richer in CO_2 downward (66.5% - 95%) Magmatic, Pliocene-Recent lamproite intrusion Leucite Hills Rock Springs uplift charged
Bravo Dome (NM)	***Res***: Ark congl SS, Perm. Tubb SS ***Trap***: Anticlinal nose, (E-SE plunging) Faulting/unconformity trap ***Seal***: Permian Cimarron Anhydrite, Chinle mudstone	May be still filling today Ultramafic to alkali basalt Within Raton
Jackson Dome (MS)	***Res***: SS, Smackover LS, Eolian Buckner Fm, Norphlet Fm ***Trap***: Anticlines and salt structures ***Seal***: Mudstone within Jurassic section	Overpressured, 35% H_2S, CO_2 65-95%, mixture varies well to well Magmatic, phonoletic and mafic alkaline intrusions
St Johns Dome, (AZ. NM)	***Res***: Perm Supai Arkosic SS, Frac. Bsmt ***Trap***: Reverse fault, NW-SE asym anticline ***Seal***: San Andreas Anhydrite, Moenkopi Mudstone	Dawsonitic travertine at surface Magmatic alkali olivine basaltic field White Mts. And Springerville V.F. (30Ma - Recent)
Escalante (UT)	***Res***: Perm-Triass Cedar Mesa SS, Karst in Kaibab LS ***Trap***: N-NW Laramide anticline ***Seal***: Permian Organ Rock Fm (shale)	Mio-Pliocent volcanic field nearby Likely magmatic. 0.1% Argon (Ar)
McElmo Dome (CO)	***Res***: Miss. Leadville Dolomite ***Trap***: NW plunging anticline ***Seal***: 125-450 m Paradox salt- anhydrite	98.5% CO_2 Magmatic
Val Verde Basin (TX)	***Res:*** Ellenburger ***Trap:*** Fault-bend folds Marathon Thrust ***Seal:*** Simpson shale and dolostone	Up tp 97% CO_2 Magmatic
McCallum Dome (CO)	***Res***: Dakota SS, Lakota SS, Muddy SS ***Trap***: Laramide-related anticlines ***Seal:*** Cretaceous shales	Mid-Tertiary Braddock Peak Volcanic Field
Farnham Dome (UT)	***Res***: Navajo SS, Jurassic; Sinbad LS ***Trap***: Anticline (N-S trending) ***Seal***: Carmel shale and limestone	Ttravertine at surface w/ Dawsonite (Na-Al carbonate)
Sheep Mountain (CO)	***Res***: K Dakota SS, J Entrada SS ***Trap***: NNW-SSE anticline, Laramide Thrust ***Seal***: Pierre Shale, Laccolith seal (24 Ma)	Only field in region that has top seal that may be the source Magmatic source, late Mid-T
Madden Field (WY)	***Res***: Madison dolomite ***Trap***: NW-SE anticline ***Seal***: Miss. Madison dolomite, karst and and sabka dvlp	Near LaBarge

See Volume I for references and details

2.2.2 Characteristics of CO_2 Fields

A review of CO_2 reservoirs from the lower 48 states demonstrates that they are not substantially different from the region's exploited conventional natural gas reservoirs. Gas is trapped in conventional structures capable of holding low-density fluids. These are found in open, upright to gently inclined, symmetrical double-plunging anticlines with a 3.5:1 (length:width) aspect ratio. In all cases the geometry of folded reservoirs are such that the horizontal dimension greatly exceeds the vertical dimension. Often reservoir thickness is in the order of 150 ft net (450 ft gross) pay and a horizontal dimension of about 6 miles, or a ratio of 1:200.

Reservoir units (i.e., producing intervals) often possess 10 to 20 mD (millidarcy) of permeability and average 5 to 20 percent porosity, whereas overlying, lower permeability sealing units of anhydrite-salt-sabkha breccia, shale-mudstone-siltstone or dolomite have a fraction of a mD permeability. Many traps have a fault-bound component or involve various combinations of sealing unconformities, pinch-outs and lateral facies changes within the sealing unit. Gross permeability anisotropy of the trapping structure is commonplace. Differential fracturing, lateral lithologic changes and the effect of post-depositional alteration-mineralization dramatically change porosity/permeability (P/P) distributions within reservoir and seals. Many of the CO_2 fields consist of multiple reservoirs within a given stratigraphic succession as well as in multiple stacked reservoirs in different formations (La Barge, WY, and Escalante, UT).

The age of reservoir rocks extended from fractured-mineralized Precambrian basement, Ordovician Ellenburger Formation, Mississippian Madison and Leadville Formations, Permian Supai, Cedar Mesa, White Rim and Sangre de Cristo Sandstone, Triassic Sinbad and Moenkopi dolomite and Chinle sandstone, Jurassic Navajo Sandstone, and Cretaceous Dakota-Entrada sandstone. Sandstone and carbonate (dolomitized limestone) are the most common subsurface CO_2 reservoirs. Four-way, anticlinal trapping structures are temporally and spatially related to crustal shortening associated with late Sevier-early Laramide crustal compression spanning Late Cretaceous-Early Tertiary (80-56 Ma) time; or to a lesser extent Eocene Laramide shortening and early Oligocene decompression, uplift and doming.

Reservoirs often show many unusual characteristics including: density stratification of contained gases (Doelger et al., 1993) with CO_2 having its greatest concentration in the deeper parts of the reservoir, whereas methane (CH_4) concentrations are pronounced near the highest portion of the reservoir, and produced CO_2 gas varies greatly from 19-99 percent along with associated CH_4, H_2S, nitrogen (N_2), helium (He), neon (Ne), argon (Ar), krypton (Kr) and xenon (Xe). The composition of noble gases reported by Gilfillan et al. (2007) from Bravo, NM; Sheep Mountain, CO; McCallum, CO; St. Johns, AZ; and McElmo, CO. These CO_2 fields have $CO_2/^3He$ ratios consistent with a predominate magmatic source. The most recent volcanic/intrusive rocks in the region date from 8-10,000 years ago and are spatially associated with the St. Johns/Springerville, AZ and Bravo, NM CO_2 fields. Older magmatic activity in the region includes: 42-70 Ma (million years) at McElmo, CO; 26-22 Ma at Sheep Mountain; 30-16 Ma at Raton-Clayton (north of Bravo, NM); and 8 Ma-Recent near St. Johns/Springerville and Raton-Clayton. Spatially related intrusive complexes are likewise unusual. They typically consist of mafic to extremely alkalic felsite complexes accompanied by lesser amounts of ultra-mafic kimberlite, lamprophyre, basanite, lamproites (La Barge, WY) and carbonatites (northeast of McElmo, CO) intrusions.

The perfect trap-reservoir-seal combination is rare; consequently, most traps leak to some degree. Soil gas surveys have demonstrated that they are capable of identifying surface anomalies which were drilled and where trapped fluids were discovered at depth (Schumacher and Abrams, 1996). Evidence of subsurface CO_2 leakage to the surface is common in eastern Utah (near Crystal Geyser south of Green River, between Farnham anticline and Woodside, UT) and east of the St. Johns/Springerville CO_2 field, AZ. In all of these instances, dense, massive, banded to fibrous masses of light tan to brown carbonate (travertine) is being precipitated around natural bicarbonate-rich springs, seeps, bubbling pools, intermittently erupting geysers and uncapped drill holes. The widespread occurrence of travertine deposits in Utah, Arizona, Colorado and New Mexico are indicative of present, recent and Neogene charge and migration of CO_2 over a large area of the Colorado Plateau and the Southern Colorado Rockies. The presence of travertine deposits spatially associated with Tertiary ultramafic/mafic alkalic and alkalic felsic intrusions are considered excellent CO_2 pathfinder indicators and their presence increases the favorability of discovering significant subsurface CO_2 reservoirs in the immediate area.

3 Play Fairways and Leads—Undiscovered

Using the exploration methodology presented in Section 2, a number of play fairways and leads were defined in this study and are presented below. While this effort does not represent comprehensive assessment of the U.S. (such was beyond the scope of this effort), it does indicate areas in which CO_2 could be found. Exhibit 3-1 inscribes the principal undiscovered fairways and recognized leads, which span from the mid-continent, west Texas and New Mexico, across the Colorado Plateau and southern Rocky Mountains into Montana. Representative fairways are reviewed successively from oldest episode of magmatism and consanguineous CO_2 charge. Exhibit 3-2 identifies twenty-six hypothetical leads identified during this study. This section describes present lead location maps, and exhibits depicting geologic descriptions and parameters, and risk weighting, recovery and access factors, including their rationale.

Exhibit 3-1 Undiscovered CO_2 fairways and leads

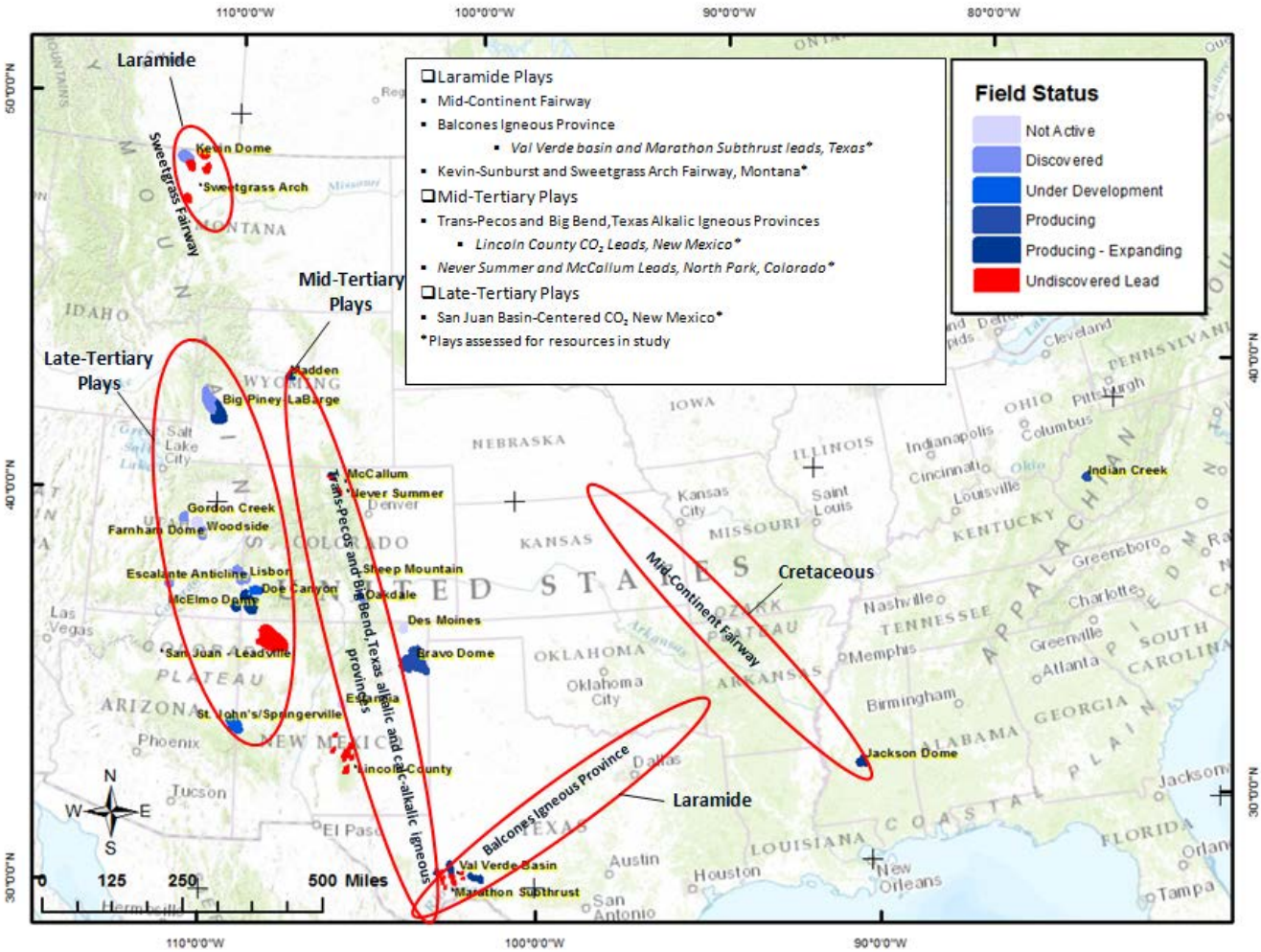

Exhibit 3-2 Undiscovered CO_2 leads

Area	Play/Lead	State	Age	Source	Play Type
Val Verde Basin	Marathon Thrust 1	TX	Penn-Cret-Olig?	Magmatic	Structural
Val Verde Basin	Marathon Thrust 2	TX	Penn-Cret-Olig?	Magmatic	Structural
Val Verde Basin	Marathon Thrust 3	TX	Penn-Cret-Olig?	Magmatic	Structural
Val Verde Basin	Marathon Thrust 4	TX	Penn-Cret-Olig?	Magmatic	Structural
Val Verde Basin	Marathon Thrust 5	TX	Penn-Cret-Olig?	Magmatic	Structural
Val Verde Basin	Marathon Subthrust 1	TX	Penn-Cret-Olig?	Magmatic	Structural
Val Verde Basin	Marathon Subthrust 2	TX	Penn-Cret-Olig?	Magmatic	Structural
Val Verde Basin	Marathon Subthrust 3	TX	Penn-Cret-Olig?	Magmatic	Structural
Val Verde Basin	Marathon Subthrust 4	TX	Penn-Cret-Olig?	Magmatic	Structural
Val Verde Basin	Marathon Subthrust 5	TX	Penn-Cret-Olig?	Magmatic	Structural
Val Verde Basin	Marathon Subthrust 6	TX	Penn-Cret-Olig?	Magmatic	Structural
Val Verde Basin	Marathon Subthrust 7	TX	Penn-Cret-Olig?	Magmatic	Structural
Val Verde Basin	Marathon Subthrust 8	TX	Penn-Cret-Olig?	Magmatic	Structural
Sweetgrass	No. 1 - Conventional Anticline	MT	Eocene	Magmatic	Structural
Sweetgrass	No. 2 - Great Falls Anticline	MT	Eocene	Magmatic	Unconventional - Stratigraphic
Sweetgrass	No. 3 - Unconventional Stratigraphic	MT	Eocene	Magmatic	Structural
Sweetgrass	No. 4 - Conventional Dome	MT	Eocene	Magmatic	Stratigraphic
Lincoln County	Conventional 1	NM	Mid Tertiary	Magmatic	Structural
Lincoln County	Conventional 2	NM	Mid Tertiary	Magmatic	Structural
Lincoln County	Conventional 3	NM	Mid Tertiary	Magmatic	Structural
Lincoln County	Conventional 4	NM	Mid Tertiary	Magmatic	Structural
Lincoln County	Unconventional 5	NM	Mid Tertiary	Magmatic	Unconventional - Stratigraphic
Lincoln County	Unconventional 6	NM	Mid Tertiary	Magmatic	Structure - Stratigraphic
North Park	Never Summer Subthrust	CO	Mid Tertiary	Magmatic	Structural
North Park	McCallum Footwall	CO	Mid Tertiary	Magmatic	Structural
San Juan	Leadville Basin-Center	NM	Mid to Late Tertiary?	Magmatic	Unconventional - Basin-Centered

3.1 Identified Late-Cretaceous Laramide Fairways and Undiscovered CO_2 Leads

Exhibit 3-3 shows the Laramide Fairways. Each of these fairways is described below. Due to time and resource constraints, not all play fairways were fully evaluated for leads.

3.1.1 Mid-Continent Fairway

Introduction and Background

In the 1960s, while exploring for oil and natural gas, Shell Energy and Land inadvertently discovered CO_2 at Jackson dome. Jackson dome CO_2 gas deposit, one of the deepest commercial CO_2 gas fields in the world, is located in central Mississippi. In 1996, Airgas purchased Jackson

dome for industrial, medical, and specialty usage. At the time of purchase, CO_2 reserves were placed at 800 Bcf.

Denbury Resources, Inc., eventually purchased Jackson dome from Airgas in 1999 for $42 million and Denbury agreed to honor existing industrial contracts written by Airgas. Technically recoverable resources are now estimated to be over 10 Tcf. With the purchase, Denbury also took ownership of a 185 mile, 20 inch diameter, high-pressure pipeline that runs from the NE Jackson dome area to White Castle, LA.

Exhibit 3-3 Late Cretaceous igneous intrusive fairways

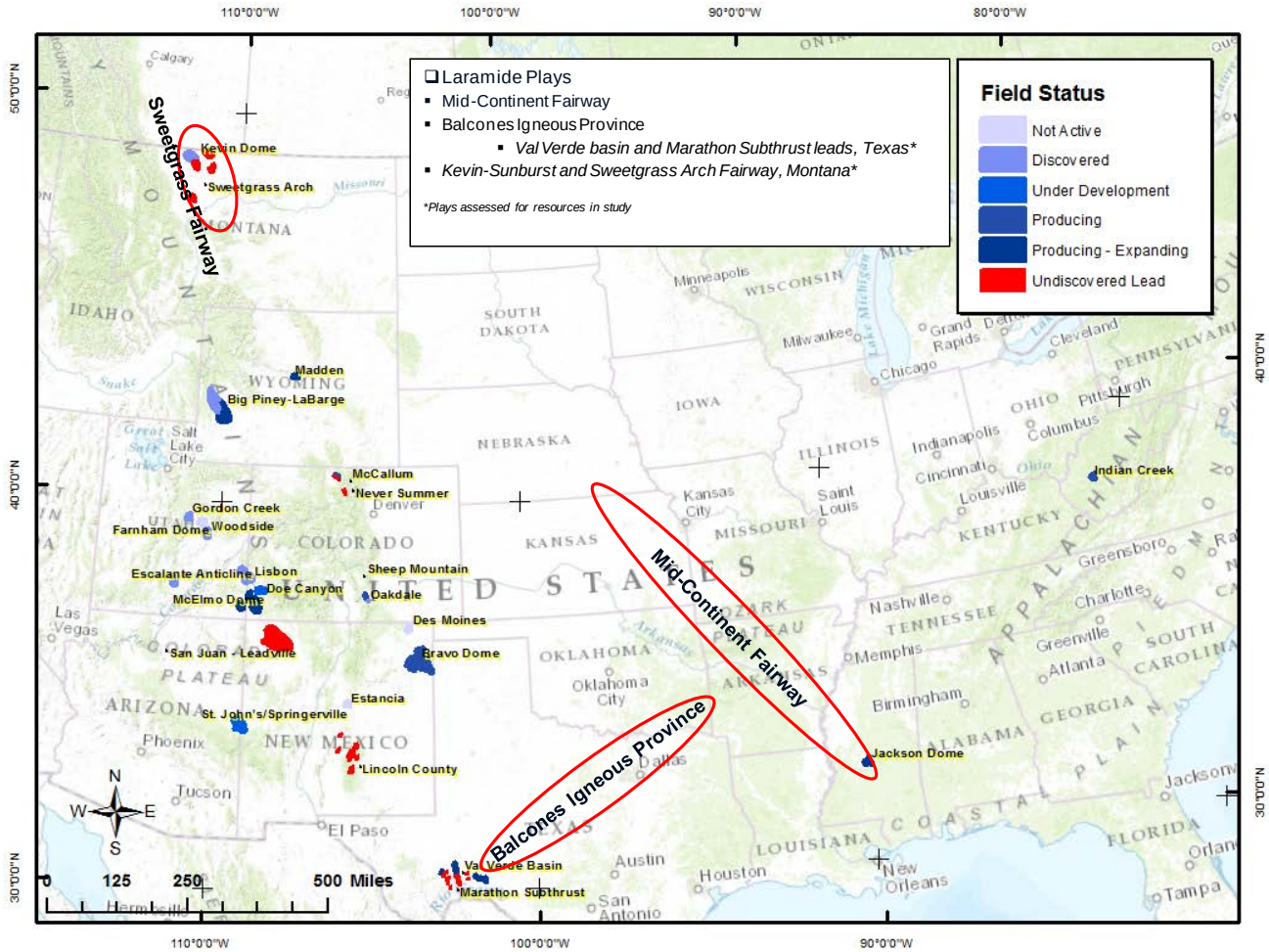

Tectonostratigraphic Setting of the Jackson Dome

Exhibit 3-4 summarizes the tectonostratigraphic setting of the Mississippi Interior Salt Basin, which is the most petroliferous basin in the northeastern Gulf of Mexico region along with the North Louisiana Salt Basin. Exhibit 3-4 shows extent of the Mississippi embayment and location of the NW-SE-trending Kansas-Arkansas-Mississippi belt of ultramafic-mafic-alkalic-carbonatite intrusive complexes. The U.S. Geological Survey (USGS) has recently ranked this region as one of the more important provinces in North America for oil and gas accumulations. Their study of the world's oil and gas provinces, the North Louisiana Salt Basin and Mississippi

Interior Salt Basin are ranked 29th in gas provinces and 34th in oil provinces with a gas volume of 42.8 Tcf, oil volume of 7.1 billion barrels, and natural gas liquids of 1.3 billion barrels.

Exhibit 3-4 Sketch map summarizing principal structural and stratigraphic elements of the Mississippi Interior Salt Basin (modified after Pilger, 1981)

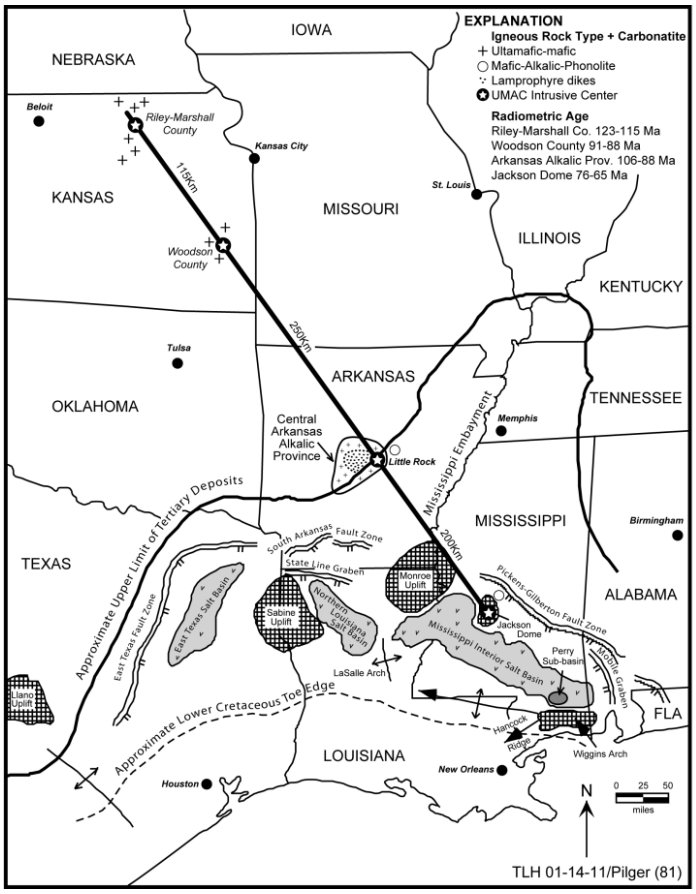

Republished by permission of the Gulf Coast Association of Geological Societies, whose permission is required for further publication use

The structural architecture of the Mississippi interior salt basin was formed largely as a result of salt flowage and extensional rift tectonics. The thickest Jurassic salt deposits (+ 6000 ft) lie within two prominent belts: an inner belt consisting of the Mississippi interior, North Louisiana, East Texas, and South Texas salt basins, and a middle belt containing the Louisiana-Texas coastal and inner shelf salt domes. The Jackson dome is part of the Interior Salt Basin, which when, as a part of the Llano, Sabine, Monroe and Wiggins uplifts, forms a semi-circular arc defining the overall geometry of the basin. The individual uplifts are separated by co-tectonic salt thicks, including the East Texas, northern Louisiana and Mississippi interior salt basins (Exhibit 3-13).

All of the above regional framework elements are localized in the hanging-wall of a continuous, semi-circular, en echelon network of depth flattening listric normal faults of Middle-Late Cretaceous age. The fore-mentioned semi-circular uplifts, salt thicks, and dome help define the hanging-wall culmination of the Late Cretaceous rollover. The Jackson dome is integral to the tectonic evolution of the interior Mississippian salt basin and elevation of the adjoining Late

Cretaceous-Early Tertiary Monroe uplift. The critical moment for oil and gas maturation/generation, migration, trap formation, reservoir, and seal along the interior east Texas, South Arkansas, and Mississippi interior basin extended from the Late Cretaceous into the Paleocene.

The Jackson dome is centered on the city of Jackson, Mississippi. It has produced significant amounts of natural gas and minor crude oil since the 1930s. As shown in Exhibit 3-4, the dome is bounded on the north by the Pickens-Gilbertown fault system, the up-dip limit of the Jurassic Louann Salt, and on the south by basement highs of the Wiggins and Lasalle uplifts of southern Mississippi. CO_2 reservoirs are located in the Jurassic Buckner, Smackover and Norphlet formations at depths of about three miles. However, what was not expected before drilling was the discovery that the dome is cored by an exotic suite of alkalic igneous intrusions of Late Cretaceous (early Laramide) age. At least seven deep boreholes have penetrated igneous rocks in the center of the dome and provide data adequate enough to now characterize the petrography, petrology, geochemistry, alteration-mineralization, and overall age of the igneous rock suite.

Jackson Dome Intrusive Rocks

Intrusive rocks fall into two broad categories: mafic alkalic and phonolite. Mafic alkalic rocks contain variable amounts of nepheline, clinopyroxene (aegerine, aegerine-augite, or titanaugite), biotite, magnetite, garnet, and sphene. The latter rocks are best classified as ijolite, melteigite, nephelinite, and jacupirangite based on their relative mineral abundances. Jackson dome phonolite consists of phenocrysts of sanidine and nepheline in a fine-grained groundmass of similar composition. Whole-rock analyses indicate that the rocks are nepheline-normative, are silica deficient, with silica (SiO_2) as low as 26.7 weight percent, and are enriched in titanium (titanium oxide [TiO_2] as high as 8 percent) and alkalis with sodium (Na) + potassium (K) typically exceeding 14 percent. K-Ar age dates were determined on whole-rock samples and biotite separates from four core samples from two different wells. Radiometric ages range from 79 ± 2.9 to 69 ± 2.9 Ma (early Laramide in the western U.S.) indicating that volcano-plutonic activity at the Jackson dome progressed over a ten million year period. Ultramafic, mafic alkalic and alkalic igneous activity was coeval with the differential elevation of the Monroe uplift, extension, and denudation.

Arkansas Alkalic Province (AAP)

The literature review confirmed the presence of the Magnet Cove kimberlite-carbonatite occurrence and the extensive Arkansas alkalic province (see Exhibit 3-4) 124 miles at N40°W of Jackson, Mississippi. Little Rock is situated between the Ouachita Mountains on the NW and the Gulf coastal plain to the SE. Exhibit 3-5 shows the spatial distribution of several of the more important ultramafic, mafic alkalic, alkalic and lamprophyre-carbonatite occurrences, which compose the province. Highlighted in red in Exhibit 3-5 is a NE-SW oriented belt of ultramafic, mafic and alkalic intrusions, which extends from Prairie Creek through Granite Mountain. These intrusions delimit the AAP lying along the northern edge of the Mississippi embayment. There is a spatially-related variation from lamproites (Prairie Creek) at the southwestern end through several carbonatite complexes (Magnet Cove and Potash Sulfur Springs), a lamprophyre dike swarm (Benton), and at the northeastern end several large syenite plutons (Saline County and Granite Mountain). Lamprophyre and syenite dikes also crop out at the V-intrusive complex and carbonatite dikes are found at Perryville and Morrilton. Regional drilling has revealed numerous other subsurface carbonatite, lamprophyre, and syenite intrusions.

The Arkansas alkalic province consists of intrusive bodies ranging in lithology from lamproite to carbonatite to nepheline syenite. Apatite and titanite fission-track and $^{40}Ar/^{39}Ar$ ages define three groups of intrusions: ~106, 101-94 and ~88 Ma. The apatite and titanite fission-track ages are concordant indicating rapid cooling due to the emplacement of these intrusions at high levels during a time of regional uplift and extension. There is also a general relationship between age and petrology: (a) lamproites are emplaced at ~106Ma, (b) carbonatites and associated silica-under-saturated alkalic rocks are emplaced between 101 and 94 Ma, and (c) large nepheline syenite bodies intrude at ~88 Ma. It is clear that provincial magmatism is intimately related to concurrent regional uplift and extensional reactivation of faults associated with the Mississippi graben.

Exhibit 3-5 Map of principal intrusions comprising the AAP and general limit of lamprophyre dikes (adapted from Eby, 1987)

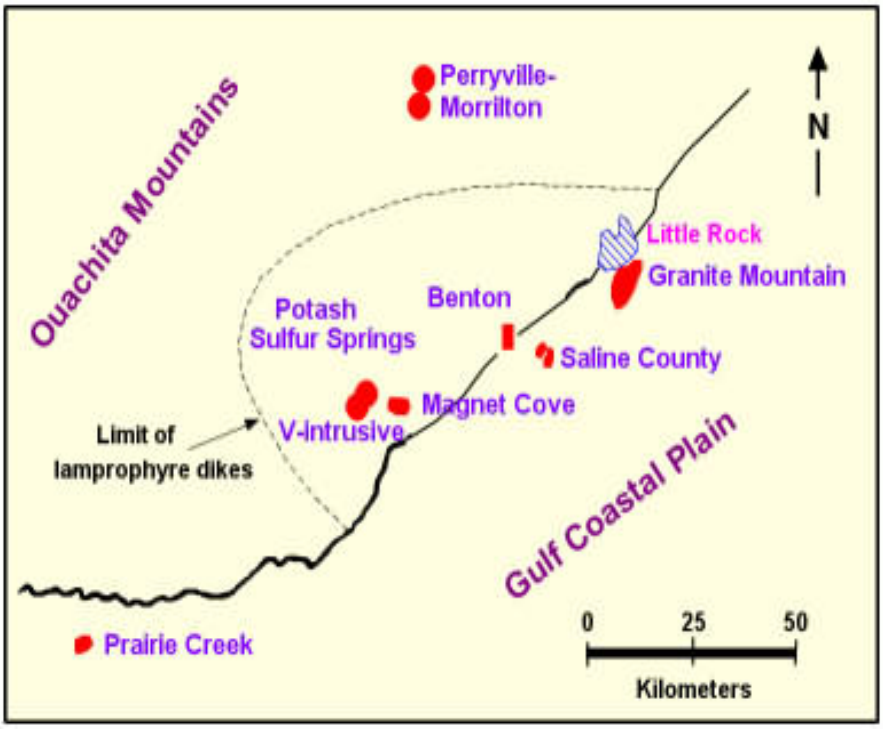

Source: USGS

There is a general consensus that the distinctive Arkansas alkalic suite of magmas (~106-88 Ma) are readily subdivided using strontium (Sr)-neodymium (Nd)-lead (Pb) isotopic compositions of olivine lamproites rather than other alkalic rock types, including carbonatite, ijolite, alkalic lamprophyres, tephrite, malignite, jacupirangite, phonolite, trachyte, and latite. Isotopic compositions of diamond-bearing olivine lamproites from Prairie Creek and Dare Mine Knob point to Proterozoic lithosphere as an important source, and previous rhenium (Re) – osmium (Os) isotopic data indicate derivation from subcontinental mantle lithosphere. Both sources were probably involved in lamproite generation. Magnet Cove carbonatites and other alkalic magmas were likely derived from a partially melted asthenospheric source.

Lamproites of the Arkansas alkalic province are isotopically quite different from other rock types in Sr-Nd-Pb isotopic space. Although lamproite samples from Prairie Creek have a large range of SiO_2 contents (40-60 weight percent), initial values of εNd (-10 to -13), $^{206}Pb/^{204}Pb$ (16.61-16.81), $^{207}Pb/^{204}Pb$ (15.34-15.36), and $^{208}Pb/^{204}Pb$ (36.57-36.76) are low and similar. Only $^{87}Sr/^{86}Sr(i)$ ratios display a wide range in the Prairie Creek lamproites (0.70627-0.70829). A lamproite from Dare Mine Knob shows the most negative εNd(i) of -19.

There is no other Laramide ultramafic-mafic alkalic intrusive complex that is more thoroughly mapped and studied than the Magnet Cove complex (Exhibit 3-6). Magnet Cove is an elliptical basin with a maximum NW-SE diameter of about 3 miles and encompasses an area of about 5 mi^2. The rim area consists of an outer belt of light-colored nepheline syenite and an inner belt of phonolite-trachyte. Much of Magnet Cove's interior is covered by deep residual and alluvial soils that are underlain by ijolite. Within the ultramafic ijolite core there are least two large masses of carbonatite (vermicular, light yellow).

Exhibit 3-6 Magnet Cove intrusive complex (adapted from Howard and Chandler, 2007)

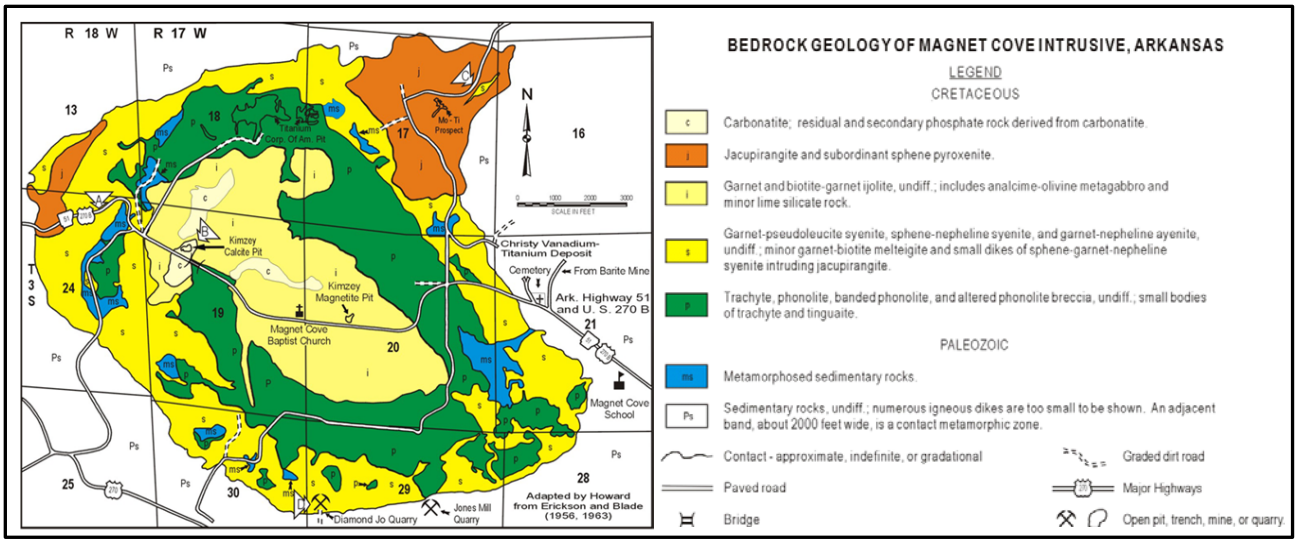

Source: Arkansas Geological Survey (AGS)

The intrusive complex and the surrounding host rock alteration zone are well documented and gemologists worldwide come here to collect over a hundred unusual minerals (niobium [Nb]-rich perovskite, molybdenite and brookite, etc.). Explorationists in search of additional undiscovered CO_2 resources should contemplate the possible existence of Magnet Cove-like geology beneath the numerous Laramide and Cenozoic alkalic complexes scattered across the western United States. Samples of carbonatite, ijolite, and jacupirangite from Magnet Cove and Potash Sulphur Springs exhibit the most depleted Sr-Nd isotopic signatures of all isotopically samples examined. For the rock types, $^{87}Sr/^{86}Sr(i)$ is 0.70352 - 0.70396, and εNd(i) is +3.8 - +4.3. Other rock types have a narrow range of εNd(i) (+1.9 - +3.7), but a wide range of $^{87}Sr/^{86}Sr(i)$ (0.70424 - 0.70629). These samples also form a tight cluster of Pb isotopic values: $^{206}Pb/^{204}Pb$ (18.22-19.23), $^{207}Pb/^{204}Pb$ (15.54-15.62), and $^{208}Pb/^{204}Pb$ (38.38-38.94), suggesting very little crustal assimilation. Published ages of crustal amphibolite xenoliths from the Prairie Creek lamproite are Proterozoic (~1.32- 1.47 billion years ago [Ga]), in keeping with isotopic evidence for crustal assimilation.

Syenites from the Magnet Cove alkalic igneous complex form a diverse mineralogical and geochemical suite. Compositional zoning in primary and late-stage minerals indicates complex, multi-stage crystallization and replacement histories. Residual magmatic fluids, rich in fluorine (F), chlorine (Cl), CO_2, and H_2O reacted with primary minerals to form complex intergrowths of minerals such as rinkite, fluorite, V-bearing magnetite, F-bearing garnet and aegerine. Abundant sodalite and natrolite formed in pegmatitic segregations within nepheline syenite where Cl- and Na-rich fluids were trapped.

By extending the line connecting the Jackson dome and Arkansas carbonatites an additional 155 miles further on the same N40°W-bearing, the line intersects ultramafic kimberlite-carbonatite intrusions drilled at Woodson, Kansas. Additionally, by continuing another 71 miles on the same bearing the well-documented kimberlite-carbonatite intrusive complexes in Riley and Marshall Counties Kansas (Exhibit 3-4) are also intersected. The general chemical and radiometric age characteristics of the ~350 mile long Kansas, Arkansas and Mississippi alkalic kimberlite-carbonatite (KAMA) belt are summarized in Exhibit 3-7.

Exhibit 3-7 Radiometric summary of Mississippi, Arkansas, and Kansas lamproite and mafic-alkalic Laramide intrusions (data summarized from Brookins [1967, 1970], Brookins and Nasaer [1971], and Cullers et al. [1982])

Location	Age (Ma)	Method, Rocks Dated, Notes
Kansas		
Riley-Marshal County (13 pipes)	123-115 ±12	Fission Track (FT), apatite; kimberlite, carbonatite,
Leonardville, Stockdale and Winkler		phlogopitic kimberlite pipes; age suspect
Randolph No.1, 2 and Bala		Lamprophyric kimberlite pipes
Woodson County	91-88	Rose dome lamproite, 250 km N40ºW from Prairie Creek, Kansas; near Silver City
Silver City Dome	91-88	Ultra-potassic lamproite-peridotite at Hills Pond
Arkansas*		
Prairie Creek Lamproite Field	106-97	Zartman, 1977; Gogineni et. al., 1978, K/Ar
Arkansas Alkaline Province	101-86	Mullen, 1987, includes quartz syenite, ijolite, nepheline syenite, sannite, phonolite, trachyte
Magnet Cove (3 episodes)*	102-100	FT apatite
	102-96	FT apatite
	88	FT apatite
Mississippi		
Jackson Dome	76-69	Mafic alkalic (ijolite, melteigite, nephelinite, and jacupirangite) and phonolite intrusions
	65	Single $^{40}Ar/^{39}Ar$ age on Jackson dome volcanism, Monroe uplift, extension and denudation

*Note: Three Arkansas alkaline provincial episodes of emplacement are recognized:

1) Lamproites	108-106	Prairie Creek diamond-bearing pipe
2) Carbonatites	102-94, 89	Province-wide
3) Nepheline syenite plutons	90-88	Granite Mountain

Woodson and Riley-Marshall County Alkalic Complexes

The Woodson County intrusions belong to the family of ultra-potassic lamproites that are enriched in incompatible elements (light rare-earth elements [LREE] or, barium [Ba], thorium [Th], hafnium [Hf], tantalum [Ta], Sr, rubidium [Rb]), and have moderate to high initial strontium isotopic (Sri) compositions (0.7042 and 0.7102). Sill-like intrusions of lamproite show signs of vertical fractionation of some elements due to either volatile transport or variations in the abundance of phenocrysts relative to groundmass due to flow differentiation. Hills Pond is a 60 ft thick sill within the northern portion of the Silver City dome (ring fracture zone). The Rose dome is a nearby intrusion that is closely associated with the above sill. The Silver City and Rose dome intrusions were initially referred to as phlogopite-rich kimberlite; now they are recognized as lamproite (Cullers and Berendsen, 2006), a K-rich, intermediate to ultramafic alkalic rock with high K/Na and K/aluminum (Al).

Analyses of cuttings and core from the Woodson intrusions show them as ultra-potassic (potassium oxide [K_2O]/sodium oxide [Na_2O] = 2.0–19.9), alkalic (molecular [K_2O/Na_2O]/Al_2O_3 = 1.3-2.8), enriched in mantle-incompatible elements (LREE, Ba, Rb, Sr, Th, Hf, Ta) and have nearly homogeneous initial Sr isotopic compositions (0.7078-0.7081). Unlike the Magnet Cove ultramafic intrusions, diamonds were not noted. Radiometric ages of phlogopite collected from the Hills Pond (Silver City) and Rose domes lamproites consistently yield ages between 91-88 Ma. Riley and Marshall Counties, Kansas, are located 70 miles N40°W of Woodson County. Thirteen separate ultra-potassic lamproite intrusions are identified and mineralogic-geochemical analyses demonstrate that they have characteristics very similar with the Magnet Cove intrusive complex of central Arkansas and lamprolites encountered in Woodson County. Intrusive rocks associated with the respective sub-vertical pipes are subdivided into two distinct petrologic groups: 123-115 ±12 Ma phlogopitic kimberlite pipes (Leonardville, Stockdale and Winkler); and lamprophyric kimberlite pipes (Randolph No. 1, 2, and Bala) with apatite FT radiometric ages varying between 123-115 ±12 Ma. Primary calcite (carbonatitic) is believed present in all the kimberlites, based on petrographic examination, and definitely present in the Bala, Randolph No. 1 and 2 kimberlites, as evidenced by Sr isotopic studies. Diamonds have not been identified in any of the pipes to date. Exhibit 3-8 is a location map of the Riley and Marshall County kimberlites. The south-southwest (SSW)-trending cluster of kimberlite pipes (1-6) appears to step-left ~6 miles across the N40°W-bearing Big Blue River before continuing north north-east (NNE) into Marshal County (7-12). Exhibit 3-9 shows the character of NE-SW-striking structural elements of the Proterozoic Mid-Continental rift and Abilene anticline. The Big Blue River shear zone (blue) and suggested offset of the southern Riley and northern Riley-Marshall kimberlite-carbonatite fields (shown in red) were added to the location map based on pipe distribution, mapped transfers shown in Exhibit 3-9 and documented elongated magnetic anomalies by Enegis.

Drilling in conjunction with detailed ground and aeromagnetic surveys show the “emplacement of the kimberlite bodies is controlled by N40°W-striking structures” (Berendsen and Weis, 2001). In this context, it is important to realize the Riley-Marshall kimberlite pipes cluster is also aligned at a regional scale with a longitudinal NE-trend. The NE orientation tracks the trace of the Proterozoic Mid-Continent rift system, an aborted rift extending from the Lake Superior region to SW Oklahoma. NE-trending structures are high-angle, normal and reverse faults associated with the 1.10 Ga mid-continental rifting event. On a regional basis, an older, high-angle normal and reverse, NW-SE-striking, transverse set of reactivated transfer faults offset portions of the rift (Exhibit 3-9). The presence of the rift is identified by regional gravity surveys, detailed gravity data sets, and evidenced in core and cuttings recovered from drill holes that penetrate juxtaposed Precambrian basement blocks.

Kimberlites are steeply-dipping, pipe-like bodies oriented more or less normal to the Abilene anticline as indicated by magnetometer surveys. See clusters 3-6 and 7-9; however, as suggested earlier and noted in Exhibit 3-9, the more regional trend of all intrusions once the left-step across the Big Blue River is restored is distinctly NE parallel to the axis of the Proterozoic Mid-Continental rift. Kimberlite emplacement was at low temperatures (75-150ºC) and is distinctly different from the Woodson County peridotitic kimberlites, which crystallized from hypabyssal melts during a high temperature, explosive, rapidly emplaced intrusive event at ~90 Ma (K-Ar, phlogopite).

Exhibit 3-8 Location map of the Riley and Marshall Counties kimberlite occurrences (modified after Berendsen and Weis, 2001; with fault interpretation by Enegis, LLC; used with permission)

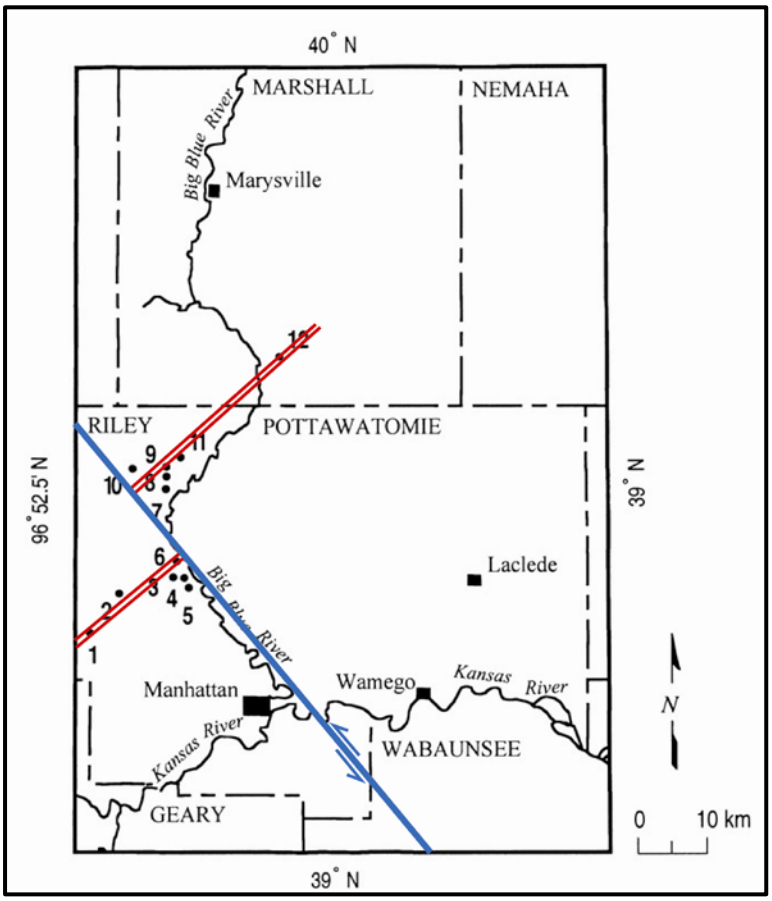

1. Bala, 2. Leonardville, 3. Tuttle, 4. Lonetree A and B, 5. Stockdale, 6. Baldwin Creek, 7. Fancy Creek, 8. Randolph-1, 9. Randolph-2, 10. Winkler, 11. Swede Creek, 12. Antioch.

Conclusion

The CO_2 source for the Jackson dome field is not from the breakdown of sedimentary carbonate. The ultramafic, mafic alkalic, alkalic and carbonatitic assemblage described from the KAMA belt is unquestionably lamproitic kimberlite-carbonatite dominate. The noted alkalic rock suites, alteration-mineralization assemblages, presence of carbonatitic magma, geochemical-petrochemical characteristics are not unlike those found further NW in the Black Hills of South Dakota and across the Montana alkalic province in general. The presence of significant CO_2 production at Jackson dome demonstrates that lamproitic kimberlite intrusions are CO_2 prone and capable of charging large, well-sealed, conventional reservoirs at reasonable depths. These findings reinforce our assumption regarding the potential ability of the Leucite Hills lamproite volcanic center to charge the up-dip, giant Big Piney-La Barge anticlinal trap. The distribution of favorable alkalic intrusive centers localized along the KAMA belt are remarkably similar to those noted along the Mid-Tertiary East Mexican alkalic –Trans-Pecos-Lincoln County belt.

Exhibit 3-9 Geologic map of Precambrian basement with major lithologies, Riley and Marshall Counties, Kansas (adapted from Berendsen and Weis, 2001; used with permission)

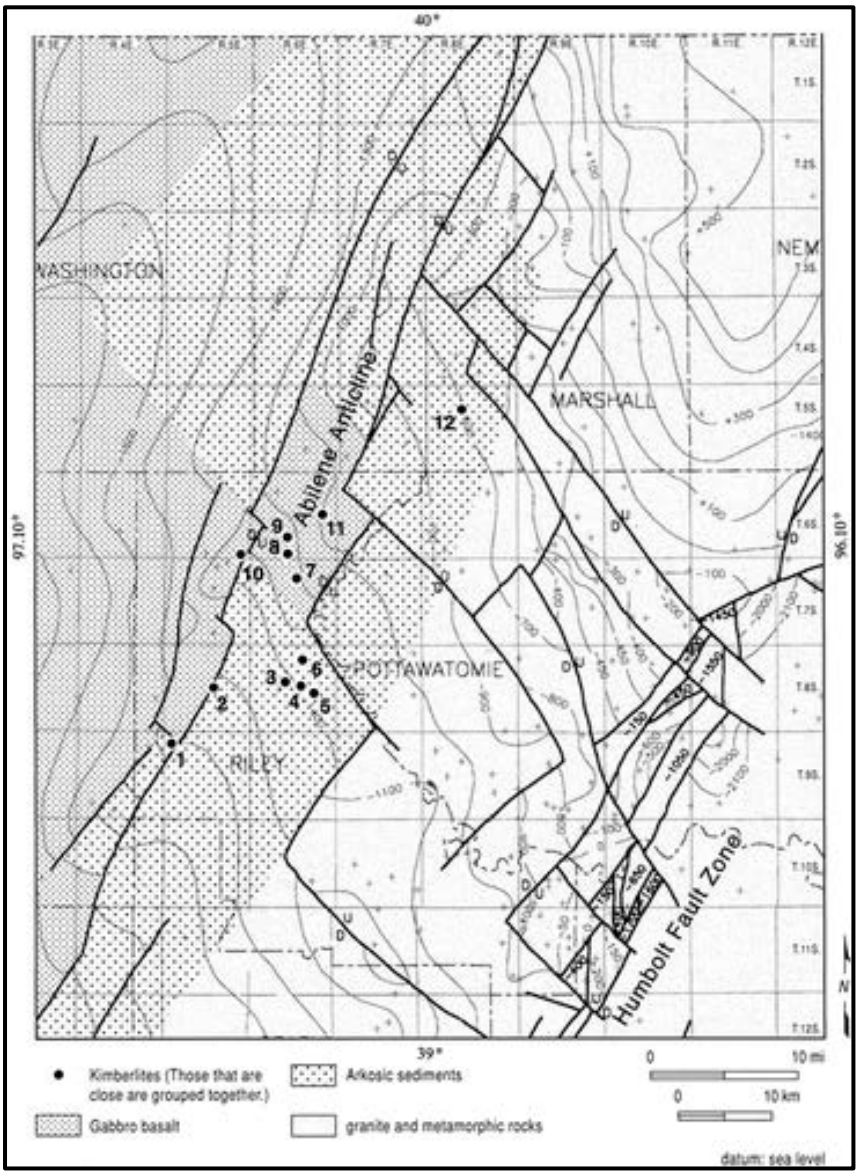

Kimberlite pipes. 1. Bala, 2. Leonardville, 3. Tuttle, 4. Lonetree A and B, 5. Stockdale, 6. Baldwin Creek, 7. Fancy Creek, 8. Randolph-1, 9. Randolph-2, 10. Winkler, 11. Swede Creek, 12. Antioch, 13.

The following brief commentaries are integrated in our developing exploration philosophy for undiscovered CO_2 deposits in the western United States:

- The Mid-Continental kimberlite-carbonatite belt is remarkably narrow, linear, trends N40°W ±5°, traverses numerous cratonal terrane boundaries and contrasting crustal rock types, and appears semi-contiguous for over 750 miles. It does not appear to follow any previously recognized or published "lineament" defined by gravity, aeromagnetic, remote sensing, etc.

- At last count, the number of documented lamproite-lamprophyre kimberlite and/or carbonatite pipes localized along or near the mid-continent fairway is 24: Mississippi, 1; Arkansas 10; and Kansas, 13. Most engineers and geologists agree that two points determine a line—in this instance twenty-four consanguineous points, forming a narrow, linear array of N40°W ±5° bearing for +750 miles seem adequate to justify the "Laramide fairway."
- Where detailed fracture analyses within the kimberlite pipes and ground magnetic surveys are available, there is definite statistical preference for the development of an orthogonal fracture system which controls the emplacement and elongation of alkalic and ultramafic intrusions.
- Focused depth-penetrating crustal and mantle extension, transtension and dilation appear to induce semi-regional decompression. This leads to partial melting mantle/mantle lithosphere and subsequent degassing. In instances where the decompressed zone migrates laterally and intersects a pre-existing crustal-scale shear zone like the Proterozoic Mid-Continent rift system (Exhibit 3-8 and Exhibit 3-9) or other major shear zone or crustal-scale lineaments, mafic lamproite, lamprophyre or other mantle-derived mafic-alkalic melts charged with coexisting CO_2/F/H_2O/^{3}He gain access to regional, through-going migration routes leading upward to epicrustal levels.

3.1.2 North American Kimberlite-Carbonatite-Lamproite Occurrences

Introduction

Kimberlite magmas are small, very rare, and according to Eggler (1989) are derived from the mantle at depths in excess of 90 miles. Kimberlite magmas have very low viscosities and high buoyanacies due in part to their enrichment in CO_2 fluid and Cl. Fresh, unaltered olivine-hosted melt inclusions are set in a fine-grained mantle-derived matrix of alkalic carbonates (5-15 weight percent), abundant alkali elements (5 weight percent Na_2O), high Cl content (3-5 weight percent), and halite and sylvite (Kamenetsky et al., 2008). They are often closely associated with parental carbonatite magmas depleted of H_2O (<0.5 weight percent) with primitive group 1 isotopic values: $^{87}Sr/^{86}Sri$, 0.7043-0.7049 and ƐNd near +5. On occasion, they are economically important for their diamond content (Maas, 2005).

Historically, kimberlite magmas were viewed as products of anorogenic plutonism positioned far inboard from contemporaneous subduction and volcanic arc regimes. Sharp (1974) challenged this interpretation and proposed they were indeed subduction-related as subsequently championed by McCandless (1999). Convincing research on the tectonic and magmatic evolution of the western United States and adjoining Mexico and Canada shows that there is a persistent, long-term, westward-younging progression of kimberlite/carbonatite and lamproite intrusions across the western U.S. If correct, it seems unlikely that the North American kimberlite/carbonatite occurrences are associated with anorogenic magmatism and are indeed subduction-related. The following section captures the essence of this space-time, westward-younging wave of kimberlitic-carbonatitic magmatism across North America.

Plate and Regional Tectonic Evolution

Huge volumes of Panthalassa ocean floor were subduced beneath the North American plate since the opening and subsequent spreading of the North Atlantic basin (150 Ma-Recent). Convergence between the various Panthalassa plates (Farallon and Kula) during the Cretaceous and Cenozoic are somewhat speculative. It is generally accepted that: (a) from 175-125 Ma, the orientation of the net convergence vector between Panthalassa/North America was E-ESE-directed with convergence decreasing by a factor of two over the 50 Ma period; (b) North American kimberlites emplaced between 175-125 Ma are located along the easternmost region of the continent (Quebec, Ontario, Michigan); (c) after 125 Ma, convergence rotated counter-clockwise and nearly doubled in velocity between 125-75 Ma; (d) widespread kimberlite magmatism heralded the onset of the Laramide orogeny (80-34 Ma) reaching far to the north (Somerset Island, Slave Province, Alberta, Saskatchewan and NW-SE across Kansas, Arkansas and Mississippi); (e) during the Middle and Late Laramide, respective slab windows and calc-alkalic magmatic gaps evolved in the American Northwest (circa 54-48 Ma) and later in the American Southwest (circa 30 Ma-Recent); and (f) as respective slab windows expanded, marginal Farallon subduction zones were progressively converted to transform fault zones. Shortened North American Cordilleran foreland areas experienced widespread extension, emplacement of metamorphic core complexes, detachment style tectonism, emplacement of ultramafic kimberlite/carbonatites and consanguineous calc-alkalic plutonism rapidly transitioned to more alkalic intrusions characterized by syenodiorite, syenomonzonite, alkalic granite, syenite, phonolite, trachyte, and fine-grained equivalent volcanic lava, flow breccia, and radial dike swarms.

Exhibit 3-10 and Exhibit 3-11 summarize the distribution of North American radiometric ages for kimberlite-carbonatite and associated lamproite, lamprophyre, and alkalic intrusions. Instantaneous convergence vectors for the Farallon (F)/North American (NA) plate at 150, 125, 75, and 25 Ma are after Cox et al. (1989). Motion vectors vary from 5-8 in (inch) /yr (year) to 2.5-4 in/yr down to 1-0.5 in/yr. Stylized intrusion isochrone lines for 150, 100, 50, 25, 5 Ma, and supplemented data points for the western U.S. are from this study. Note the persistent westward younging of radiometric ages across the continent. This pattern appears less consolidated following the post-125 Ma counterclockwise rotation of F/NA convergence from E-W to NNE-directed with commencement of Laramide mountain building. Laramide, Mid-Tertiary and Late Tertiary (75, 25, and 5 Ma) isochrones continue to get younger westward; however, migration patterns are considerably more compartmentalized. Los Angeles (L) and Vancouver (V) are labeled for location purposes. It is apparent that reported ages: (a) become progressively younger from E to W and NE to SW across the continent; (b) isochrones become more condensed through time; (c) after termination of Laramide compression in the American Northwest (~50 Ma) and Southwest (~35 Ma), kimberlite-carbonatite emplacement migrated rapidly SW coincident with the dramatic decrease in Farallon/North American convergence and Farallon plate rollback/dismemberment; and (d) kimberlite-carbonatite emplacement culminated along a N-S line sympathetic to the western margin of the Colorado Plateau, northward to the southern Wyoming craton at Leucite Hills.

Synopsis and Exploration Relevance

The observed spatial and temporal relationship of kimberlite-carbonatite intrusions across North America and their persistent younging pattern toward the Pacific shows that the observed distribution is related to the interaction of the continent and over-ridden/subducted plates of the

proto-Pacific ocean (Panthalassa). It appears that Farallon subduction progressively back-stepped toward the W and SW through time. The Mid-Continent alignment of kimberlites were emplaced coincident with the marked increase in arc magmatism along the Sierra Nevada orogen at 125 Ma. This was the last major episode of magmatism recorded along the eastern Sierran arc, which continued to ±90 Ma. A review of Exhibit 3-7 shows this event precisely brackets the older Kansas-Arkansas out-break of kimberlite-carbonatite that ceased circa 88 Ma, when the dip of the Farallon plate commenced to flatten beneath the entire southern Rocky Mountain Cordillera arc orogen extending across northern Mexico, Arizona, New Mexico, and north beneath the Colorado Plateau. Concurrent with flat-slap subduction beneath the American Southwest, CO_2-bearing mafic alkalic and advanced alkalic intrusions at Jackson dome (76-65 Ma) were emplaced along with the E-W-trending Laramide Balcones intrusive belt 90-65 Ma).

Exhibit 3-10 North American kimberlite-carbonatite-lamproite occurrences (125-1 Ma)

Location	Age (Ma)	Rock Type
Mid-Continent Kansas-Arkansas-Mississippi		
Kansas: Riley, Marshall, Woodson Counties	123-88	Kimberlite, carbonatite,lamprophyre, K-lamproite
Arkansas: Prairie Crk, Magnet Cove	106-88	Carbonatite, lamproite, lamprophyre, phonolite
Mississippi: Jackson Dome	76-65	Mafic-alkalic suite, nephelinite, phonolite, CO_2 field
Balcones Intrusive Field, Texas		
	90-65	Basanite, phonolite, nephelinite, serpentine plugs
Montana Alkalic Province; South Dakota; and Wyoming		
Haystack Butte	48	Monticellite peridotite, kimberlite/carbonatite
Bearpaw Mountains	54-50	Rocky Boy carbonatite, nepheline syenite, lamprophyre
Missouri Breaks	48-47	Williams kimberlite, biotite lamprophyre (alnöite)
Judith Mountains	47	Kimberlite/carbonatite
Grass Range	50	Homestead kimberlite/carbonatite
Porcupine Dome	<56	Carbonatite, aillikite, lamprophyre
Black Hills, South Dakota	<46	Carbonatite, phonolite
Rattlesnake Hills, Wyoming	44-40	Phonolite, trachyte, latite
Smoky Butte, Wyoming	27	Lamproite
Clayton-Raton Volcanic Field		
	24	Basanite, lamprophyre dikes
	30	Kimberlite diatreme
Utah, Summit Co.		
Kamas, Moon Canyon	40	Lamproite
Silver King Tunnel, Park City	39	Mica peridotite, alnöite dikes
White Creek, 25 mi NW Vernal	13	Lamproites
Leucite Hills, Wyoming		
Rock Springs Uplift	2-1	Phlogopitic lamproite

Exhibit 3-11 Map of the North American continent showing the location of several kimberlite, carbonatite, and lamproite intrusive complexes for the 175-1 Ma timeframe (150, 100, 75, 50, 25, and 5 Ma isochron lines by Enegis, LLC; modified after McCandless, 1999; used with permission)

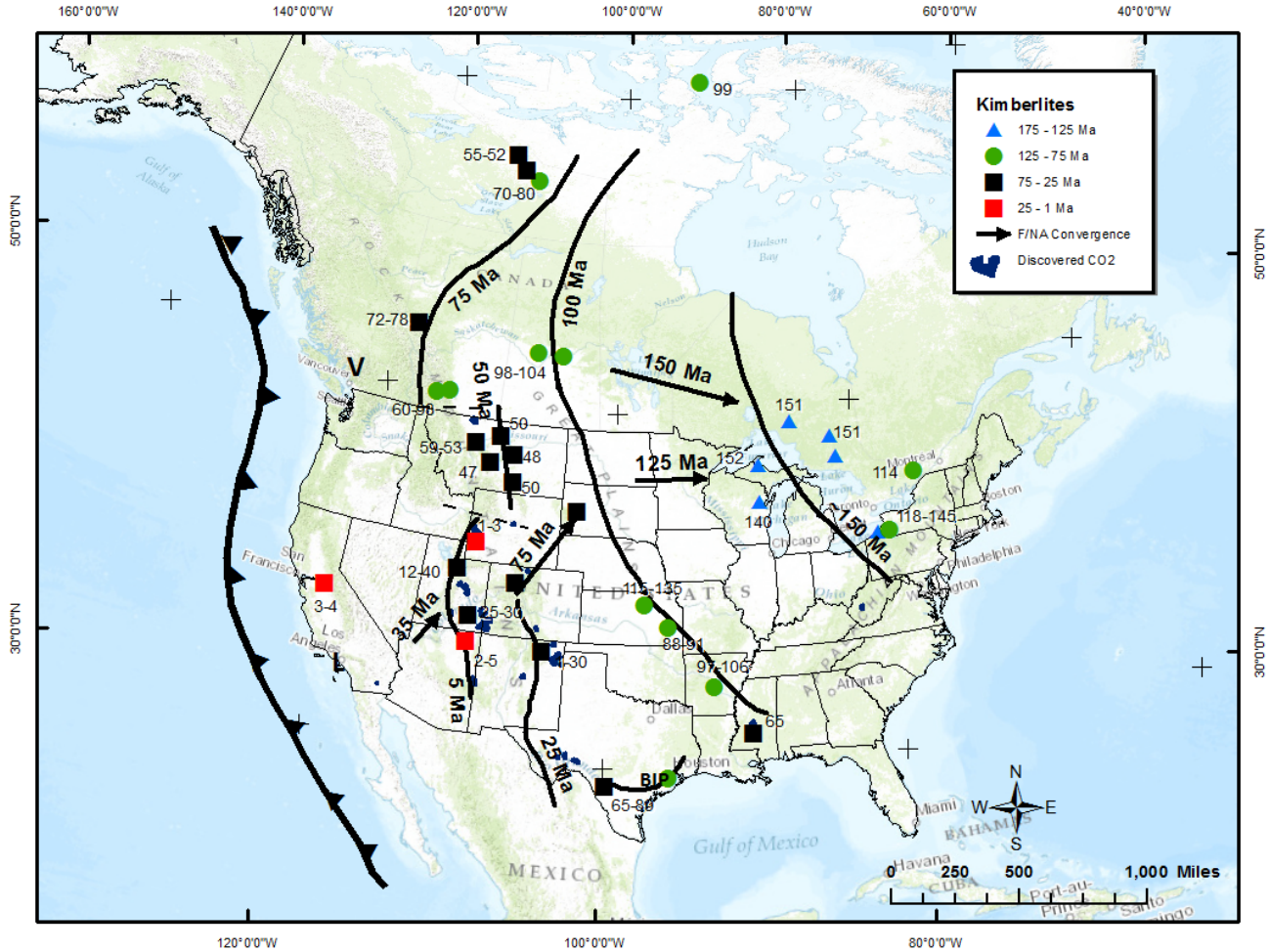

As noted at Magnet Cove, advanced alkalic intrusive systems can exceed 19 mi^2 in outcrop. Most, however, are much smaller, measuring a few miles in diameter. Exhibit 3-12 illustrates the relationship between the surficial crater, carrot-shaped diatreme pipe and deeper hypabyssal parental magma in the "root zone." Note that above the root zone and closer to the surface, layered strata or a pre-existing subhorizontal thrust or shear zones facilitates the emplacement of horizontal sill complexes. With time the sill complex evolves into convex-upward magma chambers (laccoliths) similar to those found scattered across the Colorado Plateau province. Ultramafic to mafic-alkalic intrusions regardless of age share close parental affilation with major CO_2 deposits: Jackson CO_2 dome (76-65 Ma); Kevin CO_2 and the Montana alkalic province (<56-46 Ma); McCallum CO_2 (34 Ma); Bravo dome CO_2 (30;<5 Ma); McElmo CO_2-San Juan basin (28-19 Ma); and the supergiant La Barge CO_2 and Leucite Hills lamproite field (2-1 Ma). The interpretation in this report is simplistic; size may not matter in this instance. We interpret these small, vertical, carrot-shaped, rapidly emplaced, explosive, fluid-charged intrusive systems as directly linked with the underlying CO_2 Mother Lode at a depth of ±90 miles. Once the vertical conduit penetrates to shallow crustal levels or the surface itself, hot-streaming,

immiscible, supercritical CO_2 fluid with a potentially huge volume has access to shallow, supracrustal, structural and stratigraphic traps.

This perspective is fundamental to the developing exploration strategy of this assessment. Small, carrot-shaped intrusions are invariably localized along or near the intersection of depth-penetrating lineaments or large local fault zones. Access and vertical ascent through the rigid lithosphere is apparently facilitated by the presence of previously deformed zones of deformation or along intra-plate terrane boundaries. Add to this tectonomagmatic framework appropriate size conventional structural traps or unconventional stratigraphic traps, and the explorationist will have greatly reduced the risk of drilling a duster.

Exhibit 3-12 Stylized model of a kimberlite magmatic system

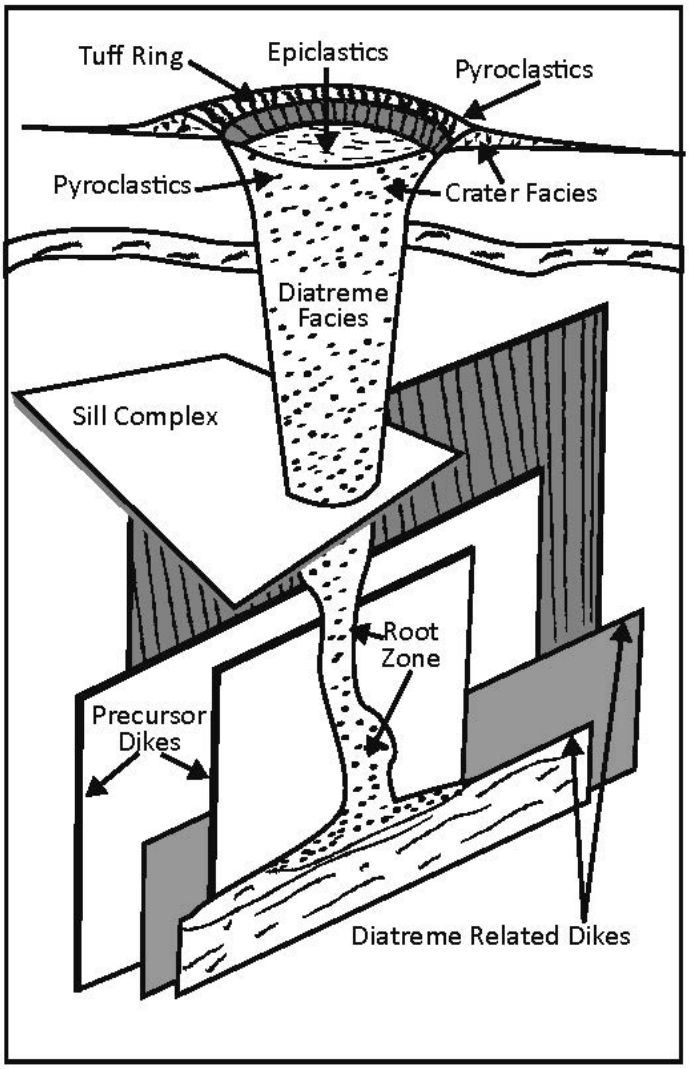

Exhibit 3-13 Location map showing the leading edge of the Marathon-Ouachita fold-thrust belt and Permian foreland basins of west Texas (adapted from Hickman et al., 2009; used with permission)

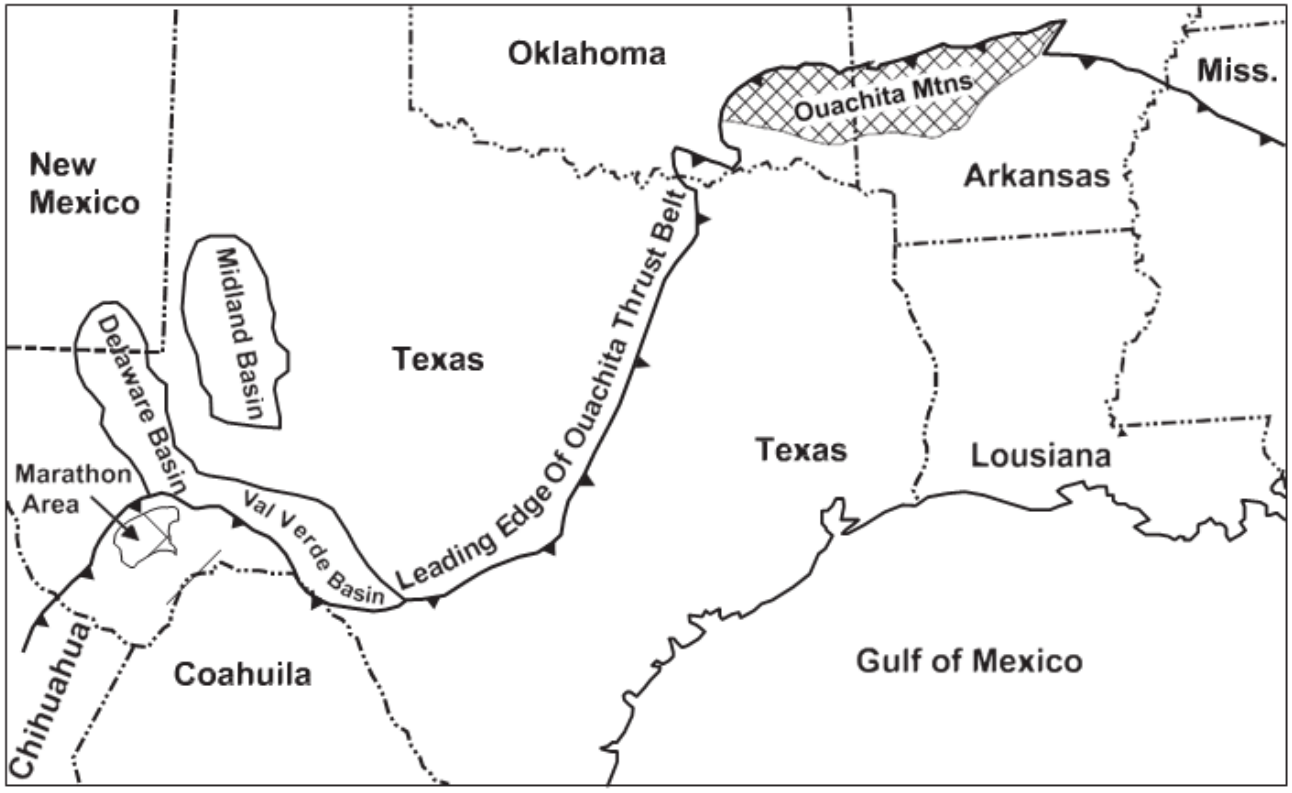

Carboniferous Plate Tectonic Restoration

Members of the team that conducted this study have a combined 65 years of oil and gas exploration-development experience working petroleum systems worldwide. The Permian basin is considered one of the more structurally and stratigraphically complex; in addition, the basin as a whole appears incompletely integrated. Regardless, the data synthesis can be leveraged by first placing the region considered within its proper global plate tectonic framework.

From a structural and stratigraphic perspective, the Permian region was dramatically altered during the Carboniferous period (360-300 Ma). The plate tectonic reconstructions at 356 and 306 Ma capture the essence of the global-scale geotectonic framework of EurAmerica (Laurentia) and Gondwanan continents (Exhibit 3-15A and B). At 356 Ma an extensive, deep, ENE-bearing seaway (relative to the calculated location of the paleo-equator) connected the Rheic (west) and Paleo-Tethys Oceans (east).

Thick accumulations of black siliceous, organic-rich shale and siliceous radiolarian ooze characterized depositional conditions across deeper portions of the seaway during Silurian through Mississippian time. A comparison of the two 50 Ma plate tectonic frames, shows the intervening Rheic and Paleo-Tethys seaway separating EurAmeria and Gondwana was completely closed during the Carboniferous. Northern South America-Africa's persistent northward movement during the period relative to the W-WSW motion of EurAmerica resulted in the oblique, left-handed collision between the two continents.

Exhibit 3-14 Map generalizing the location of several subbasins and structural compartments of the Permian basin (modified from Hanson, 1991; used with permission)

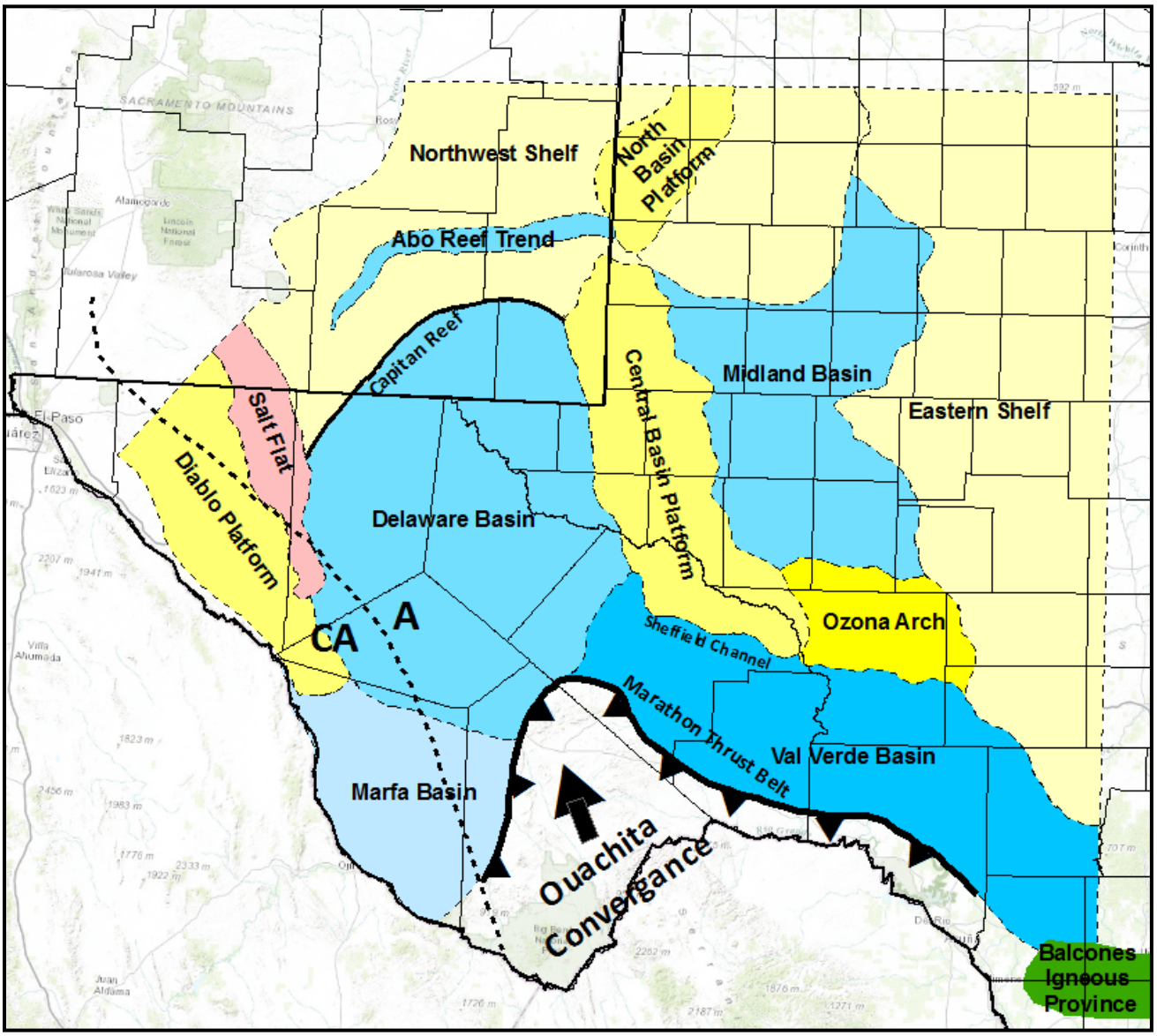

The actual welding of the two continents along the suture zone commenced in the east (Exhibit 3-15A, Appalachian Mountains), progressed westward along the Ouachita Mountains (Arkansas-Oklahoma-Kansas), and lastly the Marathon Mountains (Exhibit 3-15B, West Texas). Impact of the collision in the Marathon-Ouachita segment of the suture zone induced the differential elevation of the Ancestral Rocky Mountain chain extending from West Texas-Oklahoma, across Oklahoma-New Mexico-Colorado and as far NW as Idaho and Utah, a distance of 900 miles or more (Kluth and Coney, 1981). Clearly the effect of the North America and South America-Africa collision during the Late Carboniferous (Pennsylvanian) was profound on rocks involved, traps formed, and integrity of seals required for the long-term preservation of hydrocarbons or CO_2.

Exhibit 3-15 Early Carboniferous (3A, Tournaisian, 356 Ma) and Late Carboniferous (3B, Moscovian, 306 Ma) (Scotese, 2003; used with permission)

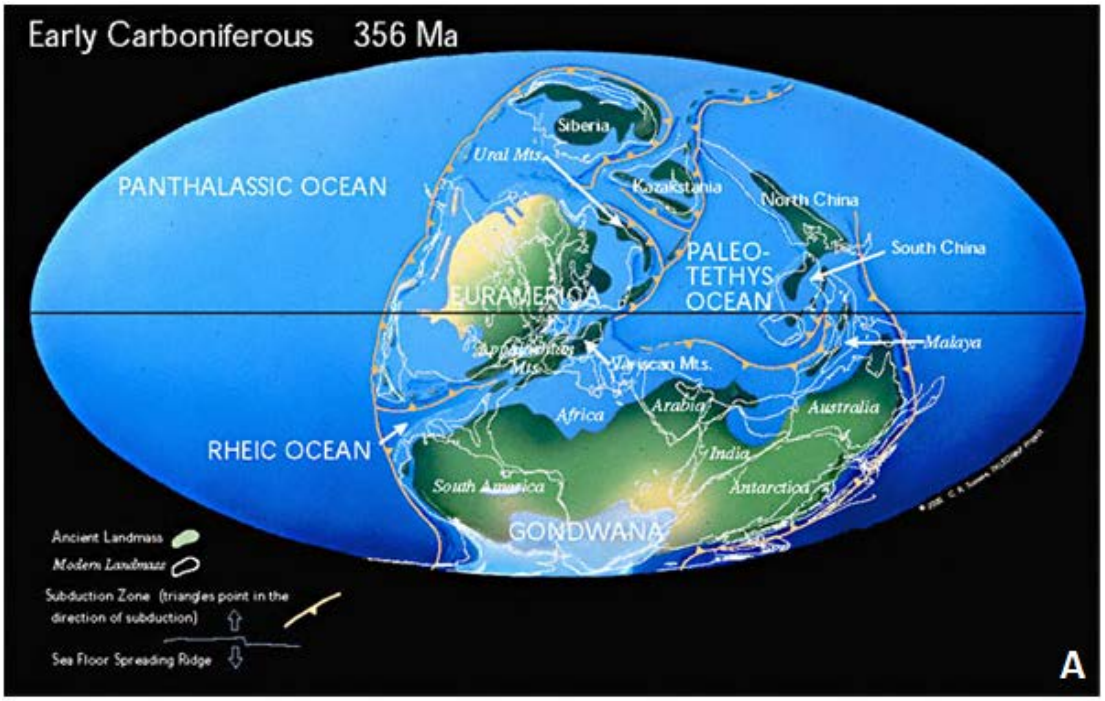

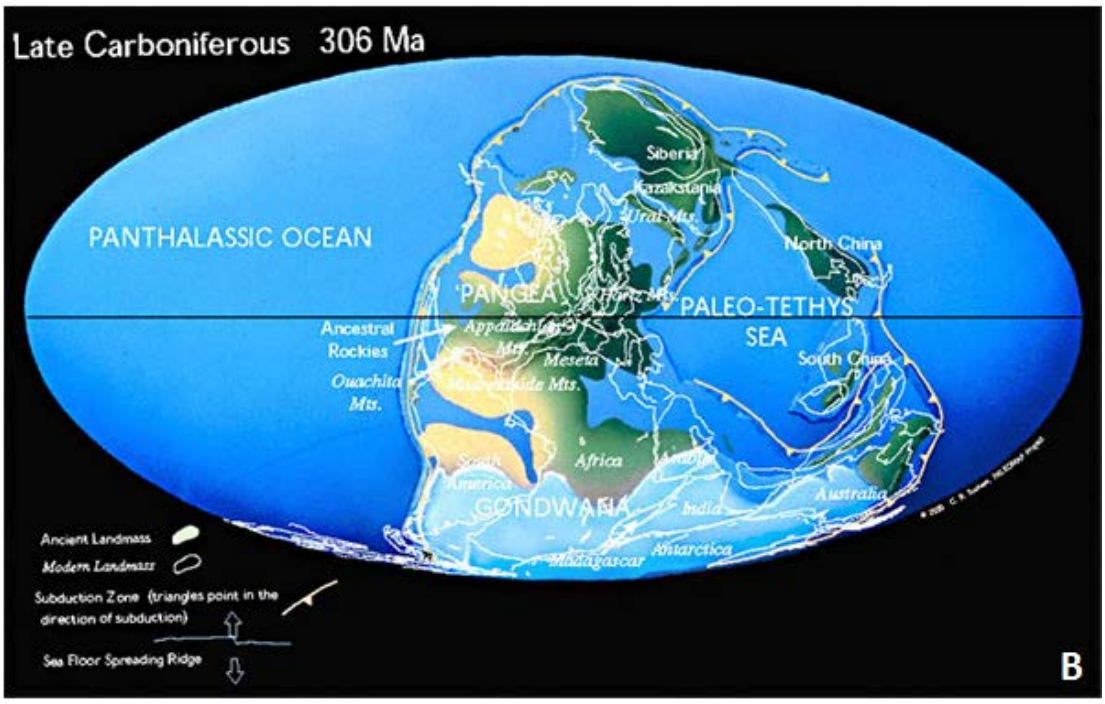

(A) Early Carboniferous (Tournaisian) plate reconstruction shows Rheic and Paleo-Tethys seaway separating the EurAmerica and Gondwana continents.
(B) Late Carboniferous (Moscovian) plate reconstruction shows the Rheic and Paleo-Tethys seaway is closed and Pangea and EurAmerica continents are sutured together along the Marathon-Ouachita-Alleghanian fold-thrust belt.

Tectonostratigraphic Evolution Marathon Allochthon and Subthrust Areas

Detailed mapping of the exposed portions of the Marathon fold-thrust belt in West Texas by P. B. King (1930, 1937, 1977, and 1980) was instrumental in defining the overall character of exposed structure, as well as, developing the stratigraphic framework of the Marathon area. The early efforts and subsequent field studies when integrated with sub-surface structure, well control and regional stratigraphic interpretations detailed the Paleozoic tectonostratigraphic history of the region.

Stratigraphy

Thrusted and complexly folded strata of the Marathon thrust belt are usually referred to as pre-tectonic "Marathon facies or Marathon allochthon." Included in the pre-tectonic Marathon facies is an early sequence of Late Cambrian–Devonian strata and a diagnostic later sequence of Mississippian-Early Pennsylvanian strata. Early-middle Paleozoic facies include succession from the Dagger Flat Sandstone through the Caballos Novaculite (Exhibit 3-16). The younger sequence heralds an abrupt change in sedimentary environments and involves the deposition of Tesnus Formation siliciclastic sandstones unconformably deposited on the underlying marine Caballos strata. The early phase of pre-tectonic strata is dominated by thin-bedded limestone and chert deposits with subordinate thin intercalations of shale and shaley sandstone. This stratal sequence is interpreted as deposited in a continental slope to outer shelf environment. Important formations incorporated in the early Marathon facies include the Woods Hollow, Maravillas, and Caballos Novaculite (chert); and the younger late phase Tesnus, Dimple, and Haymond formations (Exhibit 3-16).

Syn-tectonic Marathon facies of latest Mississippian-Early Permian age are dominated by thick successions of flysch and overlying molasse. Syn-orogenic sediments were shed northward and eastward away from the advancing South America plate into the E-W trending Ouachita trough that formed from loading of the North American lithosphere. The thick syn-tectonic succession consist of sandy siliciclastic sandstone, shelfal limestone, siltstone, and minor intercalated conglomeratic sandstone shed from the over-riding Marathon thrust sheet. The estimated composite thickness of the syntectonic success is between 3 to 3.5 miles (King, 1977). Syn-tectonic formations of the Val Verde and Delaware foreland area included in the Canyon, Cisco and particularly thick Wolfcamp flysch deposits (Exhibit 3-16).

Exhibit 3-16 Composite stratigraphic columns for the Marathon subthrust (left) and allochthon (right), Delaware-Val Verde foreland subbasins and Marathon facies (from Barden and Franklin, 2003)

Permission Pending

Structure

The extreme levels of shortening, wide variety of structural styles of deformation and excellent outcrops exposed in the Marathon uplift of west Texas have attracted geologists to this area from around the world. Exposed Paleozoic structural elements include several orders of folds, SE-dipping thrusts, NW-trending strike-slip faults, numerous sets of joints and multiple phases of superimposed brecciation of the Devonian Caballos Novaculite. First-order folds include a synclinorium and adjacent flanking anticlinoria. Other well-displayed structural features include duplex structures, imbricate thrusts, folded and re-folded thrust faults, and disharmonic folds. In spite of the extreme degree of stratal shortening, the exposed rocks of the Marathon uplift are not metamorphosed. Major and intermediate structures are controlled chiefly by the actions of the competent Maravillas and Caballos Novaculite and spacing of major decollements. Very large-scale folds are uncommon but are observed in Late Pennsylvanian-Early Permian flysch deposits in the eastern Marathon uplift. Between 6 and 10 documented major decollement surfaces are often observed deforming Paleozoic strata along the length of the uplift.

The following fold-fault geometries and their quantified dimensions and distributions are relevant to this study; (a) internal shortening directly associated with the Marathon thrust is distributed within a 0.5-1 mile thick zone or sheet of distributed deformation; (b) deformed rocks within the disturbed zone are displaced from their location of origin and are referred to as being

allochthonous; (c) total accumulative shortening across the Marathon allochthon or thrust belt is between 75-125 miles (Muehlberger et al., 1984; Hickman et al., 2009); (d) 75-80 percent of internal shortening within the Marathon allochthon involves a diverse suite of folds and faults; (e) shortening by folding involves an array of fault-bend and propagation folds (Suppe, 1983), box, buckle and chevron folds, and tight, isoclinal to recumbent folds with steep- to shallow-dipping axial planes; (f) large-scale folds have wavelengths measured in miles with considerably smaller fold amplitudes; (g) weak, shaley units within the Marathon sequence act as detachment or decollement surfaces; forward-breaking, SE-dipping imbricate thrusts successively propagate upward from the shaley units over-riding their respective footwalls in "piggy-back" fashion; (h) sets of forward-breaking thrusts coalesce into an upper level detachment with a hanging-wall characterized by a zone of fault-bound duplexes or stacks of folded duplexes over-riding each successive duplex; (i) axes of folds are statistically oriented perpendicular to NW-directed tectonic transport; and (j) 300 to 600 ft thick Caballos Novacullite units act as competent units within the duplexes; or multiple, detached Caballos successions are imbricately stacked forming complex, high-relief fault-folds structures which act as favorable fractured traps.

Exhibit 3-17(A-E) summarizes in synoptic fashion the sequential tectonostratigraphic development of the Marathon thrust belt over a period of about 150 Ma (Middle Early Paleozoic – Late Permian). Hickman et al. (2009), integrated the well-documented sedimentologic record and successive tectogenetic events in order to reconstruct details of the collision of South and North American plates during the late Paleozoic. See Hickman et al. (2009), for details and additional supporting references.

The evolution of the Marathon Thrust Belt is summarized as follows:

> Exhibit 3-17A (±400 Ma): SW-W-facing, continental margin setting; North American cratonal source of detrital sediments; thin marine Marathon facies strata deposited (Dagger Flat Sandstone-Caballos Novaculite); Maravillas chert deposited with associated phosphorite.
>
> Exhibit 3-17B (330 Ma): Major change in Marathon facies deposition patterns; Tesnus sandstone detritus accumulates at base of slope; siliciclastics sourced from the SE-approaching South American plate and its exposed Precambrian crystalline basement; intercalated tuffaceous Tesnus beds suggest a nearby volcanic arc.
>
> Exhibit 3-17C (310 Ma): Dimple and Haymond sedimentation in deep Tesnus trench denotes proximity of the South American plate; initial imbricate thrusting of Marathon facies strata; incipient NW-vergent Marathon allochthon develops. Strong lateral compression initiates local foreland uplifts and basins associated with the Ancestral Rocky Mountain belt.
>
> Exhibit 3-17D (305 Ma): Allochthonous Marathon thrust belt driven NW over former Marathon foreland; Tesnus trench filled and inverted; syndepositional Marathon flysch and molasse sedimentary rocks folded, thrusted and overridden by other, rootless, fault-bound allochthonous blocks.
>
> Exhibit 3-17E (255 Ma): Marathon overrides the Gaptank basin; shortening along the Marathon thrust belt terminated; synorogenic clastic sediments derived from the arched allochthon; roof of Marathon allochthon exhumed; eroded detritus transported northward into the subsiding Delaware, Val Verde, and Midland basins.

Exhibit 3-17 Schematic diagram showing successive stages of tectonostratigraphic evolution of the Marathon overthrust belt (adapted from Hickman et al., 2009; used with permission)

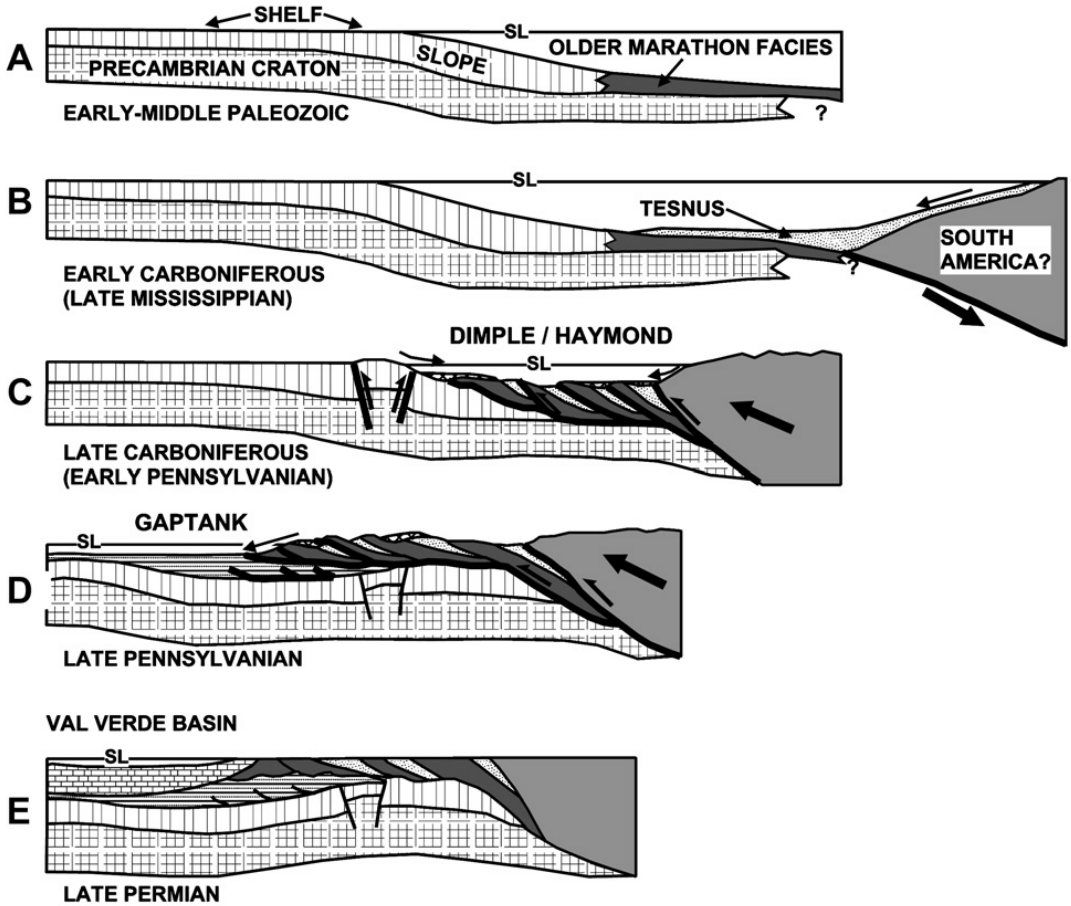

The above stylized overview recognizes three distinct and remarkably different domains that could prove favorable for undiscovered CO_2 resources. The schematic cross-section drawn across the basal frontal thrust of the Marathon allochthon shown in Exhibit 3-18 underscores two of the domains. The allochthonous Ouachita (Marathon) and its deformed Marathon facies strata are shown over-riding a weakly deformed, Ordovician Ellenberger Formation. Site 5 on the cross-section represents one of the most prolific oil and gas reservoirs of the Permian basin. In this stylized cross-section, the formation is shown intact and appears unaffected with respect to what transpired within the hanging-wall Marathon allochthon.

Contrasting interpretations concerning the style of deformation within the Marathon allochthon can be seen in a comparison of Exhibit 3-18 and Exhibit 3-19. In Exhibit 3-18 an imbricate set of forward-breaking thrusts are shown propagating upward from the basal detachment, cutting indiscriminately through the overlying Marathon facies strata. Potential traps 1-4 are readily recognized and adjoining thrust blocks have similar, well-ordered stratigraphic successions with similar identifiable traps and uniform reservoir petrophysical characteristics.

This is an ideal situation for the exploration or development geologist. Exhibit 3-19 by contrast portrays Marathon facies strata cut by a set of imbricate thrusts as above; however, in this instance: (a) there is no clear basal detachment surface, (b) a given vertical well may penetrate the same identical reservoir interval four to five different times, (c) a given reservoir like the

Caballos Novaculite is shown duplexed and wells can be located to encounter the reservoir interval where it is twice or more its normal thickness; and (d) conventional anticlinal fold traps are not upright, their location and geometry are less predictable between fault-fold blocks and folds are tight, isoclinal, and locally recumbent with horizontal axial planes. Clearly developing large undiscovered CO_2 resources within the Marathon allochthon is more difficult than in the simpler, more predictable subthrust Ellenberger setting; moreover, the geological, geophysical, and petrophysical character of the Ellenberger subthrust traps, reservoir, and topseals are well-documented from the adjoining, thoroughly drilled-out foreland tectonostratigraphic domain. According to Exhibit 3-17C-E, the Ellenberger subthrust play was once 60-120 miles further north and part of the S-SW-facing Paleozoic Val Verde slope facies. Acceptance of these simple geometric and kinematic relationships allows the explorationist to reduce geologic risk and more rigorously quantify other geometrical and petrophysical risk factors for trap, reservoir, and seal.

Exhibit 3-18 N-S schematic cross-section across the Marathon fold and thrust belt (from Barden and Franklin, 2003)

Permission Pending

Exhibit 3-19 Diagrammatic SW-NE cross-section across the Marathon fold and thrust belt (from Barden and Franklin, 2003)

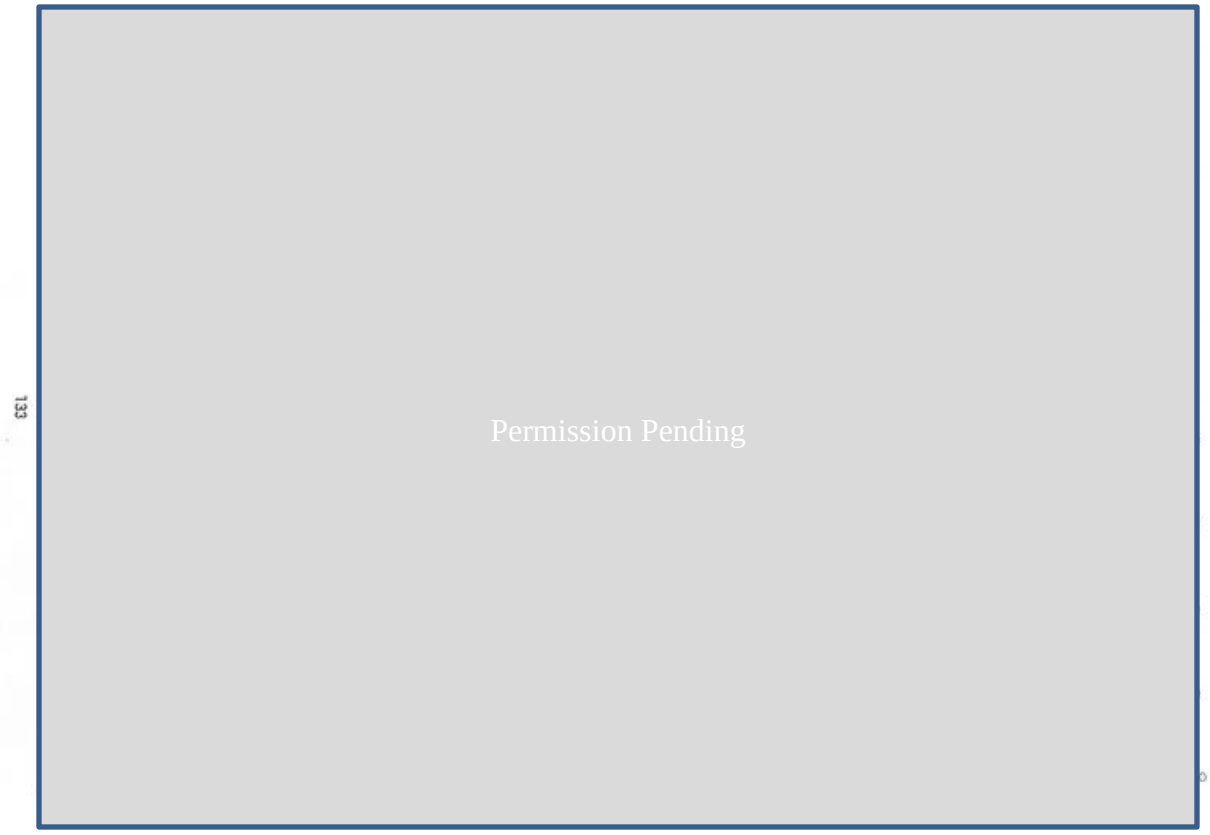

Lower Paleozoic Subthrust Tectonostratigraphic Framework

Successfully playing the lower Paleozoic subthrust underlying the Marathon allochthon requires the explorationist to place the 335-285 Ma, SE-directed conveyor belt (subducted Ellenberger) in reverse and restore 75-125 miles of overridden footwall. With current technology this is not possible; however, we are able to glean considerable perspective of what the subthrust terrain looks like by examining the areal distribution of oil-gas fields, their respective size, shapes, trap geometries, reservoir thicknesses, reservoir P/P, seal characteristics, etc., from the adjoining Val Verde and Delaware subbasins.

Ellenburger Stratigraphy Val Verde Subbasin

Thousands of wells have penetrated the prolific Ellenberger reservoirs across the Val Verde and southern Delaware subbasins. The mean gross/net pay for Ellenberger reservoirs is similar throughout the two subbasins as are the petrophysical characteristics.

The predictability of reservoir properties are a reflection of the gentle paleo-shelf to slope conditions which pervaded across the basin during the Ordovician. The relatively static, short-lived, depositional environment is manifested in the predictable gross thickness of the formation. Exhibit 3-20 shows the isopach map of the Ellenburger Formation across the Val Verde, much of the adjoining Delaware, and the southern portion of the Midland subbasins. Even at the 500 ft contour interval, the Ellenberger progressively increases in thickness southward across the basin increasing from 500 ft in the north to between 1000 to 1500 ft in the Val Verde and southern Delaware subbasins. Based on the documented isopach gradient and understanding of the

paleogeography of the S-SW-facing Ordovician shelf and slope (Exhibit 3-18) the Ellenburger Formation is expected to have: (a) a thickness of +1500 ft beneath the Marathon allochthon; (b) net/gross similar to the adjoining foreland fields in the Val Verde and southern Delaware basins resulting generally in a net thickness of about 600 ft; and (c) petrophysical and other geological characteristics in common with the neighboring fields to the north.

Exhibit 3-20 Isopach map of the Ellenburger formation, Permian Basin, west Texas (modified after Hanson et al., 1991; and Hoak, et al., 1998b; used with permission)

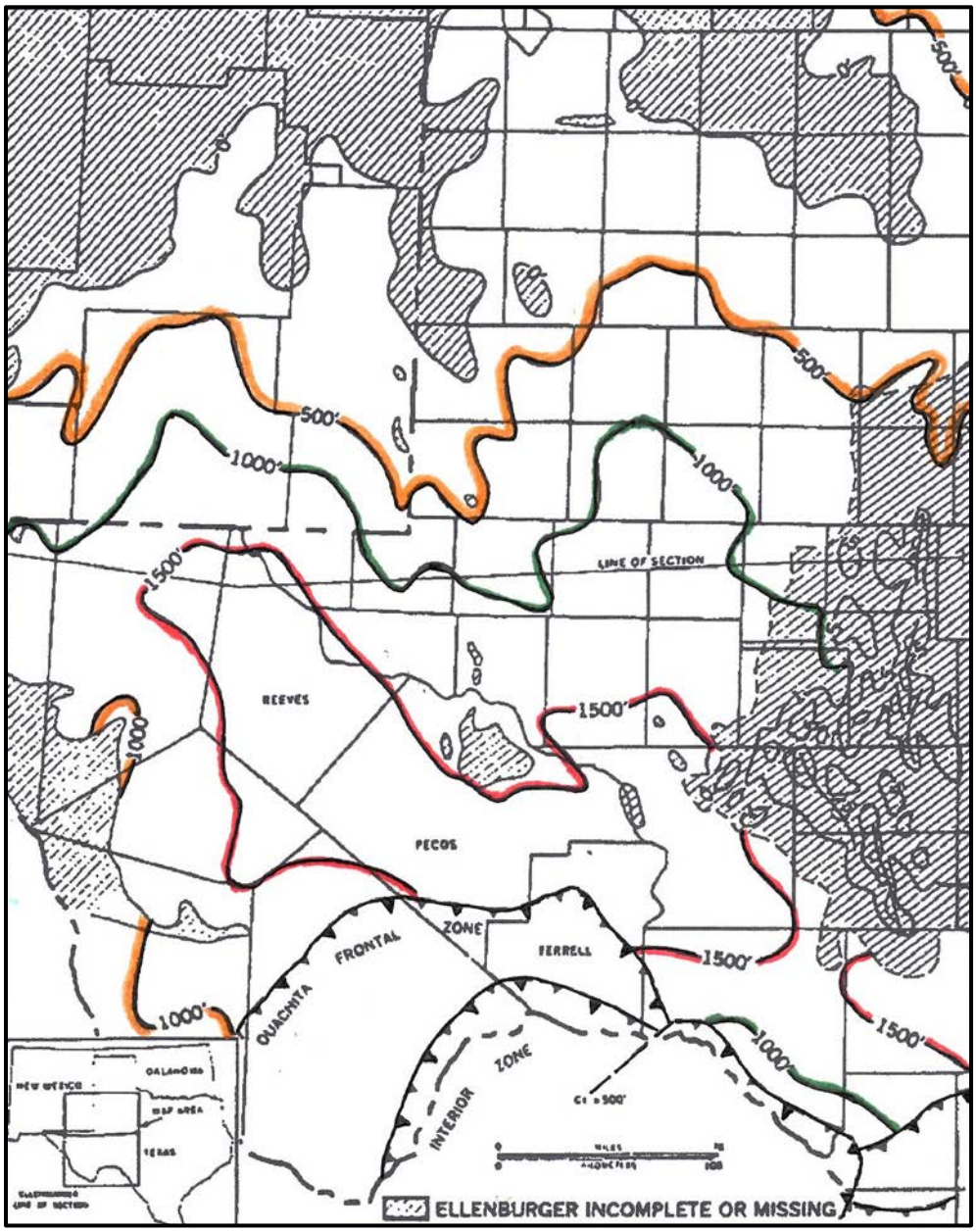

Fault and Fracture Framework, Val Verde Subbasin

Numerous papers on the Permian basin were reviewed that addressed the tectonic evolution and nature, orientation, and distribution of 1st and 2nd order structural elements. The ordering of tectonic events varied from author to author as did the relative importance placed on wrench tectonics versus shortening by horizontal compression and thrusting. It is unequivocally believed that the basin evolved rapidly and simultaneous with North American subduction, NW-directed over-thrusting along the Marathon decollement and development of the Marathon allochthon.

Concurrent wrench tectonics across the Ouachita foreland echoes earlier commentary on the oblique, left-handed convergence of North America with the persistent northward movement plan of South America. The resultant left-lateral (sinistral) shear couple is believed responsible for much of the observed foreland tectonism and attendant differential elevation and folding of respective structural traps. The impingement of South America and eventual collision with North America along the Ouachita thrust belt between 335-285 Ma produced the resultant strain field (ellipsoid) portrayed by the inset in Exhibit 3-21.

Cotectonic, first order, depth-penetrating, left-lateral, strike-slip faults are oriented parallel to the direction of the regional E-W to WNW-oriented shear couple. Major, second order, wrench-related faults strike north north-west (NNW)-NW parallel to the orientation of conjugate thrusts, fold axes and the NW-SE direction of plate convergence. The resultant mosaic of variable size polygonal structural blocks and allied shortened and folded pop-up blocks constitute the principal types of conventional oil and gas traps in this prolific basin. There is no reason why the well-documented structural framework for the Permian basin does not extend SE beneath the mapped leading edge of the Marathon allochthon. Exhibit 3-21 shows the top-basement structural contour map of the Permian basin (Hoak, et al., 1998a). It depicts several of the first and second order framework elements identified along with our derived, simple shear strain ellipsoid for the 330-305 Ma episode of foreland deformation.

Ouachita-Marathon Foreland Deformation, Stress-Strain Field, and Orientation-Geometry of Structural Elements

The maximum principal horizontal stress axis ($\sigma_{1H'}$) is oriented NE-SW across the Marathon foreland. This orientation predicts that co-tectonic, low-angle, conjugate thrusts-reverse faults and co-tectonic fold axes strike NW-SE. Fundamental to the proposed simple shear model is the presence of common, persistent, left-lateral, W-WNW-striking wrench faults throughout the foreland. Our wrench tectonic model of the Permian basin is not novel. Harrington (1963) was the first to propose wrench tectonics to explain the thin-skinned style of deformation commonly observed around the basin. Influenced by the presence of N-S-trending faults similar to the West Platform fault bounding the western margin of the Central Basin platform and related styles of deformation, he suggested a right-lateral, strike-slip shear couple oriented N-S to explain observed deformation geometries. Hills' (1970, 1985) tectonic syntheses of a larger area of the basin recognized two sets of faults: (a) ENE±15°-trending, right-lateral, strike-slip faults; and (b) co-tectonic N65°W±10°-trending left-lateral, strike-slip faults. The two sets of wrench faults were interpreted as a regional conjugate shear system. This relationship convinced Hills that $\sigma_{1H'}$ was oriented E-W although he did recognize significant right-lateral faults of NNW strike.

Exhibit 3-21 Structural contour map on top basement; contour interval is 1,000 ft, Permian basin region, West Texas (modified after Hoak et al., 1998a; used with permission; strain ellipsoid by Enegis, LLC)

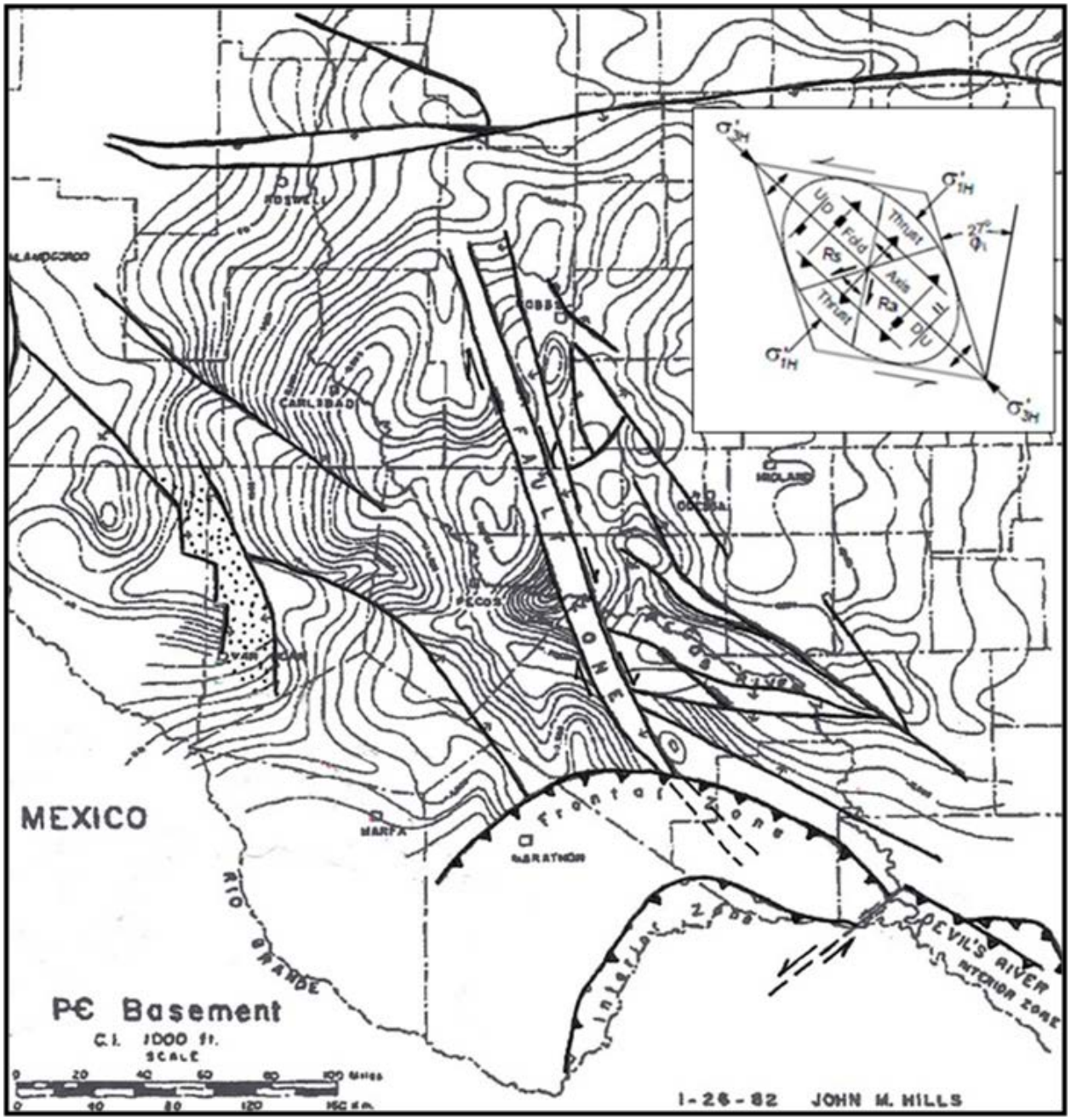

Shumaker (1992) interpreted Hill's NNW-striking faults as steep reverse faults, which link at depth with shallow, ENE-NE-dipping thrusts; moreover, the majority of the N-NNW-trending faults possessed only limited amounts of right-lateral (dextral) displacement, which he felt negated Harrington's interpretation and challenged the significance of Hills' ENE±15°-trending, dextral-slip faults. Shumaker did agree with Hills' E-W orientation of compressive stress (σ'_{1H}), but concluded there was a near penetrative, left-lateral (sinistral) shear along the system of WNW- and E-W-striking shear zones. He believed the Central Basin platform and southwestern

portion of the Permian basin was largely deformed between the Late Mississippian and Early Permian under an E-W oriented regional stress ($\sigma_{1H'}$), and significant sinistral-slip along faults of E-W and WNW-strike. He likewise stressed there was a significant, vertical axis, counter-clockwise rotation of specific structural blocks. Yang and Dorobek (1995) revisited the stratigraphic and structural evolution of the Central Basin platform and adjoining areas, and stressed the significance of en echelon, left-stepping, structures that "popped-up" under a right-lateral, clockwise rotation of structural blocks bound by NNW-trending, dextral-slip faults.

In light of the above detailed studies by interpreters who dedicated significant portions of their careers resolving the tectogenetic development of this structurally complex basin, readers should be aware of the orientation of the strain ellipsoid we propose for the Marathon foreland and inserted in Exhibit 3-21 and the orientation of derived principle stress axes. Despite this, a regional, E-W- to WNW-oriented simple shear strain field with an internal shear angle of 27° is preferred. This orientation predicts and meets the following co-tectonic basin and field relations: (a) W- and WNW±15°-striking, sinistral-slip faults are significant framework elements (Exhibit 3-21; see Hills, 1970 and Shumaker, 1992), (b) fold axes are oriented parallel to the predicted N45°W±15°-bearing; (c) thrusts and reverse faults are marginal to the "popped-up" anticlines and strike parallel to the N45°W±15°-bearing thrusts; (d) N45°W±15°-bearing thrusts and anticlinal axes are organized perpendicular to the NE-SW oriented, second order maximum horizontal principal stress axis ($\sigma_{1H'}$); and (e) second order, ENE-striking, sinistral-slip, synthetic shears (Rs) locally work in concert with WNW-striking, sinistral-slip faults resulting in vertical axis, clockwise rotated structural blocks.

Accepting $\sigma_{1H'}$ is horizontal and oriented NE-ENE during the Marathon orogeny (335-285 Ma), cross-sections with this orientation optimize bulk fold curvatures and capture maximum structural relief due to horizontal shortening. A suite of representative cross-sections from the southern Permian basin (Val Verde subbasin) by Shumaker (1992) are included in Exhibit 3-22 and Exhibit 3-23. Cross-sections are serial, oriented NE-SW, arranged SE to NW, and extend northeastward onto the Ozona arch-Central Basin platform structural block (Exhibit 3-13). Several relevant fold-fault geometries are apparent:

- folds predominately verge SW toward the Val Verde axis;
- the deformed stratal interval extends from basement-Ellenberger to synorogenic Wolcamp-Bone Spring formations;
- structural relief is enormous over short distances exceeding 24,000 ft;
- NE-dipping backlimbs are long and have flat to shallow dips;
- forelimbs are very short, characterized by steep to over-turned limbs and have low-angle to subhorizontal dipping axial surfaces;
- over-steepened forelimbs often root into underlying flat to shallow, NE-dipping thrusts;
- giant gas fields (Grey Ranch and Puckett) are low relief, double-plunging, backlimb, anticlinal culminations;
- multiple, stacked structural traps and footwall fault traps are encountered in a single vertical or directional well located over the steep to overturned forelimbs (Phillips 1EE);

- subthrusts are portrayed with minimal horizontal offsets (a few miles at most) and noted to have fault-propagation and fault-bend geometries;
- the supergiant Gomez gas field is a low relief "box fold" localized by a small backthrust on the footwall flat in the center of the Val Verde subbasin (Exhibit 3-22 and Exhibit 3-23);
- steepened forelimbs are deformed by stacked, multiple levels of low-angle thrusts;
- total estimated shortening due to folding and faulting along each respective cross-section is small (±10 percent), however the amount of shortening appears to increase toward the SE; and
- serial cross-sections constructed through the Puckett and Coyanosa fields have hanging-wall fault-fold geometries that suggest the underlying depth to the blind decollment underlying the Marathon foreland basin is at a depth of -27,000 ft subsea.

Exhibit 3-22 Transverse (ENE-NE-bearing) cross-sections showing complex fold and thrust relationships developed along the Central Basin Platform Margin, southern Permian Basin, Texas (adapted from Shumaker, 1992; and Hoak, et al., 1998a)

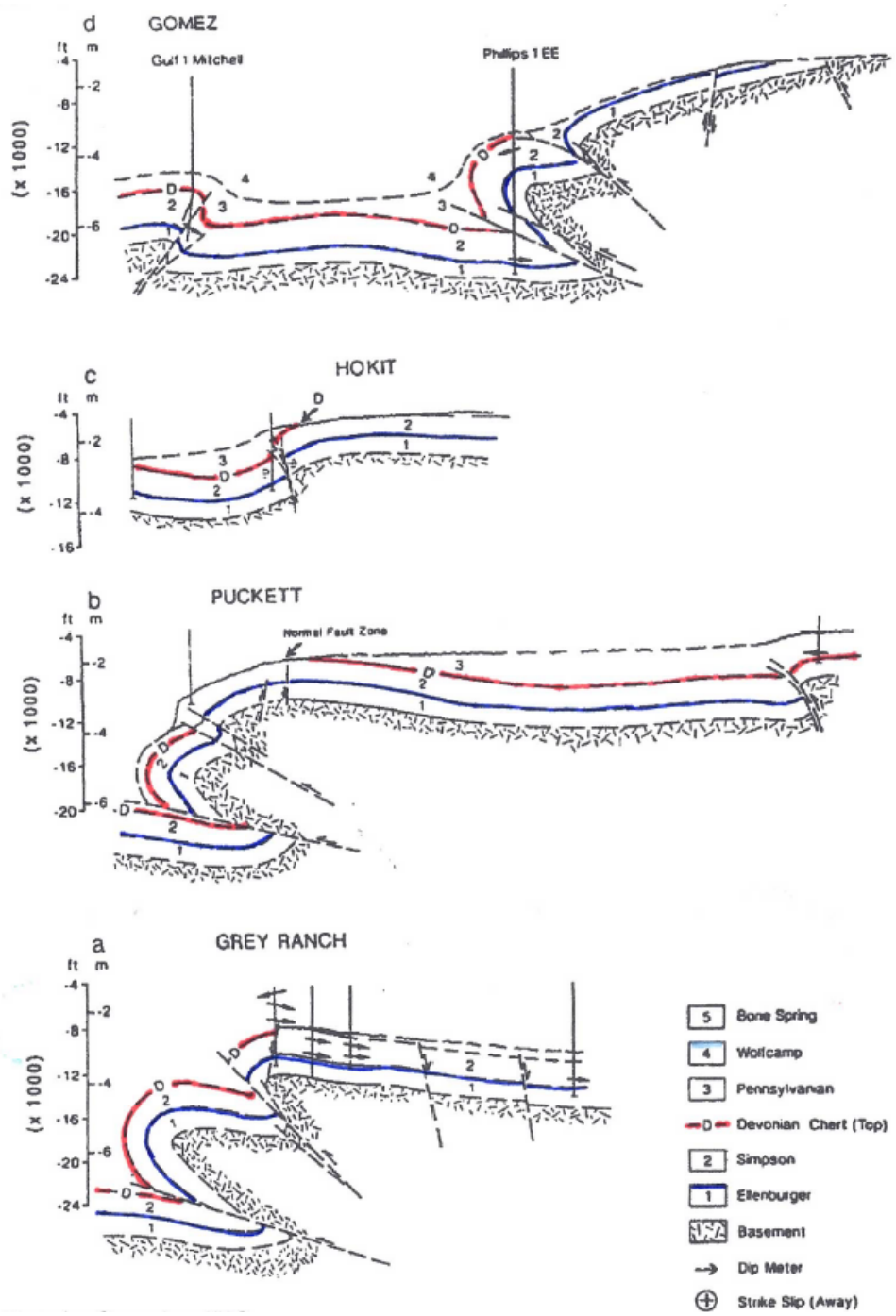

Reprinted by permission of the AAPG whose permission is required for further use

Exhibit 3-23 Structural cross-section illustrating complex Pennsylvanian-Early Permian basement-involved fold and thrust relationships along the Central Basin Platform Margin, southern Permian Basin (adapted from Shumaker, 1992; Hoak, et al., 1998a)

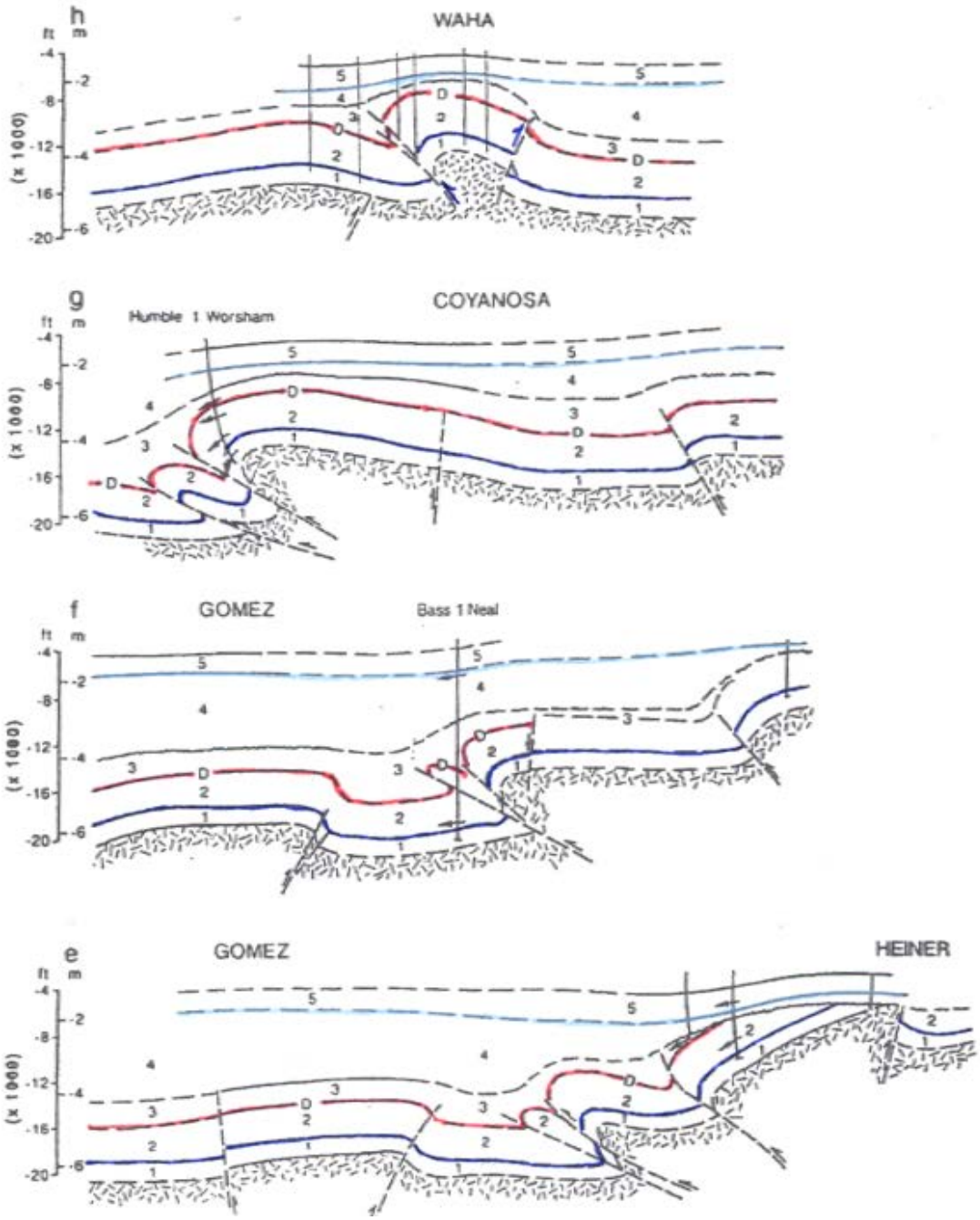

Reprinted by permission of the AAPG whose permission is required for further use

In Exhibit 3-22 note: (a) the large Puckett and Grey Ranch gas fields have over 16,000 ft of structural relief; (b) mapped faults often dip at low-angles and sole out at a depth of -30,000 ft; (c) forelimbs of the large WSW-SW-vergent folds are vertical to over-turned taking on bulk curvature common to recumbent folds with shallow-dipping to horizontal axial planes; (d) Gomez supergiant gas field is a low-relief, box fold localized on the forelimb basin of a major, SW-WSW-vergent high-relief recumbent fold; and (e) up to 15,000 ft of syntectonic Pennsylvanian-Permian flysch eroded from the advancing Marathon thrust sheets filled the syntectonic structural low areas and pull-aparts. In Exhibit 3-23: (a) most of the shortening faults have low-angle dips; (b) the majority of regional detachments lie at -30,000 ft subsea; (c) Waha structure has the characteristic syndepositional pop-up geometry involving a significant component of transpressional shortening; (d) syntectonic Pennsylvanian and Early Permian pull-aparts and structural sags were filled with 10-15,000 of coarse clastic flysch eroded from upthrusted highs and off the advancing Marathon thrust sheets.

Marathon Allochthon versus Foreland Tectonic Settings

Tectonic Transport and Stress-Strain Fields

Strata incorporated in the Marathon allochthon are collectively referred to as the Marathon facies (Exhibit 3-16 through Exhibit 3-19). Involved strata are pre-tectonic Cambrian-Early Mississippian age and had a pre-Pennsylvanian composite stratal thickness of 0.5 to 1 mile. In contrast, the contemporary, syntectonic stratal sequence deposited in the adjoining foreland basin had a composite thickness of over three miles (King, 1977). Detailed mapping and structural studies by King (1937, 1977, and 1980) through more recent analyses by Hickman et al. (2009), demonstrate fold axes within the Marathon allochthon bear NE to ENE. This reaffirms King's initial assessment that Gondwanaland (South America) collided with Laurentia over-riding North America in a NW-direction. Resultant fold axes within the allochthonous thrust sheets were oriented NE-ENE with the Ouachita-Marathon maximum horizontal stress axis (σ_{1H}) oriented normal to the fold axes bearing NNW-NW.

Deep exploration-development drilling of the Marathon allochthon at the Pinon field (6 miles ESE of Elsinore field) confirms this fold geometry and transport direction (Exhibit 3-24). Reservoirs at Pinon consist of allochthonous Devonian chert beds and 1st and 2nd Caballos Novaculite within the 2nd and 3rd Caballos thrust sheets (Barden and Franklin, 2003). Exhibit 3-25 is a 2D seismic map top 2nd Caballos Novaculite. Two right-stepping, en echelon, double-plunging anticlines are mapped bearing N70°E for a lateral distance of about 13 miles. The orientation of fold axes with identical trends for 1st Caballos reservoirs combine with numerous mapped N25°W-striking, transverse transfers and NNW-vergent fold asymmetry to fix σ_{1H} as N25°W-directed. The mapped traps involve Caballos reservoirs which vary on average between 0-150 m in thickness (Barden and Franklin, 2003). It is clear the regional direction of emplacement of the lower 1-3 Marathon thrust sheets is similar to those documented by surface mapping by King (1980). The determined Marathon allochthon transport direction is approximately perpendicular to the N45°E-S45°W±15° direction of σ_{1Hmax} proposed for the Marathon foreland basin and underlying subthrust area (Exhibit 3-21); see Hickman, et al. (2009).

Exhibit 3-24 Map of Marathon frontal thrusts, Marathon uplift, location of the Pinon field area, Longfellow-West Ranches, Thistle and Mckay Creek fields (from Barden and Franklin, 2003)

Permission Pending

Gas production from the Western Pinon- Bitterweed 2nd and 3rd thrust sheets have CO_2 contents ranging from 20-80 percent, reservoirs are over-pressured (0.62 pounds per square inch [psi]/ft gradients), have very high initial production rates, and low decline rates. These data suggest the Caballos Novaculite and associated chert reservoirs are highly fractured and laterally contiguous.

The well-documented NW±20° field elongations and fold axes trend of numerous oil/gas fields from the Marathon foreland subbasins (Shumaker, 1992; Hoak et al., 1998a), contrast markedly with co-tectonic geometries noted in fields within the Marathon allochthon. Exhibit 3-24 summarizes the distribution of frontal and hinterland thrusts of the Marathon allochthon. Major foreland fields are stippled including the NW±20°- trending Elsinore, Puckett, Grey Ranch, Brown Bassett and JM fields. The map shows the location (blue) of the intra-Marathon thrusted and folded Pinon play type, Longfellow-West Ranch area, Marathon overthrust area. Several more recent discoveries from within the lower portion of the Marathon allochthon are also shown from west to east: Pinon, Thistle, and McKay Creek. Exhibit 3-25 is a structure map on top 2nd Caballos which delineates two, right-stepping, en echelon structural closures (Barden and Franklin, 2003). The Longfellow West Ranch lead lies athwart both ranches (red boundary). The play involves anticlinally folded, N70°E-bearing Devonian Caballos Novaculite lying within a stack of NNW-vergent Marathon thrust sheets (solid line with barbs on hanging-wall). The play type is viewed as an intrafolial fold within the lower set of Marathon imbricate thrusts forming the frontal portion of the Pennsylvanian-Early Permian Marathon fold and thrust belt (Exhibit 3-19). The double-plunging anticlines extend from the eastern edge of the Allison Ranch, across West Ranch onto the Longfellow Ranch on the east, a distance of about 9 miles. Top Caballos “2” pay is at a depth of circa 10,000 ft. Drilling delineated an additional Caballos “1” pay interval at circa 7,500 ft from a similar oriented anticlinal closure.

Exhibit 3-25 Structural contour map on top Caballos Novacullite, Longfellow-West Ranch leads (from Barden and Franklin, 2003)

Permission Pending

The new cluster of Pinon discoveries and leads along with the Thistle and McKay Creek fields leave little doubt that these double-plunging anticlinal traps are trending N65-70°E with length/width aspect ratios of circa 3 to 3.5 Ma. All maps included in the Barden and Franklin (2003) reference show anticlinal traps from this trend, independent of which Caballos chert reservoir was mapped, and show respective fields and leads cut by a pervasive set of transverse fractures. These data are independent of our commentary regarding geometries documented in surface exposures that "fold axes within the allochthon have NE- to ENE-bearings, an orientation perpendicular to the dominant NW-directed tectonic transport." Our recommended orientation for the contemporaneous deformation in the underlying Marathon foreland footwall block predicts co-tectonic, double-plunging anticlines to have NW-SE-bearings, almost exactly a 90° difference in bearing. Viable, stacked CO_2 traps within the Marathon allochthon are clearly oriented NE-ENE, whereas subthrust Ellenberger traps are oriented in a transverse, NW-WNW-SE-ESE direction. It is now apparent there is a minimum of two distinctly different oriented strain fields operating simultaneously within the Marathon allochthon and underlying foreland region of West Texas. Testing and confirming/modifying the team's proposed strain field for the Marathon foreland facies underlying the allochthon, will pay huge dividends during the early phase of any exploration program focused on discovering subthrust CO_2 resources.

It is important to recall that the present highly deformed Permian basin is composed of several subbasins formed during the Marathon-Ouachita orogeny. Fortunately, most of the surrounding subbasins have similar pre-Permian lithologies and petrophysical properties, which correlate for long distances across the basin. In the case of the Ellenberger dolomite, many geologists view them as "classic fractured reservoirs" (Hoak, et al., 1998b). These reservoirs are the proto-type

fractured reservoirs developed in response to: (a) prolonged cycles of exposure, karstification, and development of extensive leached, vuggy and fractured carbonate interlayers; and (b) during post-Ellenburger deposition, the "karstified" carbonate succession experienced an intense episode (25 Ma) of shortening, low-angle thrusting, high-angle reverse faulting, fracturing along with concomitant wrench-related tectonism. The data compiled suggests the intensity of wrench-related transpression, popped-up anticlinal flexures may increase southward toward the Ouachita orogenic belt. The younger episode of Marathon-aged (335-285 Ma) fracture networks were repeatedly superimposed upon the karstified Ellenburger. Enhanced permeability and reservoir connectivity resulted through fracture linkages between formerly isolated karstified interlayers.

Reservoirs Characteristics and Tectonic Fractures

As mentioned earlier in Section 0, fault-bend and fault-propagation fold geometries are common in both Marathon foreland and allochthon settings. Exhibit 3-26 is an example of a sequential forward model of an angular, flat-ramp-flat fault-bend fold (Suppe, 1983). Both Shumaker (1992) and Hickman et al. (2009) mention the presence of fault-bend and propagation folds within the Marathon foreland and allochthon setting, respectively. Secondly, reservoir engineers and geologists working the Permian basin consider both the Ellenburger dolomite and Caballos Novaculite or chert layers as "classic fractured reservoirs." In the case of a 300 ft thick bed of Caballos Novaculite (90 percent SiO_2 with 10 percent carbonaceous shale interbeds), the formation will progressively pass through kink plane Y-B, travel up the ramp to X-B where it passes through the second kink plane, and after travelling across the upper flat for a short distance will pass yet again through another kink plane at X-A. Each time the bed of silica passes through a kink plane it becomes more fractured and brecciated, then re-fractured and phase 1 breccia is re-brecciated, etc. For this reason, the Devonian Caballos Novaculite is a proven "fractured reservoir" where individual clasts have no porosity; however, the total bulk rock porosity measures several percent with excellent permeability.

In the Marathon foreland, fracturing of the Ellenburger Formation is similarly compound, and multiple periods of superimposed fractures are observed. Extreme foreland wrench and fault-bend and -propagation thrusting pervades the Permian basin; moreover, this deformation is superimposed on pre-Marathon deformed vuggy, brecciated, fractured, karstified, and dolomitized Ellenburger. Reservoir characterization studies by Holtz and Kerans (1992) and Loucks (2007) demonstrate the compound effect of Marathon age tectonic fracturing associated with both wrench and thrust tectonics between 335-285 Ma. Their regional synthesis of Ellenburger petrophysical and petrographic data defined a 24-27 mile wide zone of "tectonically fractured dolomite" running coincident with the axis of the Delaware and Val Verde subbasins. The contribution of measured porosity due to Marathon fracturing on average increases measured porosity by 4 percent and 1 to 100 mD permeability. Possibly more important, Marathon tectonic fractures are more pervasive, wide-spaced (ft), and characterized by laterally continuity. The lengthy tectonic fractures help facilitate the linking together of previously isolated zones of karst, collapse, chaotic, and solution breccia and promote oil/gas production. It seems relevant that the 24-mile-wide "zone of tectonically fractured Ellenburger dolomite" projects SE under the frontal thrust of the Marathon allochthon (Holtz and Kerans, 1992).

Exhibit 3-27 compares and contrasts Ellenburger tectonic fracture and chaotic breccias. Exhibit 3-27A presents a Formation MicroImager (FMI) image and core photos of a tectonic fracture breccia, Ellenburger Group, Eastern shelf. Fractures are mainly vertical, appear as black, highly conductive structures transecting and brecciating a laminated mudstone. Exhibit 3-27B, shows

an FMI image and core photo of a carbonate-matrix supported chaotic breccia, Ellenburger Dolomite, Eastern shelf.

Exhibit 3-26 Sequential forward model of a flat-ramp-flat fault-bend fold (modified from Suppe, 1983)

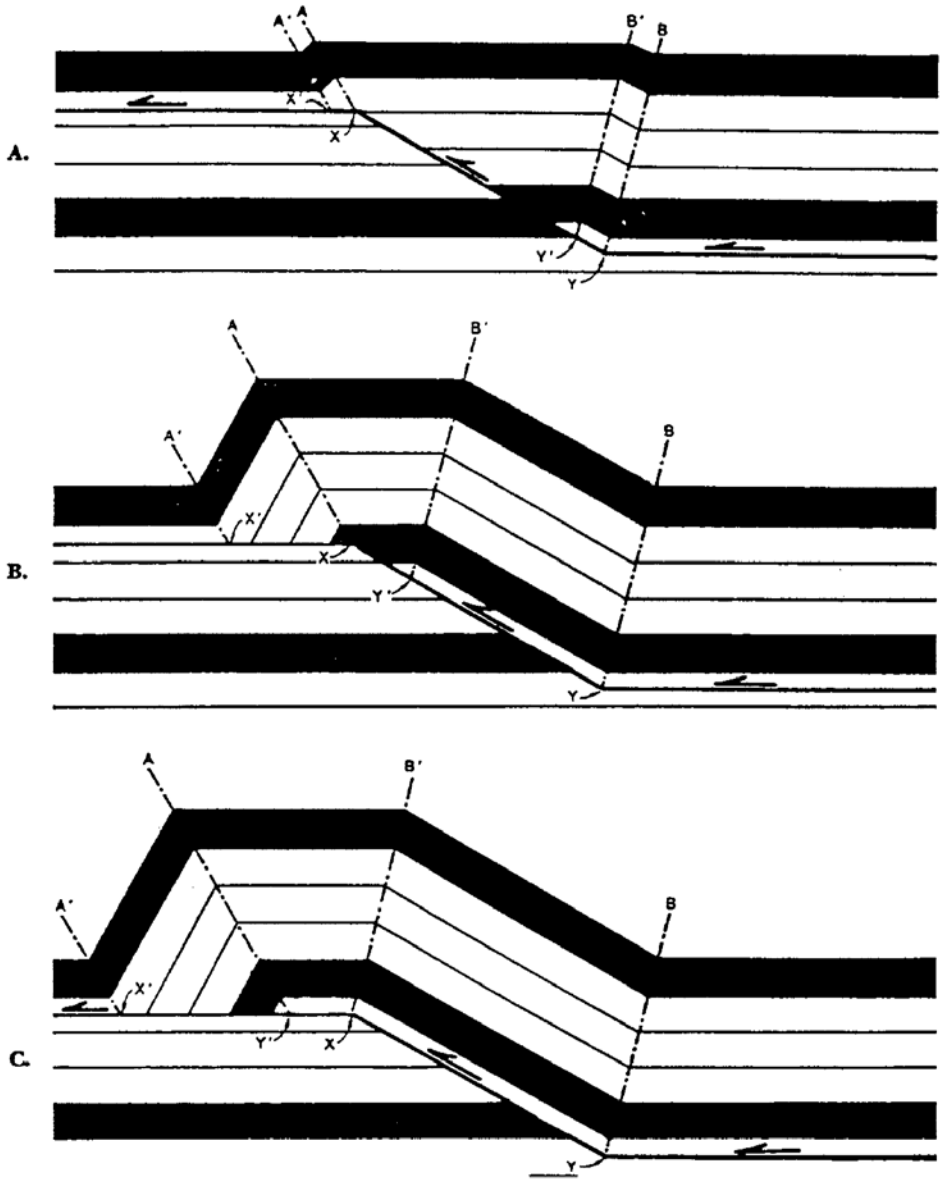

Reprinted by permission of the American Journal of Science

Exhibit 3-27 A, FMI image and core photo of Ellenburger fracture breccia development of a laminated mudstone. B, FMI image and core photo of a carbonate-matrix supported chaotic breccia, Ellenburger Dolomite, eastern Shelf, west Texas (images and core photos adapted from Cain and Hammes, 1997; used with permission)

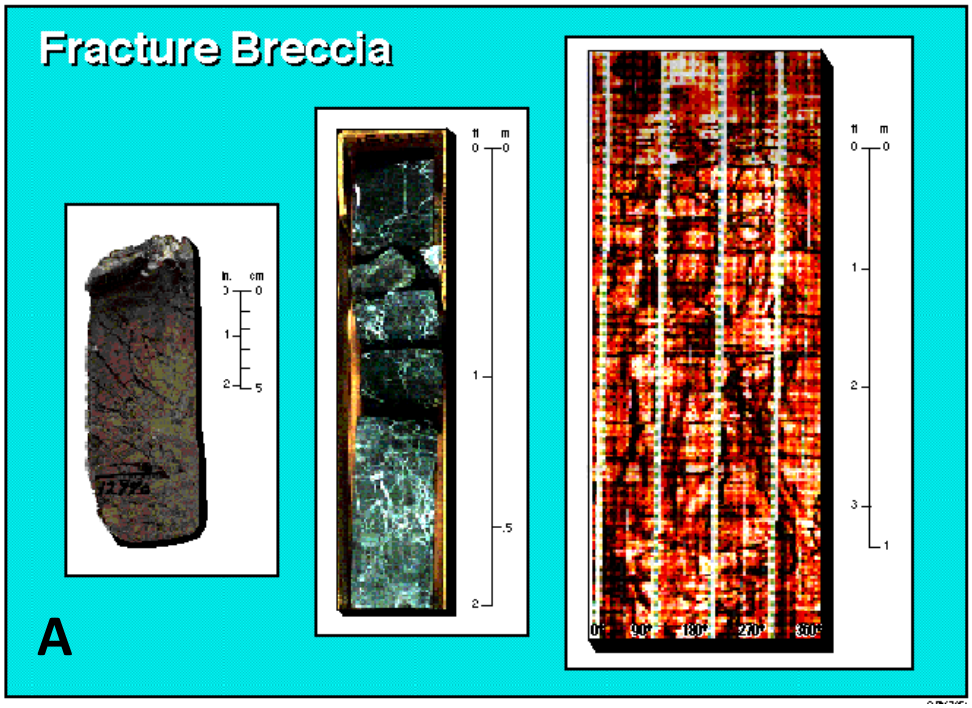

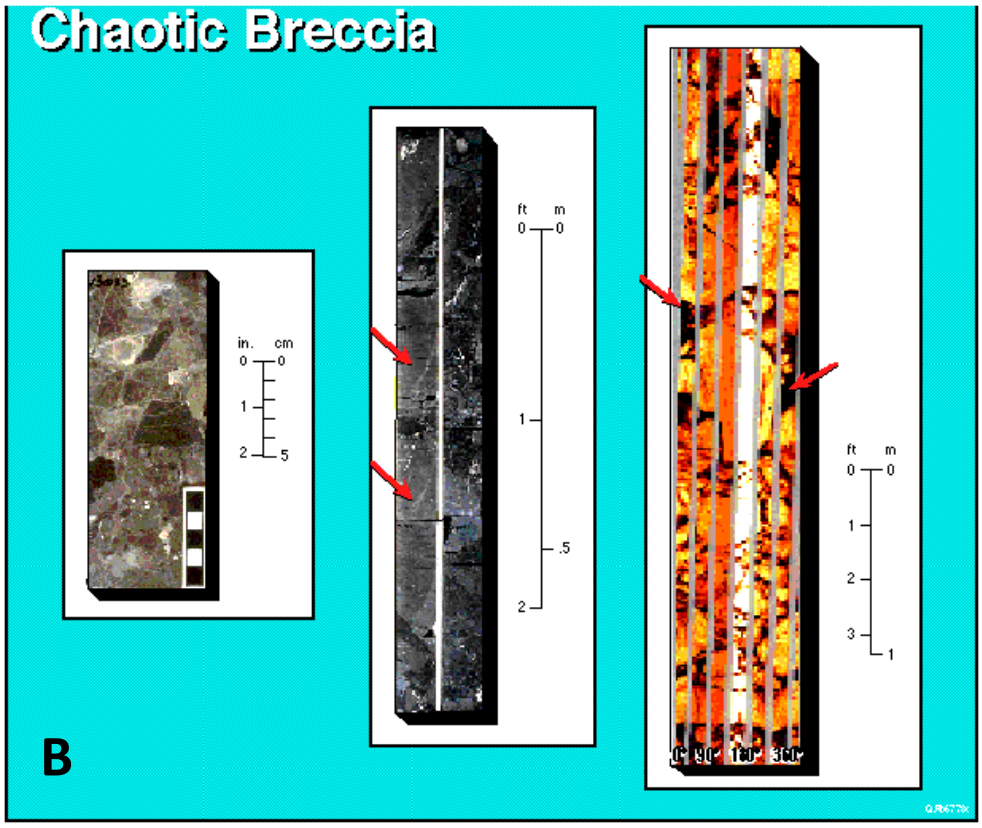

Dark conductive features next to the large clast (red arrows in Exhibit 3-27) are interpreted as combination cavernous secondary and tertiary porosity (Cain and Hammes, 1997). Finally, the literature review of Ellenburger reservoir characterization studies often identified six or more discrete episodes of superimposed, pre-tectonic fracture development followed by Marathon shortening tectonic fracturing and associated alteration-mineralization.

3.1.3 Marathon Tectonic Compartmentalization and Foreland Stress Field

The literature review concerned with the tectonic evolution of the Marathon foreland failed to uncover a structural synthesis, which would adequately explain the distribution of known elements of the Marathon orogeny. The effort by Shumaker (1992) was the most comprehensive; however, it failed to: (a) explain the +1900 mi^2 structural block of the Central Basin platform dominated by N-S-trending anticlinal traps (Exhibit 3-28, yellow region); (b) account for a NE-ENE-bearing of $\sigma_{1H'}$ when the basin is simple sheared by 1st order sinistral, wrench tectonic faults; (c) kinematically justify the 35° of vertical-axis, clockwise rotation of the Central Basin platform structural block and subordinate Puckett rotated block also highlighted in yellow; and (d) propose a 5-mile deep horizontal detachment which underlies the entire Permian basin and may extend westward beyond the limits of the Permian basin. Exhibit 3-28 also shows the location of the Central Basin Platform gas/oil boundary (dashed green line), regional distribution of Ellenburger (blue) and Silurian-Devonian (orange) fields, foreland of the Marathon fold-thrust belt.

The orientation of Enegis' derived strain ellipsoid for the Marathon orogeny is included as an inset in Exhibit 3-28, the structural framework map compiled by Shumaker (1992). Several geometrical and kinematic relationships are immediately apparent and highlighted in the exhibit:

- an ENE-NE oriented σ'_{1H} places the 1st order E-W and WNW-trending mapped faults in sinistral shear;
- four 1st order E-W to WNW-bearing sinistral strike-slip faults are identified and each shown with a hypothetical 25-mile separation;
- included in this sinistral, E-W-oriented shear couple is the regional basement fault shown in Exhibit 3-21 located north of Roswell, New Mexico;
- the major NNW-trending Central Basin platform fault is not a major, dextral wrench fault, rather it is a 2nd order, sinistral accommodation fault;
- sinistral motion on the four 1st order sinistral, E-W-striking faults are linked geometrically and kinematically by the NNW-trending, 2nd order Central Basin platform fault;
- hypothetical, sinistral displacement on each of the three E-W wrench faults (A-B, C-D and E-F shear components) are effectively summed and transferred westward along the northern-most member;
- the resultant left-lateral transfer of displacement along the Central Basin platform margin fault zone explains the tendency for this fault zone to "horsetail" northward as it merges with the E-W-trending *Mi Vida master fault*; and
- the uniform, E-W- to WNW-sinistral shear in concert with the sinistral shear along the Central Basin platform fault allows the 1900 mi^2 Central Basin platform structural block

to rotate freely 35° clockwise relative to the surrounding Permian basin structural blocks (Exhibit 3-28, yellow).

Although areally much smaller, the giant Puckett gas field is similarly rotated 20° clockwise at the juncture of the WNW-striking, Brown Basset-JM sinistral fault and the SSE extension of the Central Basin platform fault. In this geometric and kinematic model, all high-angle reverse faults and low-angle imbricate thrusts indicated on the suite of cross-sections (Exhibit 3-22 and Exhibit 3-23) root at depth into the flat-dipping, through-going, Permian basin detachment at a depth of circa five miles.

Exhibit 3-28 Map locating the Central Basin Platform (gas/oil boundary is dashed green line), regional distribution of Ellenburger (blue) and Silurian-Devonian (orange) fields, and Marathon fold-thrust belt (adapted from Shumaker, 1992)

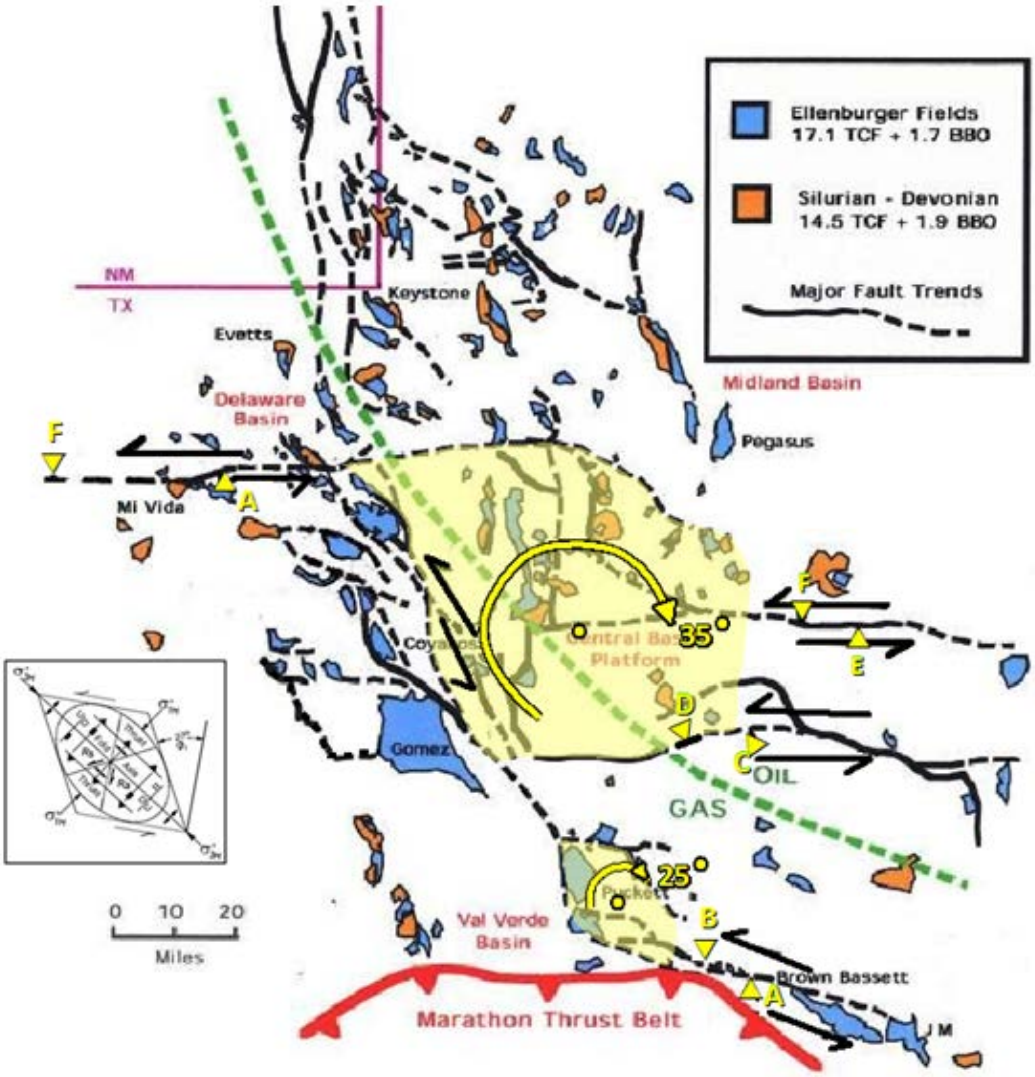

Reprinted by permission of the AAPG whose permission is required for further use

In this perspective, the Permian basin is broken up into a mosaic of rhomb-shaped fault blocks of varying sizes. Fractured, crushed, and brecciated margins of individual fault blocks possess higher net porosity and locally orders-of-magnitude higher permeability. Although flat-dipping, imbricate, intra-Permian basin detachments may not have large amounts of offset, the up-ramp-to-flat fault geometry represent releasing-bend curvatures parallel to the line of kink-bend inflection. Along this line and within the flat thrust plane, small amounts of displacement result in extensive horizontal, deltoid tube-like zones of dilation with near infinite length/width aspect ratios. Sub-horizontal deltoidal tubes act as efficient pathways for lateral, fluid migration, allowing over-pressured fluids to travel laterally for great distances away from the Marathon collision zone. Where horizontal channel ways intercept or contact highly P/P zones along crushed block margins or along block-bounding E-W-, WNW- or NNW-trending 1st and 2nd order conjugate wrench tectonic zones, over-pressured, hot fluids (60-110°C) will migrate upward from the horizontal plumes localized along the flat thrusts to accessing epicrustal, conventional, Ellenburger (blue) or Silurian-Devonian (orange) traps (Exhibit 3-28). Within this geometric-kinematic context, it is reassuring to see the the expected progressive, systematic increase in delta oxygen (O^{18}) isotopes (-9 to -4) along SE-NW fluid pathway-flow lines from the Marathon orogenic belt, across the Permian basin, toward New Mexico, a distance of 100 miles (Kupecz and Land, 1991). Hydrothermal fluids were expelled from the Marathon orogenic belt and moved laterally along: (a) karst-breccia zones and matrix pore-rich units (Exhibit 3-27A, B) or (b) permeable thrusts, wrench faults, syntectonic normal faults and fracture zones enumerated in Exhibit 3-28, where inset G summarizes the proposed orientation of structural elements after 27° of internal shear. The 2nd-order orientation of the principal horizontal stress (σ'_{1H}) bears N45°E-S45°W±15° under the assumed E-W-oriented, penetrative, and simple shear stress field. It is important to note that σ_{1H} rotates progressively counter-clockwise with increasing internal shear being oriented N20°E-S20°W after 67° of internal shear (Exhibit 3-29F). An internal shear angle of 20-30° is representative for most of the Permian basin. Exploration and development programs dedicated to quantifying the orientation of the Marathon foreland strain field will receive huge dividends through the reduction of risk when drilling offset Ellenburger and Silurian-Devonian production wells for subthrust traps beneath the Marathon allochthon.

Hydrocarbon System

The Permian basin covers 8,500 mi^2, is the largest structural basin in North America, and consists of numerous subbasins. The Pre-Pennsylvanian Delaware and Val Verde subbasins lie within the Marathon foreland and subthrust region of West Texas. Marathon facies reservoir rocks are mainly crystalline, cherty dolomite and limestone of Ordovician through Mississippian age. Involved rocks possess porous solution and vuggy porosity and are fractured, faulted, brecciated, and folded. Pre-Marathon Lower Paleozoic carbonate reservoirs are in the Lower Ordovician Ellenburger, the Upper Ordovician Montoya, and the Silurian Fusselman formations. Minor clastic reservoirs occur in the Ordovician Simpson Group. High and low-angle zones of Marathon age tectonic fractures and multiple sets of joints transect the carbonate host rocks forming adequate P/P conduits for oil/gas migration. Individual reservoir thicknesses are in excess of 500 ft and drilling depths range from 8,000 to 24,000 ft.

Hydrocarbon source rocks include: (a) Middle Ordovician shale and limestone; (b) Upper Devonian and Mississippian shale and shaley limestone (Woodford Shale); and (c) Pennsylvanian and Permian basinal shale facies. Major hydrocarbon generation occurred

concurrent with syntectonic flysch deposition during the Permian. Long distance hydrocarbon migration occurred along high P/P wrench tectonic fault zones, zones of porous tectonic breccia localized along the margins of structural blocks and joint systems in the lower Paleozoic carbonates. Trapping mechanisms are structural, involving conventional thrust- or wrench-related compressional-transpressional anticlinal structures. Traps are faulted, jointed, and brecciated concurrent with folding between 335-285 Ma (Marathon orogeny). Multiple intercalated shale and unfractured dolostone horizons serve as effective topseals.

Exhibit 3-29 Simple left-lateral shear model showing sequentially deforming of a fixed circular area with successively increasing angles of internal shear (Øi, 22-67°) (adapted from Davis and Reynolds, 1996; used with permission)

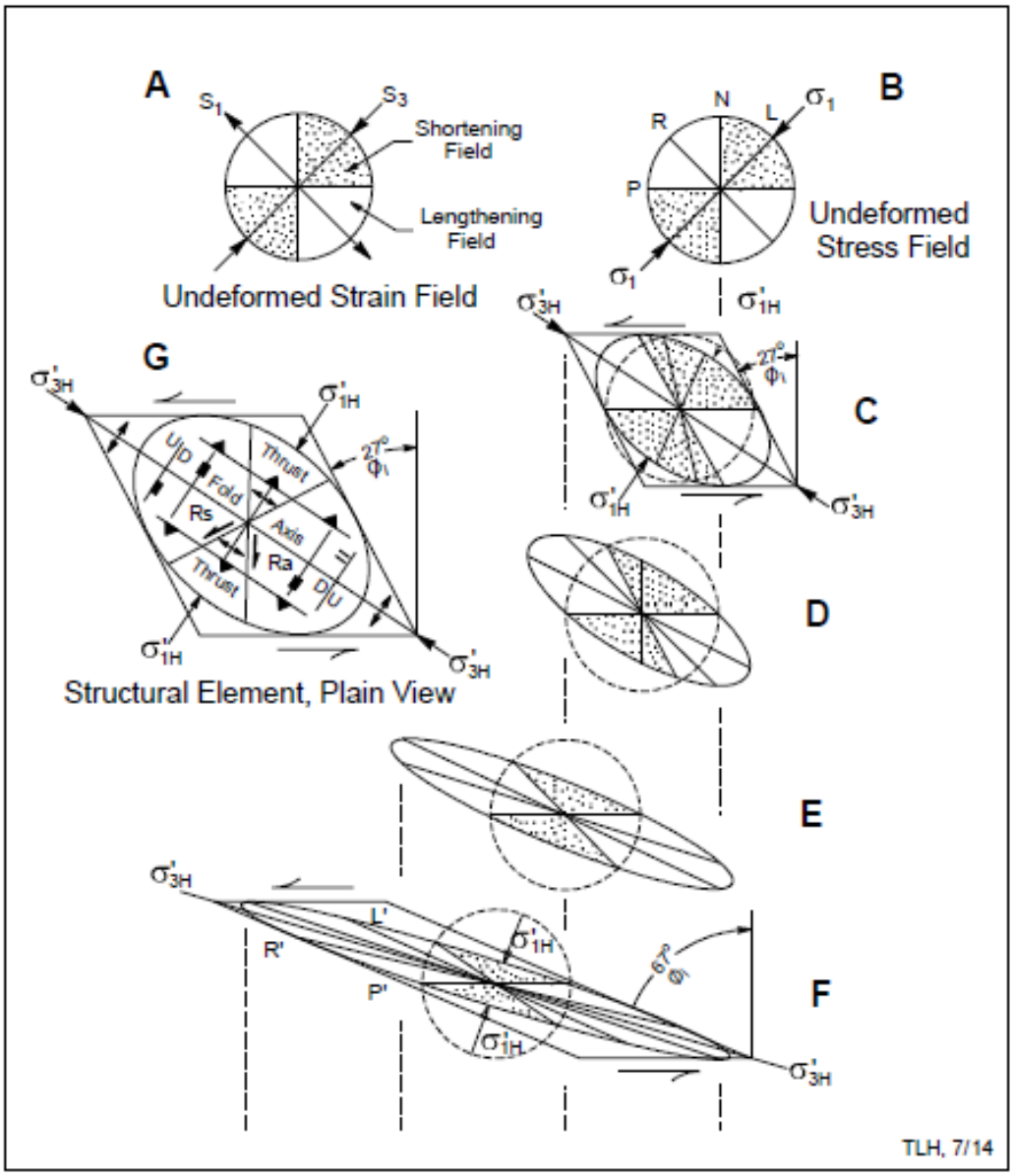

Oil was available for migration from the Late Devonian Woodford Shale into Pre-Pennsylvanian Paleozoic traps during Permian-Early Triassic time. Hydrocarbons produced from these traps are almost exclusively dry gas, indicating: (a) either initial oil in these traps was displaced by subsequent methane gas migration; or (b) early oil was cracked in place to produce the gas that is now present. A combination of these two processes seems necessary to explain the complex, varied and extensive dry-gas concentrations throughout the Val Verde subbasin. Dry-gas migration most likely continues at present. Ballentine et al. (2001) proposed that the CO_2 gas emplacement was early and methane gas was generated later and partially replaced older CO_2 charge.

Burial History, Vitrinite Reflectance and Oil/Gas Generation-Migration

Pawlewicz and Barker (2005) compiled vitrinite reflectance (Ro) data and calculated depths of the 2.0 percent Ro for rocks of all ages from the Permian basin. Exhibit 3-30 reproduces their map of Ro calculated for depths of 2.0 percent Ro. The data have been contoured at sub-sea depths of -7000, -9000, -11,000 and -13,000 ft, respectively. The contoured values produce a pronounced, NNW-bearing "synformal geometry," which extends from the Marathon fold-thrust belt along the eastern margin of the Delaware basin and western margin of the Central Basin platform. The 2 percent Ro "axial deep" is at a depth of -13,000 ft and continues SSE beneath the leading edge of Marathon fold-thrust belt.

The high-standing Ozona arch and Central Basin platform structural blocks flank the synform along its eastern margin. The giant Grey Ranch and Puckett gas fields (Exhibit 3-22, and Exhibit 3-28) are localized on the upthrown hanging-wall block, having experienced over 15,000 ft of differential elevation during Pennsylvanian-Permian loading and foreland shortening during the Ouachita-Marathon orogeny. In the foreland Permian basin, the Devonian Woodford Shale is oil generative between 0.5-1.35 percent Ro, which corresponds to -2,000 to -9000 ft below sea level. The Woodford condensate-wet gas generative window is observed between -9,000 and -14,000 ft below sea level (1.35-2.0 percent Ro) as determined by Cardott (1989). Dry gas is generated at a Ro value of 2.0-2.5 percent Ro at subsea depths of -14,000 to -22,000 in the Val Verde subbasin. According to cross-sections by Shumaker (1992), the Woodford is buried to the lower end of the dry gas window at the bottom of the 2.0 percent Ro synform.

Exhibit 3-31 summarizes established vitrinite reflectance, peak hydrocarbon generation intervals and corresponding depths below sea level for the Val Verde basin and foreland strata underlying the Marathon allochthon. The exhibit speaks volumes as to what mixture of hydrocarbons are expected from the sub-20,000 ft burial of Ellenburger, Montoya, Fusselman and Woodford source rocks beneath the Marathon allochthon. Liquid hydrocarbons are limited and include $_{13\text{-}15}$C-rich, condensate and $_{12\text{-}13}$C-rich methane gas. Methane is still being produced today. CO_2 charge is believed to precede main stage methane generation (Ballentine et al., 2001).

Exhibit 3-30 Map compiles calculated depths to the 2.0% vitrinite reflectance (Ro) values for drilled strata from the Permian Basin, west Texas and southeastern New Mexico (adapted from Pawlewicz et al., 2005)

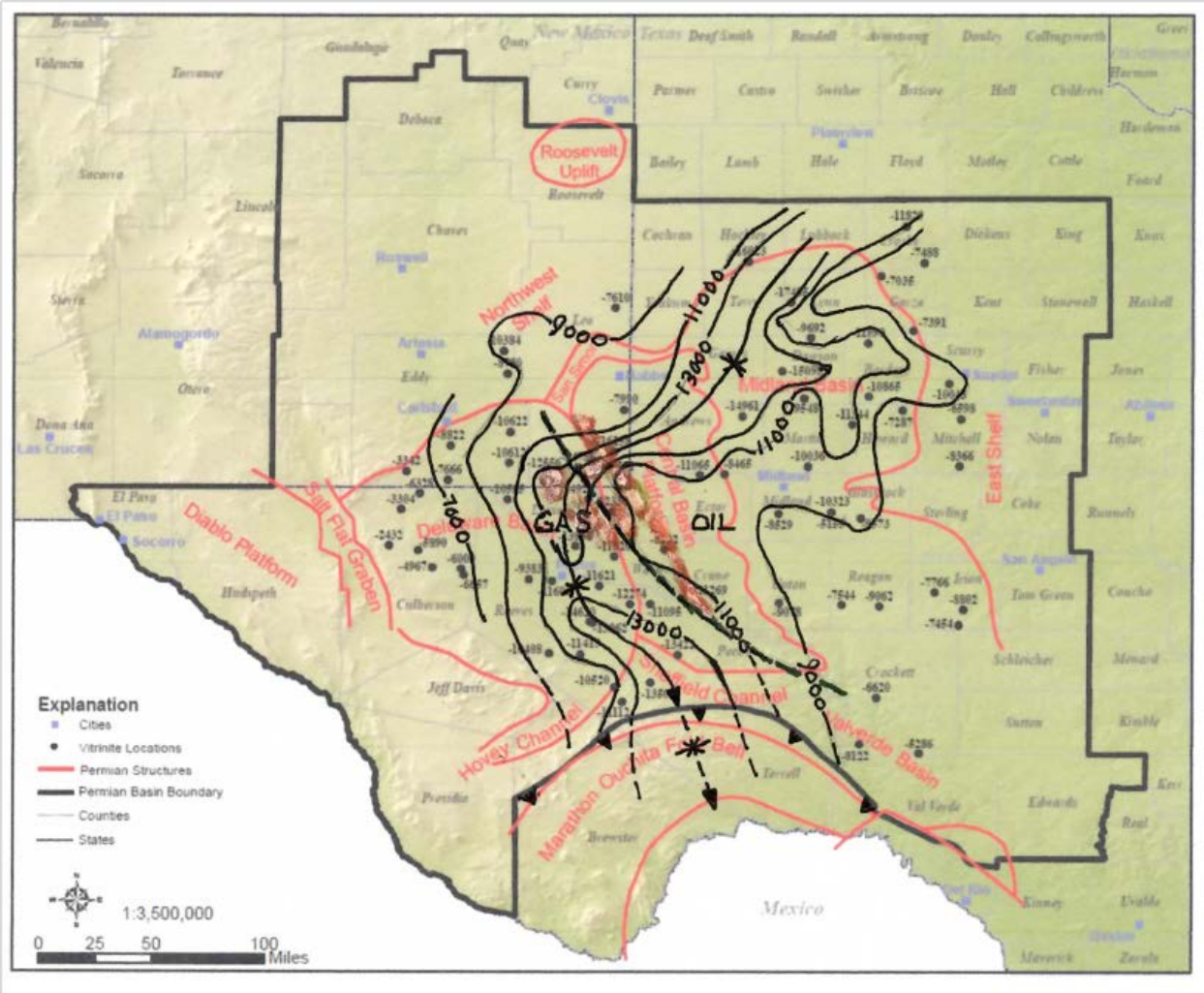

Source: USGS

Exhibit 3-31 Vitrinite thermal maturity range with corresponding depth interval and geochemical event (after Pawlewicz et al., 2005)

Vitrinite Reflectance and Hydrocarbon-Geochemical Event
0.5-1.35%Ro = Oil Window (0.9 peak oil) → Oil deposits
1.35-2.0 %Ro = Gas Window, oil destroyed; C_1-C_4 hydrocarbon gases stable → Wet gas and condensate deposits
2.0-4.0 %Ro = Only methane stable → Dry gas deposits enriched $_{12}C$
>4.0%Ro = Rock metamorphism → Over maturity, minor methane produced enriched in $_{13}C$
Emperical Vitrinite Thermal Stability , Corresponding Depth Interval (Subsea Depths), Hyrocarbon Event
0.5-1.35%Ro =- 2-9,000 ft → Oil deposits
1.35-2.0 %Ro = -9,000-14,000 ft → Wet gas and condensate deposits
2.0-4.0 %Ro = -14,000-22,000 ft → Dry gas deposits enriched $_{12}C$
>4.0%Ro = -22,000 ft → Over maturity, minor methane produced enriched in $_{13}C$

CO_2 Generation, Migration and Trapping Mechanisms

Several CO_2-bearing gas fields are seemingly localized along the leading edge of the Marathon frontal thrust and contain varying amonts of CO_2. Fields include from north to south: Gomez (4 percent); Puckett (30 percent), Thistle (78 percent), and Elsinore (97 percent); and east to west: JM (20 percent), Brown Bassett-East (39 percent), and Brown Basset-West (55 percent). Exhibit 3-32 is an enlargement of the location map of the Pinon field shown in Exhibit 3-24. The relative abundance of trapped gas increases progressively in the direction of the large black arrows. The percent of contained CO_2 gas increases north to south (4 percent to 78 percent) and east to west (20 percent to 78 percent). The highest concentrations of contained CO_2 relative to methane and other traces gases are on the west near the Elsinore and Pinon fields (97-98 percent). It is also in this area that many of the completed wells show relative in the relative percent of CO_2 produced over time. Schoell and Ballentine have researched the isotopic geochemistry of the Val Verde gases in great detail and reported their preliminary results (Ballentine et al., 2001). Based on the distribution of ^3He content and ratios of $^3He/^4He$ (R/Ra), $CO_2/^3He$ and $\delta C^{13}(CO_2)$, they concluded: (a) Rayleigh fractionation caused by partial degassing of a deep-seated magma body is consistent with observed $CO_2/^3He$ and $\delta C^{13}(CO_2)$ variations; (b) CO_2 in the Brown Bassett field is dominated by magmatic CO_2 with only a neglible crustal contribution; (c) the lowest $CO_2/^3He$ ratios are the most pristine samples, and (assuming a simple filling model) are nearest the point source for CO_2 charge; (d) JM and Brown Basset fields have the lowest $CO_2/^3He$ values and is closest to CO_2 charge for the area; (e) methane kitchens lay to the north where fields contain small amounts of residual CO_2 (4 percent), for this reason, CO_2 charge is viewed as having occurred early before methane generation; and (f) a CO_2-rich pluton is believed emplaced coincident with the uplift of the Ozona-Central Basin platform uplift (335-285 Ma) immediately north the Marathon thrust belt.

^3He is a primordial substance in the Earth's mantle and believed entrapped during planetary formation. ^3He is present within the mantle, and about 5,000 times more abundant than ^4He. Ratios of $^3He/^4He$ in excess of atmospheric are indicative of a contribution of ^3He from the mantle. Crustal sources are dominated by ^4He which is produced by the decay of radioactive elements in the crust and mantle. The enrichment of ^3He with the Val Verde CO_2 fields unequivocally indicates a buried magmatic source. Unfortunately, no intrusive rocks of post-

Mississippian age are known from the region. As noted earlier, there are favorable ultramafic and mafic-alkalic suites of intrusions 60 miles toward the SE in the Balcones region. Another possibility is the Mid-Tertiary alkalic intrusions of the Trans-Pecos and Big Bend region of West Texas which is also 60 miles toward the west. Lastly, intrusive rocks with favorable mafic-alkalic characteristics are rarely observed associated with collision zones similar to the Marathon-Ouachita belt. It remains enigmatic as to the suggested Permian age (280 Ma, Ballentine et al., 2001) versus Laramide (Balcones) or Mid-Tertiary (Trans-Pecos), which Enegis believes is more likely.

Exhibit 3-32 Map of the Val Verde subbasin specifies the direction of increase in $CO_2/^3He$ ratios toward the Marathon fold-thrust belt (black arrows). CO_2 gas emplacement precedes CH_4 generation (Ballentine et al., 2001) (Contours (4, 30, 50, and 75 percent) added by Enegis, LLC)

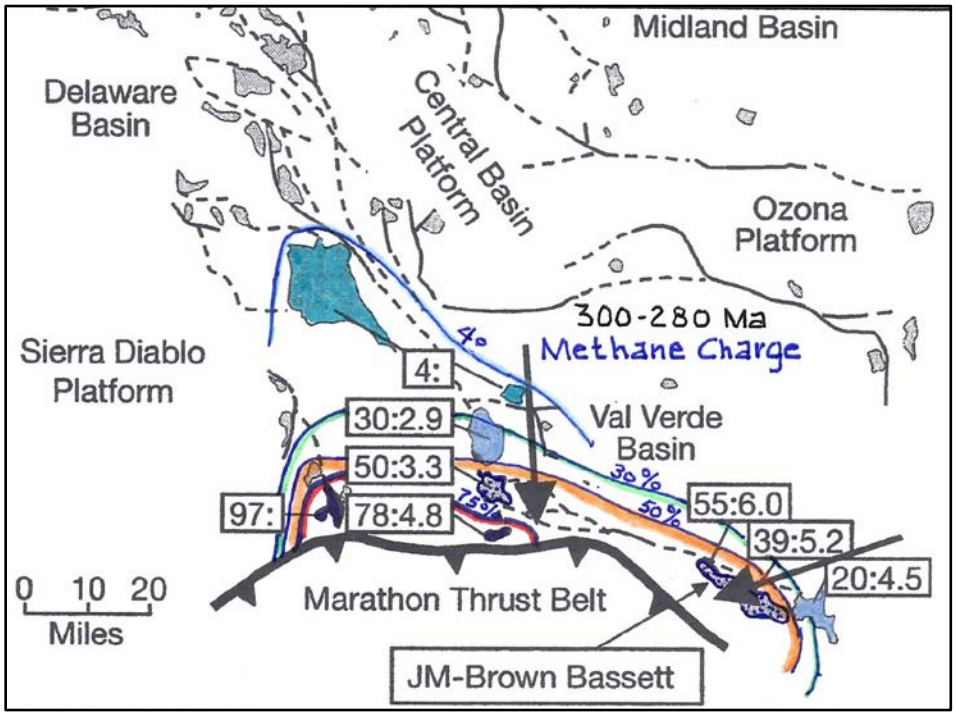

Reprinted by permission from Macmillan Publishers Ltd: Nature, copyright 2001

We have contoured percent contained CO_2 (4, 30, 50 and 75) in all the referenced fields in Exhibit 3-32. An alternative interpretation of the CO_2 field distribution is that the observed CO_2 is not localized along the leading edge of the Marathon fold-thrust belt; rather, we are looking at the northern distal edge of a blind CO_2 plume that underlies the Marathon allochthon. Exhibit 3-33 and Exhibit 3-34 respectively depict the hypothetical areal extent and CO_2 isograds in subsidiary plumes localized within the: (a) lower Marathon frontal thrust zone and (b) Permian basin detachment at approximately 4-6 miles subsea. Exhibit 3-33 depicts the lateral extent of the Marathon frontal thrust plume and hypothetically Caballo traps (blue stippled area) localized along the 1st through 3rd Caballos thrust plates of the lower Marathon allochthon.

Exhibit 3-33 Structural framework map of the Val Verde subbasin and Marathon-Ouachita fold-thrust belt, west Texas (structural details created with info from Shumaker, 1992; Barden and Franklin, 2003; and Enegis, LLC). The envisioned CO_2 plume is localized within the Marathon allochthon; contoured CO_2 isograds given in percent contained gas and is the source of CO_2 charge for Leads 1-5 (blue stippled areas). Reservoirs are multiply brecciated Caballos Novaculaite (Units 1-3), which are tightly folded along with associated strata

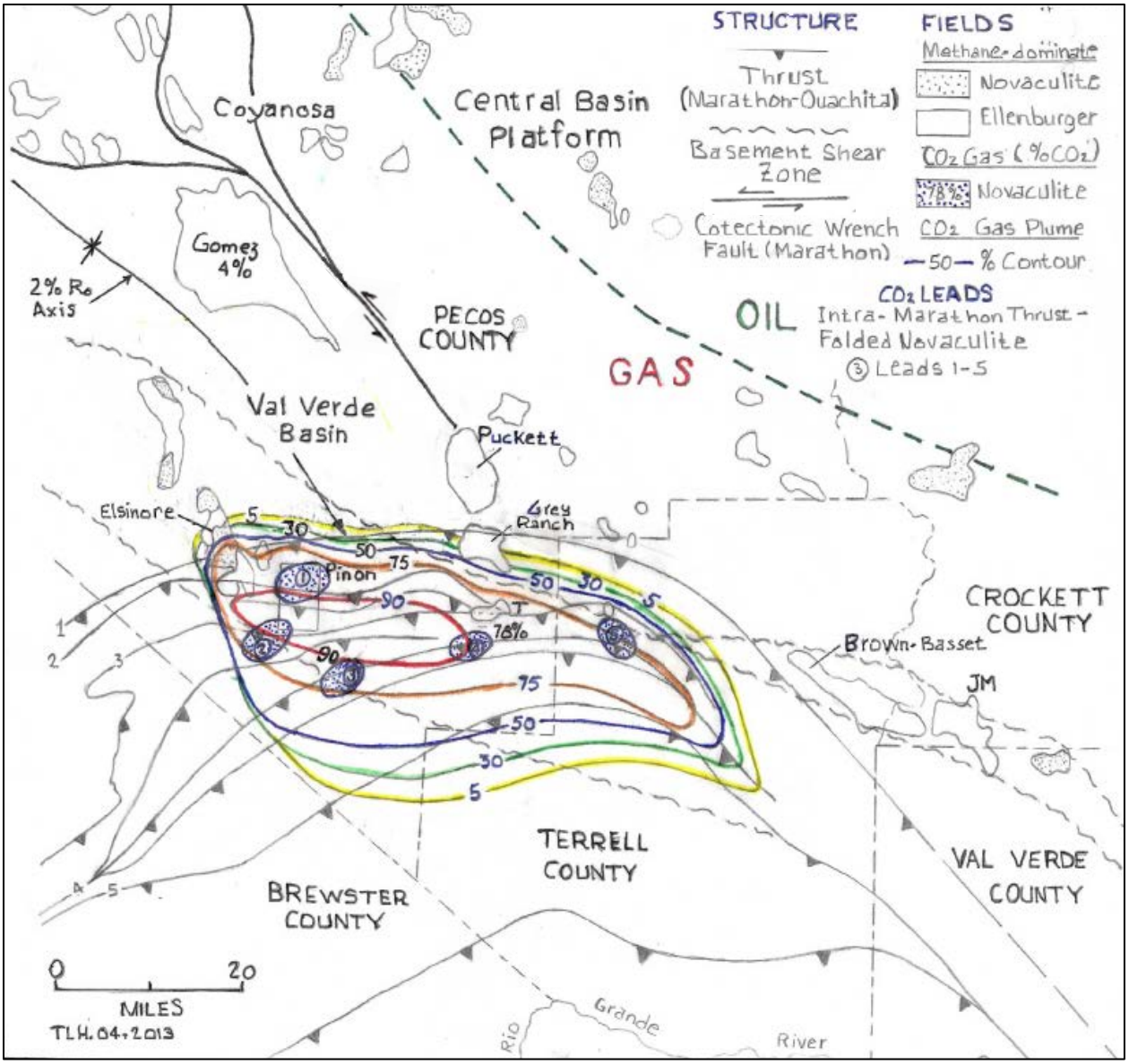

Exhibit 3-34 Structural framework map of the Val Verde subbasin and Marathon-Ouachita fold-thrust belt, west Texas (structural details created with info from Shumaker, 1992; Barden and Franklin, 2003; and Enegis, LLC). The envisioned CO_2 plume is localized along the Permian basin detachment with traps localized within the Marathon subthrust facies (principally Ellenburger Dolomite). Contoured CO_2 isograds given in percent contained gas and represents the CO_2 source plume which charged Leads 1-8 (blue stippled area)

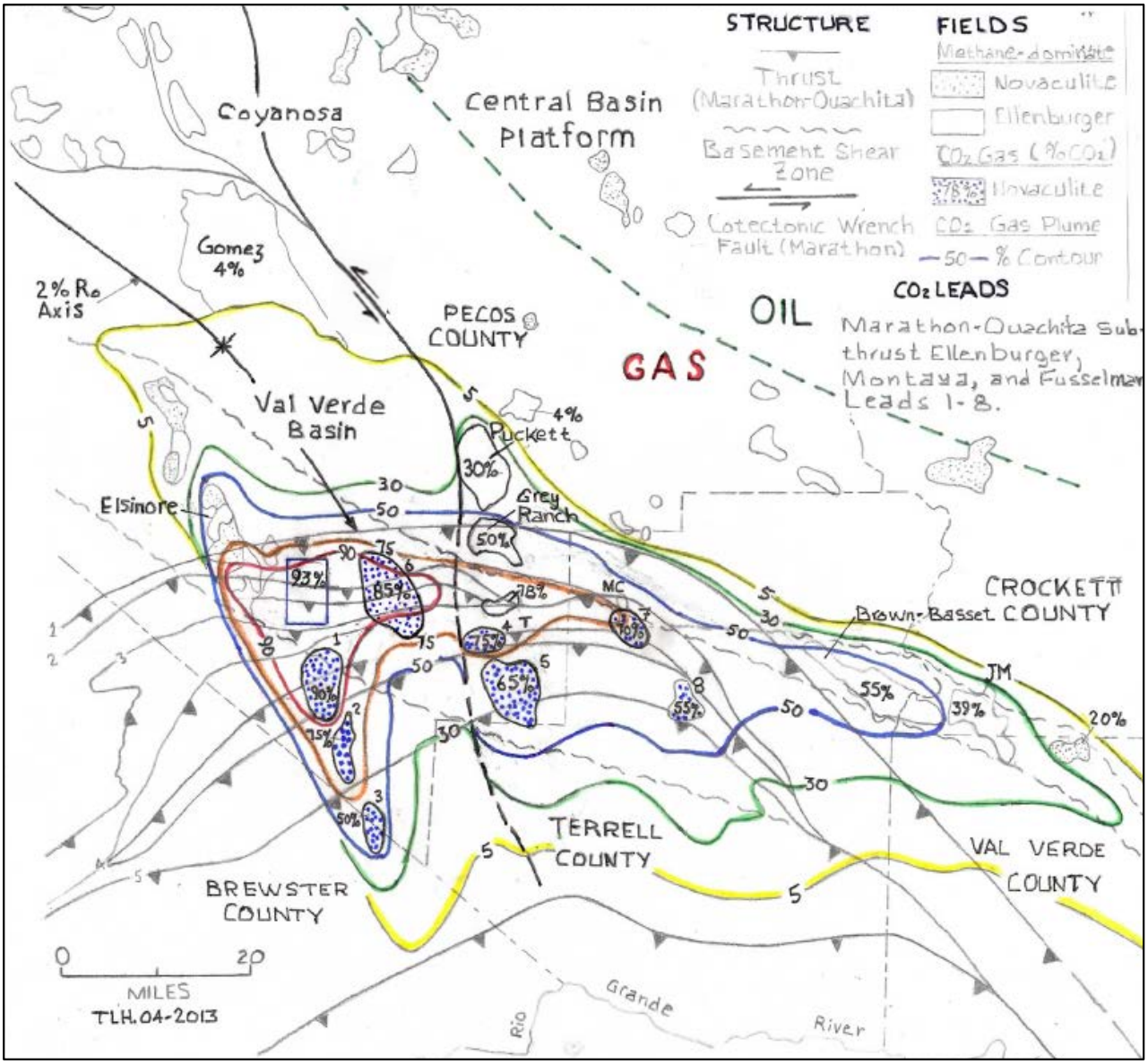

The envisioned Marathon allochthon CO_2 plume is sub-horizontal and extends from the Elsinore-Pinon area on the west to beyond the Thistle-McKay fields on the east, a distance of about 60 miles. Brecciated Novaculite localized along the hanging-walls of respective thrusts, and associated brecciation/cataclasis along individual thrusts and associated releasing bends focus the flow of supercritical CO_2 fluid. The size, shape, elongation, and distribution of Leads 1-5 are hypothetical and guided by earlier reviewed results from the Pinon area (Barden and Franklin, 2003). It is also apparent that we envision a second CO_2 point source in the Pinon area, which is indicated by the 97 and 98 percent CO_2 contents in producing reservoirs at the Elsinore and Pinon cluster of fields. A major, depth-penetrating, WNW-trending, sinistral wrench fault is projected beneath the Marathon allochthon. This shear zone is about 18 miles south of and parallel with the 1st order Brown Bassett-Puckett wrench fault highlighted in Exhibit 3-33. Both of these 1st order wrench faults are viewed as strategic in helping focus and channel migrant supercritical CO_2 fluids vertically from the Permian Pedernal basin detachment plume through the overlaying crystalline basement and linkage with lower Marathon frontal traps.

Exhibit 3-34 is similar in nature and concept with Exhibit 3-33. In this instance, we show the hypothetical distribution of CO_2 charged traps localized within the Lower Paleozoic Ellenburger, Montoya and Fusselman formations. Fields are arranged in two, uplifted and folded, NW-NNW-trending fairways along the flanks of the 2 percent Ro synformal axis detailed in Exhibit 3-30 and discussed earlier. Leads 1, 2, 3 (west), and 4, 5 (east) are conventional, upright, thrust-controlled anticlines with settings similar to the Puckett and Grey Ranch (Exhibit 3-22). Lead 6 mimics the structural setting of the supergiant Gomez gas field localized by divergent conjugate reverse faults along the 2 percent Ro synformal axis (Exhibit 3-22 and Exhibit 3-23, Gomez-Phillips 1EE and Gomez-Heiner cross-sections). Smaller Leads 7-8 are local pop-up fields along 2nd order NNW-striking restraining bends in the underlying Ellenburger (Exhibit 3-23, Waja field). The size, shape, and distribution are similar to that developed in the adjoining Val Verde, Central Basin platform and southern portion of the Midland basin (Exhibit 3-28).

The envisioned CO_2 plume is large, covers over 800,000 acres, extends from north of the Elsinore field on the west to beyond the Brown Bassett-JM fields on the east, a long dimension of 110 miles by a 25-mile width at the 50 percent CO_2 isograd. The envisioned CO_2 point source remains fixed beneath the Pinion-Thistle area. Supercritical CO_2 charge is channeled upward along sub-vertical breccia-tubes localized at left-stepping, releasing-bends along the postulated WNW- and NNW-trending 1st order sinistral shear zones. Where the vertical channelways contact extensive areas of folded and tectonic fractured and karstified porous chaotic, collapse and solution breccias of the Ellenburger, the plumes spreads out laterally parallel to the structurally subhorizontal karstified zones. The Lower Paleozoic traps are larger, laterally more extensive, easier to discover-develop, but at considerable depth where only small amounts of dry gas coexist with nearly pure, supercritical CO_2-^{3}He fluids.

Introduction

The Sweetgrass-Kevin CO_2-prone region resides with a 38,000 mi^2 area of the High Plains of north-central Montana and adjoining Saskatchewan. The area of interest is characterized by a diagnostic suite of relatively small alkalic, mafic alkalic, and ultramafic igneous within-plate intrusions. Emplacement of this unique suite of alkalic intrusions involves a narrow geologic time frame lasting only eight million years (54-46 Ma). Our analysis commences with a brief description of plate and regional tectonic frameworks of the American Northwest bracketing the middle Laramide (early-middle Eocene) timeframe.

Exhibit 3-35 summarizes the general distribution of known North American kimberlite, carbonatite and alkali-mafic lamproite-alnoite occurrences. The Farallon-Kula subduction zone is approximated by the barbed line along the west coast. Present-day Los Angeles (L) and Vancouver (V) are labeled for reference. Arrows generalize net convergence vectors between North American and Farallon plates at 150 Ma (ESE, 5 in/yr); 100 Ma (NNE, 4 in/yr); 75 Ma (NNE, 3 in/yr) and 25 Ma (≤1 in/yr). Motion vectors are generalized after Cox et al. (1989). The suggested location of kimberlite-carbonatite isochrones (150, 100, 50, 25, and 2 Ma) are from this study. Instantaneous convergence vectors for the Farallon/North American plates (arrows) are summarized for both 75 and 25 Ma which bracket the radiometric ages of representative intrusions from the Montana alkalic intrusive province (Exhibit 3-36). There is a tight and pronounced cluster of ages centered at ±48 Ma (middle Eocene). The instantaneous net motion vectors given (Cox et al., 1989) suggest that convergence vectors continued to rotate in a counter-clockwise manner with rates decreasing during the 150 Ma interval. Stylized intrusion isochrone lines for 150, 100, 50, 25, and 5 Ma and supplemental data points for the western U.S. are from this study. Note the persistent westward decrease in radiometric ages across the continent. This pattern appears less consolidated following the post-125 Ma counter-clockwise rotation of F/NA convergence from E-W to NNE-directed with commencement of Laramide mountain building. Laramide, Mid-Tertiary and Late Tertiary (75, 25, and 5 Ma) isochrone lines continue to get younger westward across the continent. Stylized migration and distribution of post-75 Ma intrusions are distinctly more compartmentalized. This is certainly the case for the cluster found on the High Plains of Montana. A more local regional tectonic event appears responsible for the observed alkalic intrusive cluster (54-46 Ma), which does not continue laterally into Canada or to the south along the Southern Colorado Rocky Mountains.

Exhibit 3-37 is a partial paleo-geographic and -tectonic sketch map of the western U.S. at circa 50 Ma (Heidrick, 2013). Several co-tectonic structural elements and terranes in the American Northwest are highlighted to help characterize the regional and plate tectonic setting in the vicinity of the Montana alkalic intrusive province. The docked, thickened Siletzia microplate is delineated in green; the shoshonitic, calcic- and calc-alkalic volcanic province encompassing the Absaroka, Challis and Clarno arcs are highlighted in pink; the double black line demarks the southern edge of the 55-50 Ma subducted Siletzia-Farallon slab (Humphreys, 1995). The sixteen alkalic, mafic alkalic, and ultramafic intrusive centers inscribing the middle Eocene Montana alkalic province are from this study. Exhibit 3-37 shows several unique regional structural and plate tectonic relationships relative to the Great Plains alkalic province. More specifically, the 310-mile-wide Siletzia oceanic microplate (green) is docked and empalled into present-day northern Oregon, western Idaho and north to near Seattle, Washington (Madsen et al., 2006).

Exhibit 3-35 Map summarizes the Mesozoic and Cenozoic distribution of kimberlite, carbonatite and lamproite intrusive complexes recognized on the North American plate (adapted from McCandless, 1999; used with permission)

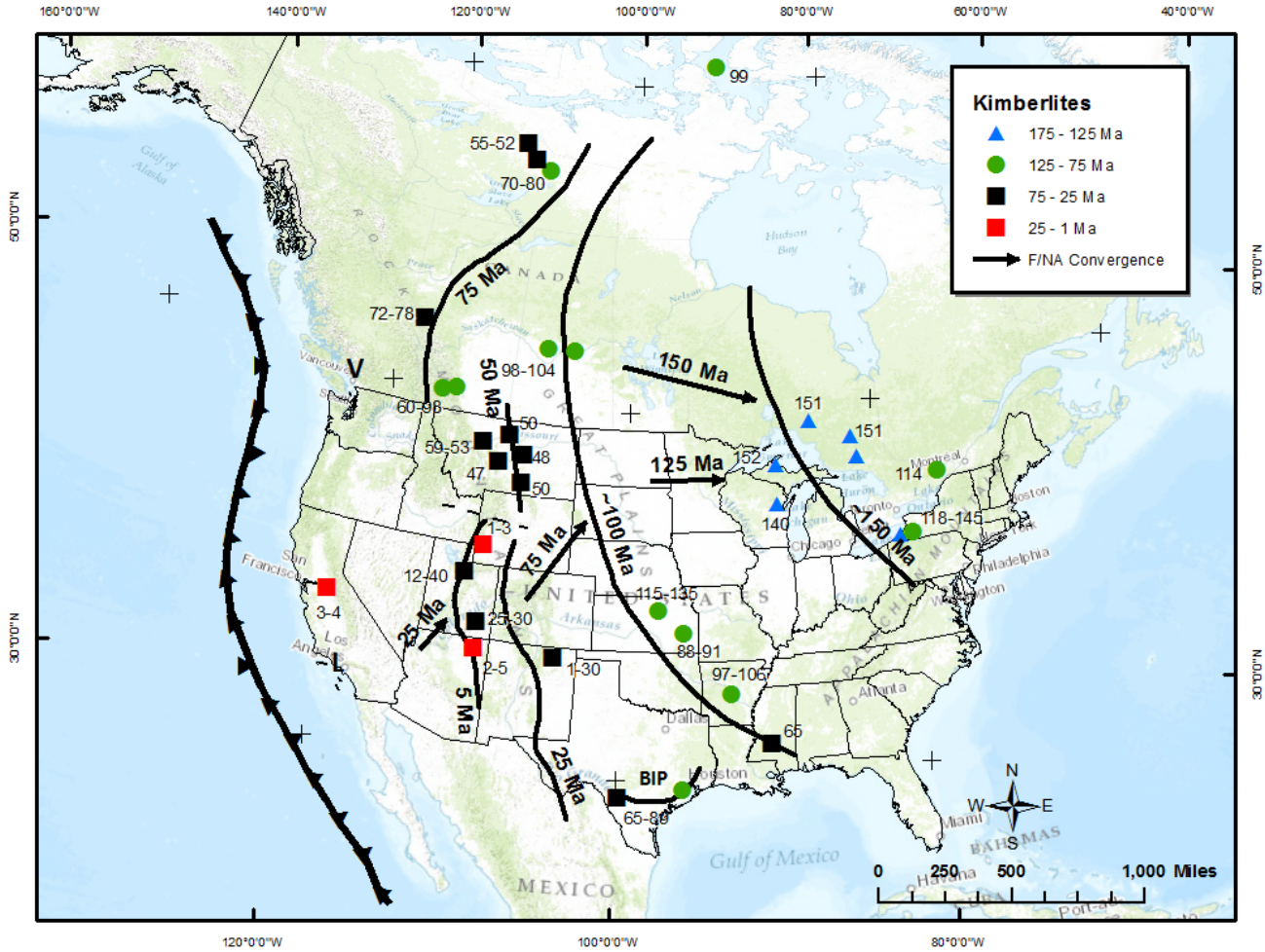

The exact orientation and palinspastic disposition of the Kula-Farallon spreading center relative to North America is portrayed as centered off Siletzia; whereas, Madsen, et al. (2006) shows the ridge further north near the northern limit of known Siletzia rock types. The general outline of the shoshonitic, calcic, and calc-alkalic Eocene Absaroka (55-39 Ma), Challis (55-44 Ma), Clarno (54-40 Ma) and Kamloops volcanic trend is highlighted in pink as modified from Humphreys (1995, 2009). The N-S trend of metamorphic core complexes (solid black) show the predominate orientation of stretching/cataclasis and tectonic transport (arrows) in several complexes (52-40 Ma) from south to north: Snake Range, Ruby Range, Raft River, Bitterroot, Priest River, and Okanogan-Shuswap. Concurrent with Siletzia accretion, Farallon-Kula subduction was re-established offshore west of Siletzia and a more normal proto-Cascadian volcanic arc commenced to develop parallel to the trench (45-40 Ma).

Exhibit 3-36 Radiometric age data, Great Plains Alkalic Province, Montana*

Formation	Age (Ma)	Description
[1]Mill River Minettes	52-49	Phlogopite-clinopx-apatite xenoliths and lamproite
Host minette dike	50	SRI's, εNd_t and Pb isotopes similar to GPAP Middle Laramide intrusions
[2]Sweetgrass Hills	54-50	Shonkinite→ syenite→ trachyte and lamprophyre
East Butte		Alkalic monzonite, syenitic trachyte, latite
Middle Butte		Diorite porphyry laccolith, Gold Butte ghost town
West Butte		Diorite porphyry, monzonite, granite
[3]Haystack Buttes		
Kimberlite-carbonatite	48	Monticellite peridotite
[4]Bearpaw Mts		
Laccolith-plugs	*54-50*	K-syenite, monzonite, latite, shonkinite, pyroxenite
Rocky Boy (K-spar)	53	Pyroxenite, shonkinite, monzonite, qtz monzonite, Ne-syenite, syenite, leucite phonolite, pegmatites
[5]Rocky Boy (Biotite)	50-51	Two K/Ar ages, both younger than Eagle Buttes K-feldspar age
[6]Highwood Mts	53-50	
[7]Missouri Breaks Diatremes		
Ainoites	52-50	SRI's = 0.717, eNdi=-34.85, Nd age of 2.9 Ga
[8]Williams kimberlites	48-47	Western region is late Laramide and ultra-mafic carbonatite
Little Rocky Mts	67-60	East of Missouri Breaks, sub-alkalic early Laramide
[9]Little Belt Mts (episode 1)	62-60	Sub-alkalic early Laramide intrusions
Little Belt Mts (episode 2)	54-52	Ar/Ar ages, quartz monzonite and monzodiorite
[10]Little Belt Mts (episode 3)		Carbonatite K-syenite biotite, vermiculite, REE, carbonate-sulfide veins; LREE, high-K, LILE/HFSE, εNd=Group 2 common
[11]Judith Mts Kimberlite	69-67; 67-62	
[12]kimberlite-carbonatite	<47	Calc-alk→ alkalic→ultramafic
[13]Grass Range UMA		Aillikite, alnoite, monchiquite
Homestead	~50	Carbonatite, associated kimberlite diatremes
[14]Moccasin Mts	66-64; 53	
[15]Crazy Mountains	51-50	Ar/Ar, Na-mafic neph syenite, Ne-syenite, trachyte
Total range	53-46	Rb/Sr, Ar/Ar; alkalic suite of intrusive rocks
Northern Mts UMAC	50.1	Ar/Ar, ultramafic, mafic neph. syenite and syenite
Comb Creek stock	51-48	Whole rock and Rb/Sr, Na-nepheline syenite
Big Timber stock	49, 46	Sub-alkalic gabbro (K-basalt, diorite, granodiorite)
Southern Mts	49	Ar/Ar, sub-alkaline Big Timber and Loco Mtn stocks
[16]Porcupine Dome	<56	Carbonatite, associated aillikite
[17]Absaroka Volcanic Prov.	55-39 (Idaho-Montana)	
Washburn Volcano	55-52	Oldest exposed rocks are calc-alkalic
Sunlight Volcano	50-48	
Western avg plugs	48-39	Bunsen Pk, Birch Hills and Washakie Needles

*See Exhibit 3-35 for superscripted locations within the Montana alkalic igneous province, where the superscripted numbers are identified in red.

Exhibit 3-37 Paleo-tectonic and -geographic map of the western U.S. circa 50 Ma. Base map personal communication (Heidrick, 2013)

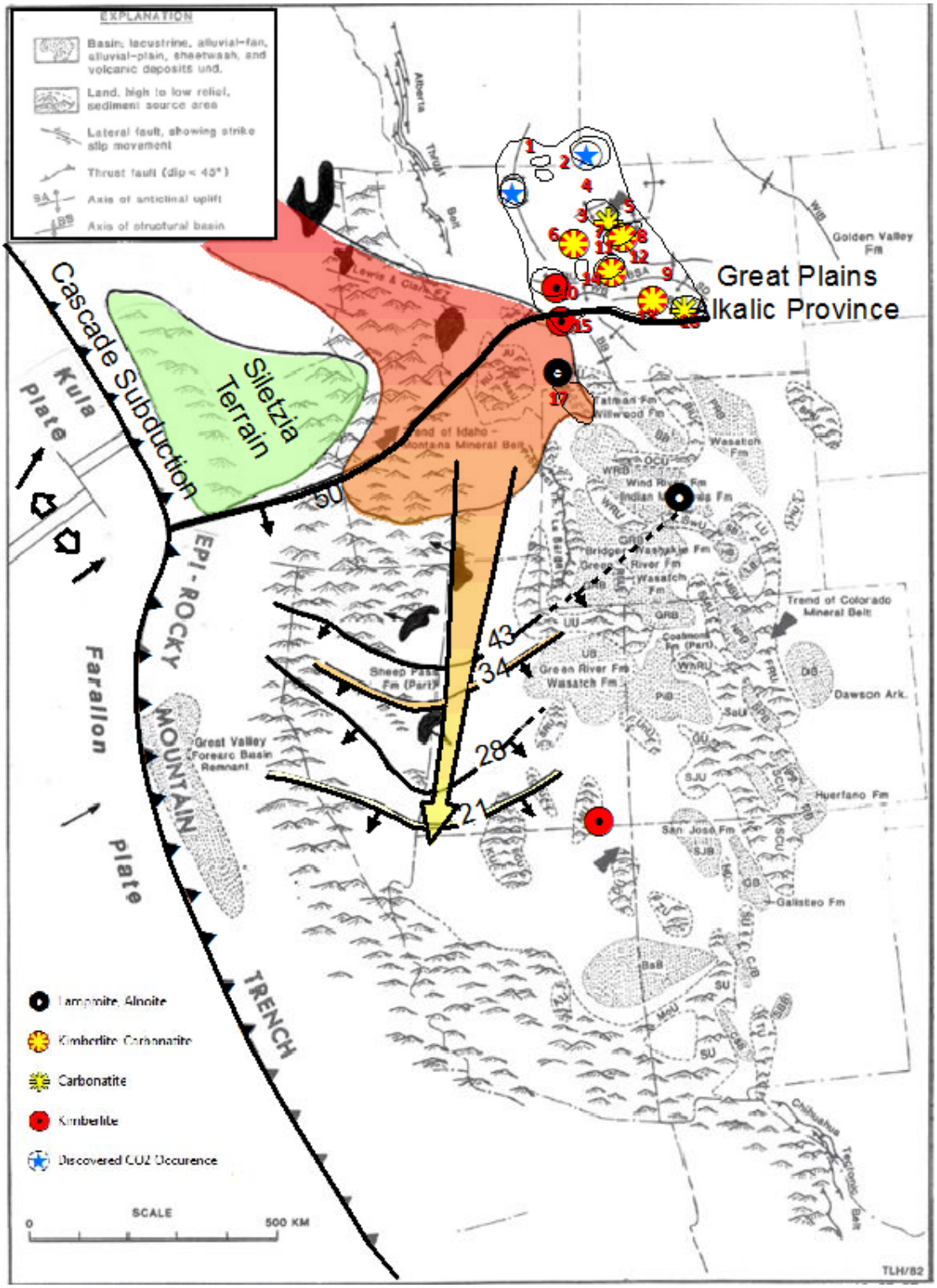

The ENE-trending, double red line extending paralleling the Trans-Idaho and Montana mineral belt (Great Falls shear zone) represents the southern edge of subducted Siletzia terrane at circa 48 Ma. At this time it represents a regional, crustal-scale transfer zone separating the flat-dipping, Laramide Farallon slab to the south from the more steeply dipping American Northwest (Kula) slab on the north (Humphreys, 1995). Major consequences of tearing cleanly through two plates and overlying North American lithosphere along the Great Falls shear zone include: (a) the northern Kula plate rolls back toward the W-WNW between 48-43 Ma, progressively extinguishing magmatism in a retrograde fashion from ESE to WNW; (b) concurrently, the southern, flat-dipping Farallon plate also rolls back more obliquely fueling the Basin and Range ignimbrite flareup; and (c) the flounding Farallon plate sinks, under goes partial melting as the slab progressively rolls back rapidly from 48-43 Ma (2 in/yr) and more slowly from 43-21 Ma (0.5 in/yr). The isochrone lines for initial volcanism along the slabs floundering trajectory are shown in Exhibit 3-37 following restorations, suggestions and insight summarized and reported by Humphreys (2009).

Lastly, note the E-ENE continuation of the southern edge of the subducted Siletzia-Farallon slab. It appears to demark the southern boundary of the Great Plains alkalic province along a curvilinear line connecting known mafic-alkalic intrusive complexes in both the Crazy Mountains (53-49 Ma) along the SW margin of the province and Porcupine dome (carbonatite and aillikite, <56 Ma) on the SE (see Exhibit 3-36). Clearly, the transition zone separating the region of normal subduction in southern Canada from the flat-slab province underlying the Southern Rocky Mountains (S of Montana and NE Wyoming) is transected by numerous depth-penetrating, crustal-scale shear zones of ENE trend (Jorgensen, 2004). Long, linear shear zones with this orientation represent important avenues of ingress for migrant, CO_2-rich, middle Eocene ultramafic and mafic alkalic intrusions and streaming, supercritical CO_2 fluids and melts channelized upward along the sub-vertical shear zones.

Exhibit 3-38 looks west at a block diagram portraying the magmatic and tectonic setting of the American Northwest at circa 50 Ma (Madsen et al., 2006). The Farallon (dark grey) and Kula (grey) plates are labeled and the Farallon-Kula spreading center is E-W oriented and terminates at the Epi-Rocky Mountain trench (barbed black line) in the vicinity of Seattle, Washington. The NA plate is underlain by flat, ENE-dipping Farallon and Kula slabs shown torn clean through along a separating jagged, zigzag suture. Above the floundering, shallow-dipping (10°) Farallon slab, the Absaroka (A) and Challis (Ch) coeval volcanic arcs are highlighted with more alkalic shoshonitic volcanoes (A, red to orange) and somewhat more calcic (B, orange-red, orange). On the more steeply-dipping Kula plate (25°), transitional alkalic volcanoes are localized next to the suture becoming more calcic to felsic calc-alkalic (yellow) northward away from the tear. The thickened Siletzia micro-plate is not shown; however, by 50 Ma it is docked and embedded in the hanging-wall of the NA plate (see Exhibit 3-37). A propagating tear in the underlying flat-dipping (10°) subducted Farallon (south) and steeper-dipping (25°) Kula (north) plates. The ENE-bearing motion vector on the Farallon plate diverges by 25° relative to the faster moving Kula plate.

Exhibit 3-38 Schematic block diagram looks WNW across the American Northwest at the envisioned subduction regime at circa 50 Ma (adapted from Breitsprecher et al., 2003)

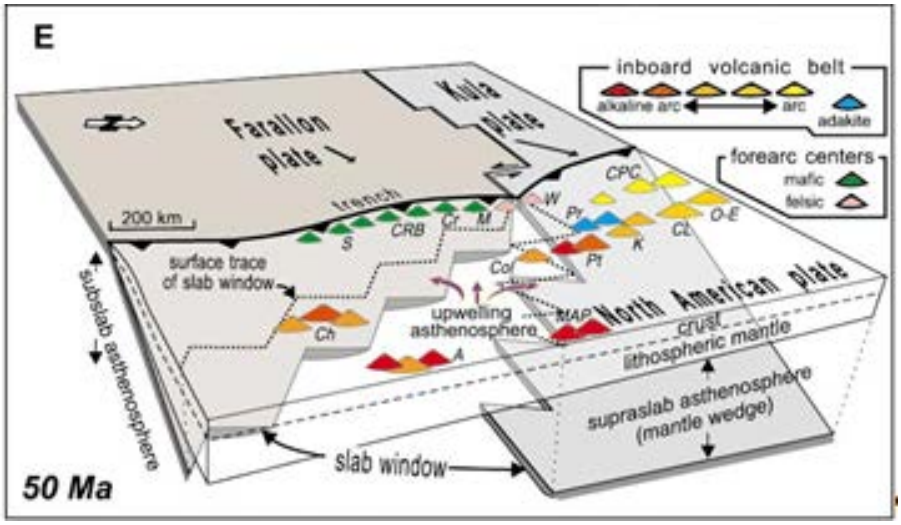

Used with permission from Geological Society of America (GSA)

The divergent motion vectors and ambient trench-ridge-trench triple junction geometry support the propagating tear and widening slab window with time. The lateral variation in magma chemistry is indicated by designated colors: inboard silica deficient alkalic (dark red, Montana alkalic province (MAP)), and alkalic-shoshonitic (red-deep orange, Absaroka, A and Challis, Ch); arc calcic to calc-alkalic (deep orange to light orange, K, Cl) and normal calc-alkalic (light orange-yellow, CPC). Mafic (green) and high silica felsic volcanic centers are localized in the Siletzia hanging-wall adjoining the Farallon trench and adjacent to the trench-ridge-trench triple junction. Adakitic (blue) magmatism is localized along the margins of the tear or around areas of upwelling asthenosphere within the slab window area. Detailed petrochemical and isotopic geochemical studies on American Northwest intrusive and extrusive rocks (Madsen et al., 2006) substantiate many aspects of the proposed working hypothesis. The integration of regional structural and plate tectonic relations summarized in Exhibit 3-37 and this 3D model (Exhibit 3-38) helps explain many of the complex petrochemical and geochemical relationships documented within the CO_2-rich High Plains alkalic province of Montana.

The N-S-trending chain of mafic volcanoes (S, CRB, Cr, and M, green) above the Epi-Rocky Mountain subduction zone represents late Eocene intrusive-volcanic centers forming the proto-Cascadian arc (oldest magmatism is ~43 Ma). Motion vectors on the Farallon and Kula plates are divergent (±25°) and helped facilitate the initial tear and subsequent separation and development of the "slab window" beneath which there is no subducted slab and the underlying hot mantle occurs at shallower depths than normal. The consequence of this unique tectonic and magmatic setting: (a) the jagged suture and intervening slab window separating the two divergent slabs, help focus upwelling heat, hot asthenosphere, primitive melts produced by slab break-up/partial melting, foundering of low-angle slablets and streaming supercritical fluids including H_2O, CO_2 and F depending on petrochemistry of consanguineous magmas; (b) accounts for the observed foreland alkalic intrusions characterizing the High Plains area of Montana and NE Wyoming; and (c) influences the co-tectonic emplacement of alkalic, silica

under-saturated intrusions and associated kimberlite diatremes and carbonatites up to 900 miles inboard in the northern Black Hills of South Dakota.

Exhibit 3-38 shows sequential NE-SW oriented, generalized cross-sections at 60, 50, and 40 Ma summarizing the evolution of subduction geometries heralding the termination of Laramide shortening in the American Northwest (Schmandt and Humphreys, 2011). The series summarizes fundamental Farallon/North American plate geometries at: (A) low-angle Farallon subduction (60-55 Ma); (B) docking of the Siletzian microplate with subsequent stalling and rollback of Siletzia/Farallon slab (53-50 Ma); and (C), terminal buoyant neutral slab geometry (45-40 Ma). The subduction of youthful, warm Farallon lithosphere under conditions of very high net convergence during the early Paleocene promoted low-angle subduction beneath the American Northwest (A). Between 55-53 Ma a thickened, cold, Siletzian oceanic microplate measuring 180-250 miles in width contacted the North American plate along the Epi-Rocky Mountain trench (Exhibit 3-37) and greatly reduced the net convergence rate between Siletzia lithosphere and North America. The marked reduction in net Siletzia/North America convergence and docking of Siletzia resulted in stalling Siletzia-Farallon subduction and a marked increase in subduction dip, rollback toward the WNW and eventual renewed subduction of oceanic Farallon lithosphere west of the Siletzia microplate (B). Between 53-50 Ma, subduction beneath the Absaroka and Challis volcanic arcs (Exhibit 3-37 and Exhibit 3-38) ceased as the Farallon-Siletzia plate progressively rolled back toward the W-WNW ultimately sinking vertically under the influence of gravity (C).

The consequence of WSW-directed rollback of the flat-dipping Farallon-Siletzia slab: (a) terminated lateral Laramide compression; (b) promoted E-W-directed crustal scale extension across the foreland of the Rocky Mountain Cordillera in Montana and Wyoming; (c) induced major instability in the mantle due to pressure release (extension), partial melting and up-welling of hot asthenosphere behind the retreating hanging-wall (mantle wedge) of the steepening slab; and (d) fostered structural, tectonic, physical, and petrochemical conditions conducive to the epicrustal localization of silica under-saturated, alkalic to ultramafic kimberlite, carbonatite and lamproite-alnoite magmas enriched in CO_2, F, and an assortment of metals across 38,000 mi^2 of the High Plains of north-central Montana (Exhibit 3-37).

Exhibit 3-39 Succession of stylized, E-W-oriented, cross-sections across the American Northwest (adapted from Humphreys, 2009; used with permission)

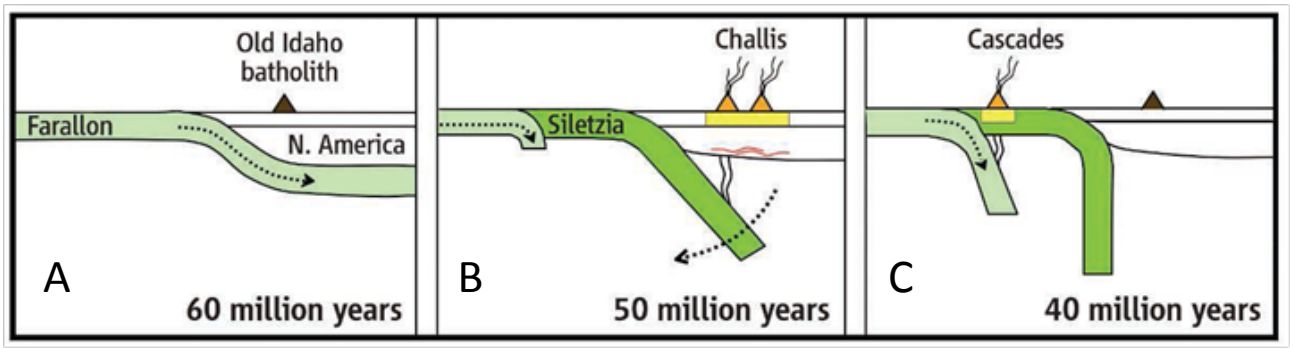

The geologic setting of NW-central Montana is summarized in Exhibit 3-40. The regional ENE-bearing Great Fall shear zone is shown centered on Great Falls, Montana, and incorporates the Bearpaw and Little Rockies Mountains. The sketch map locates the Sweetgrass arch and Kevin-Sunburst anticline lying 40 miles inboard from the leading edge of the Cordilleran fold-thrust belt. The Sweetgrass arch is a major early Paleozoic structural feature. Following Late Jurassic peneplanation through the early and middle Laramide the structure remained relatively quiescent, but was rejuvenated during middle Laramide folding and gentle Miocene upwarping into its present structural configuration – a gently NNW-plunging (2-3°), 200 mile long, asymmetric, ENE-vergent, anticline showing "10,000 ft of structural relief (south arch)" (Shepard and Bartlow, 1986). The ENE-striking Pendroy transverse transfer fault displaces the Kevin-Sunburst anticline over 30 miles in a right-lateral sense. This suggests the entire area west of the offset anticline axis and respective forelimbs are rooted at depth with a low-angle, WSW-dipping, ENE-vergent imbricate thrust. This blind Sweetgrass-Kevin-Sunburst thrust is responsible for much of the 10,000 (south arch) and 600 ft (north arch) of structural closure observed across the two Sweetgrass structural compartments, respectively. It seems relevant that the 50 mile, ENE-elongate Bearpaw Mountains parallels the Pendroy transfer and is organized with a left-stepping, en echelon geometry. The 30-mile-wide saddle which separates the South Sweetgrass arch and Kevin-Sunburst anticline is similar to the bulk curvature separating the Pendroy transfer and the Bearpaw Mountains. The intervening area between the lateral projections of the Pendroy fault and long axis of the Bearpaw Mountains may represent another 30-mile-wide zone of distributed shear. Lateral, transcurrent transfer zones of this scale, age, and foreland tectonic setting are proven routes of lateral migration for co-tectonic fluids along the entire length of the margin separating the Great Plains and the Rocky Mountains and Sierra Madre Oriental in Mexico. As emphasized previously, the western Montana foreland is traversed by numerous ENE-bearing wrench-related shear zones similar to those documented using regional gravity and 3D seismic data by Jorgensen (2004).

Exhibit 3-41 presents a geologic map of the Kevin-Sunburst anticline, north-central, Montana. Mapped alternating moderate green and tan members of the Cretaceous Colorado Formation help define the gently, ENE-vergent, double-plunging bulk curvature of the anticline. In the upper NE corner of the map depicts the general geology of the West and Middle Hills intrusive complexes of the Sweetgrass uplift. Recent detailed mapping, sampling, and geochemical-isotopic-petrochemical studies of the alkalic, mafic-alkalic, and felsic igneous rock suites of the Sweetgrass Hills and adjoining Milk River intrusions in Saskatchewan by Ruklov and Pawlowicz (2012) demonstrate: (a) emplacement ages of the olivine minettes and late stage lamprophyre intrusions have radiometric ages (K/Ar and Rb/Sr) between 54-50 Ma (Exhibit 3-36); (b) intrusions plot within the alkalic chemical field containing between 5-11 percent K_2O and SiO_2 ranging between 45-77 weight percent (foids, phonotephrite, shoshonite, trachybasalt and tephriphonolite, and rhyolite); (c) overall, intrusions having a prevailing lamproite-olivine minette petrographic-petrochemical signature; (d) intrusions enriched in titanium (Ti), K, phosphorus (P), Rb, Nb, Th, uranium (U), zirconium (Zr), Hf and LREE elements; (e) lamproites and minettes have $^{143}Nd/^{144}Nd$ (εNd) and $^{87}Sr/^{86}Sr$ ratios varying between -12.4- -19.4 and 0.7051-0.7075, respectively, which plots them within the Montana group 2 field along with intrusions from the Crazy, Bearpaw, and Highwood Mountains; (f) many of the individual intrusive complexes with associated stockwork alteration-mineralization show anomalous concentrations of F, gold (Au)-silver (Ag), tungsten (W), C (CO_2) and tellurium (Te)-selenium (Se); and (g) minette magmas are believed to have evolved at mantle lithosphere depths under

oxidized conditions with CO_2-rich fluids in the presence of primary calcite, magnesite, phlogopite, and abundant titanomagnetite.

Exhibit 3-40 Geologic sketch map of the Sweetgrass arch and Kevin-Sunburst anticline, North-Central Montana. Top Madison Limestone is contoured with a 1,000 ft interval (map modified after Shepard and Bartlow, 1986; limits of the Great Falls lineament after Mueller and Frost, 2006; used with permission)

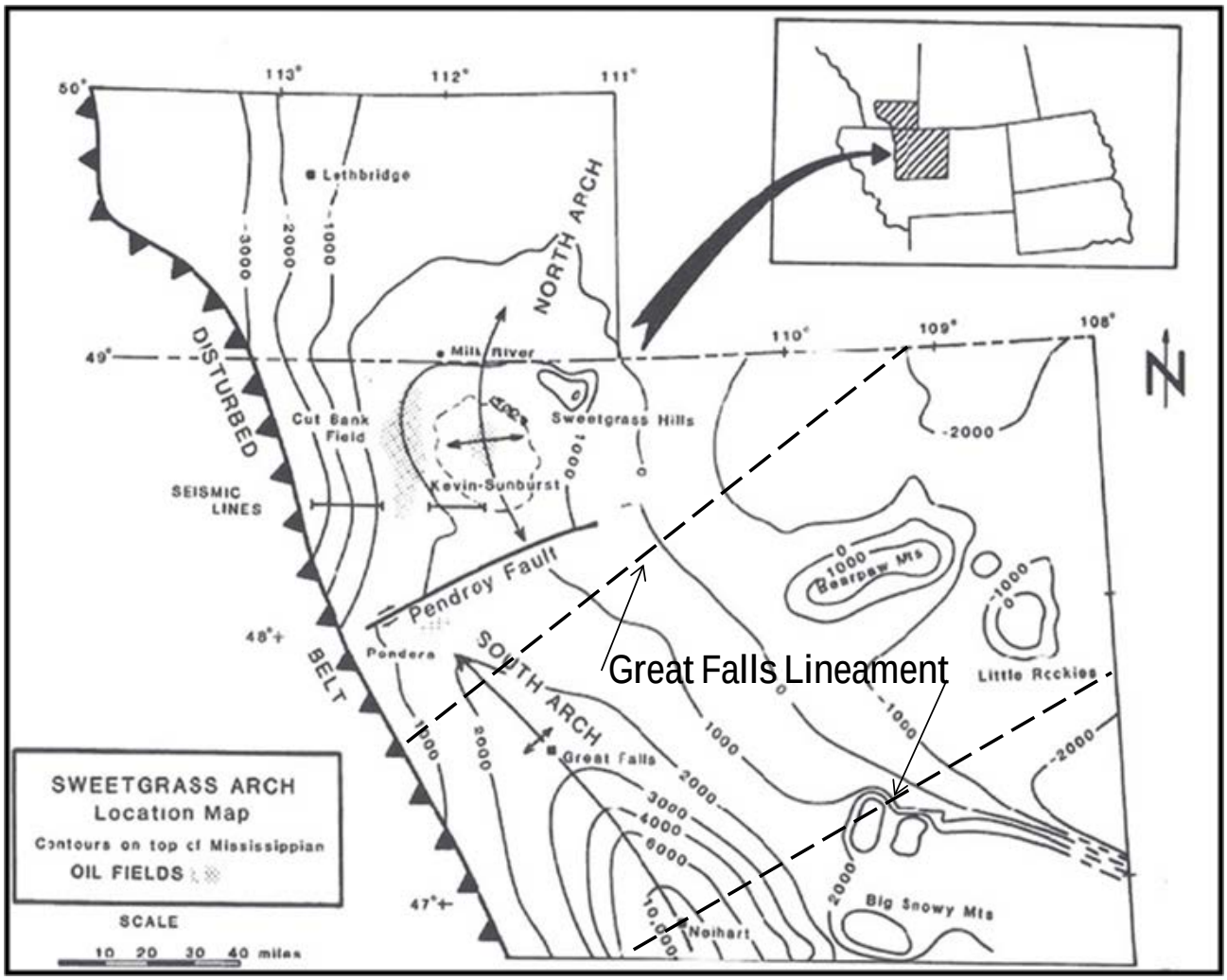

Exhibit 3-41 Geologic map of the Kevin-Sunburst anticline, north-central Montana (adapted for the Montana Geological Society, 1985; used with permission)

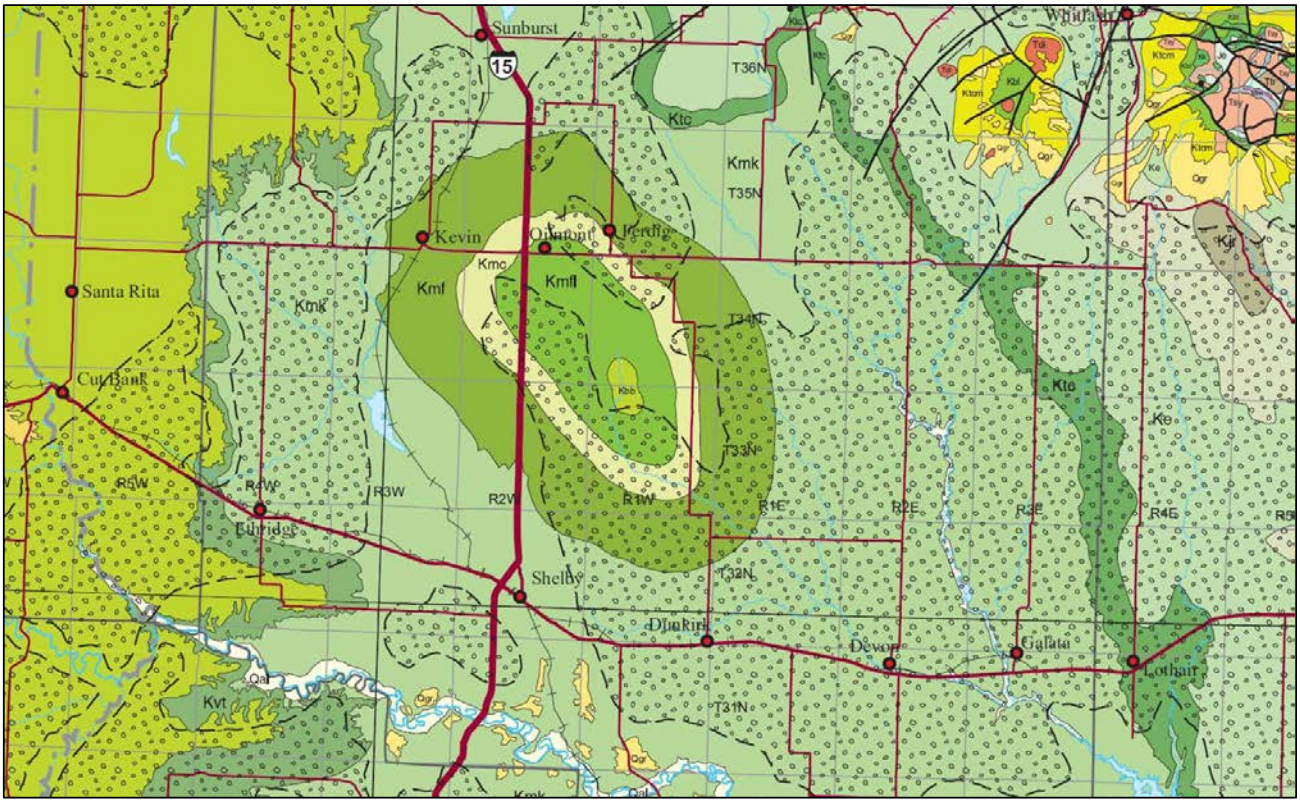

The newly reported data from the Sweetgrass Hills and Milk River region of the northern-most Montana alkalic province are viewed as favorable with a high potential of producing significant deposits of CO_2. An obliquely oriented, NW-SE diagrammatic cross-section across the Kevin-Sunburst anticline is shown in Exhibit 3-42. The cross-section shows major sedimentary units (Cambrian-Cretaceous), stylistic distribution of oil (green), methane gas (red) and local area of CO_2-bearing reservoirs within the Devonian Duperow Formation. The section shows major depositional units, axial structural relief (±600 ft) and generalized distribution of oil (green) and methane gas (red, unless labeled otherwise). Principal reservoirs include: (a) Devonian Duperow and Nisku carbonate-evaporate-grainstone succession; (b) karst-related disconformable oil and methane gas accumulations at top Mississippian Madison Limestone; (c) channelized Cretaceous sandstone units; and (d) potentially untested Cambrian and Ordovician clastic succession underlying the Devonian Duperow. Very few wells penetrate these deeper units in the Sweetgrass-Kevin area although regional isopach maps suggest their presence in the subsurface. The overall Kevin-Sunburst fold geometry is provided by multiple borehole penetrations to the top Mississippian Madison carbonate reservoir. Exhibit 3-43 shows the contoured top Madison Limestone at a 100 ft contour interval. Map projects oil-bearing reservoirs (green) and methane gas reservoirs (red). The E-W distribution of oil/gas reservoirs is suggestive of fault-controlled compartmentalization of hydrocarbon resources at Kevin-Sunburst. The hypothetical E-W-bearing compartment shear zone is a likely strand of the regional Great Falls shear zone and the mapped Pendroy fault shown immediately down-plunge (SSE) from the anticline (Exhibit 3-40). The top Mississippian Madison contour map and details are adapted from Big Sky Carbon

Sequestration Partnership studies. Contours are visibly crowded together on the NE-facing flank of the slightly elongate anticline.

Exhibit 3-42 A, Typical well log curves for principal stratigraphic units, Kevin-Sunburst field; and B, oblique, NW-SE-oriented, generalized cross-section across the Kevin-Sunburst anticline (data adapted from the Montana Geological Society, 1985; used with permission)

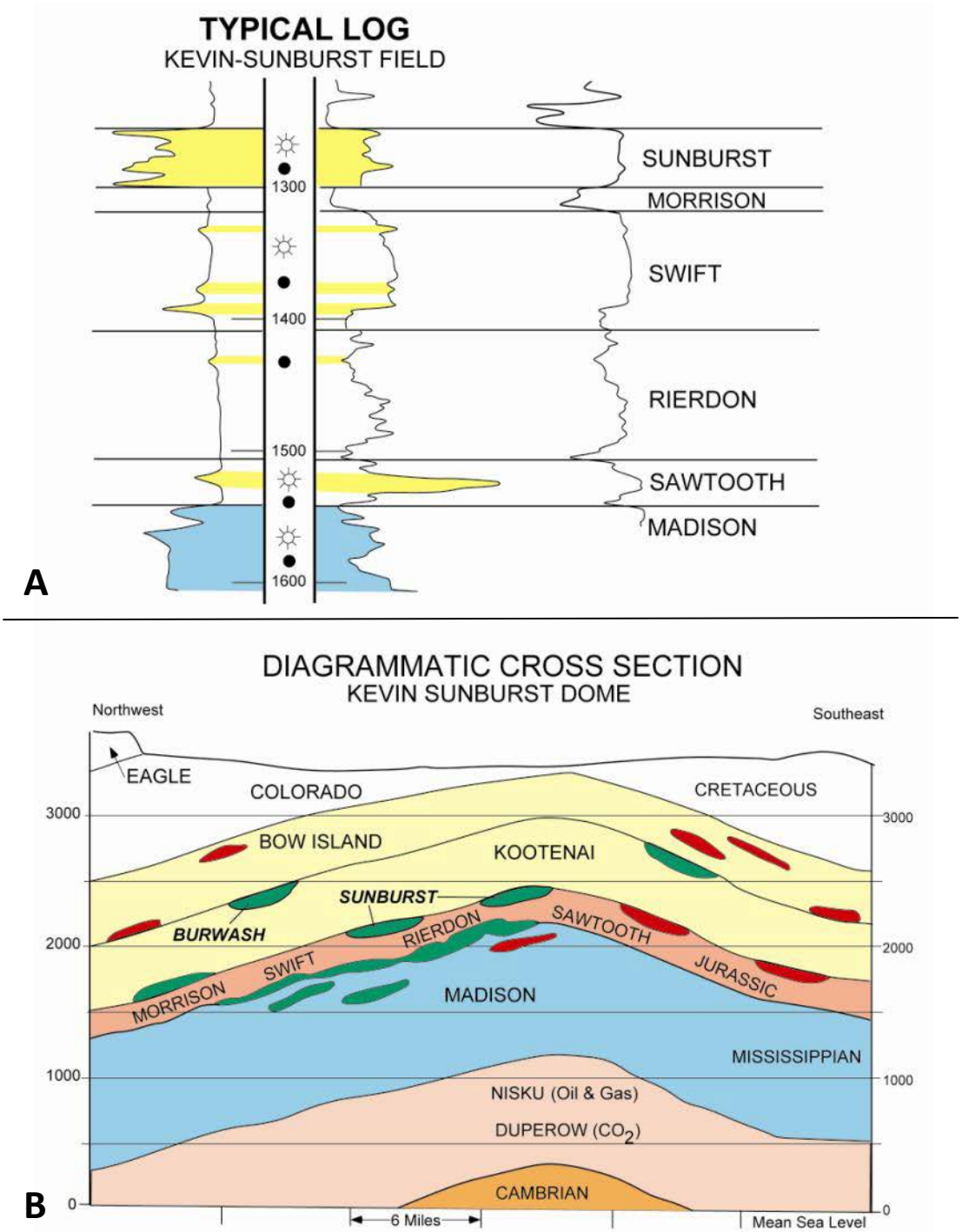

Exhibit 3-43 Structural contour map at top Mississippian Madison Limestone (100 ft contour interval) (adapted from the Montana Geological Society, 1985; used with permission)

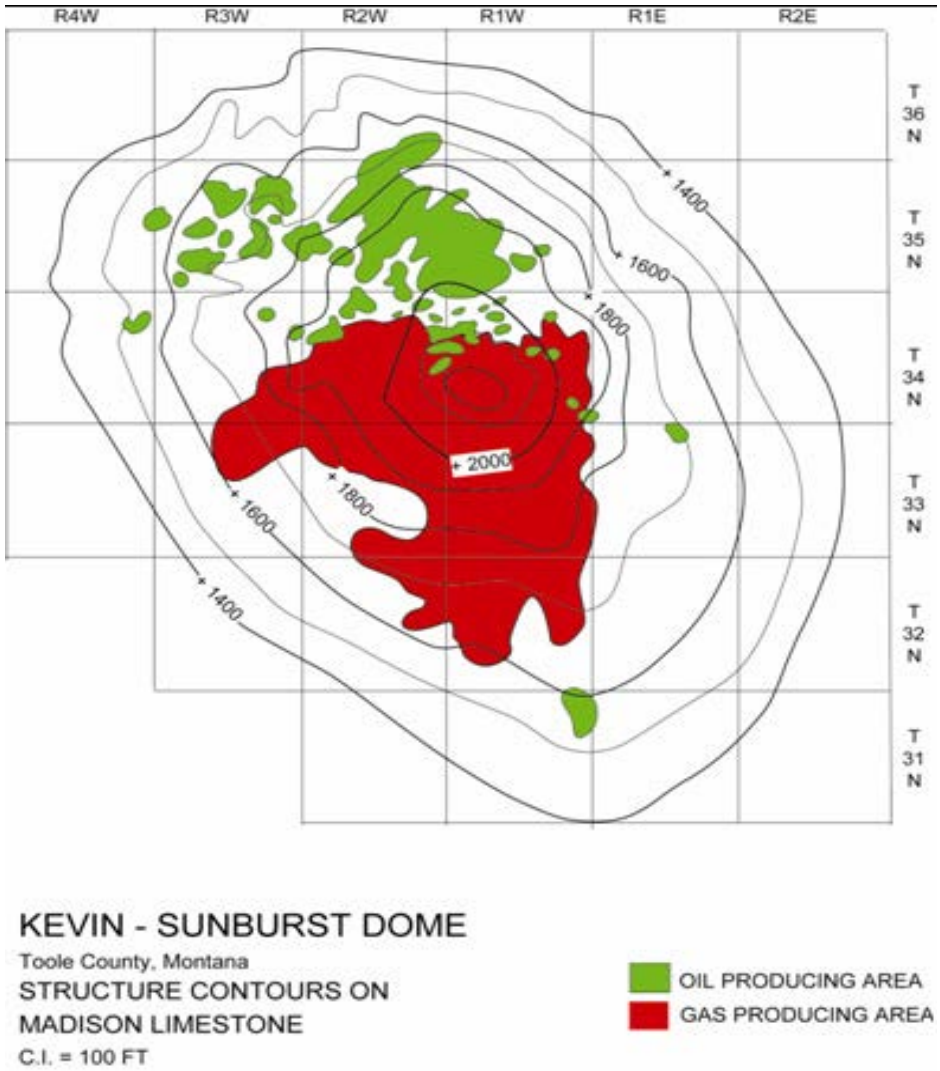

The anticline bears N30°W, plunges 2-3° SSE and somewhat steeper toward the NNW. The overall length of the Sweetgrass fold (200 miles), its close spatial position and trend parallel to the strike of the Cordilleran frontal fold-thrust belt, and apparent ENE-directed vergence (asymmetry) away from the Cordilleran deformed zone, all suggest that Sweetgrass-Kevin folding-shortening occurred within the Laramide orogeny (60-55 Ma); and there is a blind, gently WSW-dipping imbricate thrust at depth beneath the arch. The presence of a long, continuous, gently dipping, through-going thrust like the blind Sweetgrass thrust, bodes well for the lateral potential and favorability of migrant supercritical CO_2 fluids. Our international work demonstrates convincingly that over-pressured, supercritical CO_2-rich fluids readily migrate laterally along sub-horizontal thrusts for significant distances before: (a) rising vertically along co-tectonic, sub-vertical, depth-penetrating wrench faults similar to those comprising the Pendroy (and Great Falls) shear zone (Exhibit 3-40); or (b) become channeled upward along the highly fractured crestal culmination of Laramide folds similar to the double-plunging Kevin-Sunburst anticline. In this later context, it is relevant that migrant oil and methane gas at Kevin-

Sunburst are distinctly compartmentalized (Exhibit 3-43). Oil (green) is predominately reservoired in the northern portion of the field; whereas, methane gas (red) is largely restricted to the southern portion of the field. We interpret the E-W oil/gas reservoir boundary at Kevin-Sunburst as wrench fault-controlled and its lateral sealing capacity is adequate to effectively compartmentalize this huge Laramide trap.

Fewer stratigraphic control points are available for the Devonian Duperow reservoirs. We estimate that approximately fifty (50) boreholes penetrate Duperow reservoirs and less than ten wells were drilled in the South Kevin compartment. Exhibit 3-44 is a composite Kevin-Sunburst stratigraphic section showing Souris River clastic strata lying nonconformably on Proterozoic basement. Highlighted are the position of tops Souris River and Duperow CO_2 reservoirs and upper Duperow anhydrite caprock.

Also detailed is the stratal position of the two CO_2-bearing reservoirs within the Devonian Lower Duperow Formation. The accompanying well log suite shows the correlation and quantification of the CO_2 reservoirs and their stratal relationship to the overlying upper Duperow anhydrite topseal for the deep CO_2 system. The large, undiscovered/undeveloped CO_2 resources purported by the Big Sky Sequestration Partnership (Bowen, 2009 and Spangler, 2011) are trapped by the Lower Duperow reservoirs and reside wholly in the North Kevin-Sunburst compartment. If correct, the supercritical CO_2 charge accessed the Kevin-Sunburst trap from the SW, S, or SE, and migrated up-plunge toward the NW. This seems likely, the E-W-trending Kevin-Sunburst compartmental fault may continue to act as an effective seal at the Duperow reservoir level interfering with the NW, up-plunge migration of middle Eocene CO_2 charge.

Exhibit 3-45 is a tectonic sketch map of the Kevin-Sunburst area along with the North and South Sweetgrass arches. The mapped leading edge of the Laramide northern Rocky Mountain fold-thrust belt is shown as the heavy barbed line less than 100 miles west of the Kevin-Sunburst field. Regional structural architecture is highlighted by the contoured top Mississippian Madison Limestone. The regional Sweetgrass arch appears compartmentalized by the ENE-trending Pendroy shear zone which is interpreted as a strand of the regional Great Falls shear zones located ~30 miles further south. The Pendroy fault appears as a depth-penetrating structure which offsets the Sweetgrass arch by about 30 miles of right-lateral separation. The regional Great Falls and Pendroy fault zones are principal crustal and upper mantle lithosphere-penetrating shear zones. They are viewed as fundamental framework elements of north-central Montana.

It seems likely that the combination of the underlying Sweetgrass thrust and sub-vertical Pendroy wrench zone helped focus and channel alkalic, mafic-alkalic, ultramafic, and silica saturated felsic magmas from depth (+60 miles) along with consanguineous supercritical CO_2 fluids to epicrustal levels. Postulated CO_2 migration routes are shown stylistically trending NNW and S as indicated by the light blue arrows in Exhibit 3-45. The map highlights several regional framework elements: (a) leading edge Cordilleran fold-thrust belt (barbed line); (b) north and south Sweetgrass structural compartments separated by the Pendroy wrench fault (right-lateral transfer) linked kinematically to the underlying, blind Sweetgrass subthrust; (c) double-plunging Kevin-Sweetgrass dome; and (d) Bearpaw alkalic and Rocky Boy carbonatite intrusive complex (54-50 Ma). Exhibit 3-45 shows postulated supercritical CO_2 migration routes (light blue arrows) leading to respective Leads 1-3.

Exhibit 3-44 Well log correlation and quantification of reservoir properties, Kevin-Sunburst anticline, Montana (adapted from Spangler, 2011; used with permission)

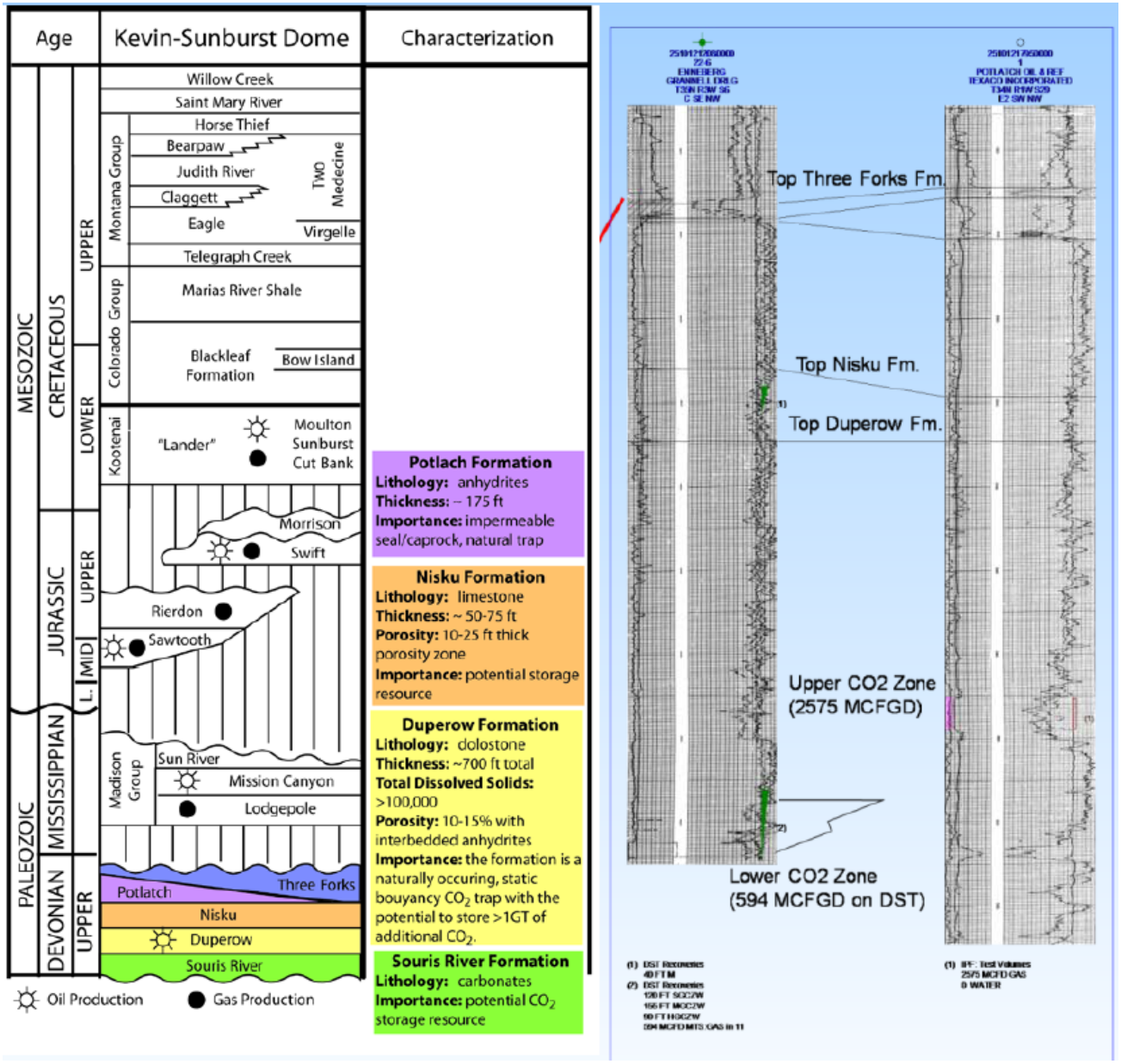

Exhibit 3-45 Regional tectonic sketch map of north-central Montana showing the location of three conventional leads (1, 2, and 4) and one unconventional stratigraphic trap (lead 3). Top Madison Limestone is contoured with 1,000 ft interval (adapted from Shepard and Bartow, 1986; used with permission)

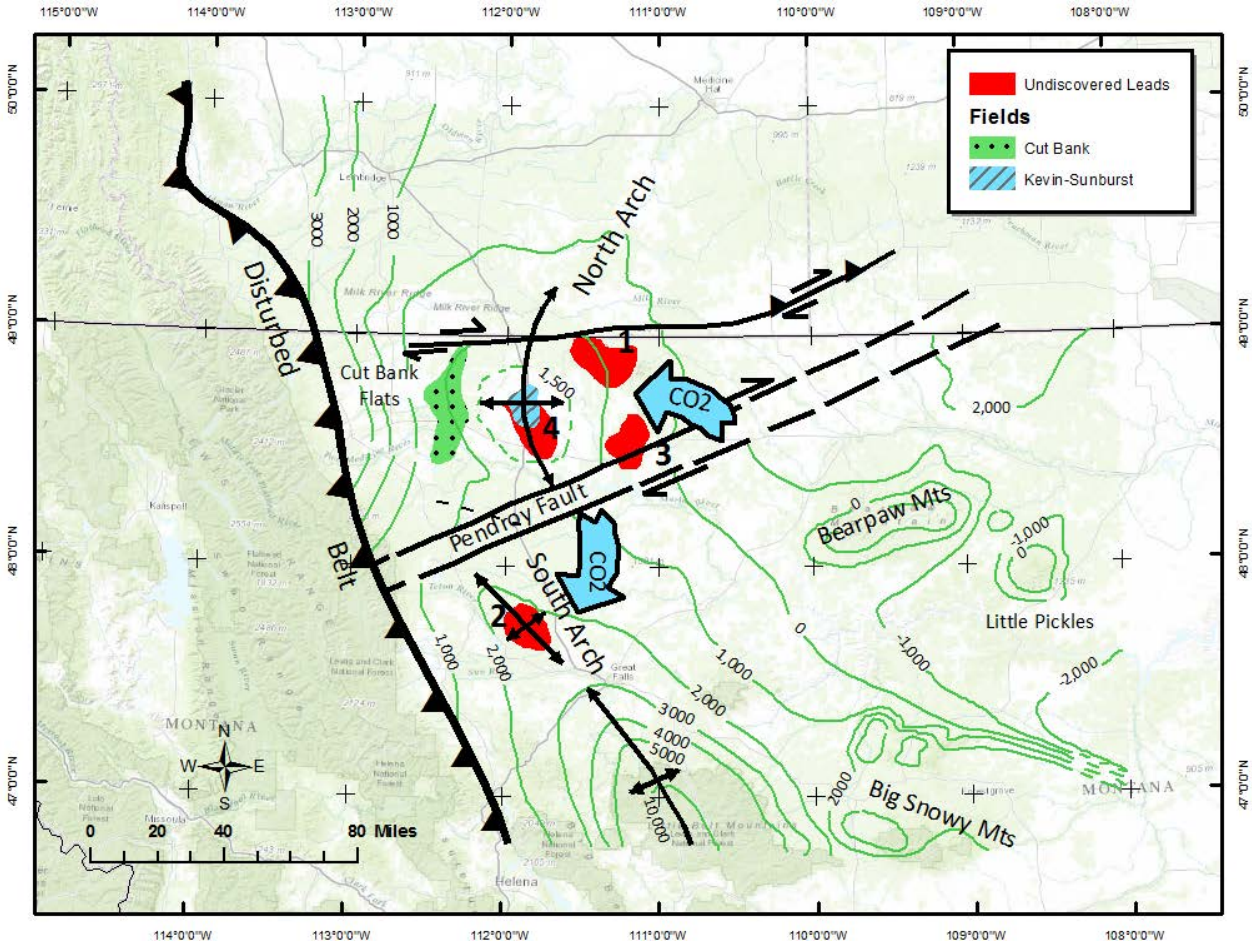

Four hypothetical undiscovered leads are identified: 1, conventional Sweetgrass dome; 2, conventional Great Falls anticline, South Sweetgrass arch; 3; unconventional stratigraphic trap east-flank of the Kevin-Sunburst anticline; and 4, conventional anticline south of the existing Kevin CO_2 deposit. Conventional traps 1, 2, and 4 have reservoir characteristics common with the Kevin-Sunburst anticline including the Devonian Duperow (lower and upper members), as well as the Mississippian Mission Canyon Limestone. Lead 3 is an unconventional stratigraphic trap along the east-dipping flank of the Kevin-Sunburst anticline. Jurassic erosion and karstification of the Mississippian Madison Limestone was followed by deposition of Cretaceous Colorado shale (seals) and sandstone of the foreland Cretaceous Mid-continental Seaway. Late Laramide folding of the Madison/Cretaceous shale unconformable pinchout and Late Tertiary doming set up the envisioned Lead 3 trap configuration. CO_2 charge for Leads 2 and 4 were up-dip toward the SW- and NE respectively- egressing from point-source releasing bend geometries within the right-lateral Pendroy wrench zone. Charge for Lead 1 was from CO_2-enriched olivine minette intrusions from beneath the Sweetgrass Hills uplift or other consanguineous CO_2-bearing phonotephrite-tephriphonolite intrusions emplaced peripheral or within the Pendroy or other subsidiary shear zones.

Exhibit 3-46 shows the contoured top Devonian Duperow (300 ft contours) and location of about 50 Duperow borehole penetrations. The map shows the location of wells that penetrate the Duperow. Respective wells are stylized, color coded (blue/black circle), and coded according to encountered quality of P/P units 1, 2, and 3. Note the: (a) scarcity of Duperow penetrations in the southern half of the structure; (b) N60°W linear array of high quality Duperow reservoir unit 2 penetrations extending beyond the principal limit of the Kevin dome; and (c) absence of well control immediately west of the dome's centroid. The distribution of Duperow penetrations with favorable P/P does not eliminate the possibility of an E-W-trending Kevin compartmental fault at top lower Duperow CO_2 reservoirs.

Exhibit 3-46 Structural contour map top Duperow Formation shows location of wells penetrating Duperow reservoirs (300 ft contour interval) (adapted from Bowen, 2009; used with permission)

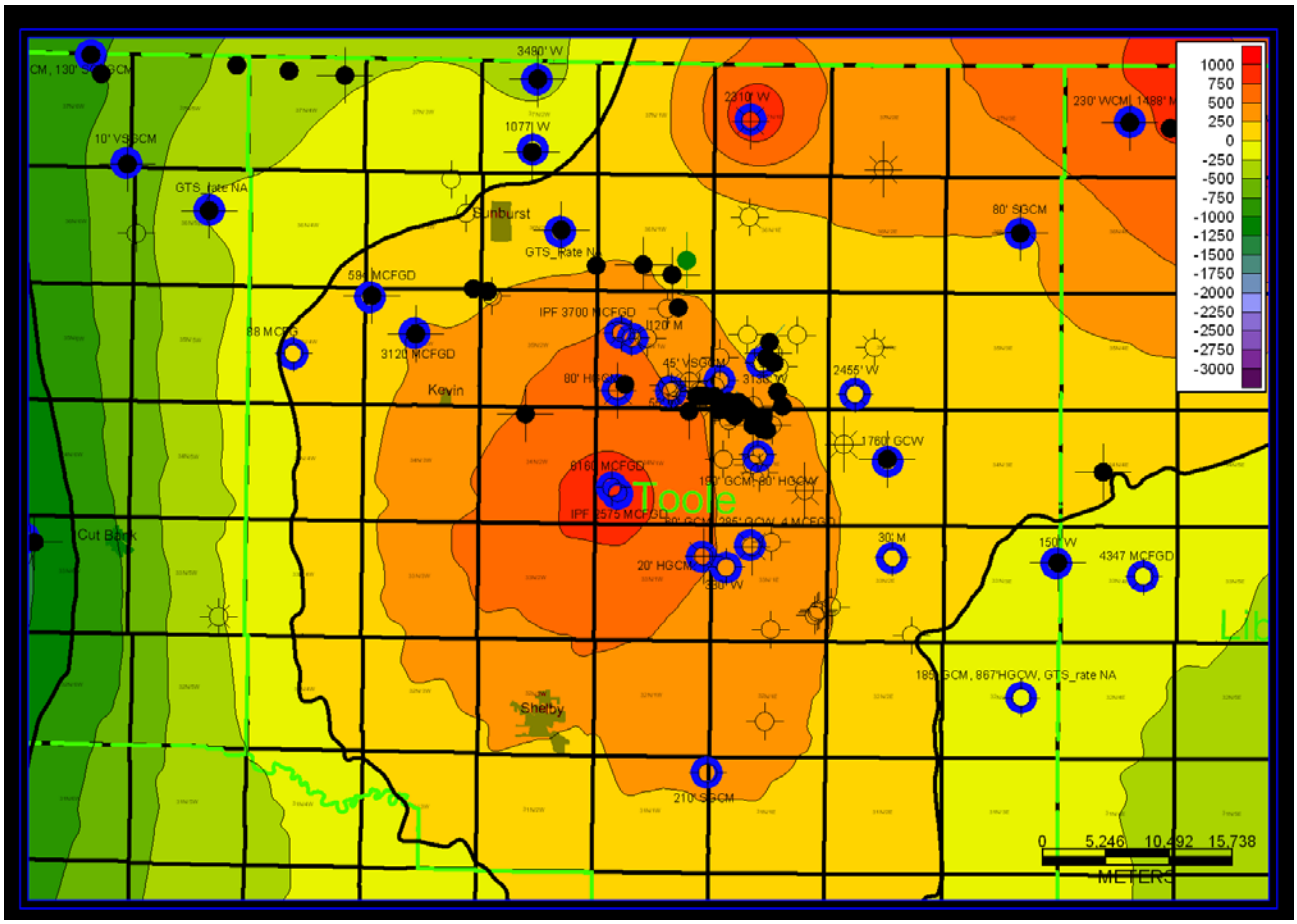

The P/P quality of lower Duperow CO_2 and sub-Duperow reservoirs are summarized in Exhibit 3-47. The Kevin-Sunburst anticline is interpreted as consisting of two large tectonostratigraphic compartments separated along a small E-W-striking, left-lateral transferred fault which is sealing at the Madison Limestone and Cretaceous reservoir levels. The location of wells which penetrate the Duperow are stylized, labeled, and colored (blue) according to the encountered quality of P/P units 1, 2 and 3. The stippled ellipsoidal area in the north compartment inscribes the area believed to contain CO_2 resource. The blue area south of the Kevin compartmental fault inscribes the inferred offset, down-plunge SE continuation of Duperow reservoirs 1 and 2 and described herein as Lead 4. The NW margin of Kevin Lead 3 is highlighted, stippled, and

labeled as "Porous/Permeable Unit 3" in the SE corner of the map. The most porous and permeable Duperow reservoir 2 is not axial symmetric with the mapped Duperow or Madison domal culminations, but rather offset several miles toward the WNW. We interpret the dome as composed of two large tectonostratigraphic compartments separated along an E-W-striking, left-lateral transferred fault. The distribution of high vs. low P/P zones encountered within Duperow reservoir units 1 and 2 are highlighted by well penetration as in the previous exhibit. The stippled ellipsoidal area in the north compartment inscribes about 215 mi^2 and CO_2 gas in high P/P Duperow reservoirs unit 2 and 325 mi^2 and CO_2 in unit 1 (not shown) following suggestions by Bowen (2009). The blue area in the south compartment represents Kevin Lead 4, the offset, down-plunge SE continuation of Duperow.

Exhibit 3-47 Structural contour map top Duperow Formation shows location of highest porous/permeable Units 1 and 2, Duperow Formation) (adapted from Bowen, 2009; used with permission)

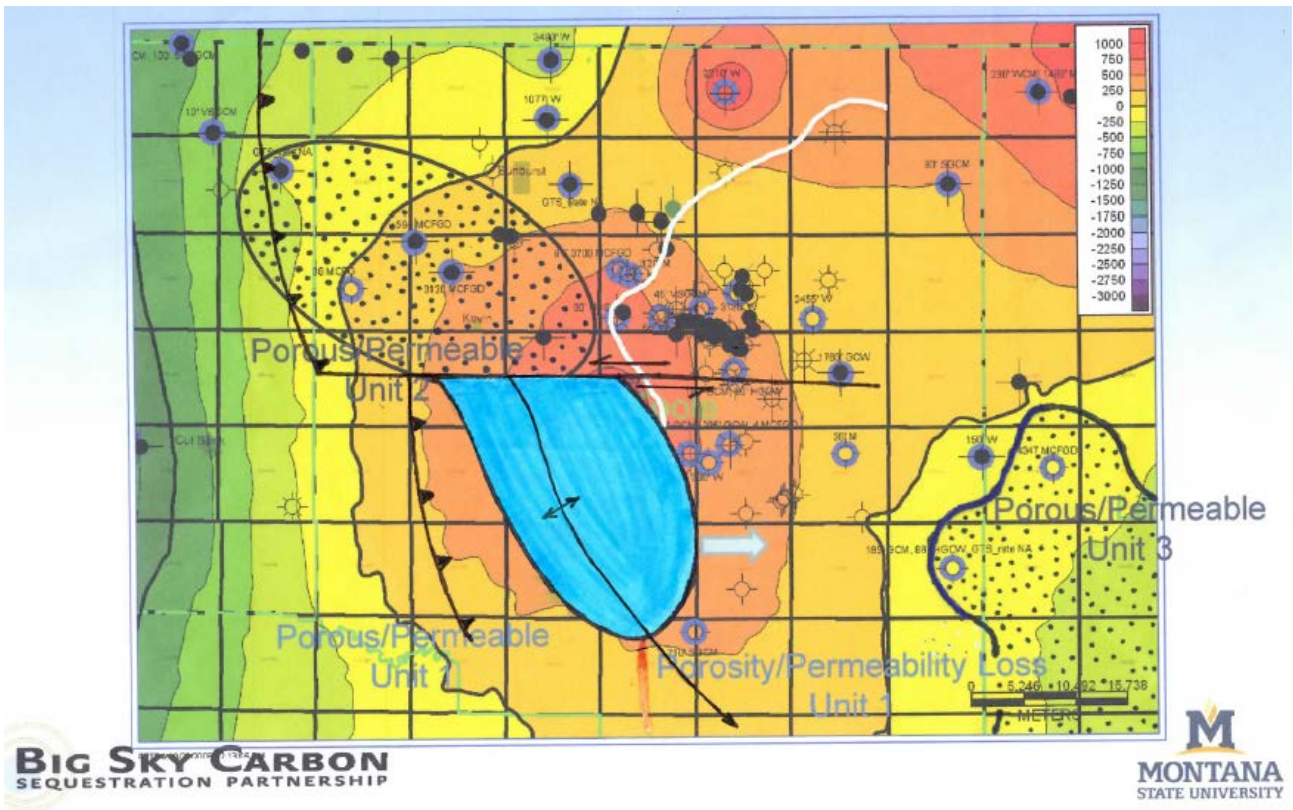

Reservoir unit 2 covers approximately 180 mi^2 and contains CO_2 as described by Bowen (2009). Duperow reservoir unit 1 (stratigraphically higher) is: (a) larger by a factor of 1.5 due to increased fold asymmetry and upward increasing radius of curvature; (b) covers approximately 270 mi^2; and (c) contains CO_2 resource as described by Bowen (2009). See the undiscovered Kevin-Sunburst resources detailed later in this report in Section 3. The NW margin of Kevin Lead 3 is highlighted, stippled, and labeled as "Porous/Permeable Unit 3" along the eastern margin of the map. See the accompanying Kevin Lead 3 map and potential CO_2 resource contained in pre-Bakken strata and Souris River clastics successions along the SE-facing flank of the southern tectonostratigraphic compartment of the Kevin anticline. The CO_2 charge for the south Duperow compartment and SSE-plunging reservoirs is envisioned as sourced from right-

stepping, releasing bend geometries within the Pendroy shear zone. Streaming, supercritical CO_2 fluids accessed the shear zone: (a) directly by decompressed partial melts in the upper mantle/mantle lithosphere at depths of +60 miles or (b) via crystallization of CO_2 saturated high K minette intrusions emplaced at depth but not exposed at releasing, pull-apart bends within the Pendroy shear zone down-plunge (SE) along the Kevin-Sunburst culmination. Differential lateral migration of streaming CO_2 is enhanced along the gently WSW-dipping blind Sweetgrass thrust and up-plunge to the NNW along the crestal culmination of the Kevin-Sunburst anticline.

3.2 Identified Mid-Tertiary Fairways and Undiscovered CO_2 Leads

Exhibit 3-48 shows the Mid-Tertiary CO_2 Fairway.

Exhibit 3-48 Mid-Tertiary CO_2 fairway

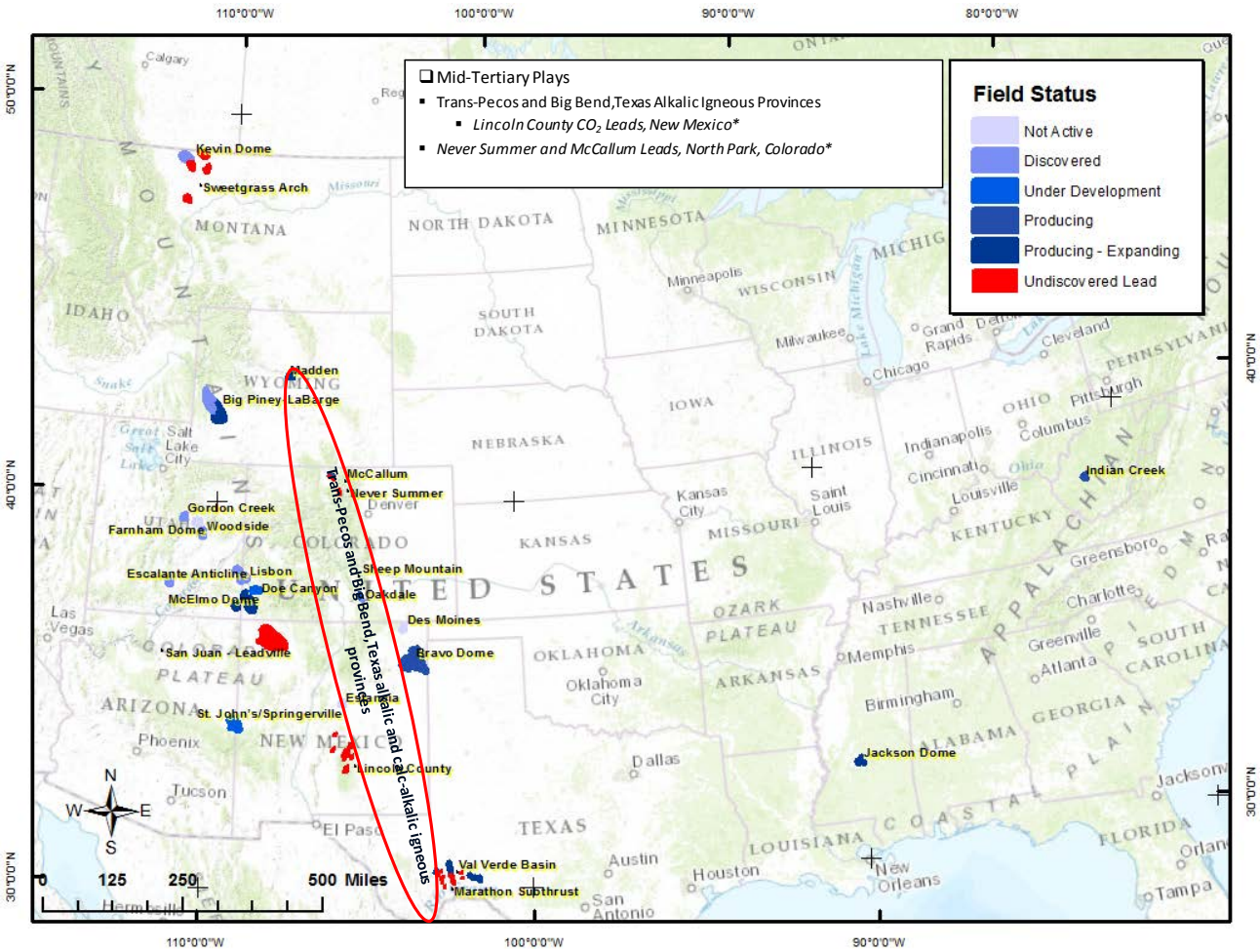

Introduction

The Lincoln County magmatic belt is localized along the N-S-trending, regional Pedernal arch in east-central New Mexico (Kelley and Thompson, 1964). This major Permo-Pennsylvanian structure extends across New Mexico linking to the north with the co-tectonic, NNE-bearing, Sierra Grande arch in the NE corner of the state. The Sierra Grande uplift was fundamental in localizing the large Bravo Dome and subordinate Des Moines CO_2 fields in NE New Mexico. Exhibit 3-49 shows the location of historically productive CO_2 accumulations in context of mapped basins and uplifts (Broadhead et al., 2009). Included are Bravo dome (Harding Co.), Des Moines (Union Co.), and two small occurrences at Estancia. All fields are localized along or on the flanks of Pennsylvanian-Early Permian Ancestral Colorado Rocky Mountain uplifts. Syntectonic thinning and winnowing of sediments on the high and along the flanks are proven in reservoirs at the abandoned Des Moines and Estancia fields and at the large producing Bravo Dome CO_2 field from the Lower Yeso Formation (Tubbs Sandstone Member) and secondarily from basal conglomeratic sandstone deposited directly upon the uplifted Precambrian basement (see Exhibit 3-50). It is noted that all three fields are distributed along the projected subsurface crestal culmination of the Sierra Grande-Pedernal arch. In this context, it is relevant that the exposed centers of Mid-Tertiary igneous intrusive and volcanic areas that define the N-S-trending Lincoln County porphyry belt (LCPB) are likewise aligned parallel to and along this regional tectonic structure (Exhibit 3-50). The map depicts the Lincoln (L), Mescalero arch (MA), Ancestral Rocky Mountain Pedernal uplift (grey shaded area), Mid-Tertiary igneous rocks associated with the Sierra Blanca intrusive complex, and Lincoln County porphyry belt (pink areas). The heavy dashed line indicates the approximate limits of the Pedernal arch. This magmatic belt, in turn, is an important segment of the Rocky Mountain alkalic province (RMAP), which lies along the Rocky Mountain/Great Plains physiographic break extending from Alaska, British Columbia, Montana, Southern Rocky Mountains, New Mexico, Trans-Pecos, and East Mexican alkalic belt southeast to Chiapas, Mexico, a distance of 4,400 miles.

Exhibit 3-49 Map depicting basins and uplifts in New Mexico, locations of fields with known CO_2 production, and the N-S-trending Carboniferous Pedernal uplift (adapted from Broadhead, et al., 2009; used with permission)

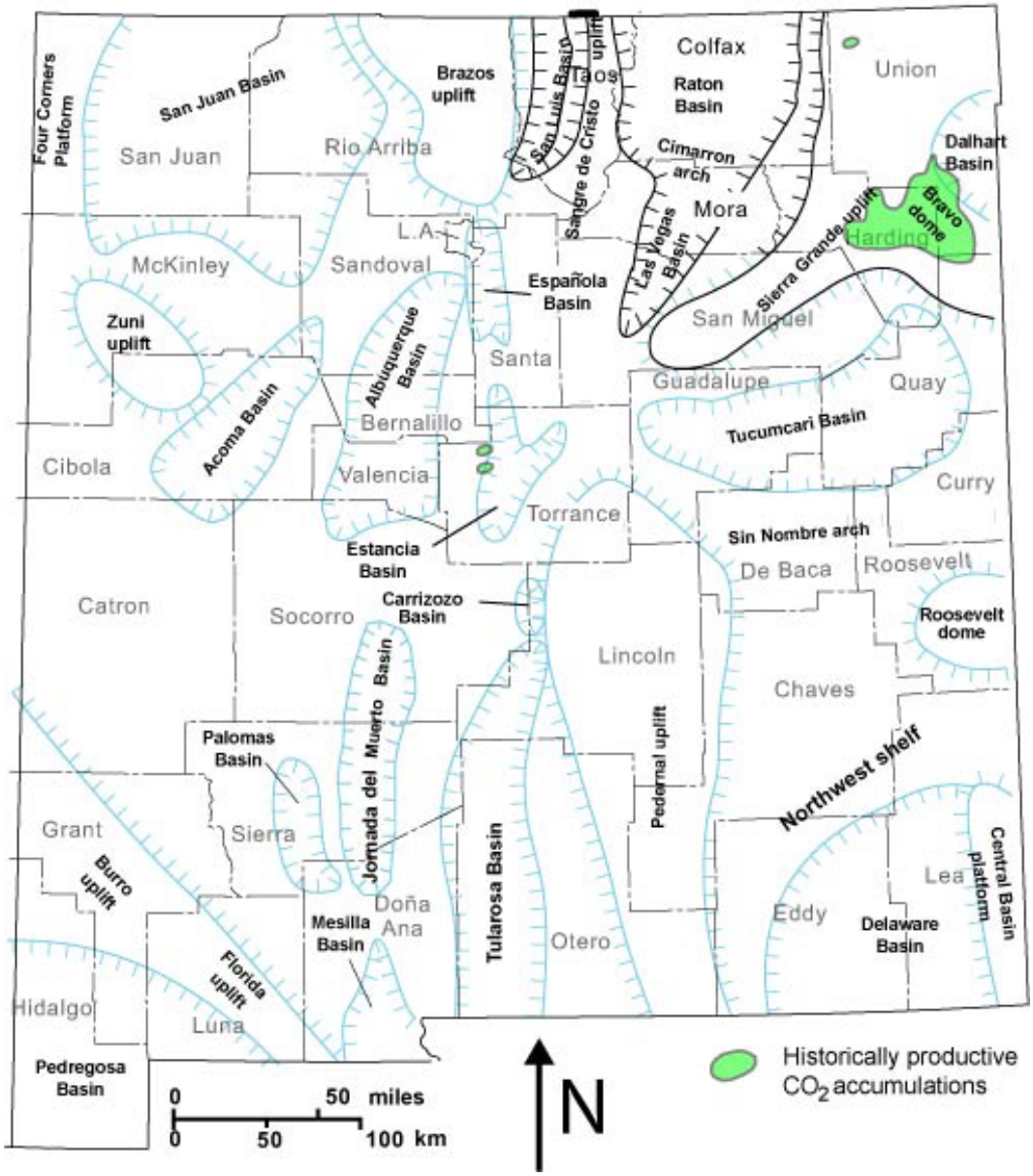

Exhibit 3-50 Regional tectonic framework map of SE New Mexico highlights the extent of the Pedernal uplift (dark grey) and principal Mid-Tertiary intrusions comprising the Lincoln County intrusive belt (modified from Kelley, 1971; and Yuras, 1991; used with permission)

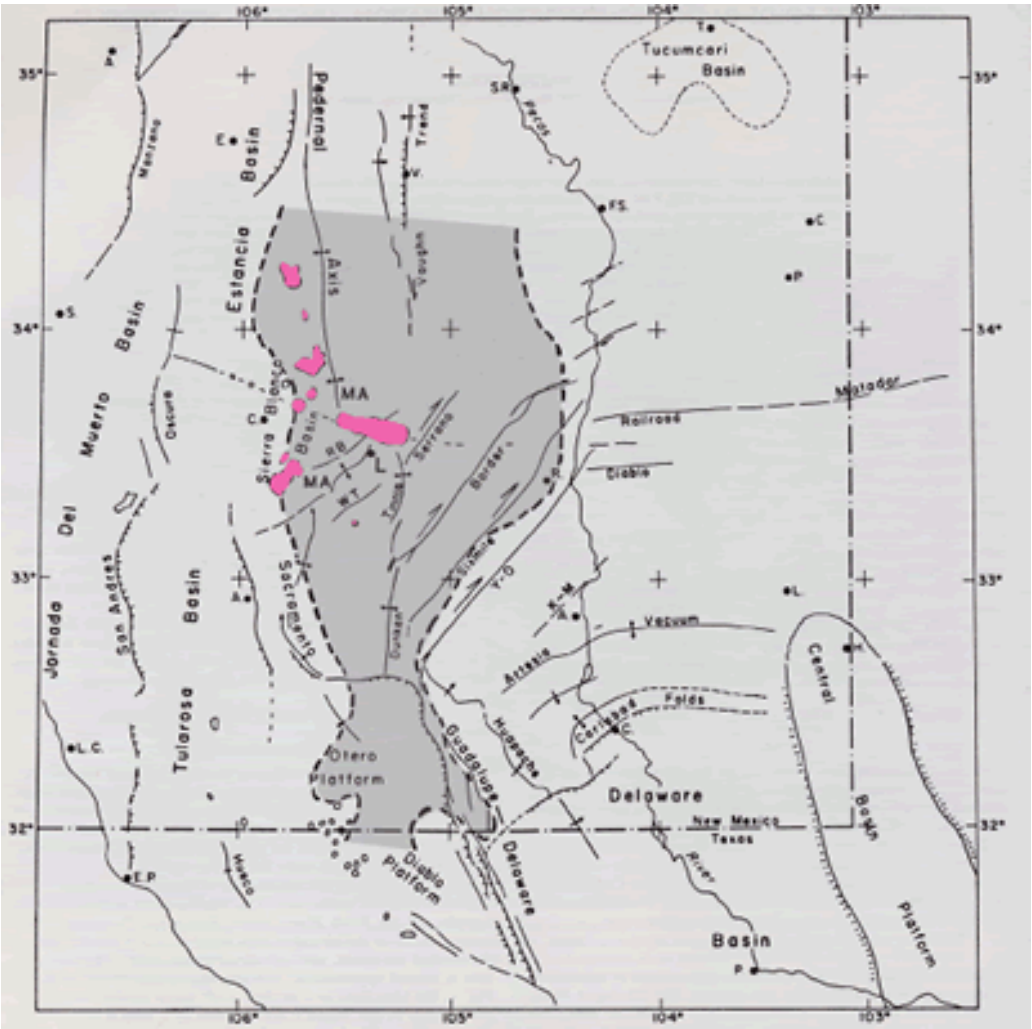

Geologic and Stratigraphic Setting

The geology and tectonics of the Lincoln County region were studied by Kelley and Thompson (1964). Their detailed work is utilized and referenced throughout this section of the report along with more recent studies by Allen and McLemore (1991) on the Capitan pluton area. Most of the early Phanerozoic geologic record and stratal events were removed from the area prior to subsidence and burial of the Pedernal uplift during the Lower Permian. During this subsidence phase, approximately 1000 ft of lower Yeso group strata were deposited with varying amounts of overlying Abo Formation (Kelley, 1971). The Yeso Formation consists of fine grained red-brown, cross-stratified sandstone, siltstone, and evaporites with intercalated limestone with interbeds of reddish colored siltstone, shale, and cross-stratified sandstone. The evaporate successions are indicative of a marginal marine, intertidal environment of deposition. The often-observed intercalated marine carbonates of the Yeso in southern New Mexico are likewise suggestive of nearby marine conditions to the east and southeast bordering the Ouachita orogenic belt during the Leonardian (284-278 Ma).

In Exhibit 3-51, the upper diagram (A) presents a generalized E-W oriented cross-section transverse to Sierra Blanca basin and Pedernal arch. The section shows a rather uniform thickness of Yeso Group strata in the subsurface along the entire length of the section. In Exhibit 3-51, diagram B shows representative gamma ray and resistivity logs for Yeso reservoirs from the Bravo dome field. Similar geological conditions are perceived for the Lincoln County region and similar petrophysical properties are believed applicable for the hypothetical undiscovered reservoirs of the LCPB.

The absence of Triassic and Jurassic age strata throughout the Ruidoso-Carrizozo implies that the Pedernal arch remained weakly positive following deposition of the Yeso. It was not until the Early Cretaceous that the entire positive area experienced deep burial by Mesaverde floodplain deposits of regional extent. Following the deposition of the Mesaverde there is little record or direct evidence of any pre-Laramide deformation of the Early Cretaceous stratigraphy.

East to ENE-directed lateral compression during the latest Cretaceous and Paleocene produced broad, open alternating anticlines and synclines with axes paralleling the lines of the old Pedernal mountains. During this phase of deformation and continuing on into the early-middle Eocene, the Mescalero arch was re-enforced and the adjoining Sierra Blanca basin to the west was formed in conjunction with the Carrizozo anticline on its western flank. This was probably the episode of maximum formation of Lincoln-type double-plunging anticlinal traps concurrent with the increased tilt along the east-facing Pecos slope. The maximum crestal altitude at the top of the Permian beds in the Sacramento uplift is near 10,000 ft; whereas, their north-directed plunge to the bottom of the Sierra Blanca basin is on the order of 6,500 to 7,000 ft in a distance of 35 to 40 miles. A similar, somewhat structural, relief is recognized along the crest of the adjoining Mescalero anticline immediately to the east, which sits up potential anticlinal traps along its axis where a dip reversal produces local double-plunging closures.

Eruption of the Sierra Blanca volcanics during Late Eocene was the harbinger of the upcoming pulse of latest Eocene intrusions of stocks, laccoliths, sills, and dikes. This eruption associated a growth across the Mescalero arch and a down-dropping of the Sierra Blanca basin (1,500-1,700 ft) along the Ruidoso fault (Exhibit 3-51) and reactivation of local fault strands parallel to the Capitan lineament. Exhibit 3-51A is a diagrammatic E-W cross-section through the Sierra Blanca intrusive complex. Permian reservoirs are mapped overlying Precambrian basement gneiss (west) and granite (east). Lower Permian Yeso strata lie nonconformably on basement and are overlain unconformably by Early Cretaceous Mesaverde Group strata. The section is topped by eruptions of the extensive Mid-Tertiary Sierra Blanca volcanic field. The Three Rivers syenite-alkalic granite stocks are emplaced between 32-26 Ma in the hanging-wall of the Mescalero thrust and WNW-dipping Ruidoso normal fault. Exhibit 3-51B is a typical gamma ray and resistivity log; Bravo Dome field highlights the character of the lower member of the Yeso Formation and principal reservoir (Tubbs Sandstone, ~83 ft net pay). In the region of the Sierra Grande uplift, CO_2 is secondarily trapped in porous basal sandstone and sandy conglomerates of the Abo Formation lying noncomformably on Precambrian basement. Similar stratal succession with comparable petrophysical properties are suspected in the subsurface beneath the Sierra Blanca basin and surrounding Lincoln County area.

Exhibit 3-51 A, presents a diagrammatic E-W cross-section through the Sierra Blanca intrusive complex and basin. Mescalero thrust added by Enegis, LLC (this study). B, typical gamma ray and resistivity logs, Bravo Dome field. (Exhibit A modified from Kelley and Thompson, 1964; Exhibit B adapted from Broadhead et al., 2009; used with permission)

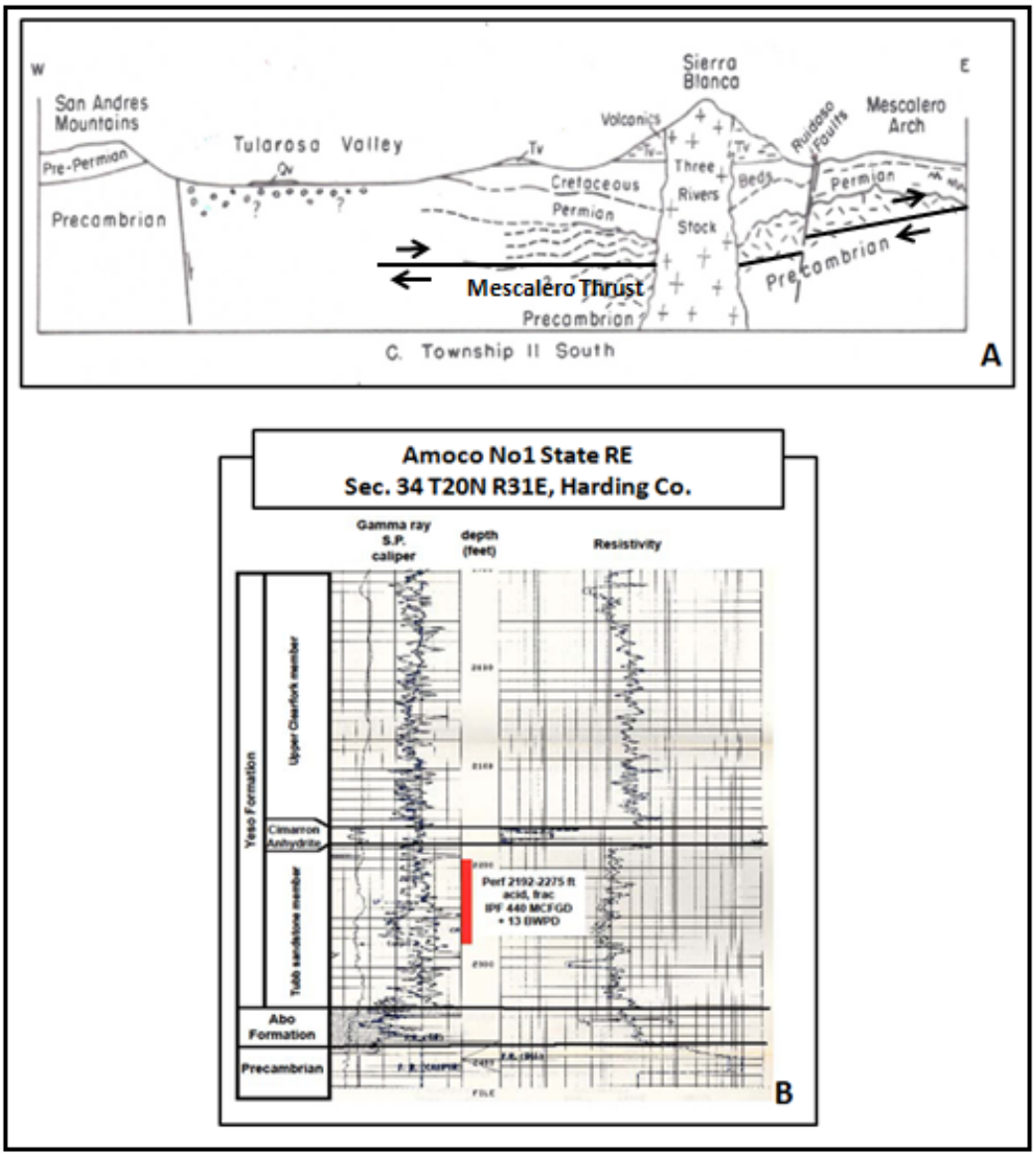

See Exhibit 3-60 for location of suspected trace of thrust tip at the base of the Pecos slope.

Between late Eocene through Oligocene time (38-25 Ma) and within the immediate environs of Lincoln County is exposed a concentration of Mid-Tertiary intrusive centers in New Mexico. Kelley and Thompson (1964) identify at least nine mapped stock-laccolith centers ranging from 5 to 25 mi^2 in outcrop area, and a single granite-granite porphyry stock (Capitan) covering over 100 mi^2. In addition, there are several smaller centers of breccia pipe development, radial and dike swarms, and sills. Within this cluster is evidence for the presence of CO_2-bearing alkalic intrusions and associated carbonatite magmas. It is proposed that the identified CO_2 point sources are capable of directly charging Lincoln-type conventional and unconventional combination stratigraphic-structural traps within and peripheral to the Sierra Blanca basin.

Tectonic and Magmatic History

The majority of alkalic igneous intrusions world-wide are associated with areas of regionally stable, continental crust that is arched and extended. Many of these "intra-continent" areas are associated with concomitant rifting and activation of deep-penetrating regional-scale fault lines or lineaments. Smaller volumes of alkalic magmatism are also associated with more voluminous calc-alkalic arc settings along convergent plate boundaries. The principal contrasts in the different alkalic intrusions are: (a) calc-alkalic and associated small volume alkalic intrusions are directly linked to shallow levels of subduction (±90 miles) beneath volcanic arcs with an interior mobile belt; and (b) intra-plate alkalic intrusions are products of deeper levels of subduction below foreland passive regions, or associated with intra-plate rifts or zones of crustal extension not directly associated with subduction. Regardless, the distal intra-plate alkalic magmas are typically emplaced along depth-penetrating lineaments or co-tectonic zones of strike-slip (wrench) tectonics. In southern New Mexico, West Texas, and adjoining Sierra Madre Oriental, calc-alkalic magmatism is sparse and widely scattered commencing at circa 78 Ma and extending through the Middle Eocene. Exterior to the Mexican Sierra Madre Oriental volcanic field, alkalic magmatism commenced in West Texas at circa 42 Ma followed by voluminous alkalic volcanism and plutonism along the length of the Big Bend and Trans-Pecos magmatic arc by 37 Ma and continuing to 32 Ma. The generalized eastern limit of the alkalic magmatism along the NNW-trending Trans-Pecos arc is highlighted in Exhibit 3-52. The map delineates the Middle Tertiary Trans-Pecos magmatic province and its northward continuation along the south-central alkalic belt of Otero and Lincoln counties, New Mexico. The dashed provincial petrologic boundary between alkalic and alkali-calcic igneous rocks is projected into New Mexico. Note the size and location of the proposed Val Verde CO_2 plume (stippled blue area) relative to the Sierra Madera "astrobleme" and the Davis Mountains volcanic field. The CO_2 charge for the proposed Val Verde plume could have come from the west linking the charged to the Trans-Pecos alkalic province. For this study, the alkalic boundary has been extended into southern New Mexico so that the continuation connecting with the LCPB alkalic volcanics and intrusions is unbroken. The Trans-Pecos belt is distinctly refracted from its N30°W trend in a clockwise manner to a more N-S to N10°E Lincoln County orientation. The exhibit also underscores the 60-mile distance separating the western boundary of alkalic magmatism and the proposed CO_2 point source for the Val Verde subthrust plume.

Exhibit 3-52 Sketch map of the Mid-Tertiary Trans-Pecos magmatic province, west Texas. The boundary between the alkalic (A) and calc-alkalic (CA) was extended to connect with the Lincoln County intrusive belt and (adapted from Barker, 1987; and Price et al., 1987; used with permission)

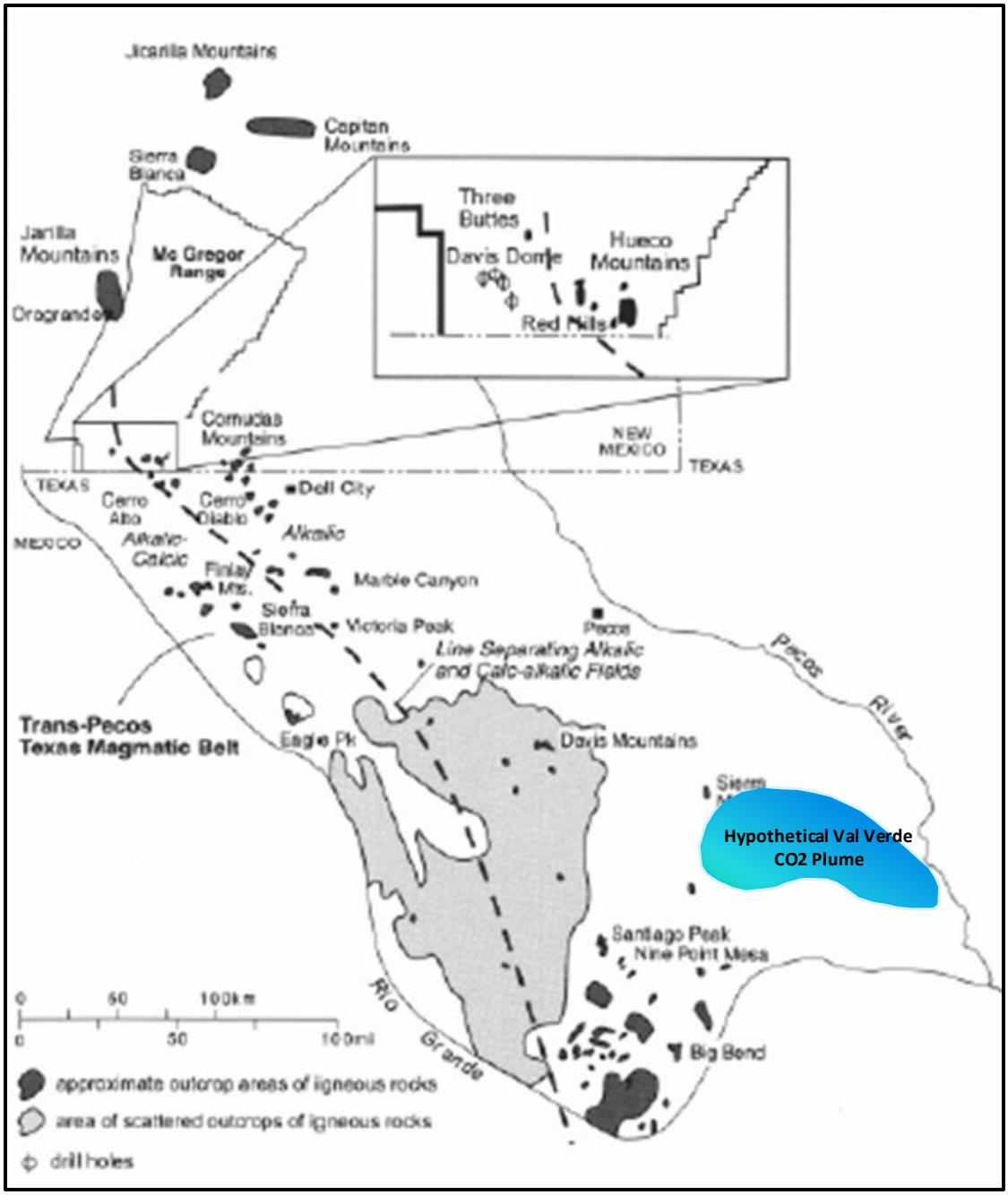

Note the close spatial relationship of the Mid-Tertiary alkalic intrusive belt and the hypothetical CO_2 plume beneath the Marathon allochthon.

The LCPB is defined by its diagnostic Late Eocene-Oligocene (37-25 Ma), N-S- and E-W-trending zone of alkali mafic to alkalic and silica oversaturated Tertiary intrusive and numerous volcano-plutonic centers (Exhibit 3-53A). The map in Exhibit 3-53A outlines major mining districts (blue) and Mid-Tertiary igneous intrusions (red). The LCPB is labeled and extends along the curvilinear N-S alignment of Mid-Tertiary intrusions and co-spatial mining districts (92-132). The Capitan lineament is believed subsidiary. It lies in the transverse direction, strikes E-W- to WNW, and helps to localize the large, Mid-Tertiary Capitan granite (91) intrusion (Exhibit 3-53A-B, 29-26 Ma).

Older ENE-trending Laramide lineaments include the Santa Rita and Morenci. The somewhat arcuate, E-facing LCPB belt is defined by a 30-mile wide zone of epizonal intrusions including plutons, laccoliths, plugs, necks, sills, and dikes (red). Compositions of plutonic rocks vary from normal calc-alkalic diorite, monzonite, and granite. K-feldspar- and quartz-rich fine grained equivalents are prevalent (red); however, correlative ultramafic, mafic-alkalic, and alkalic varieties include syenodiorite, monzodiorite, and syenite, as well as commonly associated fine-grained trachyte, phonolite, and rhyolite; see Exhibit 3-54 for details. The transverse E-W- to WNW-trending Capitan lineament is defined by the distinctly elongated Capitan granite pluton and consanguineous Railroad, Camino del Diablo, and Jones Camp dike swarms of similar orientation. In contrast to the LCMB, the composition of plutonic rocks localized along the Capitan lineament include granite-granite porphyry Capitan) and more intermediary calc-alkalic varieties. Numbered mining district outlines are those used by the New Mexico Bureau of Geology and Mineral Resources.

Intrusive rocks are characteristically porphyritic and involve shallowly emplaced stocks, laccoliths, dikes, sills, and two volcano-plutonic centers. The porphyritic rocks, which define the belt, are typically alkalic in character and are often interpreted as derived from an underlying, deep subduction system in a more passive foreland region. From south to north, the following intrusions and volcano-plutonic centers constitute the LCPB: Black Mountain stock, Three Rivers stock, Sierra Blanca volcano-plutonic center (including the Rialto and Bonito Lake stocks), Carrizo Mountain stock, Panos Mountain stock, White Oaks stock, Jicarilla Mountain stock, Tecolote Hills stock, and Gallinas Mountain stocks. The Capitan and Jones Camp dike swarms are aligned E-W and transverse to the LCPB, but are tectogenetically and petrochemically related to the belt. Volcano-plutonic complexes, which constitute the LCPB, appear sub-divided into two contrasting but somewhat overlapping pulses of igneous activity as shown in histogram format on Exhibit 3-53B. The histogram summarizes the K/Ar, Rb/Sr and Ar^{40}/Ar^{39} ages of igneous rocks from the LCPB area. $^{40}Ar/^{39}Ar$ ages are recalculated using the new decay constant. The Gallinas Mountains trachyte was dated by K/Ar methods as 29.9 Ma (Perhac, 1970). There was an abrupt commencement of latest Eocene (38 Ma) Black Mountain alkali gabbro-syenite-syenite porphyry off-lapped by Sierra Blanca nepheline syenite-essexite (foidal monzodiorite) at 32 Ma. The second younger group of intrusions commences with emplacement of the Three Rivers syenite, quartz-alkalic syenite, and lagged by syenite porphyry and Capitan alkali granite-granite porphyry (30-25 Ma). The emplacement of Lincoln County basin margin alkalic magmas heralded the termination of Laramide compression in the American Southwest and serves as the oldest harbingers of Mid-Tertiary extension and the earliest effects of Farallon rollback, break-up and deep mantle perturbation, decompression, and partial melting of the mantle.

Exhibit 3-53 A, Subdivision of volcano-plutonic complexes at the Lincoln County porphyry belt (LCPB). Map outlines major mining districts (numbered, grey areas) and principal Mid-Tertiary intrusions comprising the LCPB; and B, histogram summarizes ages of igneous rocks from the LCPB area (adapted from McLemore and Zimmerer, 2009; used with permission)

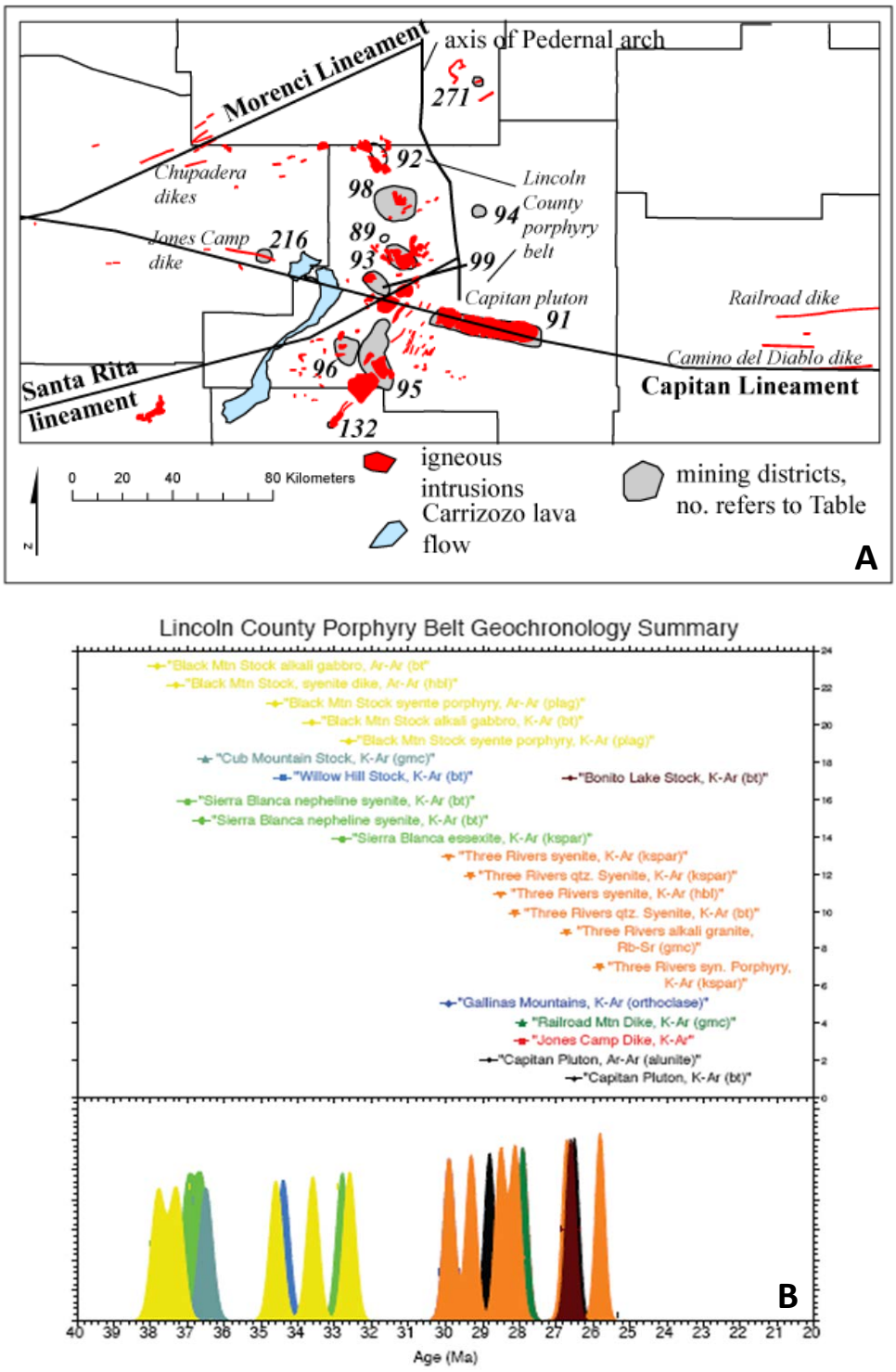

Exhibit 3-54 Summary of intrusive-volcanic events and corresponding radiometric ages, Lincoln County magmatic belt, New Mexico (sources: McLemore, 2010; Allen and Foord, 1991; and references therein)

Igneous Rock Identification	Ma	Method	Material dated, notes
Episode 1 (38-32 Ma), N-S belt of stocks, dikes, breccia pipes, and volcanic centers			
Black Mountain alkali gabbro stock	36	K/Ar	biotite
	37.8	$^{40/39}Ar$	biotite
Black Mountain bald syenite porphyry	37-33	FT, ^{39}Ar	plagioclase, zircon
Jicarilla Mountain syenogabbro	38-37	K/Ar	biotite
Baxter Mtn (White Oaks) syenogabbro	?		
Sierra Blanca volcano-plutonic centers	37-32	K/Ar	var.
Nepheline syenite and essexite	37-36	K/Ar	biotite
Sierra Blanca trachybasalt volcanics	37		
Church Mtn phonolite	31.8	K/Ar	whole rock
Three Rivers essexite	32.8	K/Ar	feldspar
Rialto stock	31.4		
Bonito Lake stock	26.6		
Three Rivers alkali granite	26.7	Rb/Sr	whole rock
Three Rivers quartz syenite	29-28	K/Ar	biotite
Three Rivers porphyry molybdenum	26.6		
Three Rivers syenite porphyry	25.8	K/Ar	feldspar
Bonito Lake syenite stock	26.6	K/Ar	biotite, Mo-Cp-Qtz veins
Rialto syenodiorite-syenite stock			breccia pipes (Mo-Cp-phlog)
Sierra Blanca trachyphonolite volcanics	28.2	FT	apatite
Godfrey Hills trachyte volcanics	26.1	K/Ar	feldspar
Tecolote Hills syenogabbro-syenite			Inferred
Gallinas Mts. trachyte, syenite and rhyolite	32-29	K/Ar	
Trachyte/syenite	29.9	K/Ar	Perhac, 1970
Episode 2 (30-26 Ma), emplacement along the E-W-trending Capitan lineament, E-W-trending Capitan intrusions			
Capitan granite porphyry	26.5		K/Ar
Jones Camp syenodiorite dikes	27.9	K/Ar	
Railroad Mtn alkali gabbro dikes	27.9	K/Ar	whole rock
Carrizo quartz syenite-granite stock	?		
Patos Mtn alkalic granite-rhyolite laccolith	?		

? - Uncertain Age

The above tabulation of compiled radiometric ages of LCPB igneous rocks defines two relatively discrete episodes of volcano-tectonic activity. The oldest N-S belt of intrusions is late Eocene-early Oligocene (38-32 Ma, Episode 1). The younger E-W-trending belt of intrusions constitute the second pulse (Episode 2) lasting from 28-25 Ma (McLemore and Zimmerer, 2009). Episode 1 marks the end of the Laramide compression and reviewed literature suggests that associated dike swarms at Black Mountain, Jicarilla, Tecolote, and Gallinas involve NE-ENE-trending dike swarms (McLemore, 2010; Allen and Foord, 1991; Perhac, 1970). By contrast, Episode 2 igneous centers are emplaced along the E-W-trending Capitan lineament where elongate stocks and dikes typically trend E-W sympathetic to the Capitan lineament or NNE similar to the Sierra Blanca basin dike and fault-vein swarm.

West of the Lincoln County, the alkalic intrusive belt coeval Episode 1 calc-alkalic magmatism is widespread continuing westward into Arizona. Exhibit 3-55 summarizes the distribution of voluminous, predominately calc-alkalic igneous rocks with radiometric ages within the 33.7-23.8 Ma timeframe. The east-central New Mexico alkalic province is highlighted (A) and projected southward from Lincoln County, across Otero County to link with the Trans-Pecos alkalic magmatic belt of West Texas. Coeval alkali-calcic and calc-alkalic (CA) igneous rocks lie further to the west and continue into Arizona.

Alkalic rocks belonging to the Lincoln County alkalic belt are inscribed and labeled A on the exhibit. If all of the plotted igneous events are indeed subduction-related arc magmas, the ancestral Laramide slab (Farallon) has commenced to roll back and steepen westward without the presence of alkalic magmatic rocks similar to the Lincoln County igneous suite. It is also noteworthy that the copious calc-alkalic volcanism of SW and Central New Mexico (Oligocene flareup and caldera development) and initiation of normal faulting along the Rio Grande rift are coincidental and, likewise, yield a circa 36 Ma age (Chapin et al, 2004; Mack, 2004).

It appears that terminal flat-slab subduction of the Farallon plate and cessation of ENE-direct Laramide compression occurred concurrent with the initiation of Episode 1 magmatism (38-32 Ma) extension along the proto-Rio Grande rift and near instantaneous development of arc-like calderas scattered across the American Southwest landscape.

The prevalence of low initial strontium ratios (Sri) for Episode 1 igneous rocks (0.7039-0.7049) and less negative and more primitive εNd (+0.5—1.9) suggest that the source of the older episode 1 LCPB magmas were derived from a deep mantle lithosphere or mesosphere (Allen and Foord, 1991). As discussed earlier in this section, Humphrey's (1995, 2009) broken and descending Farallon slab hypothesis appears applicable in this instances. As the slab sinks and breaks up, the surrounding mantle is disturbed and perturbated, creating areas of relative decompression that induce partial melting. The coalescence of these anhydrous melts commence to ascend incorporating resident volatiles (CO_2, F, H_2O, Te and ^3He) as well as entraining surrounding noble metals (Au, Ag, platinum [Pt], palladium [Pd]) and an assortment of rare earth elements (REE) (Th, U, molybdenum [Mo], Nb), and other trace and large radius elements. The ascent of these enriched, mafic-alkalic magmas are in part entrained along the line of descent of the floundering, sinking, dismembered Farallon slab and secondarily within the zone of decompression, uplift, and extension running parallel to the ancestral Pedernal arch. Ternary focus for ascending magma is along contiguous, second order, depth-penetrating, crustal-scale fault zones and lineaments.

The transverse-trending Capitan lineament was ideally oriented and facilitated/localized the Episode 2 Capitan granite-granite porphyry pluton, the largest Tertiary intrusion in New Mexico. The Capitan lineament also helped localize several smaller Episode 1 stocks juxtaposed immediately south and north of the E-W-trending Episode 2 magmatic belt. Fractional crystallization and differentiation processes during ascent of the mafic-alkalic magma appear applicable and adequate to account for the observed suite of primitive LCPB plutons, volcanics, and associated mineral deposits.

Exhibit 3-55 Map of New Mexico summarizes the regional distribution of radiometric ages of Mid-Tertiary (Oligocene, 33.7-23.8 Ma) rocks (adapted from Chapin et al., 2004; used with permission)

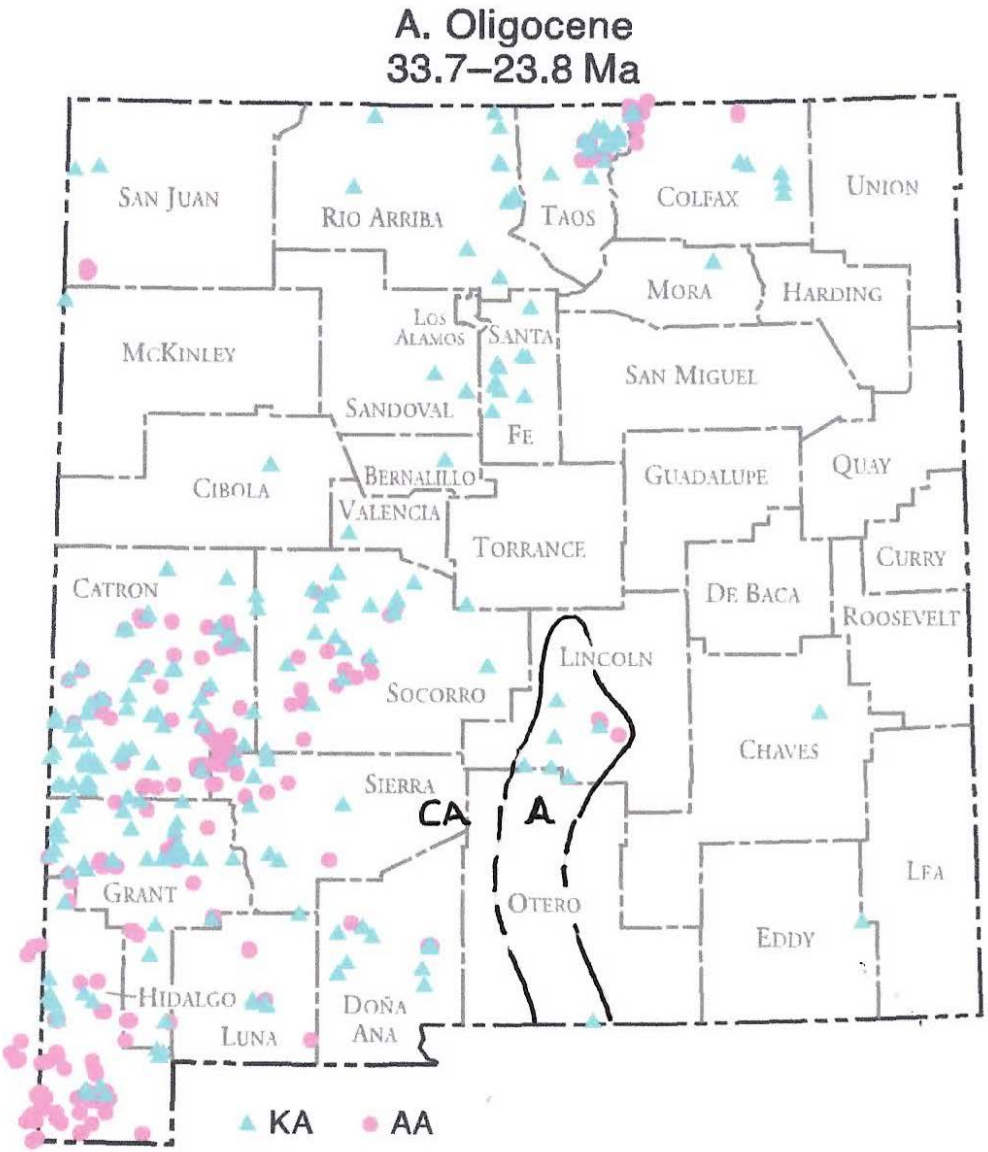

Lincoln County Ore Deposits and CO_2 Point Sources

As early as 1910, Lindgren, Graton, and Gordon stressed the apparent co-dependency between major New Mexico gold and silver deposits and: (a) the physiographic break between the Rocky Mountain Cordillera/High plains province; and (b) the linear N-S-trending alignment of Tertiary alkali-rich intrusions in adjoining Colorado and the NNW-trending Trans-Pecos alkalic province in West Texas (McLemore and North, 1987). This relationship is clearly portrayed in Exhibit 3-56 which delimits a 60-mile-wide belt of important New Mexico gold and silver deposits and consanguineous Tertiary intrusions. Identified, mining districts include: 1, Elizabethtown-Baldy; 2, Cimarroncito; 3, Laughlin Peak area; 4, Red River; 5, Cerrillos; 6, Old Placers; 7, New Placers; 8, Chupadera; 9, Gallinas; 10, Jicarilla; 11,White Oaks; 12, Capitan; 13, Nogal Peak; 14, Schelerville; 15, Orogrande; and 16, Cornudas Mountain. Districts 1-3 are Oligocene-Miocene age; 4-16 are latest Eocene-Oligocene. Note the close spatial distribution of Au-Ag districts along or near the axial culmination of the Carboniferous Pedernal arch (Exhibit 3-50). The location of the two small Estancia CO_2 fields is shown 45 miles ESE of Albuquerque (Foster and Jensen, 1971). Ages for districts 1-4 are quoted as Oligocene-Miocene (McLemore, 1994); whereas, all of the other mentioned districts have recorded alkalic intrusions within the district. Most of the state's largest gold deposits lie along this N-S belt which closely coincides with the Rocky Mountains-Rio Grande rift/Great Plains margin physiographic provinces. Various workers have referred to these deposits as alkalic-Au, alkalic-igneous-related-Au, porphyry Au, Rocky Mountain Au and Great Plains margin (Mutschler et al., 1985, 1997; Richards, 1995; and McLemore and North, 1987; North and McLemore, 1988). Alkalic igneous rocks are present in all of the districts along with associated calc-alkalic igneous rocks.

Exhibit 3-56 Map summarizes the distribution of the sixty-mile wide Great Plains margin belt of gold-silver deposits and consanguineous Tertiary intrusions of New Mexico (adapted from McLemore and North, 1987)

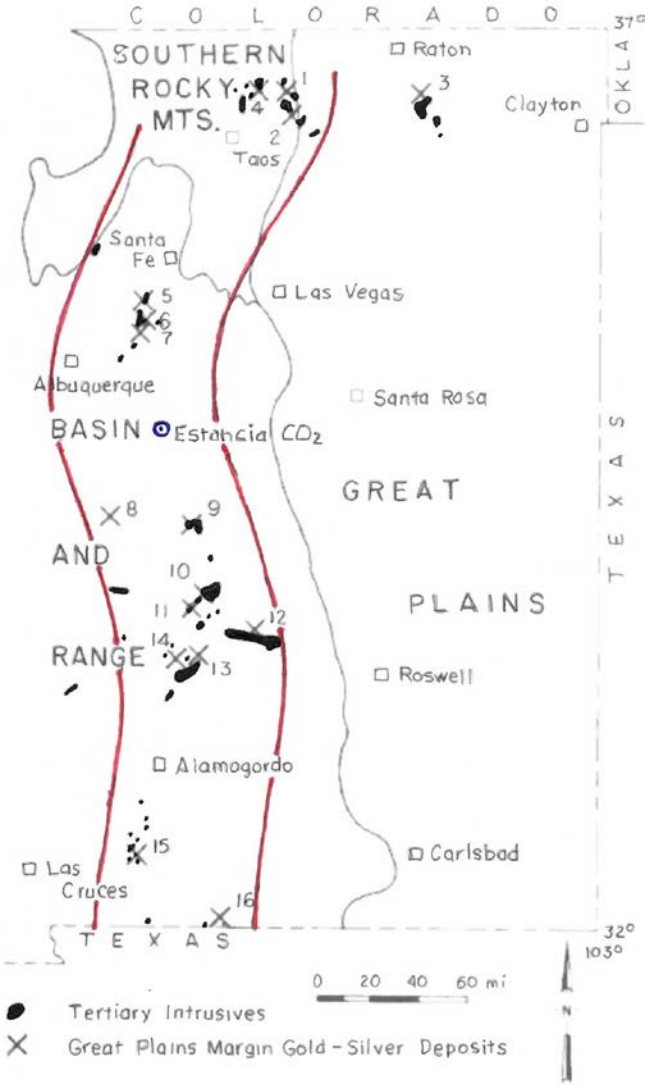

Episode 1 porphyry Mo-W-F and REE-Th-U-F vein-carbonatite deposits are spatially and (by inference) petrogenetically linked with syenite-trachyte, quartz syenite porphyry and small alkalic granite porphyry stocks and breccia pipes. Episode 2 bimodal mafic-granite assemblages tend to foster Au-Ag mineralization closely associated with silica-saturated monzonite and over-saturated quartz monzonite intrusions. Episode 1 trachyte-dominate volcano-plutonic centers tend to show progressive enrichment in Nb, Mo, Rb, and F through time (Allen and Foord, 1991). Similar positive correlation by Ta, Nb, Th, and yttrium (Y) with increasing silica content is observed at the Capitan pluton (Allen and McLemore, 1991).

Exploration efforts at the Red Cloud mining district, Gallinas Mountains appear consistent with the above petrochemical and geochemical linkage between alkalic intrusions and spatially associated mineralization. In the Red Cloud district, well developed Na and K fenite aureoles surround inferred Episode 1 syenite-trachyte intrusions, breccia pipes and veins at the northern

terminus of the LCPB. Mining operations, surface mapping and surface geochemical sampling define a geochemically anomalous area in excess of 8 mi^2. The anomalous area is characterized by high concentrations of fluorite (CaF_2), bastnaesite $(Ce,Y,La)CO_3F$, hubnerite ($MnWO_3$) and an assortment of LREE, U, and Th geochemical anomalies. Extensive mapping, geochemical sampling, and drilling by numerous mining companies helped document the likely nature of the underlying source intrusion responsible for noted surface mineralization. Exhibit 3-57A, B summarizes the conceptual petrogenetic model responsible for the rare earth mineral deposits. All authors agree there is a buried, metal-bearing Mid-Tertiary alkalic syenite-trachyte pluton beneath the Red Cloud district (Exhibit 3-57A). This conceptual petrogenetic model accounts for the peculiar mineral deposits found in the Gallinas Mountains, Lincoln County, New Mexico. We perceive there is a buried, metal-bearing, Mid-Tertiary alkalic syenite-carbonatite intrusion underlying the district (Exhibit 3-57A). This extreme alkalic differentiate is "anhydrous," charged with CO_2 and residual magmatic fluids contain anomalous concentrations of incompatible large radius elements including Fe-REE-Th-U-Mo-(Cu) copper and abundant fluorine. The widespread occurrence of Mo-Cu, the mineral bastnaesite, magmatic-hydrothermal breccia pipes, and fenitized porphyries prompted Cox and Singer (1986) to propose the likelihood of buried carbonatite intrusions underlying the Gallinas mining district. The widespread occurrence of the minerals bastnaesite and fluorite, anomalous concentrations of REE, Th, U, Cu, Fe, breccia pipes, and Na-K-rich fenitized porphyries prompted Cox and Singer (1986) to propose the likelihood that a concealed syenite-carbonatite intrusion underlies the Red Cloud district. Staatz (1992) envisions a somewhat similar spatial and petrogenetic relationship between mined REE-Th-U veins and an unspecified large "alkalic intrusion" with a smaller associated differentiated carbonatite stock (Exhibit 3-57B). This schematic envisions spatial relationship of mapped REE-Th-U veins to a deeper blind alkalic intrusion with a well-developed concentric zone of contact fenitization and late carbonatite magma. A well-developed concentric aureole of Na-K metasomatism is shown replacing and mineralizing wallrocks.

We were unable to find a published age for the Gallinas REE-Th-U alteration and mineralization (32-29 MA; Perhac, 1970, and McLemore, 2010) and assume that the observed alteration-mineralization belongs with Episode 1 magmatism. Thompson (1972, 1973) mapped the area surrounding the multi-phase, Episode 1 Sierra Blanca intrusive complex where it is juxtaposed along the southern margin of E-W-trending Capitan lineament and Episode 2 belt of intrusions. He noted that no less than three Oligocene, low-grade, bulk-tonnage, stockwork deposits were documented by various mining companies: (a) Mo-late phase Three Rivers syenite-alkali granite (26.7 Ma); (b) Mo-Cu-Bonito Lake syenite (26.6 Ma); and (c) Mo-Cu-Rialto syenodiorite-syenite stock and breccia pipes. The adjoining White Oaks syenogabbro-syenite-lamprophyre, vein-breccia deposits contain Au-Mo-W with a fluorite-selenite gangue. The intersection of the N-S- and E-W-trending Episode 1 and 2 belts greatly enhanced regional- and local-scale fracture intensity, increasing crustal-scale permeability, which repeatedly help focus the diverse suite of alkalic and calc-alkalic intrusions and multiple centers of alteration-metallization (Exhibit 3-53A). The presence of undiscovered, conventional double-plunging traps charged with mantle derived CO_2 are most likely to occur proximal to this regional tectonic intersection and lie along the axis of Au-Ag-Mo-REE-Th-U-F-Te mineralization and the ancestral Pedernal arch.

Exhibit 3-57 A, Stylized geologic cross-section depicts the blind syenite-carbonatite parental pluton and surficial intrusions and REE-Th-U alteration-mineralization (adapted from Staatz, 1992); B, envisioned petrogenetic relationship of parental alkalic intrusion, peripheral fenitized contact zone and late stage differentiated carbonatite (adapted from Schreiner, 1993; and Williams-Jones et al., 2000; with info from Richards, 1995)

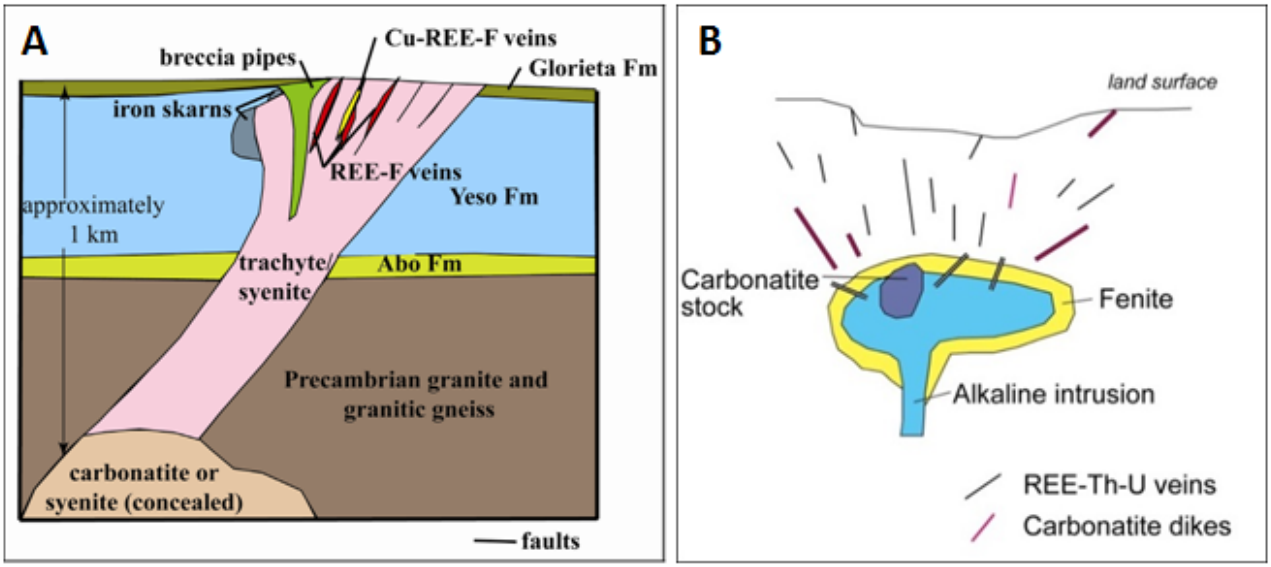

Supporting evidence for streaming CO_2 charge along the Capitan lineament is provided by encountered gas compositions in wellbores from Lea, Eddy, Chaves, and Roosevelt counties New Mexico. Exhibit 3-58 shows the measured/reported content of CO_2 gas from the Upper Permian reservoirs of SE New Mexico (Broadhead et al., 2009).

In Exhibit 3-58 the upper Permian zero isopach line is adapted from New Mexico Bureau of Geology and Mineral Resources and data from Broadhead et al. (2009). The E-W trend of enhanced CO_2 gas concentrations is coincident with the of E-W-trending Railroad-Camino del Diablo swarm of Mid-Tertiary (28 Ma) igneous dikes mapped at the surface. The spatial relationship between the dikes and the elevated CO_2 concentrations may be spurious or possibly the dikes introduced or help focus streaming, supercritical CO_2 fluids exsolved supercritical fluids from deeper crystallizing mafic-alkalic intrusions. Although the number of data points is only eight, the general E-W-trend of the 10, 5, and 1 percent CO_2 contours are unequivocal. The plotted location of the 28 Ma Episode 2 Railroad and Camino del Diablo dike swarms (red lines) is likewise coaxial with the contoured CO_2 anomaly.

Exhibit 3-58 Map summarizes the CO_2 content of gases from Upper Permian reservoirs, SE New Mexico. Content of contained subsurface CO_2 is contoured at 1, 5, and 10% (map and contoured CO_2 generalized from Broadhead et al., 2009; used with permission)

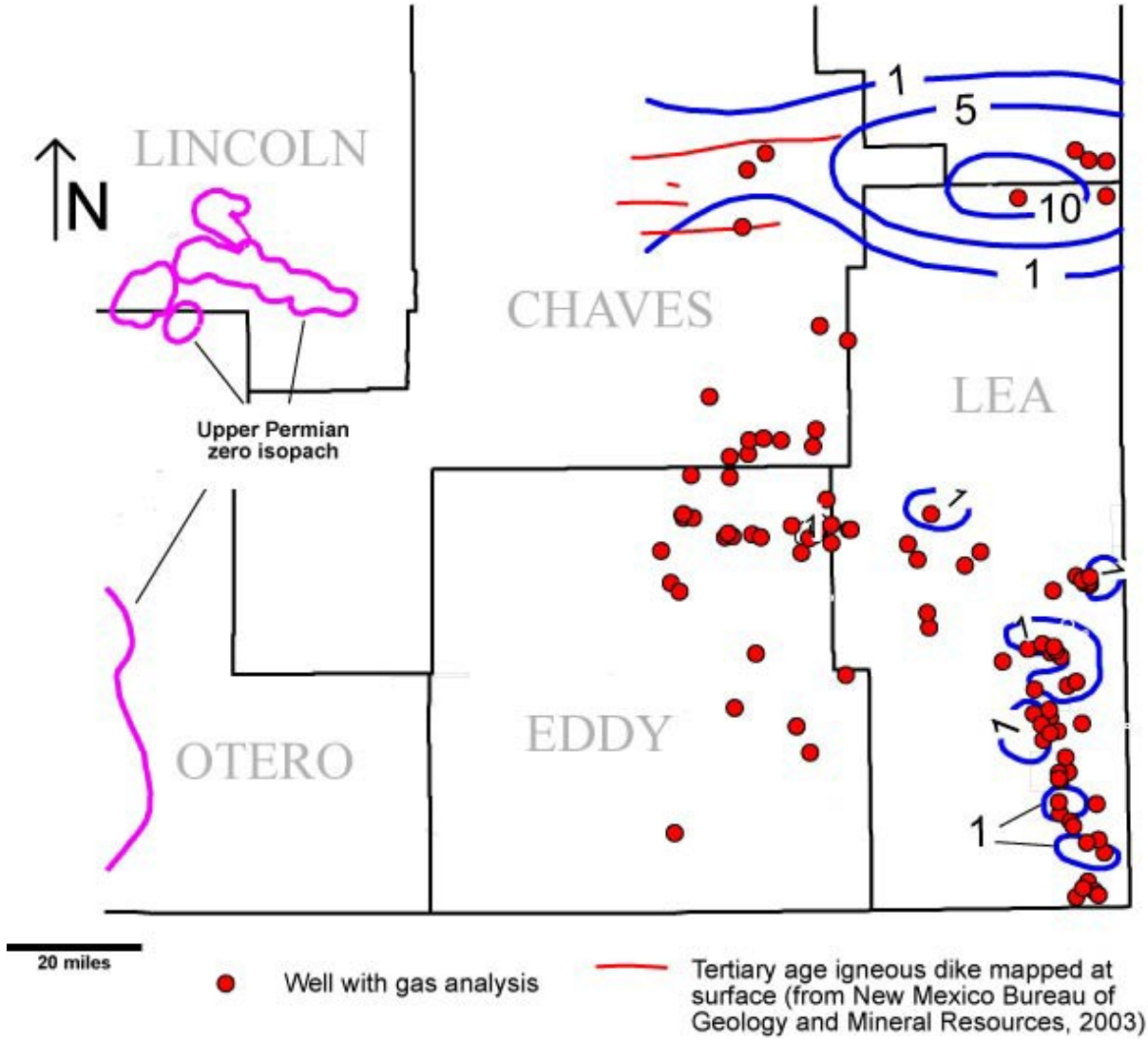

These data support either: (a) over 250 miles of lateral CO_2 migration from the proposed Sierra Blanca point source parallel to the Capitan lineament; (b) Railroad and Camino del Diablo magmas were particularly gas-rich and upon crystallization exsolves enough CO_2 to account for the mapped anomaly; (c) Railroad and Camino del Diablo dike swarms are rooted at depth directly with mantle-rich CO_2 source rocks and channeled CO_2 vertically along the Capitan lineament; and (d) some combination of the three options is operative. Regardless, either long distance vertical or horizontal CO_2 migration occurred, apparently controlled by depth-penetrating, crustal-scale structural elements comprising the Capitan lineament. Three of the five traps identified lie along the hypothetical, subvertical, W-E-directed CO_2 plume generated from a point source near the intersection of the N-S- and E-W-bearing LCPBs of Mid-Tertiary alkalic intrusions.

CO_2 Source, Migration and Trap Charge

Fundamental to this analysis is the extensive geologic mapping and documentation of structural anticlines in Lincoln County by Kelley and Thompson (1964). Exhibit 3-59 is the contour map (+1000 ft above mean sea level [MSL]) (by Kelley and Thompson) of the area at top Permian. The map shows Mid-Tertiary intrusions (stippled, S = stock, L= laccolith; 37-32 Ma), principal faults and folds (anticlines = blue), mining districts and several identified regional structural elements. Mining district abbreviations include: B, Bonito; Cc, Capitan coal; CM, Capitan Mountains; G, Gallinas; J, Jicarilla; N, Nogal; S, Schelerville or West Bonito; SC, Sierra Blanca coal; TB, Tularosa or Bent; W, White Oaks; WC, White Oaks coal; and V, Vera Cruz sub-district. Also shown are Mid-Tertiary intrusions including stocks, laccoliths, and in a few instance, dikes and dike swarms. Regional scale anticlines, synclines and the crest of the Laramide Mescalero arch are highlighted along with the east-dipping Pecos slope (flank) of the arch. Several normal faults are mapped, but as discussed earlier in Section 0 there is a complete absence of Laramide shortening along low-angle thrusts. Twenty-seven Mid-Tertiary intrusions are identified and highlighted by the added stipple pattern. Seven mining districts are identified and abbreviated including: B, Bonito; CM, Capitan; G, Gallinas, J, Jicarilla; N, Nogal; S, Schelerville (W. Bonito); and W, White Oaks. Major and secondary, double-plunging anticlinal traps are arranged in a left-stepping, en echelon pattern across the mapped area. The left-stepping pattern is structurally mimicked by the nine miles of left-lateral separation of the Mescalero arch across the E-W-striking Capitan lineament. The Laramide Sierra Blanca basin is down-dropped 1,200-1,500 ft along the NNE-striking Ruidoso normal fault (Exhibit 3-51A). The Sierra Blanca basin is the largest mapped depression, measures 24 miles in diameter, and is central to the diverse Three Rivers, Bonito, Nogal and Schelerville alkalic volcano-plutonic center and area of intense penetrative fracturing, metallization-alteration and breccia development. The Sierra Blanca alkalic intrusive complex is ranked high as a potential point source for streaming supercritical CO_2 charge with a radial, outward direct migration pattern from the basin's center. Alternatively, once the outward direct CO_2 plume contacted and gained access to the E-W to WNW-trending Capitan shear zone, a sub-vertical oriented plume could fan out eastward along the lineament and attendant Episode 2 dike swarms and deeper plugs and small stocks. The Sacramento uplift borders the map on the south and attains a current elevation of +10,000 at top Permian. The structure contour map shows top Permian is less than +4,000 ft in the center of the basin and +7,000 ft where the Mescalero arch is truncated by the Capitan granite stock. An elevation differential of 6,000 and 3,000 ft, respectively, over horizontal distances of 32 and 50 miles, respectively. These small elevation differentials spread over the large horizontal distances result in broad, open, upright structures plunging ~2-3° NNE.

Four conventional, double-plunging, anticline leads (1-4) and one unconventional, combination, structural-stratigraphic lead (5) are delineated in Exhibit 3-60. The map shows Mid-Tertiary intrusions (stippled, S = stock, L = laccolith; 37-32 Ma), principal faults and folds (anticlines = blue), mining districts and several regional structural elements. Blue stippled areas are the locations of four (1-4) hypothetical conventional anticline and one (5) unconventional stratigraphic CO_2 traps. Refer to Exhibit 3-59 for mining district annotations.

Exhibit 3-59 Structural contour map top Permian showing Mid-Tertiary intrusions, faults, folds and principal mining districts, LCPB. Contour interval is thousands of ft above sea level (modified from Kelley and Thompson, 1964; used with permission)

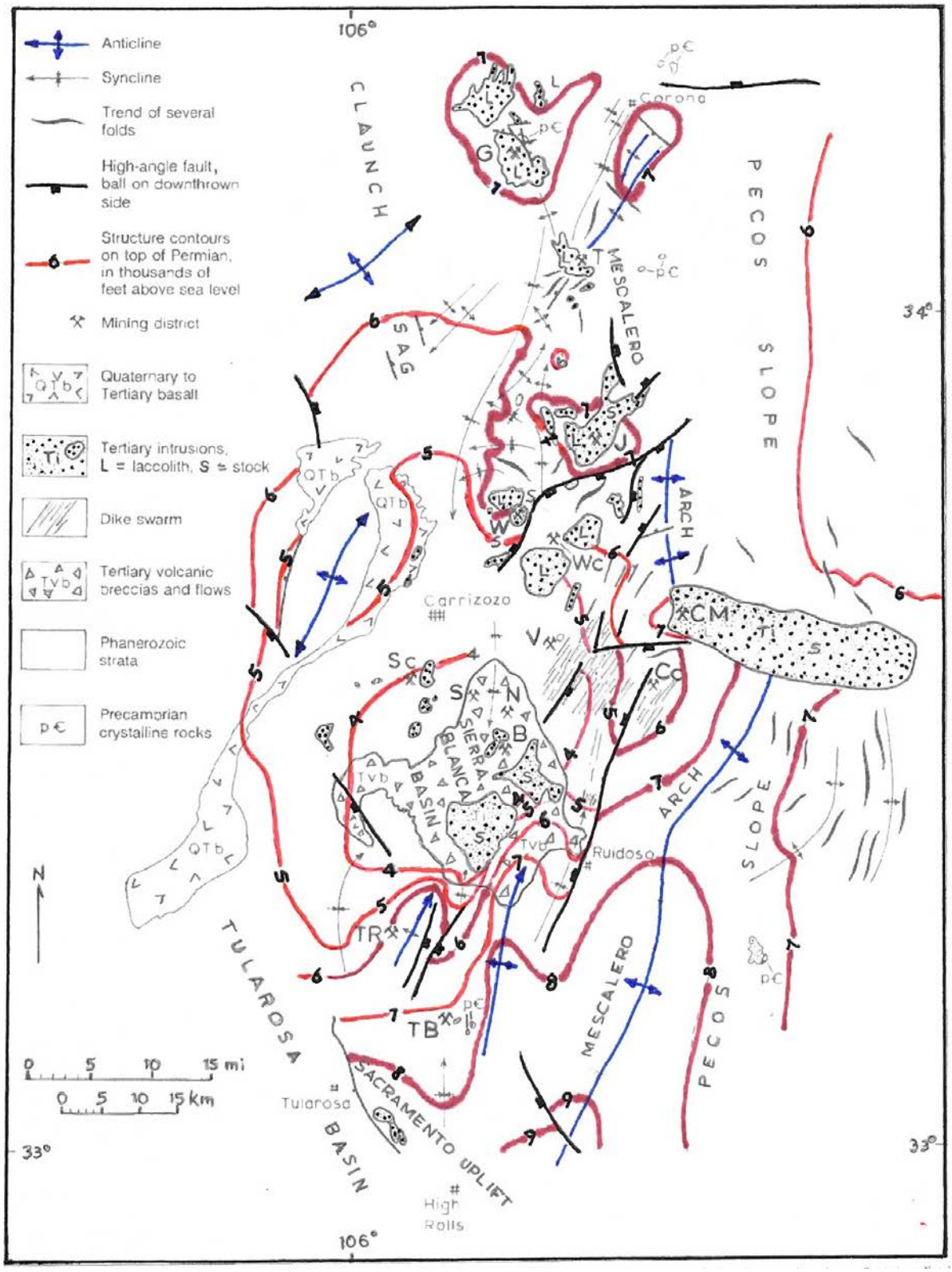

Exhibit 3-60 Structural contour map top Permian of the central portion of the LCPB showing undiscovered CO_2 conventional anticlinal Leads 1-4 and unconventional stratigraphic Lead 5 (modified from Kelley and Thompson, 1964; used with permission)

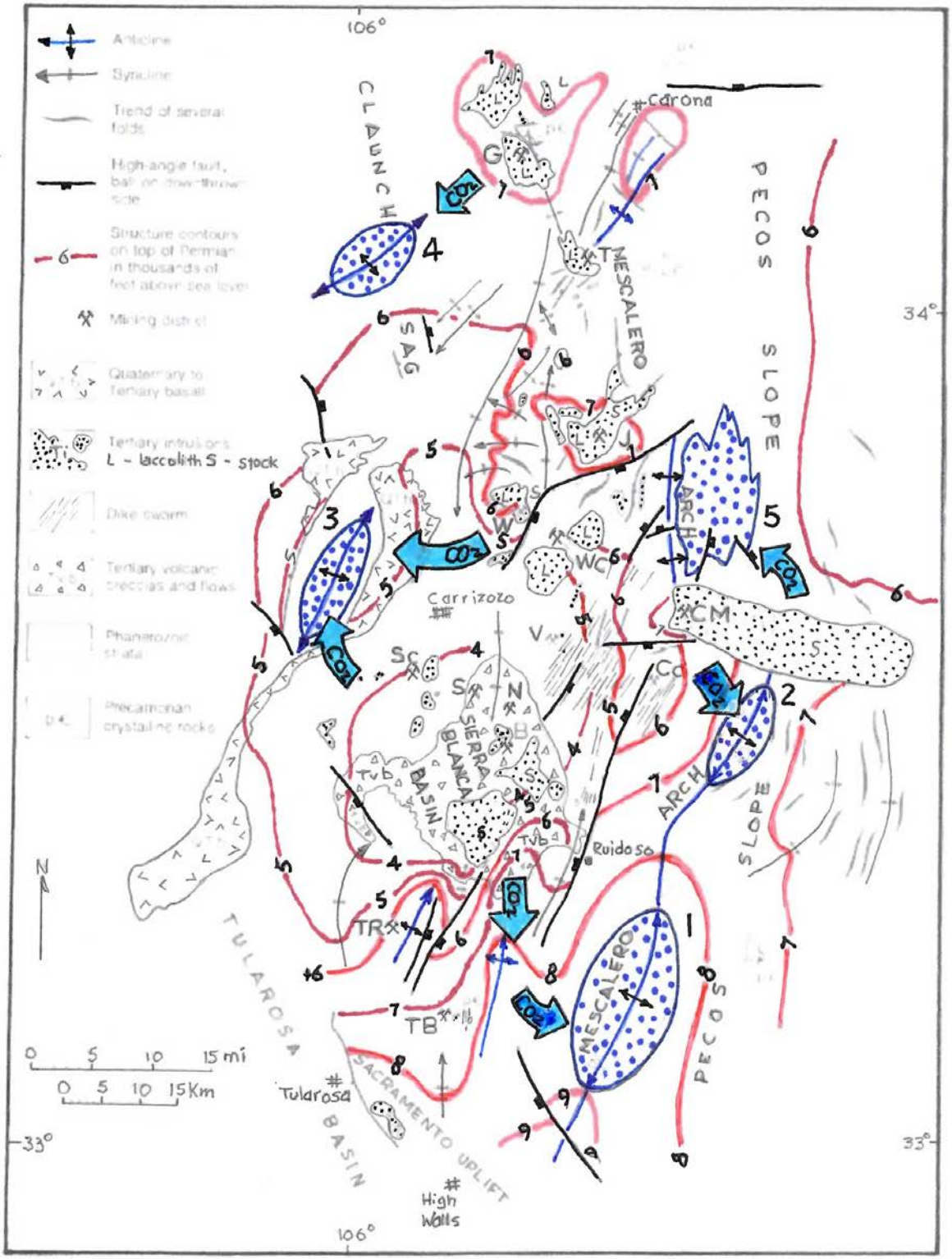

Anticlinal traps 1 and 2 are localized along the gentle, NNE-plunging crest of the Mescalero anticline. This anticline is regional tectonic in character, mapped contiguously in a general N-S direction for over 155 miles (Exhibit 3-50), and gently to actively warped, uplifted and denuded during the Eocene (?) prior to deposition of the late Eocene (37-34 Ma) Sierra Blanca volcanics (Kelley and Thompson, 1964). Although not mentioned in the literature reviewed, it is relevant to note the frontal thrusts of the Laramide fold-thrust belts are mapped only 60 miles or so WSW of the Sacramento Mountains. It was noted that Kevin, Montana, and the Sweetgrass arch were about this distance east of the frontal thrusts of the Cordilleran deformed belt. Transverse structural relief on the Mescalero arch is 1,000 to 1,200 ft which is nearly twice that noted at the Kevin dome. To produce this magnitude of structural relief along a distance of 155 miles during the Middle-Late Laramide bespeaks of lateral compression and crustal shortening. If correct, the Mescalero anticline is underlain by an E-direct, shallow, W-dipping thrust (Exhibit 3-51A). The likely tip of the blind "Mescalero thrust" is at the foot of the Pecos slope which represents the E forelimb of the regional Mescalero fold (Exhibit 3-61). At Kevin dome the blind foreland thrust underlying the Sweetgrass arch played a significant role in facilitating and channeling CO_2 fluid flow laterally away from subvertical transverse shear zones. We envision a similar Laramide geometric and kinematic solution for the Lincoln County area. The influence on potential CO_2 fluid flow along two, regional, co-tectonic shear zones is significant: (a) 11 miles of left-lateral separation, shearing and fracturing along the middle-late Laramide Capitan transfer renders wallrocks more P/P; (b) linking 11 miles of transverse Capitan transfer movement to the underlying Lincoln County thrust helps visualize and assess the physical character of Precambrian granite/gneiss involved in the shortening; (c) migrant supercritical CO_2 fluids are preferentially focused along the orthogonal set of shear zones (vertical and horizontal); and (d) the network of sub-vertical and -horizontal intra-shear zone releasing-bends channelize CO_2 fluid flow driving plumes laterally and vertically for potentially large distances.

In this four-dimensional framework, it is not difficult to visualize how each of the four conventional traps are contacted by migrant CO_2 and charged. Fluid flow is radially outward from the Sierra Blanca CO_2 point source along the gentle- to sub-horizontal-dipping Mescalero thrust. Local subvertical shear zones channel supercritical CO_2 fluids vertically until contact is made with each of the respective anticlinal culmination. Traps 1 and 2 along the Mescalero arch are products of local plunge reversal coincident with the formation of gentle structural saddles between anticlinal culminations. Traps of this type are universal along huge shallow-plunging anticlines similar to those envisioned along the Mescalero and Sweetgrass arches. CO_2 charge gains access to Lead 1 up-flank toward the SSE-SE around the SSW tip of the Ruidoso normal fault. CO_2 access to the Lead 2 is similar to Lead 1 but around the NNE tip of the Ruidoso it is normal along E-W to WNW-trending high P/P zones parallel to the Capitan shear zone.

Unconventional Lead 5 is a product of structure and stratigraphy. Carboniferous and early Permian convergence between South America-Africa along the southern edge of the North American plate (Laurentia) resulted in profound shortening across the Ouachita fold-thrust belt. Associated shortening was linked across the foreland of the American Southwest promoting uplift of the Ancestral Colorado Rockies across Texas, Oklahoma, New Mexico, Colorado and Utah (Kluth and Coney, 1981). The N-S-trending Pedernal arch and its NNE continuation along the Sierra Grande uplift of NE New Mexico are products of this huge crustal shortening event.

Exhibit 3-61 Structural contour map top Permian of the central portion of the LCPB showing location of unconventional Lead 6 associated with the Sierra Blanca intrusive center and basin flank (adapted from Kelley and Thompson, 1964; used with permission)

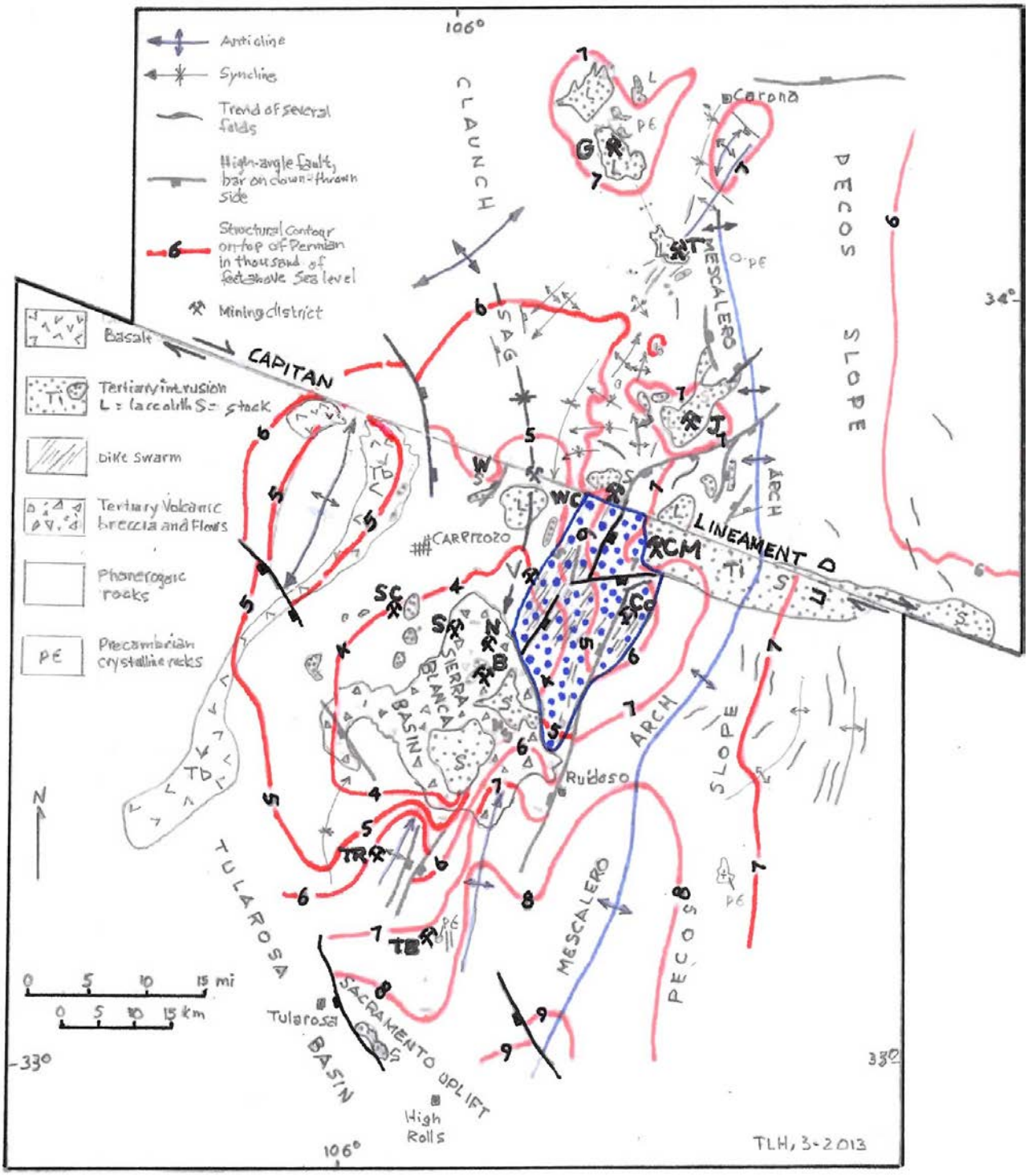

Eleven miles of left-lateral separation across the WNW-trending Capitan lineament are shown restored and recontoured.

As mentioned previously, the Pedernal arch experienced wholesale denudation during the Ouachita orogeny. The entire Cambrian through Pennsylvanian section was removed from the crestal portion of the arch. Subsidence during the early Wolfcampian promoted the deposition of the lower Tubbs Sandstone and laterally equivalent strata Exhibit 3-51B. As noted in Exhibit 3-59, the Pedernal and Sierra Grande arches locally remained high and resulted in depositional windows or areas of erosion and non-Tubbs and –upper Yeso Formation deposition (inscribed red area). Lead 5 is a hypothetical unconformity pinchout by the lower Yeso sandstone member westward against the eastern flank of the Pedernal arch north of the Capitan lineament. Charge for the trap is facilitated by its proximity to the E-W to WNW-striking Capitan transfer and underlying Mescalero thrust. Both regional shear zones are believed to have experienced periodic CO_2 plume development during a prolonged period (38-26 Ma) of mafic-alkalic, alkalic and calc-alkalic Episodes 1 and 2 volcanism and plutonism.

The blue stippled area highlighted in Exhibit 3-47 outlines an extensive area of pervasive, NNE-trending, Mid-Tertiary fluid fracturing and calc-alkalic, mafic and alkalic dike and vein emplacement. The map shows the contoured top Permian (red, thousand foot contours), structural framework and Tertiary intrusive and extrusive igneous rocks. Highlighted by the blue stippled area delimits the areal extent of pervasive, NNE-trending, Mid-Tertiary hydraulic fracturing and mafic, calc-alkalic and alkalic dike emplacement. The map restores 11 miles of left-lateral, oblique-slip along the WNW-trending Capitan lineament. Contours and structural framework elements are modified to accommodate the left-lateral oblique-slip movement. Mining district annotations are similar to those shown in Exhibit 3-59. Lead 6 is an unconventional “basin-centered” fractured reservoir play. See Section 2.2 for description of the unconventional basin-centered stratigraphic and combination fractured-basement play concept. A proximal analog of Lead 6 is the southern, small CO_2 field at Estancia, New Mexico. The two Estancia fields are localized along the medial axis of the Mid-Tertiary, New Mexico Au-Ag belt and the west flank of the Pedernal swell, 190 miles NNW of the Sierra Blanca intrusive complex (Exhibit 3-50 through Exhibit 3-56). Sixteen wells were drilled in the two field areas. Most of the wells drilled encountered small to economic quantities of CO_2. Production is most likely from the lower Pennsylvanian Sandia Sandstone Member. Drill depths are from 1600 to 2000 ft. Where significant quantities of CO_2 were encountered (800-1,000 thousand cubic ft per day [Mcfd] and 400 psi pressure) produced gas was 99 percent CO_2 with 0.04 percent He. Interestingly, the final well drilled (Lee 16) was a redrill from 1840 to 2000 ft (total depth [TD]). Initial production from the Sandia was apparently non-economic; however, the redrilled interval penetrated the underlying Precambrian schist and metaquartzite. Drill records report at TD the well produced 12,000 Mcfd CO_2 without mention of the percent contained CO_2. The well was never produced and the fields were abandoned in 1941 (Foster and Jensen, 1971). Lead 6 plays on this theme of highly fractured Precambrian basement rendered porous and permeable due to multiple sets of fractures. Similar conditions are reported from deep wells from the St. Johns field in western New Mexico. There are few areas in New Mexico, which evidence more intense, continuous, planar hydraulic fracturing than in the Sierra Blanca basin. Envisioned reservoirs include the clean, basal, Permian Yeso Sandstone and underlying Precambrian gneiss, quartzite and schist. The topseal is shaley units in the Yeso and intercalated evaporate successions immediately overlying lower Yeso Sandstone. The regional topseal includes thick mudstone, shale, and siltstone successions in the lower Cretaceous Mesaverde Formation. CO_2 charge is proximal related to protracted Sierra Blanca intrusive and peripherally emplacement of breccia pipes, small circular plugs and alkalic-carbonatite intrusions (37-26 Ma, Exhibit 3-54).

Introduction

The McCallum field in northern Colorado represents the northern most intrusive center and consanguineous CO_2 field allied with Mid-Tertiary tectonism and magmatism. As indicated in Exhibit 3-35, the North and Middle Park areas are considered integral to the Southern Rocky Mountain Cordilleran/High Plains alkalic province. The McCallum CO_2-bearing anticline is located in north-central Colorado about 17 miles south of the Wyoming-Colorado state line. This NNW-NW-bearing, double-plunging anticline lies five miles NE of Walden, Colorado, along the inverted eastern margin of the North Park basin (Exhibit 3-62). The map shown in Exhibit 3-62 is modified from compilations by Blackstone (1977) and Tweto (1979) for the purpose of this study. Low-angle thrust faults (solid triangles on hanging-wall) and high-angle reverse faults (open triangles on hanging-wall) are highlighted and differentiated.

In Exhibit 3-62 two significant, regional conjugate transfer zones were identified and added, including: (a) ENE-trending, left-lateral Ring Mt; and (b) WNW-trending, left-lateral Delaney Butte-Cameron Pass (DB-CP) transfer. The footwall cutoff of the WNW-trending Independence thrust was initially located along I°-I' prior to late Laramide compression. Shortening was rotational with a maximum of 4.5 miles at I' decreasing eastward to the null point at I° near Kings Canyon, Colorado (Blackstone, 1977). The discovered McCallum CO_2 field is stippled. The tectonostratigraphic and magmatic evolution of the North and Middle Park basins is summarized in Exhibit 3-63. Measured and compiled composite stratigraphic sections by Steven (1960) and Blackstone (1977) suggest the maximum stratal thickness preserved in the basin is between 16,395 ft and 14,135 ft, respectively (Exhibit 3-64). The estimated maximum thickness of Mesozoic strata is quoted as 6,640 ft; whereas, the Cenozoic Coalmont is about 9,000 ft thick.

This suggests an accumulative maximum locally preserved Mesozoic-Cenozoic stratigraphic section of about 15,640 ft. On average, two miles of this composite stratal thickness is comprised of Late Cretaceous Pierre Shale and Paleocene-Eocene Coalmont Formations. Blackstone (1977) synthesized Late Cretaceous-Tertiary tectonostratigraphic of northern Colorado and adjoining Wyoming.

Surface mapping measured sections and borehole data indicate the lower shaley and upper sandstone units of the Pierre Shale totaled over 5,000 ft; similarly, overlying Paleogene Coalmont conglomerate, sandstone, claystone, and shale succession also totaled over 5000 ft.

The structural framework of North and Middle Park basin was further modified by the mapping and compilation work of Tweto (1975, 1979) shown in Exhibit 3-66 and with the recommended additions in Exhibit 3-67. Low-angle thrust faults (solid triangles on hanging-wall) and high-angle reverse faults (open triangles on hanging-wall) are highlighted and differentiated in Exhibit 3-67. This map highlights principal compartmental boundaries (Walden, Grizzly-Illinois, and Middle Park), transfer faults (Williams Range-Never Summer and Delaney Buttes-Cameron Pass), and relevant radiometric ages of Tertiary intrusive and volcanic igneous rocks.

Exhibit 3-62 Tertiary structural framework map of North Park Basin, Colorado and adjoining Wyoming (modified from the compilations by Blackstone, 1977; Tweto, 1979). McCallum subsurface CO_2 gas fields are stippled

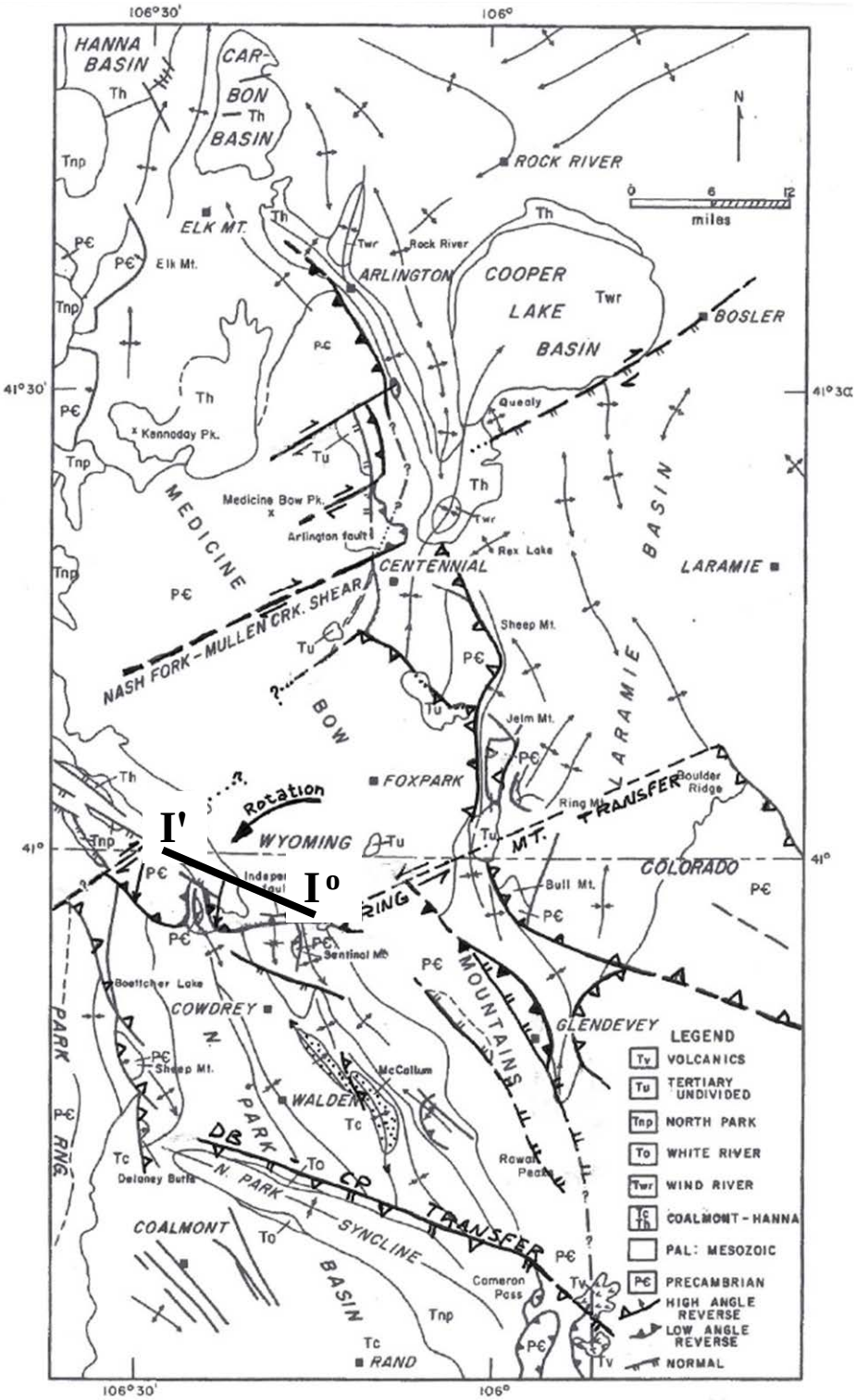

Exhibit 3-63 Tectonomagmatic evolution of North and Middle Park Basins, Colorado

Tectonomagmatic Evolultion of North and Middle Park Basins, Colorado
Late Tertiary 12-3 Ma
Late Miocene-Pliocene vertical uplift, faulting, stream incision, and drainage integration
Extensional faults strike NNW-NW including the large Northgate fluorspar fault-veins
Up to 500 m of North Park Formation (Late Miocene-Pliocene) fluvial boulder and conglomerate deposits intercalated with ashy, quartzose, conglomeratic sandstone, claystone, and limy shale in local extensional depocenters, largely removed during Pliocene uplift and incisement
Mid-Tertiary 36-21 Ma
Epeiorogeny, weathering, erosion, planation, and magmatism along the E-W Rabbit Ears and N-S intrusive belts; N- and NW-trending fault-bound basins and half-grabens. 32-23 Ma Rabbit Ears radial dikes, mafic basalt-andesite and Never Summer calc-alkalic granodiorite, granite and high-silica rhyolite stocks and plugs, lamproite, basalt-rhyolite vents, and coeval ashflows and lavas
White River Fm (To) basin-fill dominated by cgl, ss, and bentonitic slts and rhyodacite breccia (28 Ma) and basalt flows (26 Ma) erupted from the Braddock Peak intrusive center and overlies the Independence Mt thrust. Up to 500 m of Troublesome Fm (Tt, 24-13 Ma) overlies Tc and Tmp
Late Laramide 48?-36 Ma
Shortening, uplift, warping, block-faulting, subdued landscape across So. Colorado Rockies.
Intrabasin en echelon reverse faulting and folding→10,000 ft relief on bsmt and differential subsidence; igneous quiescence until 36 Ma (Wall Mtn tuff)
N-S-striking, low-angle, Never Summer thrust juxtaposes Proterozoic over folded-overturned Windy Gap (Twg) and White River Fm (To) basin-fill; 8 mi (13km) total accumulated overhang; WNW-striking, low-angle (15-20°), Independence Mt " thrust" truncates Coalmont strata without significant footwall drag folding
Middle Laramide 60-48? Ma
Low-angle (10-15°), west-vergent, Never Summer thrust overrides and overturns footwall Coalmont Fm (Tc) and Windy Gap Mbr cgls with 6 mi (9.5 km) of proterozoic basement overhang Relaxation, block-faulting, half-grabens, continued denudation of Park Range and Front Range→Middle Park and Coalmont Fms (61-48 Ma), volcaniclastic cgl, ss, arkose to braid stream-fluvio-lacustrine deposits lying disconconformably on Kp; coal beds in lower 2000ft of Coalmont Fm.; 9000 ft of Coalmont deposits = 9000ft/13 Ma = 209 m/Ma = rapid differential subsidence
Late Cretaceous-Early Tertiary 75-60 Ma
Active displacement on the Williams Range (6 km, Erslev, 1999), Bross Mt (2 km, tlh) and Never Summer thrusts. Early formed anticlinal cores eroded to top Dakota Sandstone (Erslev, 1999)
Magmatism common along the NE-SW-trending Colorado Mineral Belt (CMB); minor mafic alkaline to calc-alkaline intrusive plugs (7) in southern Middle Park
Serious thrusting, denudation to bsmt, disconformable deposition of Middle Park Fm (Tmp) and Windy Gap Mbr (Twg) on Pierre Shale after 6000 ft of erosion (~150 m/Ma uplift and erosion)
Emplacement of a 66± 4Ma cpx latite porp sill into lower Middle Park Fm (Schroeder, 2004)
Mesozoic Strata
Tr Chugwater, J Entrada-Sundance, Morrison; K Lakota and Dakota, Mowry-Benton, Niobrara and Pierre preserved

? - Uncertain Age

Exhibit 3-64 Composite stratigraphic section and lithologic descriptions of Mesozoic and Cenozoic sedimentary rocks measured in the Northgate District, North Park Basin (based on Steven, l960)

Age	Unit	Thickness (feet)	Description
Pliocene (?) and Miocene	North Park Formation		Impure silts, sands and stream gravels
Unconformity			
Oligocene	White River Formation		Grey to white tuffaceous silts and clays
Unconformity			
Paleocene	Coalmont Formation	Greater than 9,000	Grey sandy siltstone, poorly sorted arkosic sandstone, brown carbonaceous shale, and thin lenticular lignite beds. The Sudduth coal zone is 25 to 50 ft above base and Capran coal zone is about 2,600 ft above base.
Unconformity			
Late Cretaceous	Pierre Shale	3,100 - 4,200	Dark-grey fissile shale and grey sandy siltstone in lower 1,850 ft; grey sandy siltstone and a few 100 to 150 ft sandstone units in upper part
Late and Early Cretaceous	Niobrara Formation	865	Yellow to grey limy siltstone and shale
Early Cretaceous	Dakota Group	200-320	Pebbly conglomerate, sandstone and shale
Unconformity			
Late Jurassic	Morrison Formation	445	Variegated shale with monir interbedded sandstone and limestone
	Sundance Formation		
	Upper unit	70	Grey to brown thin-bedded ripple-marked sandstone with interbedded silty and sandy shale and limestone
	Lower unit	75	White to grey cross-bedded sandstone
Unconformity			
Triassic and Permian	Chugwater Formation	690	Red silty shale and sandstone
Permian	Forelle (?) Limestone	8-15	Pink to light-grey laminated limestone
	Satanka (?) Shale	0-50	Red silty shale
Unconformity			
Precambrian			Gneisses, schists, and igneous rocks

? - Uncertain Age

Exhibit 3-65 Composite stratigraphic columns summarize formation and member nomenclature for the South, Middle, and North Park Basins, NW Colorado and SE Wyoming (from Wandrey and Barker, 1991)

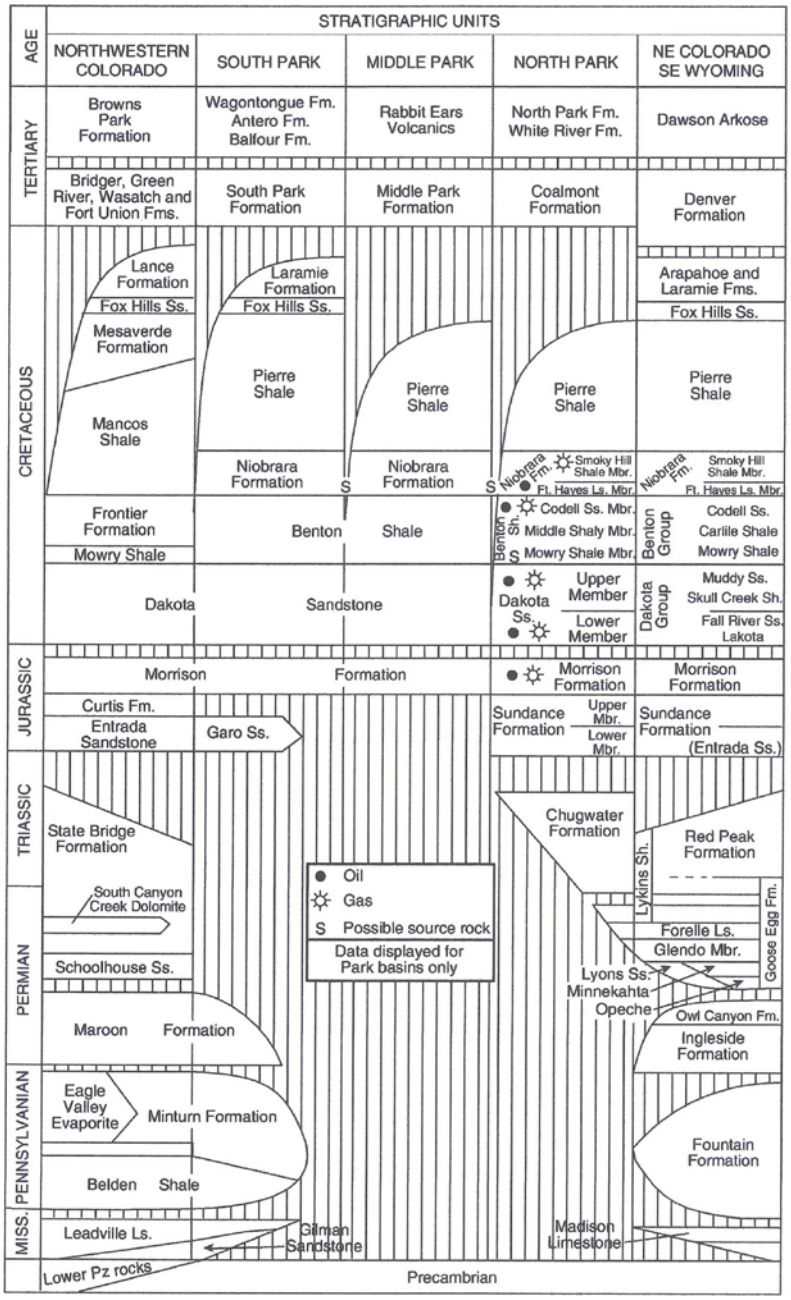

See Exhibit 3-64 for stratal thicknesses and respective lithologies for Middle Park. (Park Basin Province Colorado with a section on Upper Cretaceous Niobrara Fractured Calcareous Shale Oil by Pollastro, 1991).

Source: USGS

Exhibit 3-66 Generalized Tertiary structural framework map of the Colorado Headwaters Basin (CHB), Middle and North Park Basins, north-central Colorado (compiled from Wellborn, 1977; Tweto, 1979; recent additions from Cole et al., 2010)

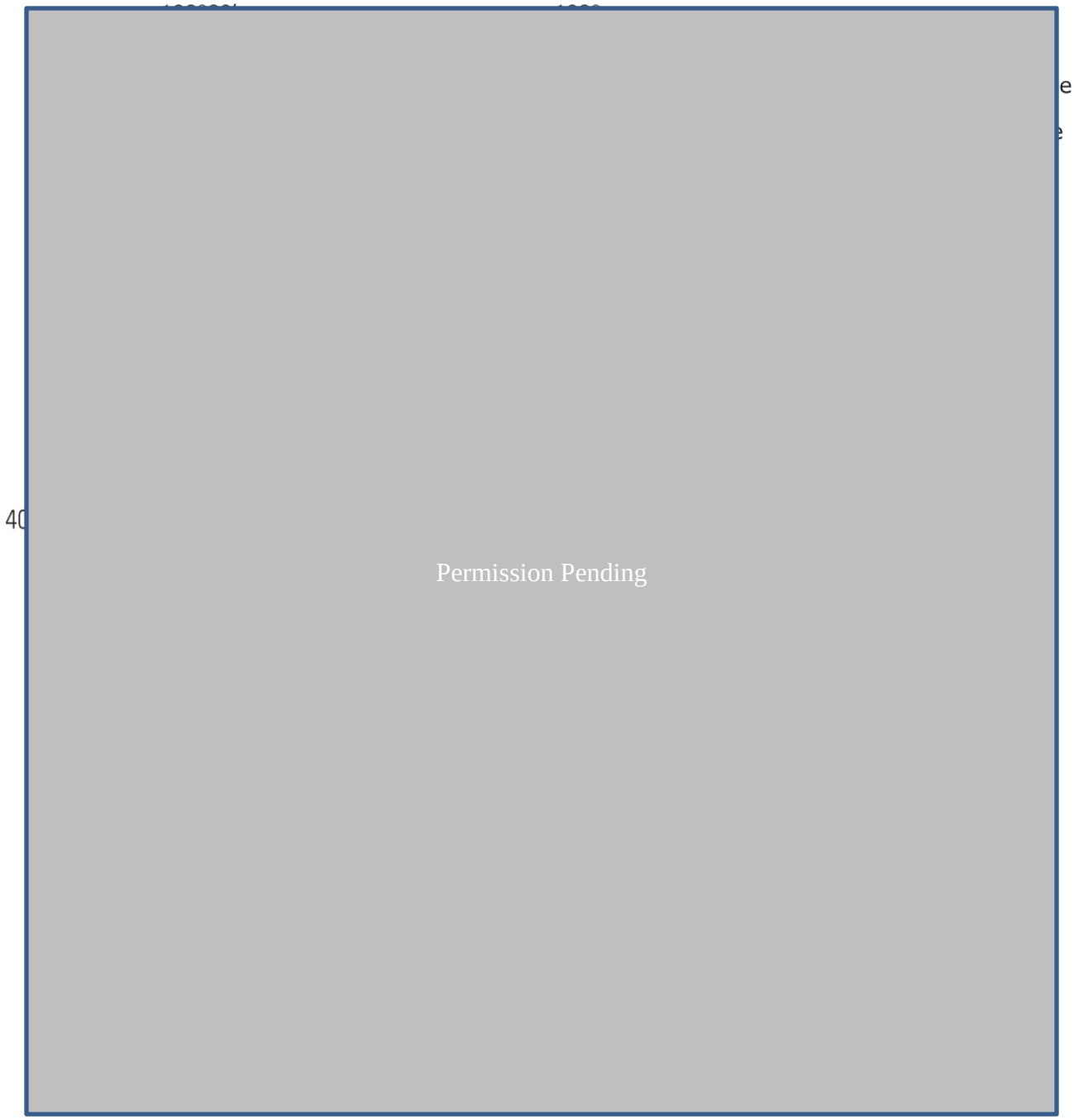

Exhibit 3-67 Modified structural framework map of Middle and North Park Basins, Colorado highlights Mid-Tertiary intrusive rocks (red boxes, which contain radiometric ages in Ma), Rabbit Ears intrusive plugs (black triangles), and principal structural compartments (modified after Cole et al., 2010; used with permission)

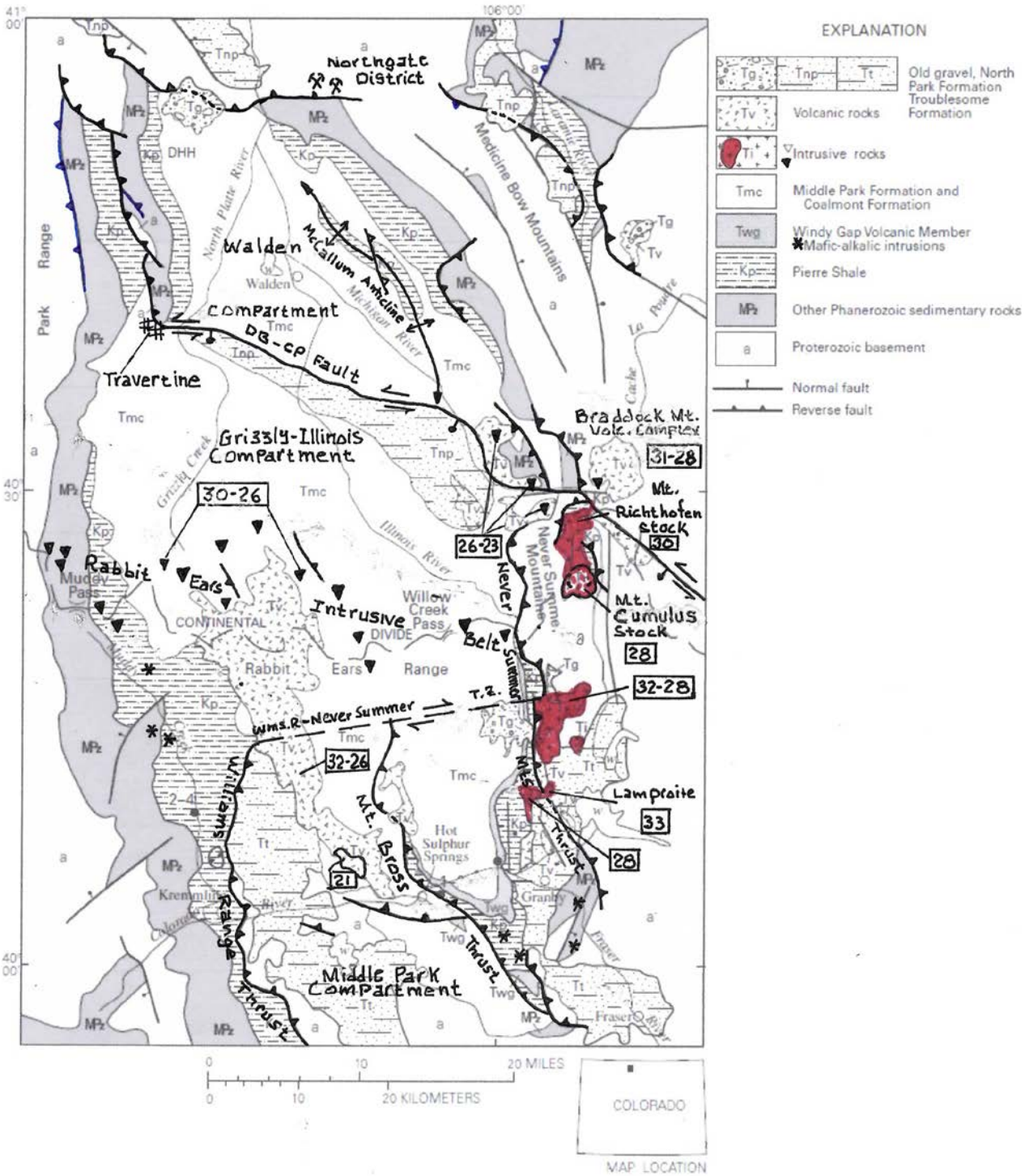

Structural Framework Definition

McCallum CO_2 field (Exhibit 3-62) lies along the NE margin of the basin and the southern end of the Precambrian basement cored southern Medicine Bow Mountains. Three important Laramide framework elements are highlighted: (a) a belt of NNW-trending thrusts extending continuously from Glendevey, Colorado for over 108 miles to beyond Arlington, Wyoming (herein, Glendevey-Arlington thrust belt); (b) the regional set of NE-ENE-trending transfers including the right-lateral Nash Fork-Mullen Creek shear zone and left-lateral Ring Mountain transfer; and (c) a set of WNW-trending shear and transfer zones interpreted as the conjugate direction to the NE-ENE structures mentioned above, including the Independence Mountain "thrust" and Delaney Buttes-Cameron Pass (DB-CP) transfer zone.

The Laramide tectonostratigraphic evolution of North and Middle Park basins involves three recognizable episodes: Late Cretaceous-Paleocene (75-60 Ma, F_{EL}), Paleocene-Eocene (60-48? Ma, F_{ML}), and Eocene (48-36 Ma, F_{LL}). Mid-Tertiary (36-21 Ma) and Late Tertiary (12-3 Ma) include two distinctly non-shortening episodes of predominately extensional and transtensional deformation. Exhibit 3-63 provides, in synoptic fashion, diagnostic tectonostratigraphic characteristics of each respective episode of syntectonic deposition, coeval tectonism and magmatism.

Magmatism, Volcanism and CO_2 Sources

The exhibits provided in this report of Middle and North Park basins of Colorado were mapped in detail by an assortment of field geologists from the U.S. Geological Survey, Colorado Geological Survey, numerous professors from nearby universities in Wyoming, Colorado, and Utah as well as geologists from both major and minor oil/gas exploration companies.

A review of Exhibit 3-67 demonstrates that Cenozoic rocks are present, but not widespread. The most pronounced alignment of intrusions is along the eastern margin of the Headwaters basin. Several small calc-alkalic to alkalic granite stocks are aligned N-S, extending from north of Granby, Colorado to the Braddock Mountain volcanic complex at Cameron Pass. The Never Summer magmatic belt has arc-like chemical affinities and was emplaced during the early Oligocene (32-28 Ma). The N-S elongate plutons intruded at shallow epicrustal levels and seemed to feed extrusive andesitic, rhyodacitic, and rhyolitic out-flows arranged centripetally to parental stocks, plugs, and volcanic necks. The local preservation of coeval eruptive volcanics is indicative of relatively low rates of post-emplacement exhumation. A second obvious alignment of intrusive-extrusive rocks is along the E-W to WNW-trending Rabbit Ears intrusive belt (Exhibit 3-67). Numerous small, fine-grained plugs and necks of basalt, trachyandesite, and andesite are scattered along the belt. Many of the small plugs and vents are subvolcanic in character and viewed as the roots of a more extensive basic-to-intermediate volcanic carapace. Radiometric ages of Rabbit Ears intrusive and extrusive igneous rocks are tightly grouped between 30-26 Ma, which are coeval with rocks comprising the Never Summer igneous belt to the east. The only alkali-mafic intrusion encountered during the literature search was a small lamproite plug located six miles north of Granby, Colorado, near the southern end of the Never Summer belt, showing in Exhibit 3-67 (Thompson, et al., 1997). The small intrusion is ultrapotassic in composition (+10 weight percent K_2O), has chemical affinities similar to the Leucite Hills lamproite volcanic yield (1-3 Ma) located down structure from the supergiant La Barge, Wyoming, CO_2 field, and is interpreted as sourced from a similar mantle lithosphere at a depth of 90-125 miles or deeper. Exhibit 3-68 shows an asymmetric character of the NW-

trending, NE-vergent, North and South McCallum anticlines with their steep-to-vertical NE-dipping forelimbs relative to the 20-40°-dipping backlimbs.

Exhibit 3-68 Structure contour map top Dakota Sandstone, Middle and North Park Basins, Colorado, and the McCallum anticline (500 ft contour interval). A-A' is the location of the cross-section across the North Park Basin (adapted from Wellborn, 1977)

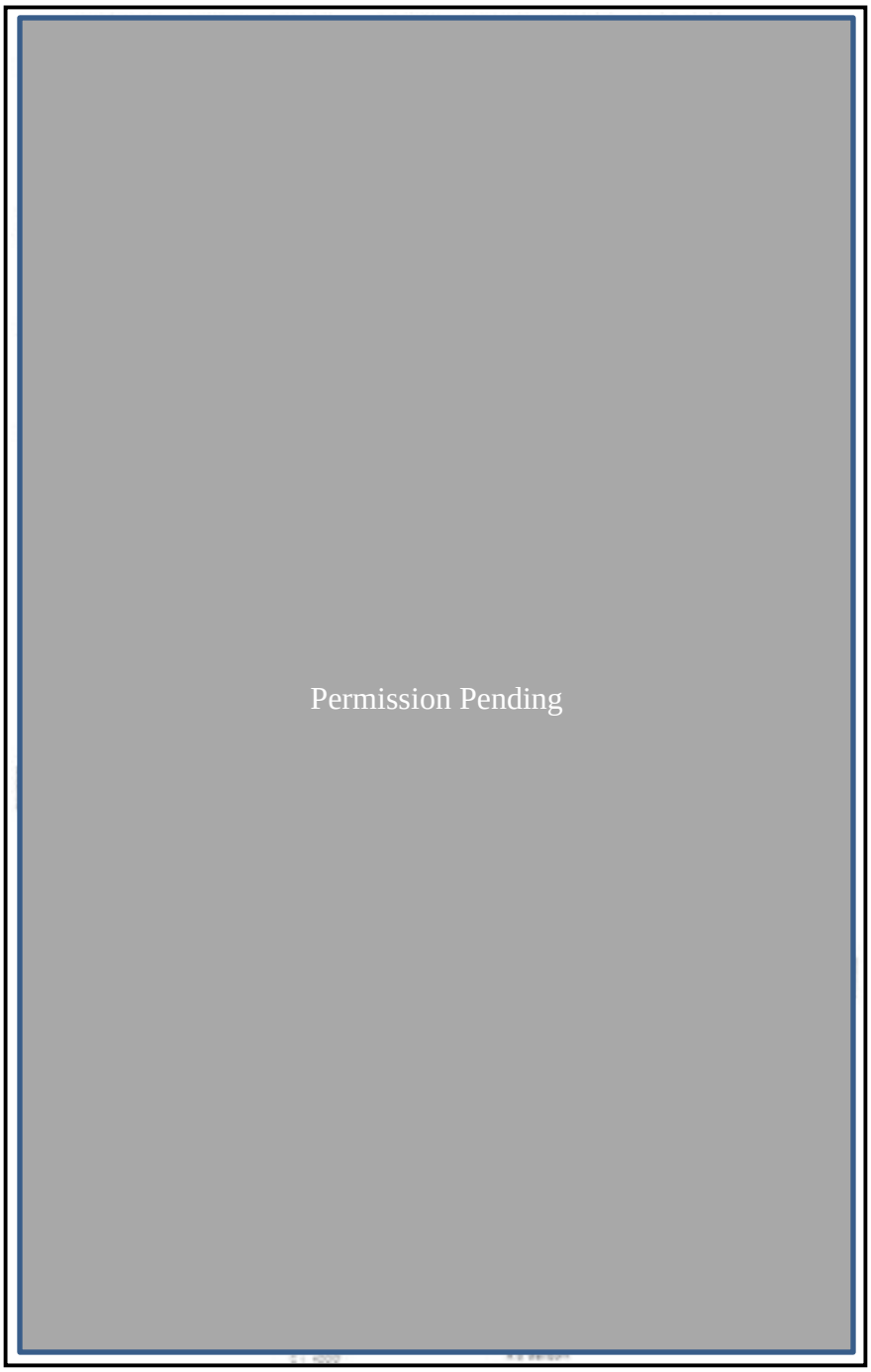

Strategic wells at McCallum are pre-1977. Line A-A' shows the location of the Walden compartment transverse cross-section, included in Exhibit 3-69. The geometry of dip panels is controlled by surface geology, subsurface boreholes, and constrained by the knowledge that the: (a) Coalmont Formation (Tc) is at least 9,000 ft thick in the axial portion of the North Park syncline; (b) Pierre Shale (Kp) is 4,200 ft thick; and (c) the combined thickness of sub-Pierre Shale Paleozoic and Mesozoic strata (PMz) become thinner ENE from 0.6 to 0.3 miles across the North Park basin (Sims and Goth, 1957 and Wellborn, 1977). The overall "shovel-shaped" kink geometry of the basin is well documented as well as respective ENE- (McCallum) and WSW- (Sheep Mountain) verging anticlines. Asymmetric limbs dip at 50-90° while back-limbs dip at 20-40°. Basin-bounding reverse faults underlying McCallum and Sheep Mountain anticlines are steep, typically dipping 65-70°. Depth to the detachment underlying the North Basin is not controlled and arbitrarily placed at a depth of 7.5 miles where the Sheep Mountain back-limb kink plane intersects the WSW-vergent Sheep Mountain reverse fault. All faults and axial surfaces are assumed linear, and folds have angular fault-bend fold geometries. The restored Precambrian/PMz contact is 25 miles in length while the deformed length of the cross-section is 20 miles in length. This suggests the true-scale cross-section is shortened by 5.5 miles, or 21.5 percent.

The ultrapotassic lamproite intrusion is located about 15 miles south of the partially buried, 23 mi^2 Mount Cumulus intrusion (Exhibit 3-67). This pluton yields a 28.2 Ma age and is a highly differentiated alkalic granite-granite porphyry, which appears closely associated with numerous small, consanguineous rhyolite porphyry intrusions a nd a rhyolite tuff-breccia ring fracture zone in the Upper Illinois River drainage (Exhibit 3-70, UI on map). The combination of ultrapotassic lamproite (33 Ma) and off-lapping Mount Cumulus alkalic granite-granite porphyry and rhyolite (28.2 Ma) leads to the possibility of potential sources for significant CO_2 charge in the North Park basin.

Exhibit 3-69 Schematic ENE-WSW oriented cross-section (A-A' in Exhibit 3-67) constructed from Sheep Mountain, across North Park Basin and through the McCallum anticline

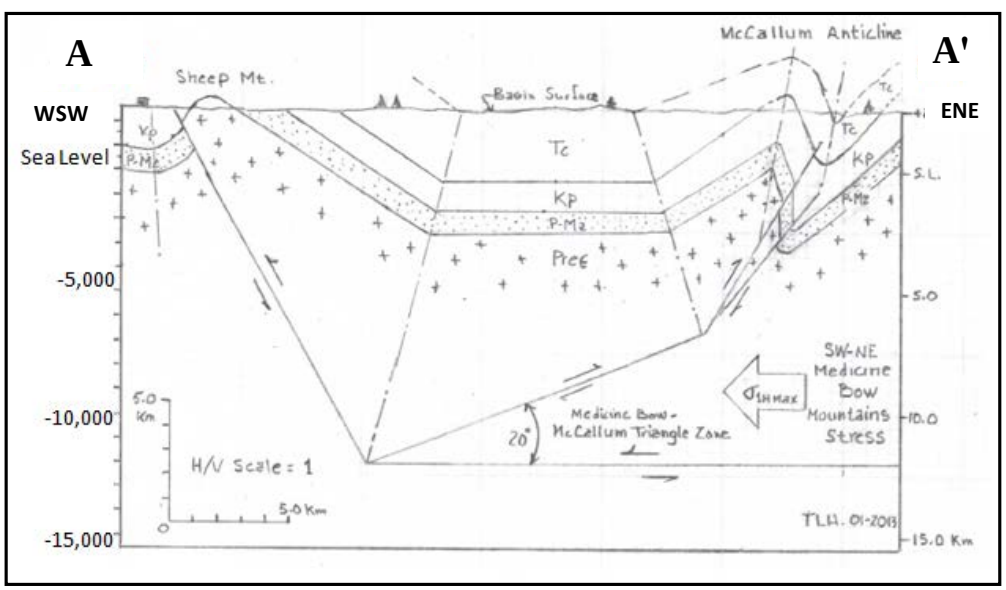

CO_2 Source, Migration Pathways and Trap Charge

As shown in Exhibit 3-67, the Never Summer-Braddock intrusive belt trends NNE and is 22 miles long. Note that the belt terminates on the north at the Braddock intrusive complex. More specifically, the belt is interpreted as localized at the marked, left-stepping, releasing bend geometry produced by the proposed left-lateral, DB-CP lateral transfer fault (Exhibit 3-64, Exhibit 3-67, Exhibit 3-69, and Exhibit 3-71). Geologic features shown in Exhibit 3-70 include: oval gravity low (red dashed, hachured line enclosing buried granite porphyry at Jack Creek (JC) and Mount Cumulus (MC) stock; Colorado River fault (CRF); Michigan River fault (MRF); North Fork thrust (NFT; and Never Summer thrust (NST)). Geographic features shown in Exhibit 3-70: Braddock Peak (BP); Chambers Lake (CL); Cameron Pass (CmP); Clark Peak (CP); Kawuneechee Valley (KV); Little Yellowstone (LY); North Park (NP); Owl Mountain (OM); Specimen Mountain (SM); and Seven Utes Mountain (SU). Symbols include: Pre€, Proterozoic basement; PMz, Paleozoic-Mesozoic und.; Kp, Pierre Shale; Twg, Windy Gap Volcanic Member (65-60 Ma alkali basalt, andesite intrusive plugs); Tmc, Middle Park and Coalmont formations; Tertiary intrusive (Ti), volcanic (Tv) rocks; Troublesome (Tt) and North Park (Tnp) formations; and older gravel deposits (Tg). Blue arrows show principal CO_2 fluid migration pathways during Braddock Peak plutonism and volcanism (32-23 Ma). The noted intersection of source rocks endowed with CO_2 at releasing fault-kink geometries are crucial in the focusing of migrant supercritical CO_2 fluids. Detailed mapping of the Braddock intrusive complex (Cole and Braddock, 2009) demonstrates that the proposed DB-CP transfer links with numerous WNW-striking wrench faults, which were experiencing left-lateral shear movement concomitant with Mid-Tertiary plutonism and volcanism.

Exhibit 3-70 Detailed geologic map of the Braddock Peak intrusive and volcanic complex, Northern Never Summer Mountains, North Park, Colorado (modified after Cole and Braddock, 2009)

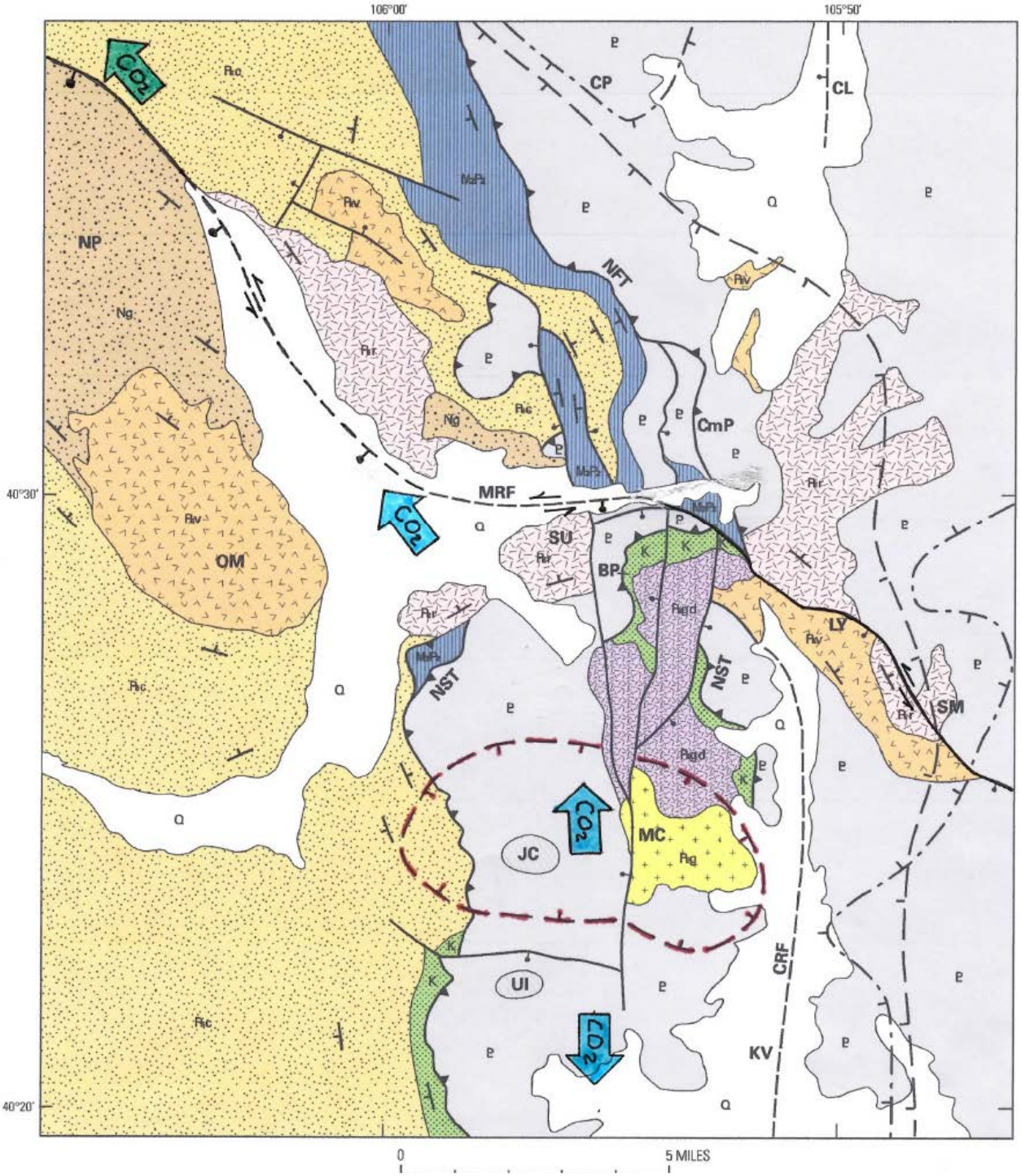

Source: USGS

Exhibit 3-71 Structural framework map of North and Middle Park Basins, Colorado (adapted after Wellborn, 1977). Fourteen km of total shortening assumed and conserved along the Williams Range-Never Summer thrust belt (Erslev and Holdaway, 1999, and Erslev et al., 1999).

Permission Pending

Produced overhang on the Never Summer thrust belt is indicated by dashed footwall cut-off line. Highlighted in blue are hypothetical, blind, footwall CO_2 leads beneath the Never Summer and McCallum South thrusts. Blue arrows denote suspected supercritical CO_2 migration routes

Left-lateral, left-stepping, kink-bend fault geometries (±25°) are highly dilational in nature and act as areal "suction pumps" during periods of displacement. Supercritical CO_2 expelled from the late differentiated fractions of the Mount Cumulus magma chamber were naturally "sucked" or focused into the dilated-brecciated area of the bend. Similar arguments hold for the focusing of streaming, supercritical CO_2-charged fluids associated with the emplacement of other blind ultrapotassic lamproite intrusions emplaced along the Never Summer-Braddock intrusive belt. The consequence of having favorable: (a) CO_2 source intrusions; (b) co-tectonically active, sub-vertical, depth-penetrating wrench faults; and (c) presence of local, dilatant-releasing fault kink geometries occurring in concert only 12 miles SW of the McCallum CO_2 field is no coincidence. Exhibit 3-71 summarizes the resultant migration route from the Never Summer-Braddock intrusive belt into the McCallum trap. Once entrained, supercritical CO_2 reaches the general area of the geo-suction pump, and vertical migration is impeded by thick regional topseals succession within the fissile Pierre shale and carbonaceous Coalmont shale. Lateral migration beneath the thick shale topseal is facilitated by: (a) differential brecciation and cataclasis localized along and within the DB-CP transfer zone; (b) zones of high permeability within brecciated and fractured Dakota Sandstone juxtaposed along the DB-CP transfer zone; (c) differential lateral migration of streaming CO_2, which is likewise channeled along the sub-horizontal Medicine Bow detachment underlying the Walden structural compartment (Exhibit 3-69); (d) upward movement along the WSW-dipping (20-55°) McCallum backthrust; or (e) direct up-plunge migration (N30°W) from the DB-CP transfer along the highly fractured crestal culmination of the Dakota Sandstone into the double-plunging McCallum trap. The potential for multiple, stacked reservoirs in the footwall of the McCallum backthrust seem highly likely, and their location is indicated on Exhibit 3-71. This top Dakota Sandstone contour map (500 ft contours) shows the distribution of principal thrusts/reverse faults, estimated shortening on respective shortened faults (miles), Mid-Tertiary intrusions (Tib, lamproite; Tg, Cumulus granite; Tgd, Richthofen granodiorite; Ti, undifferentiated) and volcanic rocks (Tv) localized along the Never Summer-Braddock intrusive belt. Perceived CO_2 point sources are the Cumulus alkalic granite pluton (Tig) and the Never Summer lamproite plug (Tib). Proposed Never Summer and McCallum subthrust leads are shown with stippled blue pattern. Relatively long-distance migration of CO_2 charge along the DB-CP transfer (35 mi) is suggested by the mapped travertine deposits south of Delaney Buttes (Exhibit 3-71).

Another suspected subthrust lead underlies the huge, shallow, east-dipping Never Summer thrust. The envisioned anticline involves lower and upper Dakota reservoirs and the underlying Jurassic Morrison Formation. All reservoirs are in direct contact with the Mount Cumulus granite CO_2 source intrusions. Charge could also involve other blind CO_2-rich lamproite intrusions emplaced along the Never Summer-Braddock intrusive belt. The structural setting for this subthrust play is structurally complex; moreover, the Precambrian footwall cutoff is at least another six-to-seven miles further east. The possibility of blind CO_2-charged structural traps beneath the Never Summer thrust is favorable; however, locating large, uncompromised traps is difficult without adequate seismic coverage. Sub-thrusted, folded, and fractured Precambrian basement (granite) could prove a viable unconventional productive reservoir in this particular structural setting involving 7.5 miles or more of overhang.

3.3 Identified Mid- to Late-Tertiary Fairways and Undiscovered CO_2 Lead

Introduction

The San Juan basin is the largest in New Mexico and located in the Four Corners area. Its lateral extent is delineated in Exhibit 3-72, which shows it continues northward into adjoining Colorado. Also depicted is the location of known CO_2 fields and occurrences including La Barge, Wyoming; Gordon Creek, Farnham dome, and Escalante, Utah; Lisbon and the McElmo cluster of fields, McCallum dome, and Sheep Mountain, Colorado; Des Moines, Bravo dome, Estancia, and St. Johns dome, New Mexico; and St. Johns/Springerville, Arizona. Inscribed and indicated in red in Exhibit 3-72 is an assortment of Tertiary igneous rocks. Major volcanic fields constituting the "ring" of volcanism surrounding the Colorado Plateau include (clockwise from East to West) Rio Grande rift in southern Colorado-northern New Mexico, Taos, Mt. Taylor, Zuni-Bandera, and Springerville field, New Mexico; White Mountains and San Francisco volcanic fields, Arizona; Western Grand Canyon fields, northern Arizona, and southern Nevada; and Marysvale, Utah. The present-day basin is a distinctly asymmetric, rhombic-shaped depression with thick accumulations of Tertiary and Cretaceous strata overlying a more deformed and thinner Paleozoic succession deposited on Precambrian crystalline rocks.

Exhibit 3-72 Map of the Colorado Plateau locates the San Juan Basin and highlights several, large Late Tertiary volcanic fields peripheral to this huge regional structural block (adapted from Gilfillan et al., 2008 and 2009)

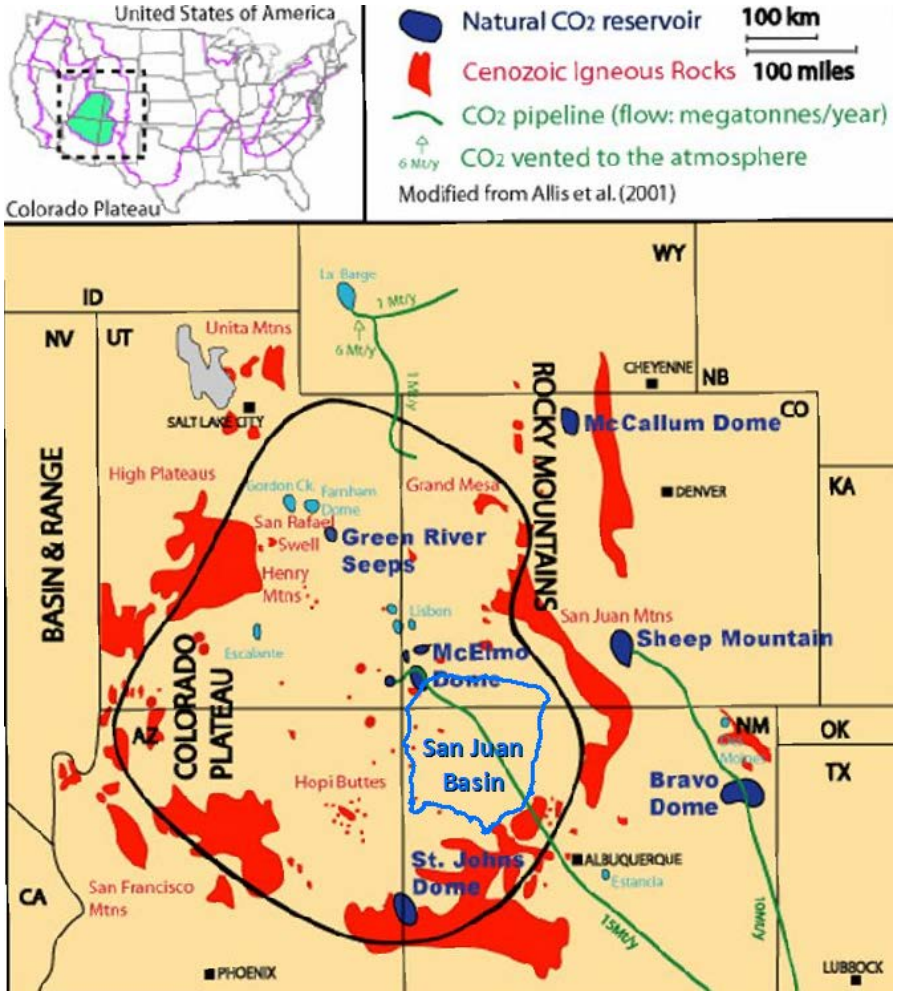

The prominent NE-trending Defiance-Hogback monoclinal structure separates the Four Corners platform on the NW from the San Juan basin to the SE (Exhibit 3-73). The map highlights subsurface (black) and surface (blue) faults, anticlines (green), Tertiary igneous dikes (red) and reverse faults (orange). In the upper left, an orthogonal system of WNW- and NNE-striking faults are indicated, underlying much of the San Juan basin. A diverse suite of uplifts surround the basin, including: (a) on the west (Defiance uplift-Four Corners platform), (b) on the north and northeast (Archuleta arch), and (c) on the east (Nacimiento uplift) and south-southeast (Zuni uplift and Chaco slope). Exhibit 3-72 places the basin well within the Colorado Plateau physiographic province, transposed on the east by the NNE-trending Rio Grande rift. The boundary of the Colorado Plateau is defined by a well-developed, Middle-Late Tertiary "ring of volcanic fire." Major volcanic fields are basalt-dominate, including (clockwise from East to West): Rio Grande rift in southern Colorado/northern New Mexico; Ocate, Taos, Mt. Taylor, Zuni-Bandera, and Springerville fields, New Mexico; White Mountains and San Francisco volcanic fields, Arizona; Western Grand Canyon fields, northern Arizona, and southern Nevada; and Marysvale field, Utah. The San Juan basin is a geologically and physiographically tectonostratigraphic element of the Colorado Plateau province.

Exhibit 3-73 Regional structural framework map of New Mexico shows mapped subsurface (black) and surface faults (blue); major Tertiary intrusive centers and dikes (red); and major reverse faults (orange) (adapted from Broadhead et al., 2009; used with permission)

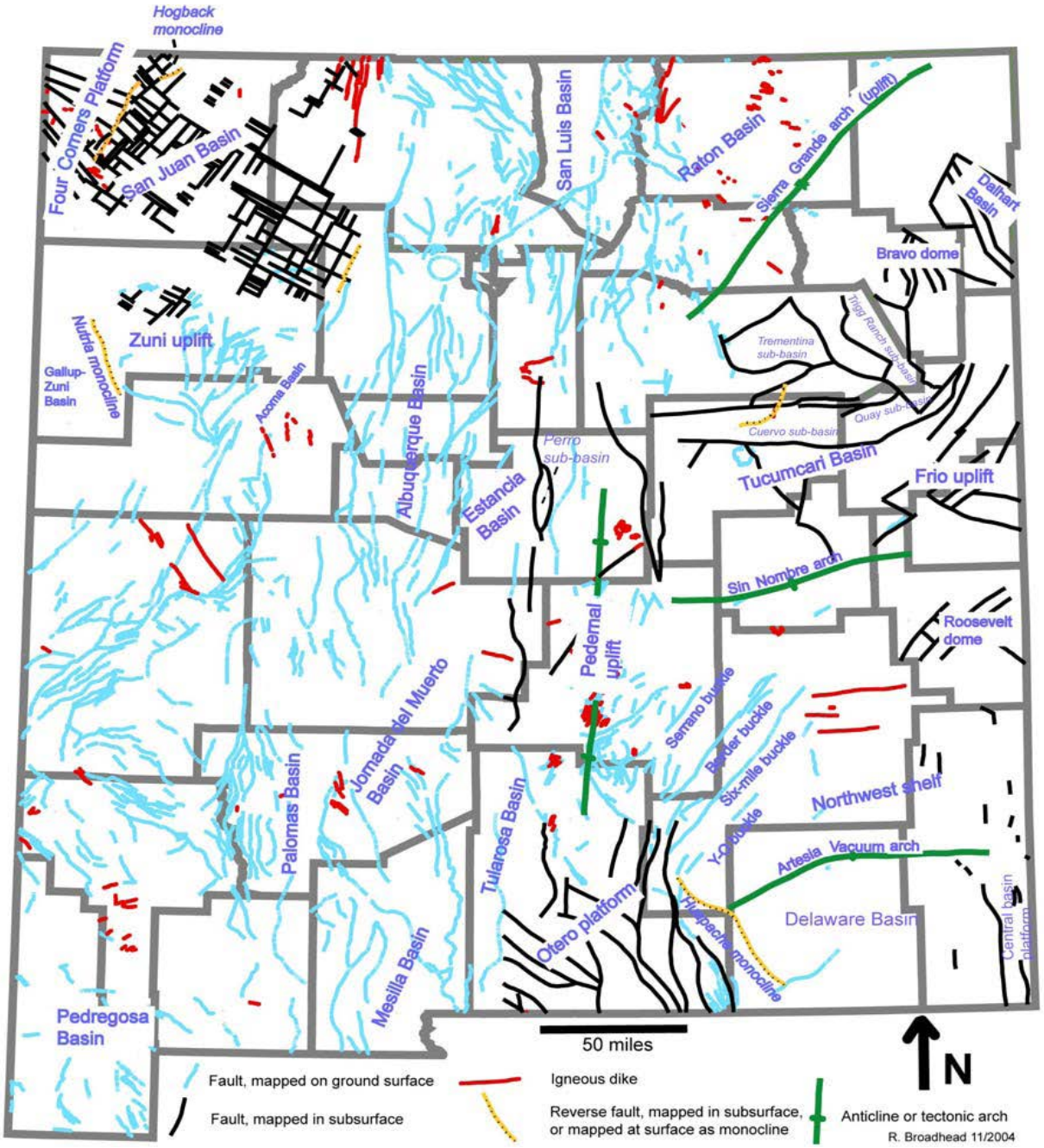

Note the subsurface orthogonal system of WNW- and NNE-striking faults underlying the San Juan Basin. Blank areas indicate an absence of subsurface control.

Structural and paleogeographic restorations of the San Juan basin, and particularly during deposition of the important Mississippian Leadville reservoir strata, are challenging without abundant data (Baars, 1966). Surface outcrop sections adjacent to the basin are widely spaced from uplift to uplift, platform to arch; moreover, there are very few deep wells that penetrate the basement within the deeper portion of the basin. Regional framework elements are well-established on the adjoining plateau. With the aid of regional gravity and aeromagnetic surveys, these elements are located and correlated across the basin. Seismic surveys cover most of the basin, but parameters utilized during data collection were often set for imaging shallow Mesozoic or Paleogene strata at the expense of high definition in the deeper Paleozoic sections.

An abundance of favorable mafic-alkalic and alkalic igneous rocks are mapped surrounding the basin (Exhibit 3-72). Few favorable Tertiary intrusions are noted or cut by wells drilled within the basin proper. The presence of over 80 mafic minette intrusions (Central Navajo volcanic field, 27-18 Ma) surrounds the basin on the SW and W, extends for over 60 miles toward the SW; and are mapped over 120 miles west of the basin. Many of these intrusions are pipe-like, filled with ultramafic serpentine breccia and correlated with the underlying mantle lithosphere. The abundance of ultra-mafic, mafic, and lamprophyric dike swarms immediately north of the basin greatly reduced the risk of not having an adequate blind CO_2 source rock beneath the San Juan basin.

Regional Four Corners and Local San Juan Structural Frameworks

The New Mexico Bureau of Mines and Mineral Resources (NMBMMR) group at Socorro, New Mexico, and associated geological societies have compiled, synthesized and published relevant geological and geophysical data for the public sector and industry. Most of the data reviewed for this portion of the report come from this association. Exhibit 3-73 is an example of the type of work routinely provided by the NMBMMR organization. The regional structural framework map of New Mexico highlights both sub-surface (black) and surface verified elements (blue). Anticlines are highlighted in green, reverse faults in orange, and Tertiary intrusions in red. In the upper left corner of the map, an orthogonal system of WNW-and NNE-striking faults are documented underlying the San Juan basin (Kelley and Clinton, 1966). This orthogonal pattern is fundamental to the basin and observed elsewhere throughout most of the Colorado Plateau region (Exhibit 3-74). A comparison of these two maps (Exhibit 3-73 and Exhibit 3-74) shows that the orthogonal fracture system does not appear to persist across the younger set of N-S-trending faults associated with post-34 Ma, E-W-directed extension associated with Rio Grande rift development. Regional mapping and detailed stratigraphy and stratigraphic correlations demonstrate that the second order W50°W-trending fracture zones (lineament) were produced concurrent with the collision and indentation of South America (Gondwanland) with south-central North America (EurAmerica) along the Marathon fold-thrust belt between 335-265 Ma (King, 1977). The resulting Marathon orogeny in West Texas, produced crustal-scale shortening adequate to differentially elevate large, NNW-NW-trending crustal blocks of the “Ancestral Rocky Mountains” of New Mexico, Colorado, Utah, and Arizona (Kluth and Coney, 1981). The large NW-trending “Uncompahgre uplift” and foreland “Paradox basin” highlighted on Exhibit 3-74 is of Late Mississippian, Pennsylvanian, and Early Permian age (Huffman and Condon, 1993). The Marathon orogeny of West Texas and co-tectonic deformation associated with the formation of the Ancestral Rocky Mountains was directly responsible for producing Marathon facies stratigraphic trapping geometries, which characterize the San Juan and Paradox basins (Baars, 1966).

Exhibit 3-74 Regional structural framework map of the Four Corners portraying dominate lineament orientations

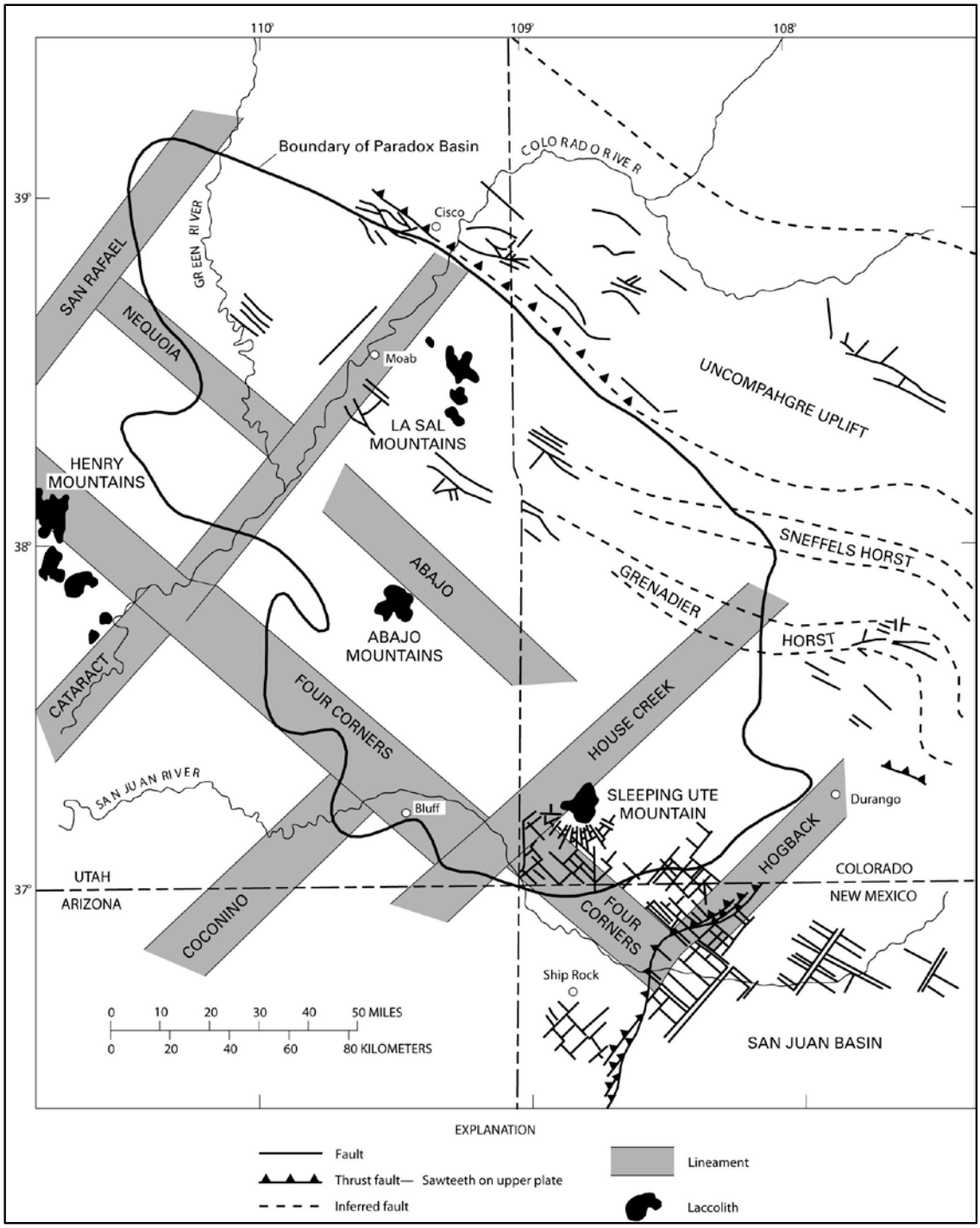

Enegis-interpreted image of data from Kelley and Clinton (1960), Baars (1966), Baars and Stevenson (1982), and Huffman and Taylor (1997)

ENE-WSW-directed Laramide shortening associated with low-angle Farallon subduction beneath the American Southwest, formed the widespread monoclines, folds, and associated thrust-reverse faults of the Colorado Plateau (Davis, 1978). The N-NNE-trending Defiance uplift-Hogback monocline depicted in Exhibit 3-73 through Exhibit 3-75 effectively "down-drops" the San Juan basin several miles relative to the structurally high-standing Four Corners platform. Exhibit 3-75 shows that the San Juan basin is located central to several positive structural elements of Precambrian, Carboniferous (Ancestral Rocky Mountains), Laramide, Mid-Tertiary, and Late Tertiary age. Syn-tectonic and depositional high-standing fault-fold terrane surrounding the basin restricts the lateral migration of CO_2 out of the basin.

This transverse-trending hogback monocline is interpreted as a regional structural zone of near vertical folding of the brittle, crystalline basement that is rooted in a high-angle, WNW-dipping reverse fault. It is noted with interest that the continued NNE projection of the Defiance-Hogback structure deflects the mapped Grenadier horst, Sneffels horst and leading edge of the SW-vergent Uncompahgre allochthon in a 15-mile-wide, right-handed oroclinal flexure. This magnitude of flexing of structural elements of the Uncompahagre block bespeaks of significant right-lateral, strike-slip displacement. A possible simplistic and likely explanation is that the Hogback monoclonal structure roots into a regional-scale transverse, transfer of Marathon age with miles of offset and cataclasis of all pre-tectonic (pre-Permian) synorogenic strata. Huffman and Taylor (1999) published seismic cross-sections and suggested the Defiance-Hogback trend was a zone of major structural weakness, which accommodates right-lateral shear of unknown but important offset. A transpressional zone of deformation of this magnitude could represent the perfect fault-seal for post-tectonic expelled fluids attempting to migrate SW, W, or NW out of the San Juan basin.

The sinuous, N-S-striking, eastern hinge of the basin (Archuleta arch and Nacimiento uplift) shows syndepositional/tectonic thinning of most preserved strata from the Mississippian Leadville Formation through Paleocene strata (Woodward and Callender, 1977). They also mention that there is between 10,000-13,000 ft of structural relief between the culmination of the east rim and the adjoining basin (1977). Differential syntectonic thinning of Late Cretaceous-Paleocene strata are particularly apparent, documenting two stages of compressional activation during the Laramide orogeny: (a) an early phase of right-lateral offset totaling two-to-three miles was distributed along the western margin of the Nacimiento uplift (Woodward et al., 1992), and (b) a second phase of later Laramide transpressional overthrusting with minor overhang occurred immediately west of the uplift (Woodward, 1987). Coincident shortening and dip-slip reactivation of the Defiance-Hogback fault zone is expected and would result in the near-vertical dipping, observed in the monoclonal flexing of the post-Marathon facies strata across the buried transfer. The effect of Laramide reactivation and resultant fault-fold geometry across the Defiance-Hogback fault zone and Nacimiento uplift are captured by the E-W cross-section extending from the Four Corners platform to the Nacimiento uplift (Exhibit 3-76). On this cross-section, there is an absence of deep wells drilled in the middle of the basin. In addition, (a) lower Paleozoic strata pinchout eastward and southward against the Nacimento, Archuleta, and Chaco-Zuni uplifts; and (b) steeply east- to vertical-dipping strata associated with W-dipping reverse faults underlying the Hogback monocline may serve as regional topseal to migrant CO_2 fluids along the western margin of the basin.

Exhibit 3-75 Regional sketch map outlining principal positive structural blocks surrounding the San Juan Basin (yellow, stippled area). Syndepositional elements that were active and positive during the deposition of Leadville Limestone include the Zuni-Chaco slope, Paradox-Uncompahgre and Archuleta Arch-Nacimiento-uplift. The Four Corners platform block was inverted and uplifted during the Laramide orogeny (modified after Huffman and Condon, 1993)

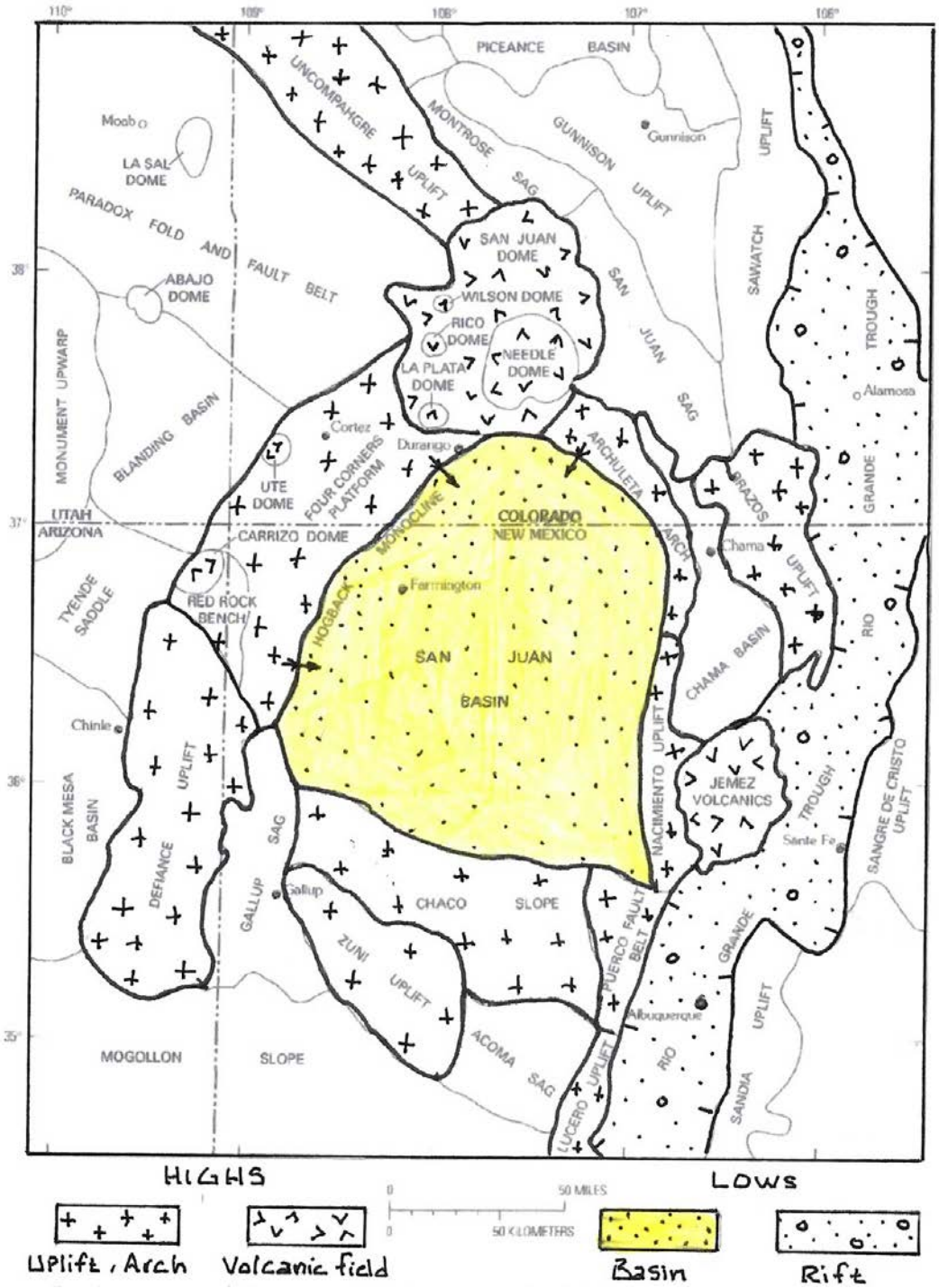

Source: USGS

Exhibit 3-76 E-W oriented cross-section across the San Juan Basin depicts the lower Paleozoic strata pinching out eastward against the syntectonic Archuleta, Nacimiento and Zuni-Chaco uplifts and highlands (adapted from Peterson, 1965)

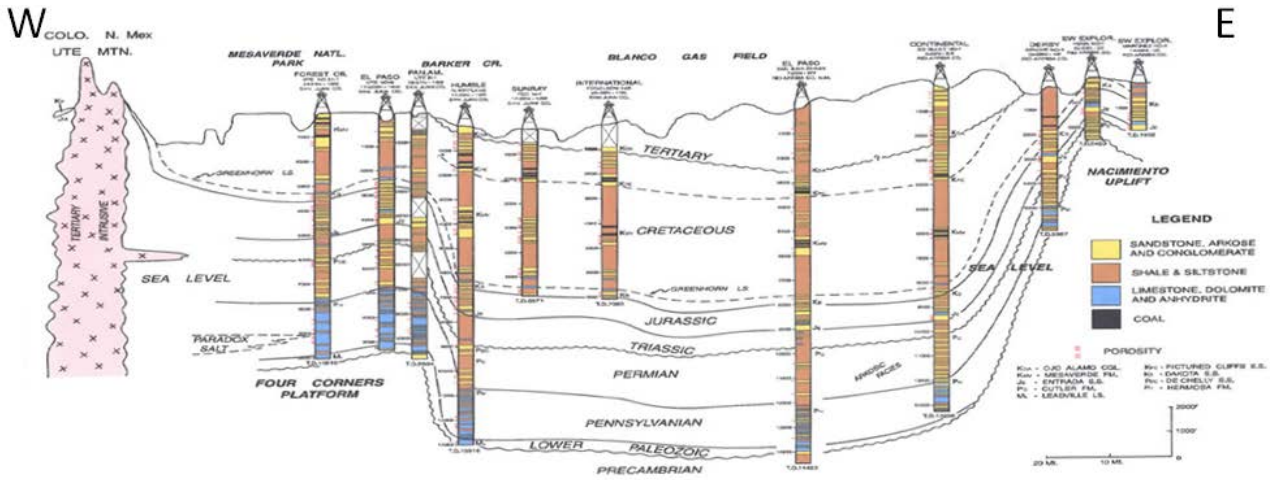

Note the general absence of deep wells in the central portion of the basin.

Reprinted by permission of the AAPG whose permission is required for further use

Regional Paleozoic Stratigraphy

Armstrong and Holcomb (1989) were able to incorporate considerable unpublished Shell Oil Company micropaleontologic data and formerly proprietary processed electric logs and regional correlation studies to help accurately reconstruct the paleogeographic and paleotectonic environments during the Carboniferous development of the San Juan basin. In the area within and surrounding the San Juan basin, Mississippian age strata were mapped and correlated as Leadville Limestone. Lateral Leadville time-stratigraphic correlatives include the Redwall Limestone, Arroyo Penasco Group, and Log Springs Formation. In the northern and western portion of the basin, Leadville strata unconformably overlie the Devonian Ouray Limestone. Along the eastern rim of the basin (Archuleta arch, Nacimiento uplift, and San Pedro Mountains), Marathon orogenesis resulted in the nonconformable pinchout of Mississippian strata against Precambrian igneous and metamorphic rocks (Exhibit 3-76). Drill results along the: (a) northern margin of the basin (NW Archuleta and south Needle dome area) and (b) Zuni uplift and N-dipping Chaco slope (Exhibit 3-75) demonstrate Mississippian strata pinchout unconformably against syndepositionally uplifted Precambrian crystalline and metamorphic basement. Repeated syndepositional reactivation of the NW-trending lineaments (Baars and Stevenson, 1982) promoted eastward-directed transgression of the marine Antler foreland seaway. Marine incursion gained access to the region from the west via a 120 mile wide embayment centered on the Ute-San Juan-Cabezon axis. Shallow marine conditions persisted across the embayment; although, during low-stand conditions, supratidal, arid to semiarid environments (sabkha), persisted for short periods of time.

The resulting Leadville Limestone is a complex suite of cratonal carbonate strata virtually void of intercalated terrigenous clastic material. Replacement dolomite in the Leadville is common and often involves limy mudstone to coarse grained crinoidal interbeds. McKee (1951)

published isopach maps of the Devonian and Mississippian systems of northwest New Mexico. He correlated the lower part of the Leadville with the Redwall Limestone of the Grand Canyon area and the upper portion of the Leadville with the Mooney Falls Member in the Black Mesa basin, northeastern Arizona and, more locally, the Arroyo Penasco Group strata cropping out along the eastern flank of the basin (Exhibit 3-77). The location of the Pennsylvanian and Permian boundary is uncertain. The principal CO_2 gas reservoir underlying the San Juan basin is the karstified, dolomitized, and weathered Leadville Limestone. Shales, siltstones, and argillaceous sandstone/conglomerate of the Mississippian Molas Formation overlie the Leadville and serve as the regional topseal for this unconventional "basin-centered" CO_2 gas play.

Exhibit 3-77 Carboniferous-Permian correlation columns for the San Juan Basin, New Mexico (adapted from Huffman and Condon, 1993)

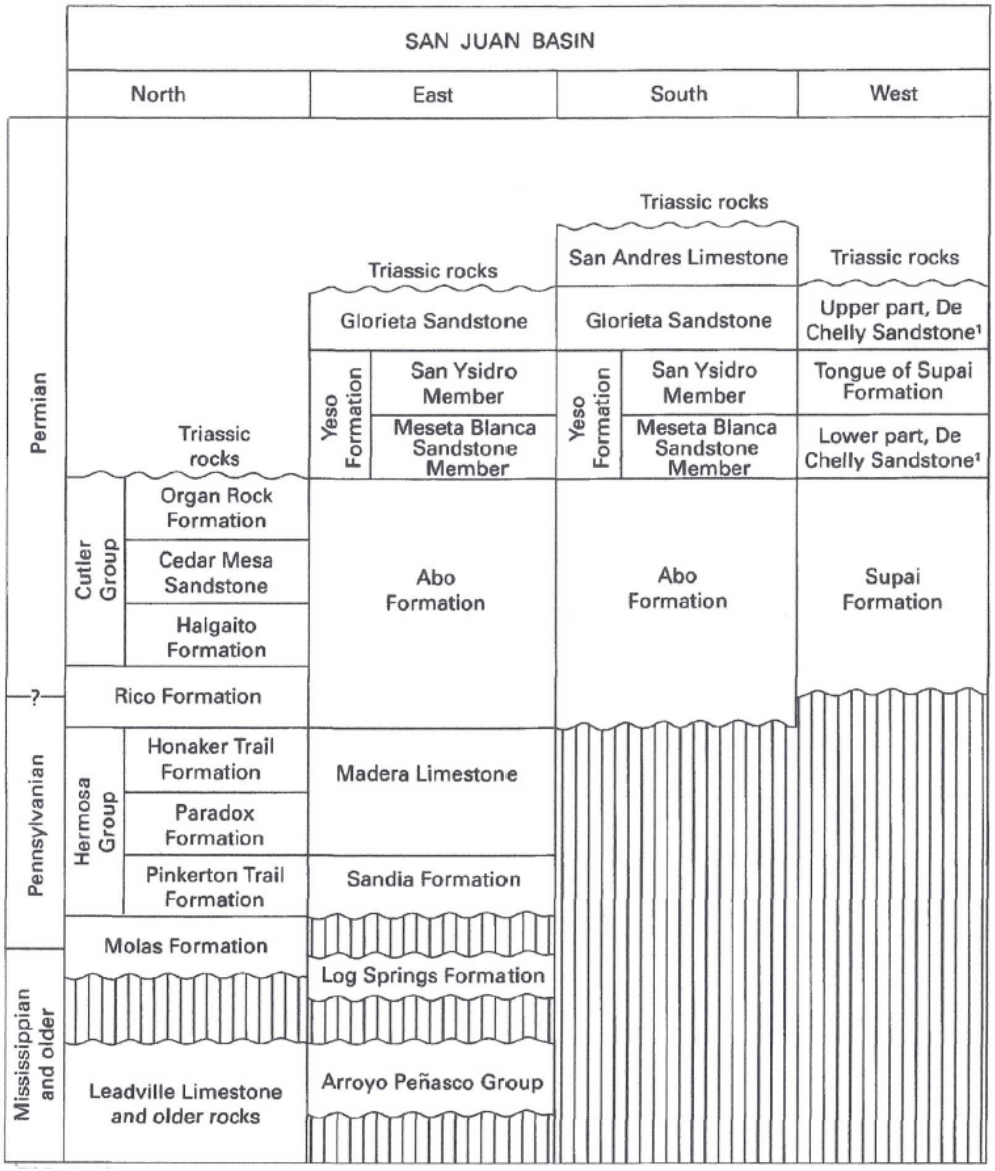

Source: USGS

During the Pennsylvanian and Early Permian time maximum convergence occurred along the Marathon-Ouachita suture. Wrench tectonism and associated NE-SW-directed crustal shortening across the Ute-San Juan-Cabezon seaway elevated, eroded, and dissected Mississippian strata and completely removed the Leadville from the Zuni-Defiance/Uncompahgre and portions of the Pedernal uplifts. As highlighted in Exhibit 3-75, rejuvenation of NW-trending structural elements along the Uncomphagre and Zuni-Defiance trends produced "Ancestral Rocky Mountain" highlands south and north of the seaway. This paleogeography promoted the accumulation of appreciable Leadville Limestone along the axial deep. The principal CO_2 gas reservoirs in the deeper portions of the San Juan basin involve the karstified, dolomitized, weathered, leached, and brecciated Leadville Limestone.

Armstrong and Holcomb (1989) updated earlier isopach maps integrating available wellbore data and correlated 2-3D seismic data. Their map is included in Exhibit 3-78. Mississippian gases in the deeper interior portion of the basin (i.e. that part of the basin east of the Four Corners platform) contain 65 to 96 percent CO_2. The very limited data available indicates that CO_2 constitutes more than 90 percent of Mississippian gases throughout most of the deeper portion of the basin. This gas is likely Miocene magmatic in origin and virtually untested at this time[1]. Although there were numerous intermittent periods of syndepositional uplift, erosion, and karstification of exposed Leadville, a significant marine Leadville section accumulated along the axial sag of the San Juan basin.

The configuration of the zero isopach or non-depositional edge of the embayment is demarked by the NW-SE-trending erosional edge of the Zuni uplift; whereas, the ancestral Uncompahgre-San Luis-Penasco highland-uplift defines the W- to SW-dipping northern unconformable zero edge. On-lapping Leadville stratal thickness increases rapidly basinward to 100 ft, and then more gradually westward to 150-200 ft before progressively thickening westward into the open foreland seaway exceeding 400 ft in the Four Corners area.

Topseal - Molas and Log Springs Formations

Lower Pennsylvanian Molas and Log Springs formations disconformably overlie the Leadville. Lithologies are typically variegated clastic redbed succession intercalated with silty shale interbeds with occasion chert and limestone. Armstrong and Holcomb interpreted the lower portion of the Molas as "residual soil that covers a karst surface on the Leadville Limestone" (1989). They state that the Molas is, in part, a regolith formed in late Chesterian time and subsequently reworked by marine transgressions. The Log Springs Formation crops out on the San Pedro-Nacimiento uplift and on the adjoining Zuni Mountains-Chaco slope. Extensive ground-water solutioning of the underlying limestone strata resulted in the development of intra-formational collapse breccia and zones of solution cavities. Most of this secondary porosity became filled with basal ferruginous, pisolitic shale of the Log Springs Formation. The sealing shales rest with angular unconformity on the karst surface of the Arroyo Penasco Group or Leadville Limestone. These strata are, in turn, overlain along an angular unconformity with marine limestone of the Sandia Formation (Exhibit 3-77).

[1] See Broadhead et al., 2009, for geologic, petrophysical, and geochemical details.

Exhibit 3-78 Isopach map of the Mississippian Leadville limestone, San Juan embayment, New Mexico shows the distribution of strata contoured at a 50 ft interval (adapted from Armstrong and Mamet, 1977; used with permission)

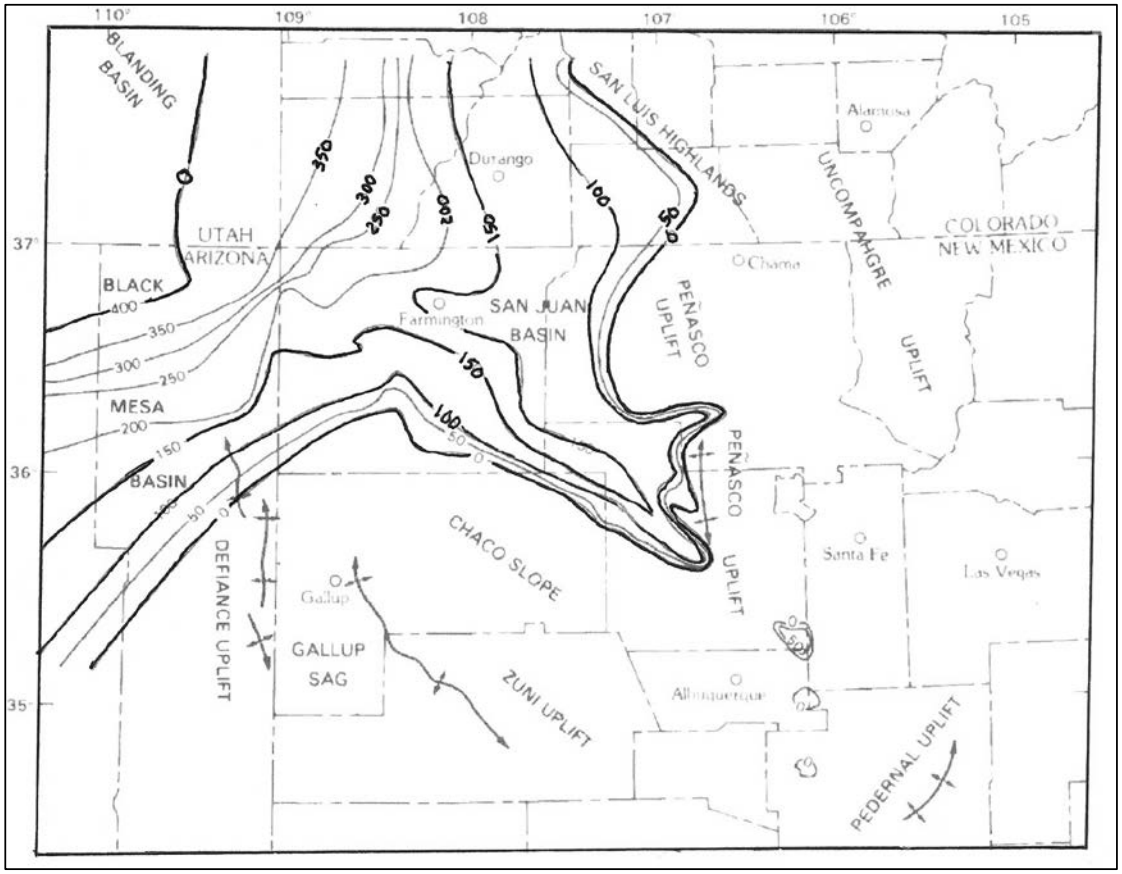

Note the deeper untested portion of the basin is underlain by ±150 gross ft of Leadville reservoir

CO_2 Source Intrusions

Following termination of Laramide compression at circa 34 Ma, the flat-dipping Farallon slab became unstable due to: (a) the diminution in convergence rate; (b) the impingement of the East Pacific Rise with the North America plate; and (c) the N to S rollback of the Farallon slab (48-21 Ma) in the American Northwest (Exhibit 3-37) (Montana, Wyoming, and Nevada). Coney and Reynolds (1977) demonstrate the rapid westward-directed sweep of Oligocene and Miocene (34-12 Ma) igneous activity across the American Southwest. On a smaller scale, the "rollback" of igneous activity is also evident in New Mexico. The initiation of favorable CO_2-rich mafic-alkalic plutonism at circa 38-34 Ma extending from the East Mexican alkalic province through Trans-Pecos West Texas and along the Lincoln County intrusive belt, New Mexico. The release of Laramide compression and initiation of Mid-Tertiary extension perturbed the mantle lithosphere and deeper mantle mesosphere. This induced decompressional partial melting, induced production of mafic-alkalic melts, and focused mantle sourced CO_2 and ^3He. It is suspected that the identical mafic-alkalic production of magmas saturated with CO_2-^3He accompanied the Middle-Late Tertiary rollback of igneous activity younging westward across the American Southwest.

A review of radiometric ages of the igneous rocks surrounding the San Juan basin highlighted on Exhibit 3-72 heralds the proposed westward youthfulness of intrusions. Exhibit 3-79 compiles the distribution of about 80 known potassic lamprophyres (minettes), ultramafic serpentine-bearing microbreccia pipes, and other exotic ultramafic-mafic intrusions of the Navajo volcanic field. Individual events are the products of structurally-controlled magma ascent, explosive eruptions, and deep post-eruptive exhumation. Igneous rock types include potassic lamprophyres, serpentinized tuffs, and exotic mafic and ultramafic intrusive rocks. The intrusions, along with a variety of incorporated crustal and mantle xenoliths, are used to map the petrology and history of the lithosphere and upper mantle beneath the Colorado Plateau. Dark circles on Exhibit 3-79 indicate minettes; open triangles represent serpentine ultramafic microbreccia pipes. Monoclines are indicated by heavy lines. Abbreviations are as follows: AP, Agathla Peak, Arizona; BB, Boundary Butte, Utah; BP, Buell Park, Arizona; CRM, Comb Ridge Monocline; CV, Cane Valley; EDM, East Defiance Monocline; GN, Green Knobs; GR, Garnet Ridge; ME, Mule Ear; MHM, Mesaverde Hogback Monocline; MR, Moses Rock; NM, New Mexico; RM, Red Mesa; SR, Ship Rock; UT, Utah.

Exhibit 3-79 Location map of the Navajo Volcanic Field, Colorado Plateau, shows over 80 Tertiary age (28-19 Ma) volcanoes, dikes, sills and breccia pipes. Numerous petrochemically favorable intrusions are localized along the MHM-thrust belt placing them within the limits of the San Juan basin (adapted after Smith and Levy, 1976; and McGetchin et al., 1977; used with permission)

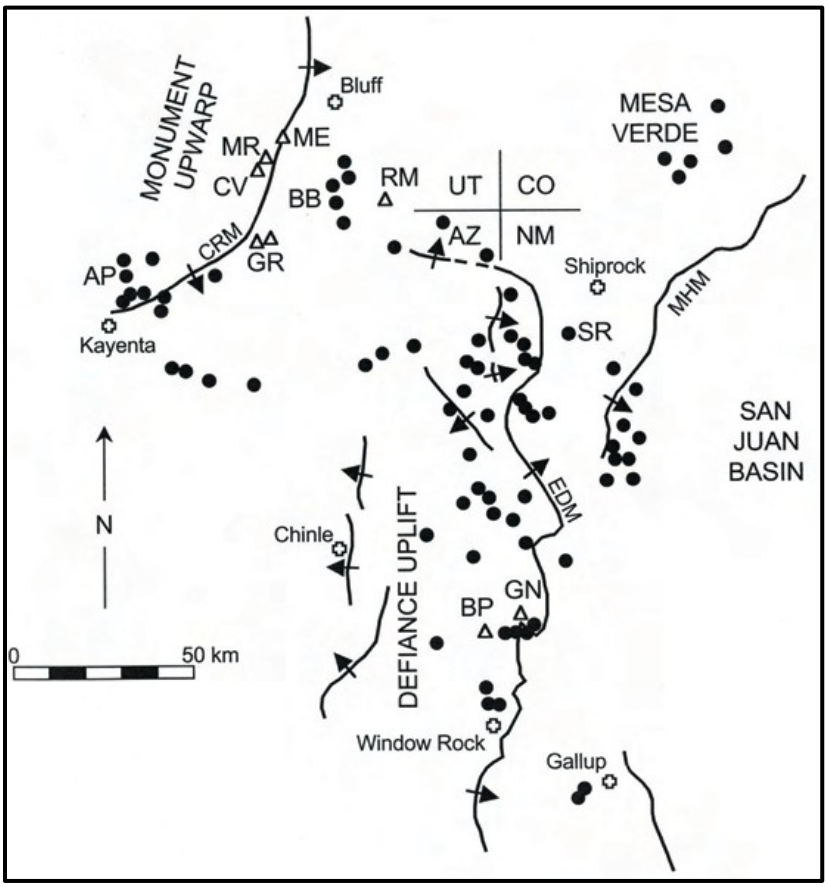

The Navajo volcanic field is distributed across the Colorado Plateau in a roughly crescent-shaped array extending from the Window Rock-Gallup area of New Mexico 180 miles NW to the Four Corners and Mesa Verde, and then 80 miles WSW to the Monument upwarp on the Utah-Arizona border. Many centers lie along the Laramide Defiance, Comb, and Monument-Hogback monoclines. The NE-facing crescent-shaped distribution has an arc distance of nearly 180 miles and covers a large portion of the Colorado Plateau. It is also relevant that the depth penetrating Defiance-Hogback shear zone (MHM, Mesaverde-Hogback monocline) localized ±25 percent of the mantle and derived potentially CO_2-rich intrusions along its trace. See Semken (2003) for details and additional empirical information.

The age of the Navajo minettes and ultramafic microbreccia intrusions vary between 28-19 Ma (Semken, 2003). Immediately north of the basin is the N-S-striking, Pagosa Springs-Archuleta minette dike swarm. The age of this dike swarm is unknown; however, published maps infer a "Miocene" age (Dane, 1948; Segerstrom and Henkes, 1977). It is evident the intrusions comprising the Navajo volcanic field are outside this report's "Mid-Tertiary" window of Great Plains margin mafic-alkalic intrusions. For this reason, the San Juan basin CO_2 lead is placed with the "Late Tertiary" sourced fields and plays.

It is apparent from the distribution of large volcanic fields surrounding the Colorado Plateau that there is a possibility that the observed CO_2 charge for the San Juan basin is Late Miocene-Recent (Exhibit 3-72). Associated intrusions and the extensive lava fields involve basanites, alkali-olivine basalts, tholeiites (25 percent), and evolved alkalic basalts. The younger igneous rocks are distinctly deficient in K_2O; however, they are still alkalic and viewed as favorable CO_2 source candidates. The larger fields include: (in a clockwise manner, East to West): northern Raton-Clayton-Ocate-Taos fields (8 Ma-Recent); Mount Taylor-Zuni-Bandera (4 Ma-Recent); Springerville (30 Ma-Recent); White Mountains (38-12 Ma, 9 Ma-Recent); and San Francisco (12 Ma-Recent). The ability of these young basanite-olivine basalt-evolved alkalic basalt to carry and exsolve large amounts of CO_2 is suggested by their close spatial relationship with several large CO_2 deposits: Bravo dome and Des Moines, New Mexico; St Johns/Springerville, Arizona-New Mexico; and La Barge, Wyoming, with the adjoining Leucite Hills lamproite volcanic field (2 Ma –Recent).

The number of intrusions, expansive region intruded, diachronous potential sources, and favorable composition of igneous rocks surrounding the San Juan basin greatly reduce the likely risk of not having an adequate CO_2-bearing source rocks beneath the basin. This contention is strengthened by the nearby McElmo Dome-Doe Canyon cluster of CO_2 fields. The McElmo Dome occurrence is aligned along the Four Corners lineament and only 30 miles NW of the bounding Hogback fault zone and NW edge of the San Juan basin.

San Juan Basin-centered CO_2 Lead

Broadhead et al., 2009, noted the high concentrations of CO_2 gas in wells drilled along and on the hanging-wall of the Hogback monocline and Defiance uplift (3-80). Twenty-five wells were recognized as showing abnormal concentrations of CO_2 gas within the Mississippian Leadville Limestone. Five of the wells contained in excess of 65 percent with the highest concentration of 96 percent. Although there is a complete absence of deep tests within the central and deepest portion of the basin, available data show the concentration of CO_2 gas increases basinward.

Exhibit 3-80 Map of CO_2 content in gases from Mississippian reservoirs in the San Juan Basin, New Mexico shows the progressive basinward increase in contained CO_2 and He gases (0.1 to 95.3% CO_2) (adapted from Broadhead et al., 2009; used with permission)

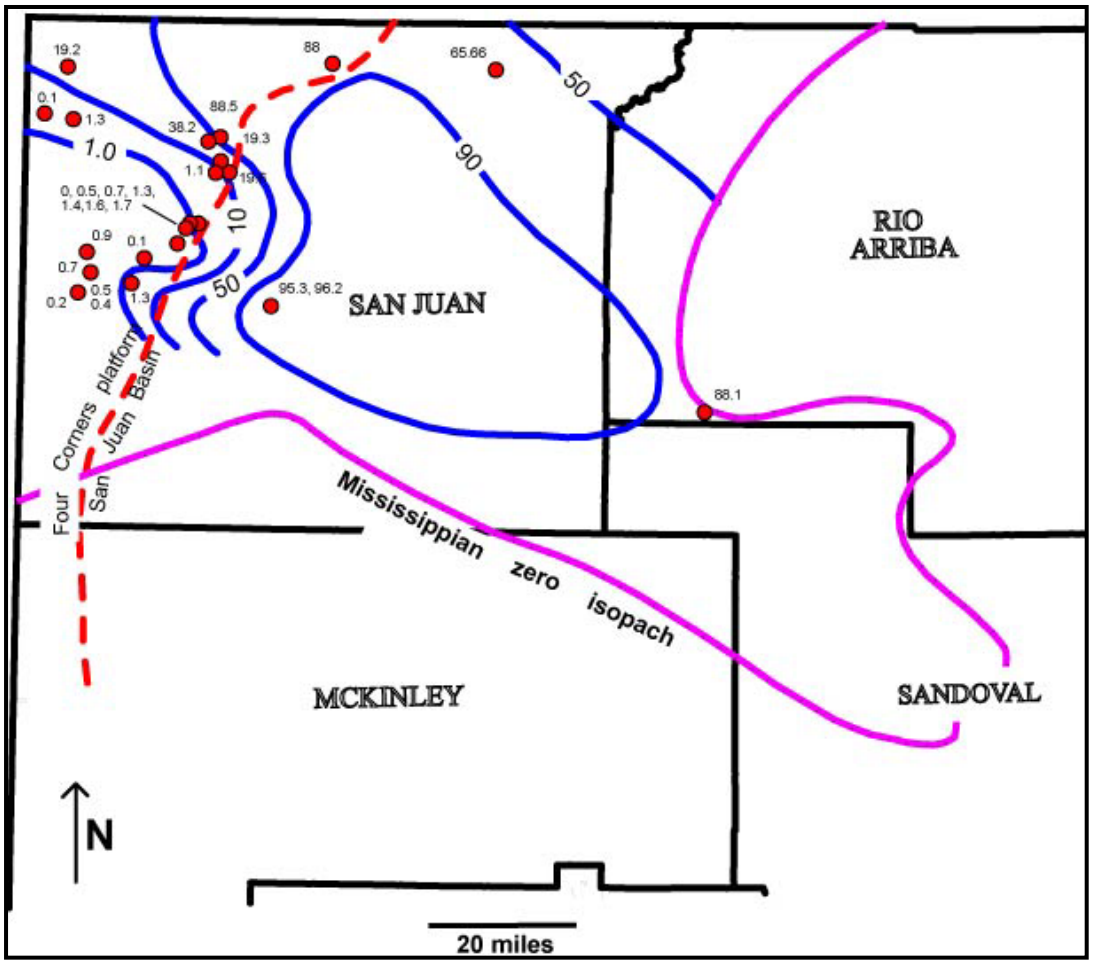

The zero isopach line indicated on Exhibit 3-80 is adapted from Armstrong and Mamet (1977) and incorporated in the San Juan Lead map in Exhibit 3-81. The size of the Leadville-CO_2 play was restricted to just the deeper, basin-centered portion play bounded on the north and south by the Four Corners lineament and Tocito horst, respectively. Kelley and Clinton (1960) and Baars and Stevenson (1982) have tracked the Four Corners lineament or its equivalent laterally across the Colorado Plateau, which demonstrates its regional importance. It was found to have a second order structural character, a crustal-scale depth-penetrating nature, an ability to help localize the McElmo Dome-Doe Canyon CO_2 deposits, and a series of higher-than-average concentrations of CO_2 in on-trend wells (66, 85, and 88 percent). The intersection of the Four Corners lineament with the Hogback transfer/overthrust zone is viewed as a likely CO_2 point source for the San Juan basin. A similar site occurs at the intersection with the Tocito horst. Once the Leadville Limestone is contacted by the rising, focused, supercritical stream of CO_2-^{3}He, it will dissipate laterally across the basin. The developing plume is initially focused along the mapped, penetrative grid of orthogonal NW- and NNE-trending systems of sub-vertical fractures.

Exhibit 3-81 San Juan Basin-centered lead map locates the primary Leadville Limestone CO_2 objective (shown in blue)

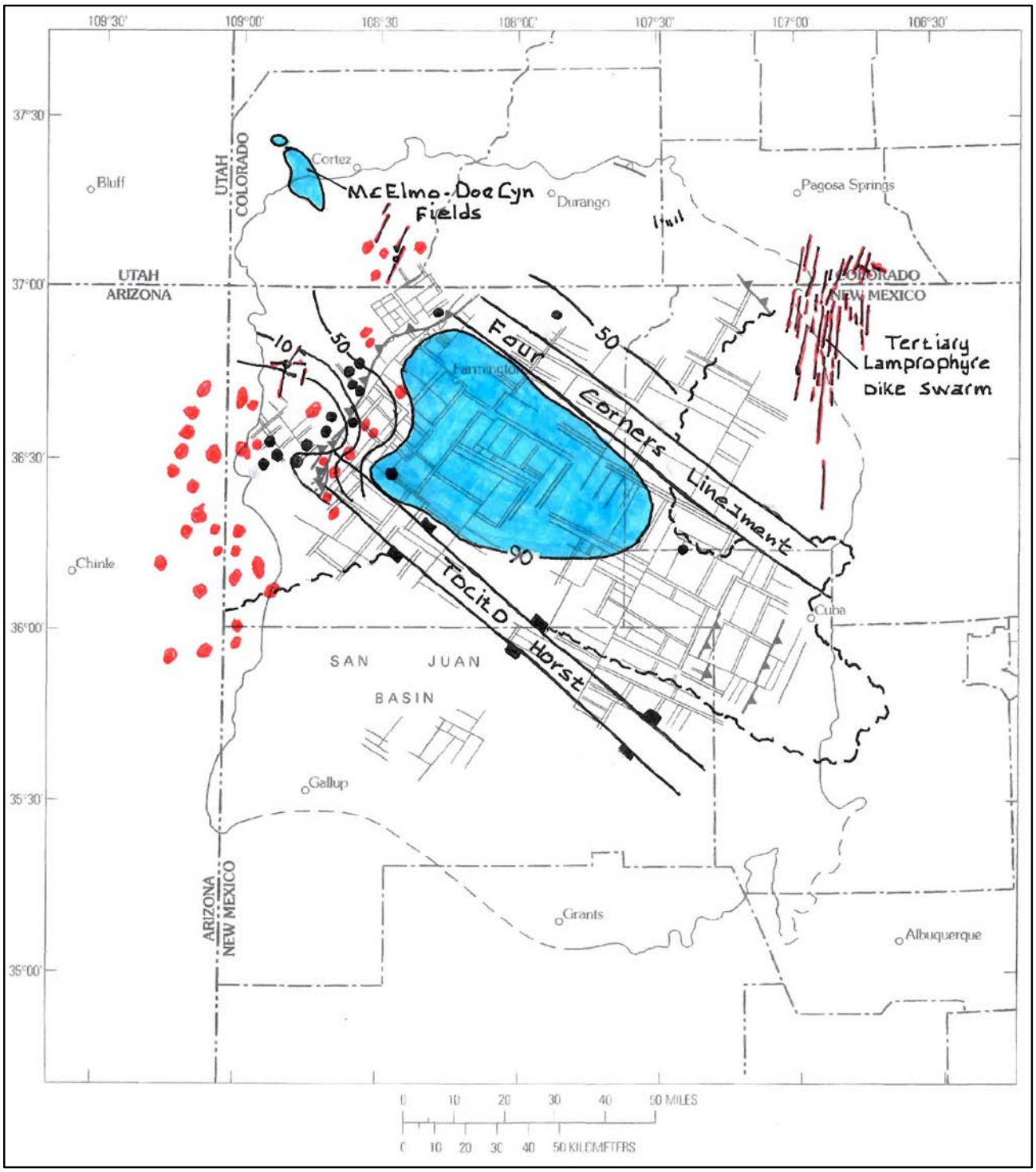

Enegis-interpreted image of data from Huffman and Taylor, 1997 and Baars and Stevenson, 1982 (base map structural framework elements); Smith and Levy, 1976 and McGetchin et al., 1977 (Miocene intrusions of the Navajo volcanic field [red]); Dane, 1948 (distribution of Miocene [?] Jiracilla lamprophyre [minette] dike swarm NE of the basin).

Secondary migration occurs laterally along intra-layers of collapse- and solution-breccia and multiple zones of karstified, vuggy, dolomitic Leadville. Up-dip migration along the southern Zuni-Chaco slope, eastern Nacimiento uplift, and northern Archuleta arch-San Juan-Needles uplift occurs along nonconformable pinchouts along the deeply weathered, regolithic crystalline basement. The surrounding ancestral highlands remained structurally positive during the early phase of Marathon transpression and crustal shortening across the NW-SE elongate, Late Mississippian embayment (Exhibit 3-74, Exhibit 3-75, and Exhibit 3-78). SW-, W- and NW-directed CO_2-^3He migration was blocked by cataclasis and gouge development along the 1st order Defiance-Hogback, right-lateral, Marathon vintage transfer and subsequent reactivation during early and late Laramide crustal shortening and inversion. The envisioned sealing capacity of the Defiance-Hogback shear zone is believed significant. Leadville CO_2 concentrations in the 21 hanging-wall wells on the Four Corners platform average 9 percent CO_2. In contrast, the three wells drilled penetrating the basin-center play and one well drilled within the Four Corners lineament, average 85 percent CO_2.

Lastly, all anomalously high CO_2 wells on the upthrown hanging-wall structural block either lie along the NW-trending projection of the Four Corners lineament or are concentrated in the NW corner of the maps shown on Exhibit 3-80 and Exhibit 3-81. The wells in question are all closest to the McElmo Dome-Doe Canyon fields. It is possible that a migration/dispersion pathway exists, connecting the San Juan basin-centered lead and the McElmo Dome.

4 Estimates for GIIP and TRR

In conducting the analysis of CO_2 systems in the United States and evaluating the leads for undiscovered resources, the authors collected information about the leads to support estimates for GIIP and TRR. Equation 1 was applied to estimate the GIIP for each of the leads. Each lead was modeled as having a single depth, uniform thickness, and a single value for pay, porosity and etc. throughout its entire volume. The GIIP estimates for the leads are risked to account for the fact that they are undiscovered. The companion NETL document on discovered CO_2 reservoirs contains details of how the formation volume factor was derived from a phase diagram for CO_2 and how estimated temperature and pressure gradients were applied to estimate reservoir conditions. Equation 2 shows how degradations for recoverability of the resource and access to the land overlying the resource are applied to GIIP to estimate TRR. The degradation for land access was estimated by overlaying GIS information on land use plans, national parks, population centers and other areas where access for resource extraction is limited. The degradation for produce-ability is adjusted from realized values at known CO_2 accumulations based on the lithology in the area and strata of the undiscovered leads.

Equation 1

$$GIIP_R = \frac{C_{Vol} \cdot A \cdot H \cdot \phi(1 - Swc)}{B_{gi}} \cdot \varsigma . F_R$$

Where:

$GIIP_R$ = Risked Gas-initially-in-place, in standard cubic feet (scf) for CO_2

A = Area (acres)

H = Pay thickness (feet)

Φ = Porosity (fraction)

Swc = Connate water saturation (fraction)

Bgi = Initial gas formation volume factor in reservoir ft^3 per scf (reservoir cubic feet (rcf)/scf)

C_{Vol} = A volumetric constant, 43560 ft^3/ ac-feet (cubic foot/acre-foot)

ς = CO_2 concentration (volumetric percent)

F_R= Risk Factor, estimated likelihood that the undiscovered reservoir exists

Equation 2

$$TRR_R = GIIP_R . F_T . F_A$$

Where:

TRR_R = Risked Technically-recoverable Resource

$GIIP_R$ = Risked Gas-initially-in-place, in Standard

Exhibit 4-1 presents key inputs for the volumetric calculation of risked GIIP and also the degradations for access and recoverability used to estimate TRR. Twenty-six leads in five geographic areas are estimated to contain 63 Tcf of risked CO_2 initially in place and 42 Tcf of risked technically recoverable CO_2 resource (TRR). Thirty-three Tcf of the risked TRR is contained in two areas: the San Juan basin in northwest New Mexico and the Val Verde basin in southwest Texas, both of which are near a pipeline infrastructure that feeds the Permian Basin, a center of CO_2 use for enhanced oil recovery (EOR). This risked TRR is similar in magnitude to the 30 Tcf of combined TRR (net of cumulative production) from the known subsurface sources that currently supply the Permian basin.

The aggregate estimates of GIIP and TRR should not be considered comprehensive within the lower 48 states. The number of areas examined was limited by the project budget. Particular areas for study were selected where there was available data to support an analysis. At the same time, the results indicate that there are likely undiscovered CO_2 reservoirs in the United States of a magnitude that could contribute materially to CO_2 supply for enhanced oil recovery.

Exhibit 4-1 Estimates of gas-initially-in-place and technically recoverable resources for undiscovered leads for CO_2 in the United States, and key input variables for the volumetric calculations

Area	State	# leads	Area (all leads), M ac.	Pay, ft	Porosity %	Depth, Mft	Formation Volume Factor Rcf/000scf	CO_2 %	Risk Factor	GIIP, Tcf	Access %	Recovery %	TRR, Tcf
San Juan (Leadville)	NM	1	1000	75	12	14	2.8	90	33	33.7	95	70	22.4
Val Verde (Marathon Sub thrust)	TX	8	96	650	5	15	2.5	74	31	10.2	95	70	6.8
Val Verde (Marathon thrust)	TX	5	49	225	16	12	2.3	77	33	6.9	95	70	4.6
Sweet Grass	MT	4	410	117	9	3.5	5.2	90	31	8.0	95	75	5.7
Lincoln County	NM	6	252	120	15	1.7	12.6	97	23	2.5	82	65	1.3
North Park	CO	2	36	95	18	5.5	2.9	95	27	1.9	51	70	0.7
Total		**26**	**1,844**							**63.2**			**41.5**

Conversion Factor: 52.9 $MMmtCO_2$/Tcf

Values for pay, porosity, depth, formation volume factor, CO_2 concentration, risk factor, access, and recovery are the weighted average (based on area) of the values for the leads within an area

5 Closing Ideas, Concepts, and Observations

The following are ideas, concepts, and observations that could inform further exploration of subsurface CO_2 deposits in the Western U.S. and Mid-Continental U.S., including the Balconces and West Texas magmatic provinces.

1. Traditionally it is taught that CO_2 gas fields were primarily sourced from carbonate-bearing strata, which, when buried to sufficient depths and temperatures, react yielding supercritical CO_2 fluid plus non-CO_2-bearing mineral by-products. However, this is no longer exclusively the case. CO_2 gases collected and analyzed from the major producing fields of the western U.S. contain a suite of definitive isotopes which are: (a) sourced as a supercritical CO_2 liquid directly from the earth's mantle or overlying mantle lithosphere; (b) primitive, CO_2-saturated, mafic alkalic fractions of partially melted mantle or mantle lithosphere, which become mobile and emplaced at various levels in the earth's crust; or (c) residual differentiated fractions of primitive mafic alkalic magmas, which are felsic and contain very high amounts of Na_2O and K_2O, and are super-saturated with CO_2 gas.

2. Previous studies of CO_2 deposits of North America and this study demonstrate that CO_2 gas fields in the western U.S. are not uniquely sourced by Late Tertiary basaltic intrusions or allied volcanism. As summarized earlier (Section 2.1.5), there are three discrete episodes of ultramafic, mafic alkalic, or felsic alkalic igneous activity, which yielded significant quantities of gases containing 85-98 percent CO_2 gas. CO_2-associated igneous intrusions have a diagnostic suite of whole rock and trace element chemical/geochemical, mineralogic, petrographic, and isotopic signatures. Pathfinder characteristics vary widely through time and space; however, variations are not random and developed criteria help the explorationist focus on the more CO_2-prone intrusive systems.

3. Discovered and undiscovered CO_2 deposits and leads do not occur at random, scattered across the western U.S. They are ordered in both time and space; moreover, fields and leads occur along discrete linear belts or fairways. Intrusions and associated alteration-mineralization are emplaced within narrow geologic episodes: Early Cretaceous (Mid-continent, 125-85 Ma); associated with Laramide tectonism (80-34 Ma including Jackson Dome, Balcones, and Montana alkalic province), Mid-Tertiary (38 Ma-22 Ma); and Late Tertiary/Quaternary (12 Ma-Recent). Ballentine et al. (2001) also suggest there is an additional episode of CO_2 charge at circa 300 Ma in the West Texas Permian Basin (see Section 3 for discussion).

4. Our North American field studies completed for this report demonstrate that the majority of natural occurring CO_2 deposits are localized on large, uplifted and folded Laramide or Ancestral Rocky Mountain (320-255 Ma) structural blocks. The more promising structural blocks are located within 75 mi of a major fold and thrust belt and juxtaposed or cut by one or more crustal-scale lineaments. Supercritical CO_2 comes directly from decompressed mantle or mantle lithosphere or CO_2-charged ultramafic; mafic-alkalic or felsic alkalic differentiated magma must travel vertically through the overlying lithosphere and crust (+75 km without tortuosity). For this reason, CO_2-charged fluids and magmas become localized along crustal-scale breaks (zones of decompression that cut clear through the lithosphere) and migrate upward along vertical migration pathways. As demonstrated by Exhibit 3-8, Exhibit 3-9, Exhibit 3-40, Exhibit 3-45, and Exhibit 3-60 one large through-going regional lineament is adequate; however, two "intersecting X's" is even better for helping focus CO_2-rich migrant fluids and favorable magmas. Still better are those structural settings with compound X's. As indicated by Exhibit

3-34, Exhibit 3-69, Exhibit 3-71, Exhibit 3-74, and Exhibit 3-81, low-angle imbricate thrusts, when viewed in cross-section, possibly represent the most significant "lineament" in the Rocky Mountains and Marathon fold-thrust belt. We have demonstrated in this report that imbricate thrusts act as very effective, laterally contiguous, horizontal migration pathways for migrant supercritical CO_2 charge. This seems to be the case in the Val Verde/Marathon thrust belt; Lincoln County-Sierra Blanco basin/Mescalero thrust (Exhibit 3-51A); San Juan/Hogback thrust; Kevin dome/underlying Sweetgrass thrust; and McCallum/Never Summer thrust and backthrust. Crustal migration pathways (double X's) work and demonstrate the 75-mile supposition for proximity to the nearest major thrust belt.

6 References

Allen, M.S., and Foord, E.E., 1991, Geological, geochemical and isotopic characteristics of the Lincoln County porphyry belt, New Mexico: Implications for regional tectonics and mineral deposits: New Mexico Geological Society Guidebook, 42nd Field Conference, Sierra Blanca, Sacramento, Capitan Ranges, p. 97-113.

Allen, M.S., and McLemore, V.T., 1991, The geology and petrogenesis of the Capitan pluton, New Mexico: New Mexico Geological Society, Guidebook 42.

Allis, R., Chidsey, T., Gwynn, W., Morgan, C., White, James M., Adams, E., Moore, J., 2001, Natural CO_2 Reservoirs on the Colorado Plateau and Southern Rocky Mountains: Candidates for CO_2 Sequestration, Proceedings 1st National Conference on Carbon Sequestration, May 14-17, 2001, Washington DC, DOE-NETL CD DOE/NETL-2001/1144, 19p.

Allis, R., Bergfeld, D., Moore, J., McClure, K., Morgan, C., Chidsey, T., Heath, J., and McPherson, B., 2005. Implications of results from CO_2 flux surveys over known CO_2 systems for long-term monitoring. Proceedings 4th National Conference on Carbon Sequestration, May 2005, Alexandria, Virginia.

Armstrong, A.K., and Holcomb, L.E., 1989, Stratigraphy, facies and paleotectonic history of Mississippian rocks of the San Juan basin or Northwestern New Mexico and adjacent areas: New Mexico Geological Society Guidebook, 40th Field Conference, Southeastern Colorado Plateau, p. 159-165.

Armstrong, A.K., and Mamet, B.L., 1977, Biostratigraphy and paleogeography of the Mississippian System in northern New Mexico and adjacent San Juan Mountains of southwestern Colorado: New Mexico Geological Society, Guidebook 28, p. 111-127.

Baars, D.L., 1966, Pre-Pennsylvanian paleotectonics: key to basin evolution and petroleum occurrences in the Paradox basin, Utah and Colorado: American Association of Petroleum Geologist Bulletin, V. 50, p. 2082-2111.

Baars, D.L., and Stevenson, G.M., 1982, Subtle Stratigraphic Traps in Paleozoic Rocks of the Paradox Basin, *in* The Deliberate Search for the Subtle Trap, Halbouty, M., AAPG Memoir 32, p. 131-158.

Ballentine, C.J., Schoell, M., Coleman, D., and Caln, B.A., 2001, 300-Myr-old magmatic CO_2 in natural gas reservoir of the west Texas Permian basin: Nature, v. 409, p. 327–331.

Barker, D.S., 1987, Tertiary alkaline magmatism in Trans-Pecos Texas; *in* Fitton, J. G and Upton, B. G. J., eds., Alkaline igneous rocks: Geological Society, Special Publication 30, p. 415-431.

Berendsen, P., and Weis R., 2001, New Kimberlite discoveries in Kansas – magnetic expression and structural setting: Transactions of the Kansas Academy of Science, v. 104, p. 223-236.

Biddle and Wielchowsky, undated, *in* Toro, J., undated, Stratigraphic traps, http://www.geo.wvu.edu/~jtoro/petroleum/petroleum_figs/review2/traps/unconf_trap.jpg

Blackstone, D.L., 1977, Independence Mountain thrust fault, North Park Basin, Colorado, *in* University of Wyoming Contributions to Geology, v. 16, no. 1, p. 1-16.

Bowen, David, undated, Geological Activities –Overview of Phase II and Phase III Activities, Big Sky Carbon Sequestration Partnership, Annual Meeting, Gallatin Gateway, Montana. Retrieved on June 1, 2013, from http://www.bigskyco2.org/sites/default/files/documents/Annual_Mtg09_Bowen2.pdf

Bowen, D., 2009, Geological Activities –Overview of Phase II and Phase III Activities, Presentation given to Big Sky Carbon Sequestration Partnership Annual Meeting, Retrieved on May 17, 2013, from http://www.bigskyco2.org/sites/default/files/documents/Annual_Mtg09_Bowen2.pdf

Barden, C., and Franklin, W., 2003, Longfellow Ranch Geological Report-West Texas Overthrust, Pecos County, Texas: Longfellow Exploration Partners Limit, 30p. Retrieved on May 17, 2013, from http://www.longfellowexp.com/downloads/GeologicalReport-WTO.pdf

Breitsprecher, K., Thorkelson, D.J., Groome, W.G., and Dostal, J., 2003, Geochemical confirmation of the Kula-Farallon slab window beneath the Pacific Northwest in Eocene time: Geology, v. 31, p. 351-354.

Broadhead, R.F., Mansel, M., and Jones, J., 2009, Carbon dioxide in New Mexico: Geologic distribution of natural occurrences: New Mexico Bureau of Geology and Mineral Resources, Open File Report no. 514, p.131

Brookins, D.G., 1967, The strontium geochemistry of carbonate in kimberlites and limestone from Riley County, Kansas: Earth and Planetary Science Letters, v. 2.

Brookins, D.G., 1970, Kimberlite at Winkler Crater, Kansas: Geological Society of America Bulletin, v. 81, p. 541-546.

Brookins, D.G., and Naeser, C.S., 197l, Age of emplacement of Riley County, Kansas Kimberlites and possible minimum age for the Dakota sandstone: Geological Society America Bulletin, v. 82, p. 1,723-1,726.

Cain, B.A., and Hammes, U., 1997 Results of 3D seismic carbonate project, West Texas, Parts 1 and 2: Retrieved on May 17, 2013, from www.netl.doe.gov/kmd/cds/disk28/NG2-10.PDF

Cardott, B.J., 1989. Thermal maturation of the Woodford Shale in the Anadarko Basin: Oklahoma. Geological Survey Circ. 90, p. 32–46.

Cathles, L.M., and Schoell, M., 2007, Modeling CO_2 Generation, Migration, and Titration in Sedimentary Basins, Ithaca and Berkeley, Cornell and Gas Consult International Inc: 34p.

Chapin, C.E., McIntosh, W.C., and Chamberlin, R.M., 2004, The Late Eocene- Oligocene Peak of Cenozoic volcanism in southwestern New Mexico: New Mexico Geological Society Special Publication 11, p. 271-293.

Cole, J.C., and Braddock, W.A., 2009, Geologic Map of the Estes Park 30′× 60′ quadrangle, north-central Colorado: U.S. Geological Survey Scientific Investigations Map 2009-3039, scale 1:100,000, 56 p.

Cole, J.C., Trexler, J.H., Jr., Cashman, P.H., Miller, I.M., Shroba, R.R., Cosca, M.A., and Workman, J.B., 2010, Beyond Colorado's Front Range—A new look at Laramide basin subsidence, sedimentation, and deformation in north-central Colorado, *in* Morgan, L.A., and Quane, S.L., eds., Through the Generations: Geologic and Anthropogenic field excursions in the

Rocky Mountains from modern to ancient: Geological Society of America Field Guide 18, p. 55-76.

Coney, P. J., and Reynolds, S. J., 1977, Cordilleran benioff zones: Nature, v. 270, p. 403-406.

Cox, A., Debiche, M.G. and Engebreteson, D.C., 1989, Terrane trajectories and plate interactions along continental margins in the North Pacific Basin: In: Z.Ben-Avraham, ed., The Evolution of the Pacific Ocean Margins, p. 20-35.

Cox, D.P., and Singer D.A., 1986, eds., 1986 Mineral deposit models: U.S. Geological Survey, Bulletin 1693, 379 p.

Cullers, R. L., and Berendsen, P., 2006, The geology, petrology, and elemental composition of kimberlites from Riley and Marshall counties Kansas, USA, Retrieved on May 22, 2013, from http://www.kgs.ku.edu/Publications/OFR/2012/OFR12_17/KGS_OF_2012-17.pdf

Cullers, R.L., Mullenax, J., DiMarco, M.J., and Nordeng, S., 1982, The trace element content and petrogenesis of kimberlites in Riley County, Kansas, USA: American Mineralogist, v. 67, p. 223-233.

Dane, C.H., 1948, Geologic map of part of eastern San Juan Basin: U.S. Geological Survey Oil and Gas Investigations Preliminary Map 78.

Davis, G.H., 1978, The monocline fold pattern of the Colorado Plateau, in Matthews, V. (ed.), Laramide folding associated with basement block faulting in the western United States: Geological Society of America Memoir 151, p. 215-233.

Davis, G.H., and Reynolds, S.J., 1996, Structural Geology of Rocks and Regions: John Wiley and Sons, 2nd Edition, 776p.

Doelger, M.J., Barlow Jr. J.A., Barlow and Haun, Inc., 1993, Low-BTU gas in Wyoming, in Atlas of Major Rocky Mountain Gas Reservoirs, New Mexico Bureau of Mines and Mineral Resources, 170 p.

Eby, G.N., 1987, Fission-track geochronology of the Arkansas alkaline province: U.S. Geological Survey Open-File Report 87-0287, 12 p.

Eggler, D. H., 1989, Kimberlites: how do they form? *in* Ross, J., Jaques, A. L., Ferguson, J., Green, D. H., O'Reilly, S. Y., Danchin, R. V. and Janse, A. J. A. eds., Kimberlites and Related Rocks: their Composition, Occurrence, Origin and Emplacement. Sydney: Blackwell Scientific Publications, p. 489-504.

Erslev, E. A., and Holdaway, S. M., 1999, Laramide faulting and tectonics of the northeastern Front Range of Colorado, *in* Lageson, D.R., Lester, A. P., and Trudgill, B. D., eds., Colorado and adjacent areas: Geological Society of America, Field Guide 1, p. 41–49.

Erslev, E. A., Kellogg, K. S., Bryant, B., Ehrlich, T. K., Holdaway, S. M., and Naeser, C. W., 1999, Laramide to Holocene structural development of the northern Colorado Front Range *in* Lageson, D. R., Lester, A. P., and Trudgill, B. D., eds., Colorado and adjacent areas: Geological Society of America, Field Guide 1, p. 21–40.

Foster, R.W. and Jensen, J.G., 1971, Carbon dioxide in northeastern New Mexico, Retrieved on May 17, 2013, from nmgs.nmt.edu/publications/guidebooks/.../33/33_p0141_p0145.pdf

Gilfillan, S.M.V., Ballentine, C.J., Holland, G., Blagburn, D., Lollar, B.S., Stevens, S., Schoell, M., and Cassidy, M., 2007, The noble gas geochemistry of natural gas reservoirs from the Colorado Plateau and Rocky Mountain provinces, USA: Geochimica et Cosmochimica Acta, v. 72, p. 1174-1198.

Hanson, B.M., Powers, B.K., Garrett, D.E., McGookey, E.D., McGlasson, R.L., Horak, SJ., Mazzullo, S.J., Reid, A.M., Calhoun, G.G., Clendening, J., and Claxton, B., 1991, The Permian Basin, in H.J. Gluskoter, D.D. Rice and R.B. Taylor, eds., Economic Geology: Geological Society of America Publication, The Geology of North America, v. P-2, p. 339-355.

Harrington, J.W., 1963, Opinion of structural mechanics of Central Basin Platform Area, West Texas: AAPG Bulletin, v. 47, p. 2023-2038.

Heidrick, 2013, Personal communication based on unpublished data.

Hickman, R.G., Varga, R.J., Altany, R.M., 2009, Structural style of the Marathon thrust belt, West Texas: Structural Geology, v. 31, p. 900-909.

Hills, J.M., 1970, Late Paleozoic structural directions in southern Permian basin, West Texas and southeastern New Mexico: AAPG Bulletin, v. 54, p. 1809-1827.

Hills, J.M., 1985, Structural evolution of the Permian Basin of West Texas and New Mexico, *in* Dickerson, P.W., and Muehlberger, W.M., eds., Structure and Tectonics of Trans-Pecos Texas, Midland, Texas, West Texas Geological Society Publication 85-81, 88-99.

Hoak, T., Jenkins, R., Ortoleva, P., Ozkan, G., Shebl, M., Sibo, W., Sundberg, K., Tuncay, K., 1998a, Naturally fractured reservoirs: Optimized E&P Strategies using a reaction-transport-mechanical simulator in an integrated approach; Chapter 3, Structural geology and tectonics; DOE/PC/91008-7 (DE98000483), Annual Report, 1996-1997, P. 53-99. Retrieved on May 17, 2013, from www.netl.doe.gov/kmd/cds/disk41/Bpercent20.../DOE-PC-91008-7.pdf

Hoak, T., Sundberg, K., Deyhim, P., and Ortoleva, P., 1998b, Fracture characterization and discrimination criteria for karst and tectonic fractures in the Ellenburger Group, West Texas: Implications for reservoir and exploration models: Annual Report, DOE/PC/91008-7, 159 p. Retrieved on May 17, 2013, from www.netl.doe.gov/kmd/cds/disk41/.../91008percent2023percent20Ptpercent206.pdf

Holtz, M. H., and Kerans, C., 1992, Characterization and categorization of West Texas Ellenburger reservoirs, *in* Candelaria, M. P., and Reed, C. L., eds., Paleokarst, karst related diagenesis and reservoir development: examples from Ordovician-Devonian age strata of West Texas and the Mid-Continent: Permian Basin Section SEPM Publication No. 92-33, p. 31-44.

Howard, J. M. and Chandler, A., 2007, Magnet Cove: Arkansas Geological Survey, Brochure Series 04, 11p. Retrieved on May 17, 2013 from http://www.geology.ar.gov/pdf/pamphlets/magnet_cove.pdf

Huffman, A.C., and Condon, 1993, Stratigraphy, Structure, and paleogeography Pennsylvanian and Permian rocks, San Juan basin and adjacent areas, Utah, Colorado, Arizona, and New Mexico: U.S. Geological Survey Bulletin 1808-O

Huffman, A.C., and Taylor, D. J., 1997, Relationship of basement faulting to laccolithic centers, southeastern Utah and Vicinity, *in*, Laccolith Complexes of southeastern Utah: Time of

Emplacement and Tectonic Setting Workshop Proceedings: U.S. Geological Survey Bulletin 2158: Coordinators, Fiedman, J. D., and Huffman, A.C., p. 41-43.

Huffman, C., and Taylor, D., 1999, Relationship of hydrocarbon resources to basement faulting in the San Juan basin, *in* Cather, M., ed., Fractured Reservoirs: Characterization and Production, Petroleum Technology Transfer Council: Farmington, NM.

Humphreys, E., 1995, Post-Laramide removal of the Farallon slab, western United States: Geology, v. 23, p. 987–990.

Humphreys, E., 2009, Relation of flat slab subduction to magmatism and deformation in the western United States: Geological Society of America Bulletin Memoir, v. 204, p. 85–98, doi:10.1130/2009.1204(04).

Jorgensen, C., 2004, Tectonic Interpretation Using Potential Field Data for the Sweetgrass Arch Area, Montana-Alberta, Saskatchewan, Presentation given to Rocky Mountain Section AAPG Meeting, Denver, Colorado, August 9-11, 2004, Retrieved on May 17, 2013, from http://www.bigskygeo.com/Sweetgrass_AAPG.pdf

Kamenetsky, V.S., Kamenetsky, M.B., Sobolev, A.V., Golovin, A.V., Demouchy, S., Faure, K., Sharygin, V.V., and Kuzmin, D.V., 2008, Olivine in the Udachnaya-East Kimberlite (Yakutia, Russia): Types, Compositions and Origins: Petrology, v. 49, p. 823-839.

Kelley, V.C., 1971, Geology of the Pecos country, southeastern New Mexico: New Mexico Bureau of Mines and Mineral Resources, Memoir 24, 75 p.

Kelley, V.C., and Clinton, N.J., 1960, Fracture systems and tectonic elements of the Colorado Plateau: University of New Mexico Publications in Geology, no. 6, 104 p.

Kelley, V.C., and Thompson, Tommy B., 1964, Tectonics and general geology of the Ruidoso-Carrizozo region, central New Mexico: New Mexico Geological Society, Guidebook 15, p. 110-121.

Kerrick, D., 2012, Personal Communication, Penn State University.

Kerrick, D., and Connolly, J. D., 2001, Quantification of subduction zone metamorphic devolatilization from computed high pressure phase equilibria. EOS, Transactions of the American Geophysical Union 82(47): 1,292.

King, P. B., 1930, The geology of the Glass Mountains, Texas; Part I, Stratigraphy: University of Texas, Bulletin. no. 3038, 167 p.

King, P. B., 1937, Geology of the Marathon Region, Texas: U.S. Geological Survey, Professional Paper 187.

King, P. B., 1977, Marathon revisited. Arkansas Geological Commission Symposium on the Geology of the Ouachita Mountains, p. 41-68.

King, P. B., 1980, Geology of the eastern part of the Marathon Basin, Texas: U.S. Geological Survey Professional Paper 1157.

Kluth, D. F., and Coney, P.J., 1981, Plate tectonics of the Ancestral Rocky Mountains: Geology, v. 9, p. 10-15.

Kupecz, J. A., and Land, L. S., 1991, Late-stage dolomitization of the Lower Ordovician Ellenburger Group, West Texas: Journal of Sedimentary Petrology, v. 61, p. 551-574.

Larson, P.B., Cunningham, C.G., And Naeser, C.W., 1994, Large-scale alteration effects in the Rico paleogeothermal anomaly, Southwest Colorado: Economic Geology, vol. 89., P. 1769-1777.

Lindgren, W., Graton, L.C., and Gordon, C., 1910, The ore deposits of New Mexico: U.S. Geological Survey Professional Paper 68, 361 p.

Loucks, R. G., 2007, Three-dimensional architecture and associated structures within a lower Ordovician Ellenburger coalesced, collapsed paleocave system, abs., Acta Carsologica, v. 36, no. 1, p. 223.

Maas, R., Kamenetsky, M. B., Sobolev, A. V., Kamenetsky, V. S. and Sobolev, N.V., 2005, Sr, Nd, and Pb isotope evidence for a mantle origin of alkali chlorides and carbonates in the Udachnaya kimberlite, Siberia: Geology v. 33, p. 549-552.

Mack, G.H., 2004, Middle and Late Cenozoic crustal extension, sedimentation, and volcanism in the southern Rio Grande rift, Basin and Range, and southern transition zone of southwestern New Mexico, *in* Mack, G.M., and Giles, K.A., eds., The Geology of New Mexico: A Geologic History: New Mexico Geological Society Special Publication 11, p. 389-406.

Madsen, J.K., Thorkelson, D.J., Friedman, R.M., and Marshall, D.D., 2006, Cenozoic to Recent plate configurations in the Pacific basin-ridge subduction and slab window magmatism in western North America: Geospheres, v. 11, p. 11-34.

McCandless, T. E., 1999, Kimberlites: Mantle expressions of deep-seated subduction: Center of Mineral Resources, Department of Geosciences, University of Arizona, Tucson, Arizona, 5 p. http://www.mccgeoscience.com/public_html/PDFs/McCandlesspercent201999.pdf

McGetchin, T.R., Smith, D., Ehrenberg, S.N., Roden, M., and Wilshire, H.G., 1977, Navajo kimberlites and minettes field guide: Santa Fé, Second Annual Kimberlite Conference, 40 p.

McKee, E.D., 1951, Sedimentary basins of Arizona and adjoining areas: Geological Society of America Bulletin, v. 62, p. 481-505.

McLemore, V.T., 1994, Placer gold deposits in New Mexico: New Mexico Geology, Science and Service, v. 16, 25 p. Retrieved on May 17, 2013, from geoinfo.nmt.edu/publications/periodicals/nmg/.../nmg_v16_n2_p21.pdf

McLemore, V.T., 2010, Geology and mineral deposits of the Gallinas Mountains, Lincoln and Torrance Counties, New Mexico; Preliminary Report, New Mexico Bureau of Geology and Mineral Resources Open-file Report OF-532, 89 p.

McLemore, V.T., and North, R.M., 1987, Metallic mineral deposits in Colfax and Union Counties, northeastern New Mexico: New Mexico Geological Society, Guidebook 38th Field Conference, p. 323-329.

McLemore, V.T., and Zimmerer, M., 2009, Magmatic activity and mineralization along the Capitan, Santa Rita, and Morenci lineaments in the Chupadera Mesa area, Central New Mexico: New Mexico Geological Society Guidebook, 60th Field Conference, Geology of the Chupadera Mesa Region, p. 375-386.

Montana Geological Society, 1985, Montana Geological Society, Symposium: Montana Oil and Gas Fields, Figure 2.

Mueller, P.A. and Frost, C.D., 2006, The Wyoming Province: a distinctive Archean craton in Laurentian North America: Canadian Journal of Earth Sciences, v. 43, pp. 1391-1397.

Muffler, L. J. P. and White D. E., 1968, Origin of CO_2 in the Salton Sea Geothermal System, Southeastern California, U.S.A. XXIII International Geological Congress 17,p. 185-194.

Muehlberger, W. R., DeMis, W. D., and Leason, J. O., 1984, Geologic cross-sections, Marathon region, Trans-Pecos Texas: Geological Society of America Map and Chart Series MC-28T, 6 p. text, scale 1:250,000.

Mutschler, F.E., Griffin, M.E., Stevens, D.S. and Shannon, S.S., Jr., 1985, Precious metal deposits related to alkaline rocks in the North American Cordillera – An interpretive review: Transactions of the Geological Society of South Africa, no. 88, p. 355-377.

Mutschler, F.E., Larson, E.E., and Ross, M.L., 1997, Potential for alkaline igneous rock-related gold deposits in the Colorado Plateau laccolithic centers, *in* Laccolith Complexes of Southeastern Utah: Time of Emplacement and Tectonic Setting Workshop Proceedings: U.S. Geological Survey Bulletin 2158: Coordinators, Fiedman, J.D., and Huffman, A.C., p. 233-247

North, R.M., and McLemore, V.T., 1988, A classification of the precious metal deposits of New Mexico, *in* Bulk mineable precious metal deposits of the western United States Symposium Volume: Geological Society of Nevada, Reno, Symposium proceedings, p. 625-659.

Pawlewicz, M., Barker, C. E., and McDonald, S., 2005, Vitrinite reflectance data for the Permian Basin, west Texas and southeast New Mexico: U.S. Geological Survey, Open-File Report, 2005-1171, 25 p.

Perhac, R. R., 1970, Geology and mineral deposits of the Gallinas Mountains Lincoln and Torrance counties, New Mexico: New Mexico Bureau of Mines and Mineral Resources, Bulletin 95, 51 p.

Peterson, J.A., Loleit, A.J., Spencer, C.W., and Ullrich, R.A., 1965, Sedimentary history and economic geology of San Juan Basin: AAPG Bulletin v. 49, p. 2076-2119.

Pilger, E.H., Jr., 1981, The opening of the Gulf of Mexico: implications for the tectonic evolution of the northern Gulf Coast: GCAGS Transactions, v. 31, p. 277-381.

Pollastro, R.M., 1991, Upper Cretaceous Niobrara fractured calcareous shale oil, *in* Wandrey, C.J. and Barker, C.E., eds, Park Basins Province (038): U.S. Geological Survey Digital Data Series DDS-30, Release 2, CD-ROM, 1 p.

Price, J.G., Henry, C.D., Barker, D.S., and Parker, D.F., 1987, Alkalic rocks of contrasting tectonic settings in Trans-Pecos Texas, *in* Mantle metasomatism and alkaline magmatism: Geological Society of America, Special Paper 215, p. 335-346.

Richards, J.P., 1995, Alkalic-type epithermal gold deposits—a review, *in* Thompson, J.F.H., ed., Magmas, fluids, and ore deposits: Mineralogical Association of Canada, Short Course Series, v. 23, p. 367-400.

Rogie, J.D., Kerrick, D.M., Chiodini, G. and Frondini, F., 2000, Flux measurements of nonvolcanic CO_2 emission from some vents in central Italy. Journal of Geophysical Research 105: doi: 10.1029/1999JB900430. issn: 0148-0227.

Ruklov, A.S., and Pawlowicz, J.G., 2012, Eocene potassic magmatism of the Milk River area, Southern Alberta (NTS 72E) and Sweet Grass Hills, Northern Montana: Overview of new data on mineralogy, geochemistry, petrology and economic potential: ERCB/AGS Open File Report 2012-01, 88p.

Schmandt, B., and Humphreys, E., 2011. Seismically imaged relict slab from the 55 Ma Siletzia accretion to northwest United States: Geology, v. 39, p 175–178: doi:10.1130/G31558.1.

Schreiner, R.A., 1993, Mineral investigation of the rare-earth-element-bearing deposits, Red Cloud mining district, Gallinas Mountains, Lincoln County, New Mexico: U.S. Bureau of Mines, MLA 99-93, 189 p.

Schroeder, D.A., 2004, Precambrian through Miocene deformation along the west flank of the Front Range around Granby, Colorado,: *in* Coates, M-M., Evanoff, E., and Morgan M.L., eds, Colorado Scientific Society and Colorado Geological Survey, Symposium on the geology of the Front Range in honor of W. A. Braddock, p. 37. http://geosurvey.state.co.us/education/Documents/fr_symp_book_web.pdf

Schumacher, D., and Abrams, M.A. 1996, eds, Hydrocarbon migration and its near-surface expression. AAPG Memoir 66.

Scotese, Christopher R., 2003, Paleomap Project website, http://www.scotese.com/

Segerstrom, K., and Henkes, W.C., 1977, Status of mineral resource information for the Jicarilla Indian Reservation, New Mexico: Administrative Report BIA-25, 11 p.

Semken, S., 2003, Black rocks protruding up: the Navajo volcanic field: New Mexico Geological Society Guidebook, 54th Field Conference, Geology of the Zuni Plateau, p. 133-138.

Sharp, W.E., 1974, A plate-tectonic origin for diamond-bearing kimberlite: Earth and Planetary Sciences Letters, v. 21, p. 351-355.

Shepard, W., and Bartow, B., 1986, Tectonic history of the Sweetgrass arch, a key to finding new hydrocarbons, Montana and Albert: Rocky Mountain oil and gas fields: Wyoming Geological Association Symposium, p. 9-19.

Shieh, Y.N., and H.P. Taylor, Jr., 1969, Oxygen and hydrogen isotope studies of contact metamorphism in the Santa Rosa Range, Nevada, and other areas: Contributions to Mineralogy and Petrology, v. 20, p. 306-356.

Shumaker, R.C., 1992, Paleozoic structure of the Central Basin Uplift and adjacent Delaware Basin, West Texas: AAPG Bulletin, v. 76, p. 1804-1824.

Sims, F.C. and Goth, J.H., Jr., 1957, McCallum field, Jackson County, Colorado: Wyoming Geological Association, 8th Annual Field Conference Guidebook, Laramie Basin and North Park p.156-158.

Smith, D., and Levy, S., 1976, Petrology of the Green Knobs diatreme and implications for the upper mantle below the Colorado Plateau: Earth and Planetary Science Letters, v. 29, p. 107-125.

Spangler, L., 2011, Kevin Dome CO_2 Storage Demonstration Project, Presented to National Energy Technology Laboratory Infrastructure Meeting, November 2011, Retrieved on May 17, 2013, from http://www.netl.doe.gov/publications/proceedings/11/carbon_storage/wednesday/BSCSPpercent20Kevinpercent20Seqpercent20infrastructure_Spangler.pdf

Staatz, M.H., 1992, Descriptive model of thorium-rare-earth veins, *in* Bliss, J.D., ed., Developments in mineral deposit modeling: U.S. Geological Survey Bulletin 2004, p. 13-15.

Steven, T.A., 1960, Geology and fluorspar deposits, Northgate District, Colorado: U.S. Geological Survey Bulletin 1082-F, p. 323–422, map scale 1:24,000.

Suppe, J., 1983, Geometry and kinematics of fault-bend folding: American Journal of Science, v. 283, p. 684-721 doi:10.2475/ajs.283.7.684.

Thompson, T. B., 1972, Sierra Blanca igneous complex, New Mexico: Geological Society of America, v. 83, p. 2341-2356.

Thompson, T.B., 1973, Mineral deposits of Nogal and Bonito mining districts, New Mexico: New Mexico Bureau of Mines and Mineral Resources, Circular 123, 29 p.

Thompson, R.N., Velde, D., Leat, P.T., Morrison, M.A., Mitchell, J.G., Dickin, A.P., and Gibson, S.A., 1997, Oligocene lamproite containing an Al poor, Ti-rich biotite, Middle Park, northwest Colorado, USA: Mineralogical Magazine, v. 61, p. 557-572.

Tweto, O., 1975, Laramide (Late Cretaceous-Early Tertiary) Orogeny in the southern Rocky Mountains, *in* Curtis, B.J., ed., Cenozoic history of the southern Rocky Mountains: Geological Society of America Memoir 144, p. 1-44.

Tweto, O., 1979, The Rio Grande rift system in Colorado, *in* Rieker, R.E., ed., Rio Grande Rift: Tectonics and Magmatism, American Geophysical Union, p. 33-56.

Wandrey, C.J. and Barker, C.E, 1991, Park Basins Province (038), in U.S. Geological Survey Digital Data Series DDS-30, Release 2, CD-ROM.

Wellborn, R., 1977. Structural style in relation to oil and gas exploration in North Park–Middle Park basin, Colorado, *in* Veal, H.K., ed., Exploration frontiers of the central and southern Rockies: Rocky Mountain Association of Geologists Symposium, p. 41-60.

Williams-Jones, A.E., Samson, I.M., and Olivo, G.R., 2000, The genesis of hydrothermal fluorite-REE deposits in the Gallinas Mountains, New Mexico: Economic Geology, v. 95, p. 327-342.

Willis, J., and Groshong, Jr., R., 1993, Deformational Style of the Wind River Uplift and Associated Flank Structures, Wyoming, *in* Keefer W., Metzger, W., and Godwin, L, eds.WGA Oil and Gas and other Resources of the Wind River Basin, Wyoming, Special Symposium 1993.

Woodward, L.A., 1987, Geology and mineral resources of Sierra Nacimiento and vicinity, New Mexico, Memoir 42, New Mexico Bureau of Mines and Mineral Resources, Memoir 42, 85 p.

Woodward, L.A, and Callender J.F., 1977, Tectonic framework of the San Juan Basin: New Mexico Geological Society Guidebook, 28th Field Conference, San Juan Basin III, p. 209-212.

Woodward, L.A., Hultgren, M.C., Crouse, D.L., and Merrick, M.A., 1992, Geometry of Nacimiento-Gallina fault system, northern New Mexico, *in* Lucas, S.G., Kues, B.S., Williamson,

T.E., and Hunt, A.P., eds., San Juan Basin IV, New Mexico Geological Society Guidebook, 43rd Field Conference, p. 103-108.

Yang, K., and Dorobek, S.L., 1995, The Permian basin of West Texas and New Mexico: Tectonic history of a "composite" foreland basin and its effects on stratigraphic development, *in* Stratigraphic Evolution of Foreland Basins, SEPM Special Publications #52, p. 149-174.

Yang, K., Pinker, R.T., Ma, Y Koike, T. Wonsick, M.M.. Cox, S.J Zhang, Y.-C, and Stackhouse, P., 2008, Evaluation of satellite estimates of downward shortwave radiation over the Tibetan Plateau: Geophysical Res., v. 113, D17204, doi:10.1029/2007JD009736.

Yuras, W., 1991, Origin of folds in the Permian Yeso Formation, Lincoln County, New Mexico: New Mexico Geological Society Guidebook 42nd Field Conference, Sierra Blanca, Sacramento, Capitan Ranges, p. 165-170.

Appendix 1 Disaggregated Field Results from CREAM

Exhibit A1-1 Risked GIIP estimates from CREAM

Area or Field	Reservoir	State	Gas Initially in Place (GIIP)																
			Area	Net Thick	ϕ	Surf Elev	Drill Depth	Rsrvr Temp	Rsrvr Press	Fm Vol Fctr	Sw	CO2 Conc	CH4 Conc	N2 Conc	He Conc	H2S Conc	Proba-bility	NG GIIP	CO2 GIIP
			Acres	Ft	%	Ft	Ft	Deg F	Psi	Rcf/Scf	%	%	%	%	%	%	%	Bcf	Bcf
Val Verde Basin	Marathon Thrust 1	TX	13,537	225	16%	3,000	12,000	-	5,196	0.002	20%	95%	5%	0%	0%	0%	33%	2,668.7	2,535.3
Val Verde Basin	Marathon Thrust 2	TX	11,897	225	16%	3,000	12,000	-	5,196	0.002	20%	85%	15%	0%	0%	0%	33%	2,238.8	1,903.0
Val Verde Basin	Marathon Thrust 3	TX	7,929	225	16%	3,000	12,000	-	5,196	0.003	20%	65%	35%	0%	0%	0%	33%	1,313.0	853.5
Val Verde Basin	Marathon Thrust 4	TX	7,661	225	16%	3,000	12,000	-	5,196	0.003	20%	55%	45%	0%	0%	0%	33%	1,174.7	646.1
Val Verde Basin	Marathon Thrust 5	TX	8,292	225	16%	3,000	12,000	-	5,196	0.002	20%	70%	30%	0%	0%	0%	33%	1,430.3	1,001.2
Val Verde Basin	Marathon Subthrust 1	TX	16,854	650	4%	3,000	15,000	-	6,495	0.002	20%	90%	10%	0%	0%	0%	33%	2,290.6	2,061.5
Val Verde Basin	Marathon Subthrust 2	TX	8,480	650	4%	3,000	15,000	-	6,495	0.002	20%	75%	25%	0%	0%	0%	25%	800.4	600.3
Val Verde Basin	Marathon Subthrust 3	TX	6,524	650	4%	3,000	15,000	-	6,495	0.003	20%	55%	45%	0%	0%	0%	20%	437.8	240.8
Val Verde Basin	Marathon Subthrust 4	TX	7,661	650	4%	3,000	15,000	-	6,495	0.002	20%	75%	25%	0%	0%	0%	33%	954.4	715.8
Val Verde Basin	Marathon Subthrust 5	TX	22,777	650	4%	3,000	15,000	-	6,495	0.003	20%	65%	35%	0%	0%	0%	33%	2,619.3	1,702.5
Val Verde Basin	Marathon Subthrust 6	TX	19,200	650	8%	3,000	15,000	-	6,495	0.003	20%	85%	15%	0%	0%	0%	33%	4,415.9	3,753.5
Val Verde Basin	Marathon Subthrust 7	TX	8,292	650	4%	3,000	15,000	-	6,495	0.003	20%	70%	30%	0%	0%	0%	33%	991.7	694.2
Val Verde Basin	Marathon Subthrust 8	TX	6,672	650	4%	3,000	15,000	-	6,495	0.003	20%	55%	45%	0%	0%	0%	33%	738.9	406.4
Lincoln County	Conventional 1	NM	58,960	90	15%	8,652	1,500	-	660	0.013	20%	97%	0%	0%	0%	0%	33%	704.1	683.0
Lincoln County	Conventional 2	NM	18,650	65	12%	6,400	1,700	-	748	0.011	20%	97%	0%	0%	0%	0%	33%	152.1	147.5
Lincoln County	Conventional 3	NM	21,050	50	15%	6,427	1,200	-	528	0.014	20%	97%	0%	0%	0%	0%	25%	98.2	95.3
Lincoln County	Conventional 4	NM	18,550	55	15%	5,791	1,200	-	528	0.014	20%	97%	0%	0%	0%	0%	20%	76.2	73.9
Lincoln County	Unconventional 5	NM	40,080	65	15%	5,404	1,750	-	770	0.013	20%	97%	0%	0%	0%	0%	25%	261.9	254.0
Lincoln County	Unconventional 6	NM	94,850	200	15%	6,530	2,000	-	880	0.012	20%	97%	0%	0%	0%	0%	15%	1,239.5	1,202.3
San Juan	Leadville Basin-Center	NM	1,012,307	75	12%	6,060	13,500	-	5,940	0.003	20%	90%	0%	5%	1%	0%	33%	37,418.7	33,676.8
North Park	Never Summer Subthrust	CO	25,891	95	18%	8,200	5,500	-	2,558	0.003	20%	95%	0%	0%	0%	0%	25%	1,285.7	1,221.4
North Park	McCallum Footwall	CO	10,070	95	18%	8,200	5,500	-	2,558	0.003	20%	95%	0%	0%	0%	0%	33%	761.6	723.6
Sweetgrass	No. 1 - Conventional Anticline	MT	128,895	165	9%	6,562	3,500	-	1,628	0.005	20%	90%	0%	0%	0%	0%	33%	4,402.3	3,962.1
Sweetgrass	No. 2 - Great Falls Anticline	MT	92,540	60	9%	3,946	3,500	-	1,628	0.005	20%	90%	0%	0%	0%	0%	33%	1,149.3	1,034.4
Sweetgrass	No. 3 - Unconventional Strat	MT	80,407	165	9%	3,443	3,700	-	1,721	0.006	20%	90%	0%	0%	0%	0%	25%	1,733.8	1,560.4
Sweetgrass	No. 4 - Conventional Dome	MT	108,540	75	9%	3,160	3,500	-	1,628	0.005	20%	90%	0%	0%	0%	0%	33%	1,685.1	1,516.6
Total																		73,042.9	63,265.3

Exhibit A1-2 Risked accessible TRR estimates from CREAM

Area	Reservoir	Accessible Technically Recoverable Resources (TRR)										
		Recovery Factor	NG TRR	Accessible portion	Accessible NG TRR	Accessible CO2 TRR	No. wells	NG TRR /well	NG EUR Tier, Average EUR Per Well			
									10%	20%	30%	40%
		%	Bcf	%	Bcf	Bcf		Bcf	Bcf	Bcf	Bcf	Bcf
Val Verde Basin	Marathon Thrust 1	70%	1,868.1	95%	1,774.7	1,685.9	7	253.5	411.8	386.4	263.6	139.9
Val Verde Basin	Marathon Thrust 2	70%	1,567.2	95%	1,488.8	1,265.5	6	248.1	403.0	378.2	258.0	137.0
Val Verde Basin	Marathon Thrust 3	70%	919.1	95%	873.2	567.6	4	218.3	354.6	332.7	227.0	120.5
Val Verde Basin	Marathon Thrust 4	70%	822.3	95%	781.2	429.6	4	195.3	317.2	297.6	203.1	107.8
Val Verde Basin	Marathon Thrust 5	70%	1,001.2	95%	951.1	665.8	4	237.8	386.2	362.4	247.3	131.2
Val Verde Basin	Marathon Subthrust 1	70%	1,603.4	95%	1,523.2	1,370.9	9	169.2	274.9	257.9	176.0	93.4
Val Verde Basin	Marathon Subthrust 2	70%	560.3	95%	532.2	399.2	3	177.4	288.2	270.4	184.5	97.9
Val Verde Basin	Marathon Subthrust 3	70%	306.5	95%	291.2	160.1	2	145.6	236.5	221.9	151.4	80.4
Val Verde Basin	Marathon Subthrust 4	70%	668.1	95%	634.7	476.0	4	158.7	257.7	241.8	165.0	87.6
Val Verde Basin	Marathon Subthrust 5	70%	1,833.5	95%	1,741.8	1,132.2	12	145.2	235.8	221.2	150.9	80.1
Val Verde Basin	Marathon Subthrust 6	70%	3,091.2	95%	2,936.6	2,496.1	10	293.7	477.0	447.6	305.4	162.1
Val Verde Basin	Marathon Subthrust 7	70%	694.2	95%	659.5	461.6	4	164.9	267.8	251.3	171.4	91.0
Val Verde Basin	Marathon Subthrust 8	70%	517.2	95%	491.3	270.2	3	163.8	266.0	249.6	170.3	90.4
Lincoln County	Conventional 1	65%	457.7	85%	389.0	377.3	30	13.0	21.1	19.8	13.5	7.2
Lincoln County	Conventional 2	65%	98.9	85%	84.0	81.5	10	8.4	13.6	12.8	8.7	4.6
Lincoln County	Conventional 3	65%	63.9	90%	57.5	55.7	8	7.2	11.7	10.9	7.5	4.0
Lincoln County	Conventional 4	65%	49.5	70%	34.7	33.6	6	5.8	9.4	8.8	6.0	3.2
Lincoln County	Unconventional 5	65%	170.2	80%	136.2	132.1	16	8.5	13.8	13.0	8.9	4.7
Lincoln County	Unconventional 6	65%	805.7	80%	644.5	625.2	22	29.3	47.6	44.7	30.5	16.2
San Juan	Leadville Basin-Center	70%	26,193.1	95%	24,883.4	22,395.1	522	47.7	77.4	72.7	49.6	26.3
North Park	Never Summer Subthrust	70%	900.0	25%	225.0	213.7	10	22.5	36.5	34.3	23.4	12.4
North Park	McCallum Footwall	70%	533.1	95%	506.5	481.2	5	101.3	164.5	154.4	105.3	55.9
Sweetgrass	No. 1 - Conventional Anticline	75%	3,301.8	95%	3,136.7	2,823.0	66	47.5	77.2	72.4	49.4	26.2
Sweetgrass	No. 2 - Great Falls Anticline	75%	862.0	95%	818.9	737.0	48	17.1	27.7	26.0	17.7	9.4
Sweetgrass	No. 3 - Unconventional Strat	75%	1,300.3	95%	1,235.3	1,111.8	31	39.8	64.7	60.7	41.4	22.0
Sweetgrass	No. 4 - Conventional Dome	75%	1,263.8	95%	1,200.6	1,080.5	56	21.4	34.8	32.7	22.3	11.8
	Total		51,452.0		48,031.8	41,528.7	902.0					

Phil DiPietro
joseph.dipietro@netl.doe.gov

Jeffrey Eppink
jeppink@enegis.com

Robert Wallace
robert.wallace@contr.netl.doe.gov

www.netl.doe.gov
Pittsburgh, PA • Morgantown, WV • Albany, OR • Sugar Land, TX • Anchorage, AK
(800) 553-7681